

COOPERATIVE AGREEMENT NO:DAMD17-97-2-7022

TITLE: X-Ray Crystallographic Studies on Acetylcholinesterase and
Related Enzymes

PRINCIPAL INVESTIGATORS: Joel L. Sussman, Ph.D.
I. Silman, Ph.D.

CONTRACTING ORGANIZATION: Weizmann Institute of Science
Rehovot 76100 Israel

REPORT DATE: October 1999

TYPE OF REPORT: Annual

PREPARED FOR: U.S. Army Medical Research and Materiel Command
Fort Detrick, Frederick, MD 21702-5012

DISTRIBUTION STATEMENT: Approved for public release;
distribution unlimited.

The views, opinions and/or findings contained in this report are those of the author(s) and should not be construed as an official Department of the Army position, policy or decision unless so designated by other documentation.

REPORT DOCUMENTATION PAGE

Form Approved
OMB No. 074-0188

The burden for this collection of information is estimated to average 1 hour per response, including the time for reviewing instructions, searching existing data sources, gathering and maintaining the data needed, and completing and reviewing this collection of information. Send comments regarding this burden estimate or any other aspect of this collection of information, including suggestions for reducing the burden, to Washington Headquarters Services, Directorate for Information Operations and Reports, 1215 Jefferson Davis Highway, Suite 1204, Arlington, VA 22202-4302, and to the Office of Management and Budget, Paperwork Reduction Project (0704-0188), Washington, DC 20503

1. AGENCY USE ONLY (Leave blank)		2. REPORT DATE October 1999	3. REPORT TYPE AND DATES COVERED Annual (15 Sep 98 - 14 Sep 99)	
4. TITLE AND SUBTITLE X-Ray Crystallographic Studies on Acetylcholinesterase and Related Enzymes			5. FUNDING NUMBERS DAMD17-97-2-7022	
6. AUTHOR(S) Joel L. Sussman, Ph.D. I. Silman, Ph.D.				
7. PERFORMING ORGANIZATION NAME(S) AND ADDRESS(ES) Weizmann Institute of Science Rehovot 76100 Israel E-MAIL: joel.sussman@weizmann.ac.il			8. PERFORMING ORGANIZATION REPORT NUMBER	
9. SPONSORING / MONITORING AGENCY NAME(S) AND ADDRESS(ES) U.S. Army Medical Research and Materiel Command Fort Detrick, Maryland 21702-5012			10. SPONSORING / MONITORING AGENCY REPORT NUMBER	
11. SUPPLEMENTARY NOTES				
12a. DISTRIBUTION / AVAILABILITY STATEMENT Approved for public release; distribution unlimited				12b. DISTRIBUTION CODE
13. ABSTRACT (Maximum 200 Words)				
14. SUBJECT TERMS				15. NUMBER OF PAGES 101
				16. PRICE CODE
17. SECURITY CLASSIFICATION OF REPORT Unclassified	18. SECURITY CLASSIFICATION OF THIS PAGE Unclassified	19. SECURITY CLASSIFICATION OF ABSTRACT Unclassified	20. LIMITATION OF ABSTRACT Unlimited	

FOREWORD

Opinions, interpretations, conclusions and recommendations are those of the author and are not necessarily endorsed by the U.S. Army.

Where copyrighted material is quoted, permission has been obtained to use such material.

Where material from documents designated for limited distribution is quoted, permission has been obtained to use the material.

Citations of commercial organizations and trade names in this report do not constitute an official Department of Army endorsement or approval of the products or services of these organizations.

N/A In conducting research using animals, the investigator(s) adhered to the "Guide for the Care and Use of Laboratory Animals," prepared by the Committee on Care and use of Laboratory Animals of the Institute of Laboratory Resources, national Research Council (NIH Publication No. 86-23, Revised 1985).

N/A For the protection of human subjects, the investigator(s) adhered to policies of applicable Federal Law 45 CFR 46.

N/A In conducting research utilizing recombinant DNA technology, the investigator(s) adhered to current guidelines promulgated by the National Institutes of Health.

N/A In the conduct of research utilizing recombinant DNA, the investigator(s) adhered to the NIH Guidelines for Research Involving Recombinant DNA Molecules.

N/A In the conduct of research involving hazardous organisms, the investigator(s) adhered to the CDC-NIH Guide for Biosafety in Microbiological and Biomedical Laboratories.

PI - Signature

Date

21.1.2000

SUMMARY

The principal objectives of the current project included:

1. Work on *Torpedo* acetylcholinesterase (*TcAChE*) involving two principal topics:
 - A) Preparation and characterization of 'aged' and 'non-aged' organophosphoryl (OP) conjugates.
 - B) Use of time-resolved crystallography in order to understand the mechanism of action of acetylcholinesterase (AChE), as well as the traffic of substrate and products through the active-site gorge.
2. Structural studies on other cholinesterases (ChEs).
3. Homology model building and detailed structural comparison of human, bovine fetal serum, snake venom and insect AChE, and of horse and human serum butyrylcholinesterase (BChE).
4. Structural studies on human paraoxonase.

The present report summarizes our principal achievements during the second year of the project. We present progress primarily with respect to Topics 1A, 2 and 4, as well as in additional areas related to the long-term aims of our research program, and also a study of specific chemical damage to *TcAChE* produced by ionizing radiation.

I. The structures of the non-aged and aged conjugates of VX with *TcAChE* were solved to 2.2 and 2.4 Å, respectively. The 3D structure of the aged adduct is essentially identical to those obtained with sarin and soman, the dealkylated OP group making a salt bridge with His440. However, the 3D structure of the non-aged conjugate revealed a disruption of the Ser200-His440-Glu327 catalytic triad due to movement of His440. Whereas in the aged conjugate, His440N δ is in H-bonding distance of Glu327O ϵ , as for native *TcAChE*, the equivalent distance is 4.5 Å in the non-aged conjugate, where the same nitrogen is in H-bonding distance (2.7 Å) of Glu199O ϵ . This disruption of the catalytic triad may explain why spontaneous reactivation of OP-AChE adducts is so slow. Movement of the imidazole is reversible, since oxime reactivation regenerates active enzyme, and the non-aged conjugate ages. Our data support the notion that the catalytic triad of serine hydrolases is mobile during catalytic function. Specifically, it supports a role for the Glu327-His440-Glu199 array in carboxyl ester hydrolysis by ChEs, and may explain

how they hydrolyze a wide range of substrates, including bulky carboxyl esters, amides, carbamates and, to a limited extent, OPs.

II. The structure of a complex of *TcAChE* with the plant alkaloid, (-)-galanthamine, has been solved to 2.3Å resolution. The inhibitor binds at the base of the active-site gorge of *TcAChE*, interacting with both the choline-binding site (Trp84) and the acyl-binding pocket (Phe288, Phe290). Its tertiary amine group appears to make a non-conventional hydrogen bond, via its N-methyl group, to Asp72, near the top of the gorge, while its hydroxyl group makes a strong hydrogen bond with Glu199. The relatively tight binding to *TcAChE* of (-)-galanthamine appears to arise from a number of moderate to weak interactions with the protein, coupled to a low entropy cost for binding due to the rigid nature of the inhibitor.

III. Radiation damage is an inherent problem in X-ray crystallography. It is usually presumed to be non-specific, and to be manifested as a gradual decay in the overall quality of data obtained for a given crystal as data collection proceeds. Synchrotron radiation, even at cryogenic temperatures, can also cause highly specific damage to proteins, as we observed for *TcAChE*. Disulfide bridges break, and carboxyl groups of acidic residues lose their definition. Highly exposed carboxyls and disulfides appear particularly susceptible. The catalytic triad residue, His440, also appears to be much more sensitive to radiation damage than other histidine residues. Our findings have direct practical implications for routine X-ray data collection at high-energy synchrotron sources. Furthermore, they provide a new and direct approach for studying radiation damage to proteins and nucleic acids at a detailed, structural level, which could provide an important tool in the search for protective pharmacological agents in both a civilian and military context.

IV. We have crystallized *Drosophila melanogaster* acetylcholinesterase (*DmAChE*) and solved the structure of the native enzyme, and of its complex with two putative insecticides, at 2.7Å resolution. The refined structure of *DmAChE* is similar to that of vertebrate AChEs in its overall fold, charge distribution and deep active-site gorge, but some surface loops deviate by up to 8Å from their position in the vertebrate structures, and the C-terminal helix is shifted substantially. While the lower part of the active-site gorges of *DmAChE* and of *TcAChE* are very similar, the

upper part of the active-site gorge of the insect enzyme is more constricted than that of the vertebrate enzymes due to the larger size of the side-chains of certain amino acids lining it. Upon binding of either of the two inhibitors, nine aromatic side-chains within the active-site gorge change their conformation so as to interact with them. Some differences in activity and specificity between the insect and vertebrate enzymes can be explained by comparison of their 3D structures.

V. A double-mutant of the PON1Q allelic variant of the gene for paraoxonase, PON1, named AA PON1Q, was obtained from Prof. Bert La Du (University of Michigan, Ann Arbor); it allows secretion of the expressed protein by permitting cleavage of the signal peptide. The clone was amplified, via PCR, and a sequence coding for a His-tag was included in the 3'-primer, to facilitate purification. The gene fragment was then cloned into an appropriate transfer vector for the Baculovirus expression vector system (BEVS). PON displaying arylesterase activity was produced and secreted in the BEVS system, and had a molecular weight 2.5 kDa lower than native PON1Q due to cleavage of the signal peptide. Scaling up permitted production of *ca.* 0.1 mg/ml of medium of AA PON1Q. Purification was achieved by selective absorption onto a nickel column that selectively binds the His-tag, followed by elution with an imidazole buffer, and subsequent dialysis so as to get rid of heavy-metal impurities. AA PON1Q can be purified to ~80 % purity by this single step, in amounts adequate for initial screening of crystallization conditions after a further purification step.

TABLE OF CONTENTS

BACKGROUND	8
Acetylcholinesterase	8
Paraoxonase	11
RESULTS	14
<i>Torpedo californica</i> Acetylcholinesterase.....	14
a) 3D structures of non-aged and aged conjugates.....	14
b) Galanthamine-AChE complex.....	15
c) Specific chemical damage to proteins produced by synchrotron radiation.....	17
3D Structure of <i>Drosophila melanogaster</i> AChE	21
Studies on Human Paraoxonase.....	23
TABLES	27
Table 1. Expression parameters of PON1.	27
FIGURES	28
Fig. 1. Structural kinetics of VX inhibition of <i>TcAChE</i> by X-ray crystallography.....	28
Fig. 2. Galanthamine (GAL).....	29
Fig. 3. Stereo view of binding of GAL in the active site gorge of <i>TcAChE</i>	29
Fig. 4. Stereo view of possible hydrogen bonds between GAL and <i>TcAChE</i>	30
Fig. 5. Comparison of GAL vs HupA binding to the active site of <i>TcAChE</i>	30
Fig. 6. Time course of cleavage of disulfide bond Cys254-Cys265 in <i>TcAChE</i>	31
Fig. 7. Time course of cleavage of disulfide bond Cys402-Cys521 in <i>TcAChE</i>	31
Fig. 8. Change in <i>TcAChE</i> B-factors due to synchrotron irradiation.....	32
Fig. 9. Alignment of three vertebrate and three insect AChE sequences.....	33
Fig. 10. Chemical formulae of reversible AChE inhibitors: ZAI, ZA and tacrine.	34
Fig. 11. Overall comparison of 3D structures of <i>DmAChE</i> and <i>TcAChE</i>	35
Fig. 12. Comparison of catalytic triads in 3D structures of <i>DmAChE</i> and <i>TcAChE</i>	36
Fig. 13. Comparison of acyl pockets in 3D structures of <i>DmAChE</i> and <i>TcAChE</i>	36
Fig. 14. Solvent-accessible area in <i>DmAChE</i> and <i>TcAChE</i>	37
Fig. 15. ZAI/ <i>DmAChE</i> interactions.	37
Fig. 16. PON cloning scheme.	38
Fig. 17. Results of Ni-NTA purification of recombinant AA PON1Q.....	39
Fig. 18. Western blot showing recombinant AA PON1Q.....	40
REFERENCES	41

OBJECTIVES

The principal objectives of this contract are to better understand the mechanism of action of AChE, and to characterize its various ligand-binding sites. These objectives are being approached by the method of single crystal X-ray diffraction, together with time-resolved X-ray crystallography, using *Torpedo californica* AChE (*TcAChE*) as the principal source of enzyme. Computational molecular model building and electrostatic characterization are being used as complementary theoretical approaches. Attempts are also being made to crystallize and, if successful, to solve the 3D structures of cholinesterases (ChEs) from other sources. These include human recombinant AChE, bovine fetal serum AChE, AChE from the venom of the krait, *Bungarus fasciatus* (*BfAChE*), and horse serum BChE. Homology model building will be used to compare and analyze the structures of these enzymes. In parallel, we are attempting to express and crystallize, with the eventual objective of solving its 3D structure, human serum paraoxonase/arylesterase.

1. Work on *TcAChE* involves two principal topics:

A) Preparation and characterization of 'aged' and 'non-aged' OP conjugates, with the objective of fully understanding the mechanistic basis and specificity of interaction of organophosphates and organophosphonates of therapeutic and toxicological interest with the active site of AChE, as well as the molecular basis of the 'aging' process.

B) Use of time-resolved crystallography in order to understand the mechanism of action of AChE, as well as the traffic of substrate and products through the active-site gorge. The experimental approaches to be adopted will be Laue crystallography and ultra-rapid freezing time-resolved crystallography. In either case, time-resolved data collection will be preceded by synthesis and characterization of suitable caged compounds, and by a study of their interaction with *TcAChE*, initially in solution and, subsequently, under steady-state X-ray data collection conditions.

2. Work on other ChEs obviously depends on the success of crystallization attempts. Particular attention is being paid to human AChE (hAChE), in view of its toxicological and therapeutic importance. In the first year of the contract, we have devoted substantial efforts to improving purification techniques already developed in our own laboratory for processing culture media containing recombinant hAChE (rhAChE), supplied by the group of Dr. Avigdor Shafferman at the Israel Institute for Biological Research (IIBR).

3. Homology model building and detailed structural comparison of human, bovine fetal serum, snake venom and insect AChE, and of horse and human serum BChE.

4. Work on paraoxonase is subject to the same restrictions as for the various ChEs, namely the availability of crystals. Thus expression and purification will precede data collection and structure determination.

BACKGROUND

Acetylcholinesterase

The enzyme, acetylcholinesterase (AChE), plays a key role in cholinergic neurotransmission. By rapid hydrolysis of the neurotransmitter, acetylcholine (ACh), it terminates the chemical impulse, thereby permitting rapid repetitive responses (1). AChE is, accordingly, characterized by a remarkably high turnover number, especially for a serine hydrolase (2), functioning at a rate approaching that of a diffusion-controlled reaction (3, 4). The powerful acute toxicity of organophosphorus (OP) poisons (as well as of carbamates and sulfonyl halides which function analogously) is attributed primarily to the fact that they are potent inhibitors of AChE (5, 6). Inhibition is achieved by their covalent attachment to a serine residue within the active site (2, 7). AChE inhibitors are utilized in the treatment of various disorders such as myasthenia gravis and glaucoma (6, 8). More recently, they have been under active consideration for use in the management of Alzheimer's disease (9). Two cholinesterase inhibitors, tacrine, under the trade name of Cognex®, and E2020, under the trade name of Aricept®, have already been approved for use in the United States by the FDA (10, 11). Finally, many carbamates and OPs serve as potent insecticides, exerting their action by selectively inhibiting insect AChE (12).

Elucidation of the three-dimensional (3D) structure of AChE is, therefore, of fundamental interest for understanding its remarkable catalytic efficacy, and of applied importance in insecticide and drug design, and in developing therapeutic approaches to OP poisoning. Furthermore, information concerning the ACh-binding site of AChE is also pertinent to an understanding of the molecular basis for the recognition of ACh by other ACh-binding proteins, such as the various ACh receptors (13-15).

Our determination of the 3D structure of AChE from *Torpedo californica* (TcAChE) (16) permitted visualization, for the first time, at atomic resolution, of a binding pocket for ACh. It also allowed identification of the active site of AChE, which, unexpectedly, is located at the bottom of a deep gorge lined largely by aromatic residues (16, 17). This unusual and unexpected structure gave us the opportunity to work out structure-function relationships for AChE. The so-called 'anionic' binding site for the quaternary moiety of ACh does not contain several negative charges, as was earlier postulated on the basis of the ionic-strength dependence of catalytic activity (18). Modeling studies suggested that the quaternary group interacts primarily with the indole ring of the conserved tryptophan residue, Trp84 (14, 16). This was confirmed by crystallographic studies on several AChE-ligand complexes, which also suggested a prominent role for Phe330 (19, 20). This implication, from the X-ray studies, that aromatic residues play an important role in recognizing the quaternary group, was in agreement with parallel affinity and photoaffinity labeling studies in solution (19, 21). The high sequence homology between mammalian AChE and the *Torpedo* enzyme suggested that their 3D structures would be very similar. Indeed, the more recent solution of the structures of complexes of recombinant mouse AChE (22) and recombinant human AChE (23) with the snake venom polypeptide toxin, fasciculin, revealed only very small differences between either of these structures and that of the

TcAChE-fasciculin complex (24), and the two mammalian structures were even more closely related. Our recent solution of the 3D structure of AChE from *Drosophila melanogaster* (*DmAChE*) reveals the structure to be similar to that of vertebrate AChEs (human, mouse, fish) in overall fold, electrostatic distribution and its deep active-site gorge; but there are substantial differences from the vertebrate enzymes, especially in the surface loops and the upper part of the active-site gorge (see Results Section).

The availability of the 3D structure of *Torpedo* AChE stimulated a large body of work, in several different laboratories, which shared the common objective of correlating the unexpected structure revealed by X-ray crystallography with the catalytic function of the enzyme. These studies can be loosely classed in four main categories, two theoretical and two experimental (some studies encompass more than one category):

- 1) Theoretical studies in which the structure of AChE or BChE from various sources is modeled on the basis of the 3D structure of *Torpedo* AChE, together with the amino acid sequence of the cholinesterase in question, obtained previously from cloning and/or sequencing studies. A necessary condition for such modeling is the high sequence identity and similarity (ca. 50% and 70%, respectively) between cholinesterases of widely different phylogenetic origin (25, 26).

- 2) Theoretical studies aimed at elucidating the electrostatic and dynamic properties of the cholinesterase molecule and their contribution to known catalytic properties.

- 3) Experimental investigations concerned with understanding the catalytic and ligand-binding properties of the cholinesterases on the basis of kinetic and spectroscopic studies with AChE and BChE from *Torpedo* and other sources.

- 4) Studies using site-directed mutagenesis to understand the contribution of particular amino acid residues to catalytic activity, substrate specificity, and to the mode of interaction with reversible and covalent inhibitors of the various cholinesterases.

Inspection of the 3D structure of *TcAChE* and of various AChE-ligand complexes, as well as of the structure of homologous enzymes, principally human AChE and BChE (inferred from modeling studies based on the 3D structure of *Torpedo* AChE), immediately led to predictions about the involvement of certain amino acid residues, almost all localized in the 'aromatic gorge', in various aspects of the enzyme's catalytic activity. Site-directed mutagenesis was the principle tool for testing such predictions. Thus, on the basis of the topology of the gorge (16), of the X-ray structure of complexes of *Torpedo* AChE with the bisquaternary inhibitors decamethonium (19) and BW284c51 (Harel *et al.*, unpublished), and on the modeling of human BChE (26), it was suggested that the so-called 'peripheral' anionic site, previously identified from kinetic (27) and spectroscopic studies (28, 29), was located at the top of the gorge. Like the 'anionic' subsite of the active site, it was thought to contain three aromatic residues, Tyr70, Tyr121, and Trp279 (*Torpedo* numbering is used here and subsequently). A kinetic comparison with BChE, which lacks all three of these residues, and with chicken AChE, which lacks two of them, provided strong experimental evidence to support this prediction (26, 30-33). In addition, a role was proposed for the acidic residue, Asp72, in the 'peripheral' site, on the basis of site-

directed mutagenesis data (34). Modeling also suggested that the two aromatic residues, Phe288 and Phe290, confer narrow substrate specificity upon AChE compared to BChE (26, 35); this suggestion, too, was clearly borne out by mutagenesis studies. Thus, our computer modeling had high predictive capacity and we have since modeled human AChE similarly, as well as more distantly related enzymes, e.g. insect AChE for studies of new insecticides (36).

Studies carried out to date have involved hundreds of mutations, principally of human, mouse, *Torpedo*, *Drosophila* and *Musca* AChE, as well as of human BChE. An updated compilation of these mutations can be obtained by accessing the Cholinesterase Data Base, at Montpellier, France, which is maintained by Drs. Arnaud Chatonnet and Xavier Cousin (see: <http://www.ensam.inra.fr/cholinesterase/>). We emphasize that these mutagenesis studies leave open numerous questions. Thus, the present data ascribe specific roles to only seven of the conserved aromatic residues in the gorge, and the role of the remainder is either not fully established or unknown. Furthermore, the role of two acidic residues, Glu199 and Asp72, respectively, near the bottom and close to the top of the gorge, is not clearly ascertained. The long-standing question of the molecular basis for substrate inhibition also is unanswered. One attractive possibility is that it involves binding of a second ACh molecule at the 'peripheral' site (30). But this contention is prejudiced by studies involving mutagenesis of aromatic residues at the 'peripheral' site (31, 37), by comparative studies on the chicken and *Torpedo* enzymes (33), and by the observation that mutation of Glu199 can strongly reduce substrate inhibition (38). A complication in analyzing all the site-directed mutagenesis data is that, in certain cases, mutations at the top of the gorge appear to affect parameters ascribed to structural factors associated with the bottom of the gorge, and vice versa (34). This is of interest, because it provides evidence that the gorge may function in an integrated fashion, but also means that interpretation of individual site-directed mutagenesis experiments must be treated with caution.

From an applied standpoint, the 3D structure of *TcAChE*, and of its complexes and conjugates with reversible and irreversible ChE inhibitors, have provided valuable information pertinent to the development of treatments for nerve gas intoxication, as well as of insecticide poisoning. Such structures can yield direct information concerning the functional groups and steric constraints governing both spontaneous and oxime-assisted reactivation and 'aging', as well as the binding of drugs of therapeutic potential, such as huperzine A (HupA) (39) and E2020 (40). These are pertinent to prophylactic and therapeutic treatment of OP intoxication, as well as to treatments which envisage administration of wild-type AChE (or BChE), whether as a scavenger (41) or as a hydrolase (42).

Inspection of the 3D structure of native *TcAChE* suggested that site-directed mutagenesis of Glu199, or of the homologous residue in the human enzyme, would retard 'aging' considerably, as confirmed by site-directed mutagenesis (43, 44). Enzyme so engineered indeed proved much more efficient in scavenging of G agents, especially when used in conjunction with oximes (45).

Modeling of BChE on the basis of the native *TcAChE* structure provided the rationale for generating a mutant, Gly117His, containing an additional histidine residue in the active site of BChE, capable of significant hydrolytic activity towards V and G nerve agents (46, 47). When a

double-mutant, Gly117His/Glu197Gln, was generated, with Glu197 being equivalent to Glu199 in *TcAChE*, aging of G agent conjugates was retarded substantially, and significant hydrolysis of soman could be achieved, whereas soman hydrolysis was undetectable with the Gly117His mutant (48).

Recent solution of the 3D structures of conjugates of the nerve agents, sarin, soman, DFP and VX with *TcAChE* (49, 50) has revealed the precise details of the multiple interactions which contribute both to the rapid inhibition of AChE by these agents, and to the irreversibility of the process. Inhibition by soman and by sarin occurs without any significant conformational change in the structure of the enzyme, but 'aging' results in formation of a salt bridge with the active-site histidine, His440, which contributes to the stabilization of the aged complex, as was already observed for the 'aged' conjugate of DFP with chymotrypsin (51). Unexpectedly, however, reaction of DFP with *TcAChE* yields an 'aged' conjugate in which the acyl-binding pocket of the enzyme has undergone a substantial conformational change in order to accommodate the residual *isopropyl* group (49). This offers a structural explanation for the slow inhibition of AChE by DFP, relative to that of BChE, which has a larger acyl-binding pocket. More recently, 3D structures were obtained for both the 'non-aged' and 'aged' conjugates of *TcAChE* with VX (50) (see Results section). Here, too, an unexpected result was obtained, inasmuch as the structures revealed conformational mobility of His440; thus, in the 'non-aged' conjugate, its imidazole is displaced by ~ 4 Å from its position in the native enzyme, forming an H-bond with Glu199, with concomitant disruption of the catalytic triad. Upon 'aging', the imidazole reverts to its position in the native enzyme. Such subtle and unpredicted conformational changes yield information, which will need to be taken into account in attempts to develop oximes with improved therapeutic characteristics.

Paraoxonase

Decontamination of OP pesticides and chemical warfare agents is a topic of considerable environmental and toxicological importance. Hence, a substantial research effort is being devoted to the discovery and characterization of enzymes capable of degrading OPs, and to utilization of 'state-of-the-art' techniques of protein engineering to enhance their catalytic power. The current status of research in this area was recently surveyed in the framework of the Proceedings of the Third International Meeting on Esterases Reacting with Organophosphorus Compounds, held at Dubrovnik on April 15th-18th, 1998 (52). Enzymes with OP-hydrolyzing capacity have been described from diverse sources. These include, in particular, bacteria (53, 54), but also squid nerve, duckweed and mung bean (55). However, especial attention has been paid to paraoxonase, due to its occurrence in human serum.

Paraoxonase (EC 3.1.8.1; PON) belongs to the family of A-esterases as defined by Aldridge (56), which are capable of hydrolyzing organophosphates, carbamates and aromatic carboxylic acid esters. They have been the subject of substantial investigation due to their potential capacity

to offer protection against intoxication by paraoxon and by other organophosphates which might serve as insecticides, as well as by OP nerve agents (for literature, see papers in (52)). Indeed, there is evidence to support the notion that serum paraoxonase (PON1) plays a significant role in the detoxification of paraoxon in the rabbit *in vivo* (57). More recently, the issue of the physiological role(s) of paraoxonase has been addressed, starting with the observation of Mackness and coworkers (58) that paraoxonase prevents accumulation of lipoperoxides in low-density lipoprotein (59, 60). Since then, paraoxonase has become the subject of clinical investigation in the context of risk factors for atherosclerotic disease (60). In parallel, fundamental research has been targeted at characterizing its endogenous substrates, and at understanding the structural and functional correlates of its action on such substrates (which include, in addition to lipoperoxides, bacterial lipopolysaccharide endotoxins) with its mode of action on OPs and aryl esters (59). A recent elegant study, utilizing a knockout mouse lacking the gene for PON1, confirmed its importance in protection against both OP intoxication and lipoprotein oxidation (61).

Paraoxonase activity has been described throughout the phylogenetic tree from microorganisms up to most mammalian species (62, 63). It remains to be established whether various esterases capable of hydrolyzing OPs in different organisms, *e.g.* the diisopropylphosphofluoridate hydrolase (DFPase) of the squid head ganglion (64), are homologous members of a small number of families displaying substantial structural similarity. In the case of the phosphotriesterase from *Pseudomonas*, which is known to hydrolyze both paraoxon and parathion (65), it has been clearly established that it shows no homology with human paraoxonase, which does not hydrolyze parathion (66). The molecular structure of the phosphotriesterase was recently solved to 2.1 Å resolution (67, 68). From the three-dimensional structure, together with kinetic and chemical data on this enzyme (69, 70), it does not appear to be closely related to human paraoxonase.

The human serum enzyme which hydrolyses paraoxon is known as human paraoxonase/arylesterase (PON1), due to its high activity on aryl esters, upon the suggestion of La Du and coworkers (71). It is one member of a multigene family (72), and has been extensively investigated by the laboratories of Furlong (73) and La Du (66). Thus it has been purified to homogeneity (74), and also cloned and expressed (75, 76). It occurs in two isozymic forms, A and B, whose pharmacogenetics have been worked out by the two laboratories. The two forms differ substantially in their specific activity towards various substrates. Notably, the B-type hydrolyses paraoxon over 6-fold faster than the A-type at high ionic strength, and hydrolyses 2-naphthyl acetate 2.5-fold faster.

The laboratory of La Du developed a procedure for obtaining highly purified PON1 from human serum (74), which allowed them to obtain both the A- and B-type enzymes purified over 500-fold from serum (77). PON1 binds tightly to apolipoproteins, and also displays a tendency to aggregate; these properties required that purification be carried out in the presence of a non-ionic detergent and glycerol. The purified enzyme so obtained is stable for months when stored at 4°C

in the presence of glycerol, a non-ionic detergent, and Ca^{++} , the cation being essential for maintaining its native conformation.

PON1 has an amino acid composition typical of globular proteins. The polypeptide chain contains 354 amino acids, and ca. 16% carbohydrate, which is attached at three glycosylation sites. Sequencing work from the laboratory of La Du (75) revealed two amino acid residues, 54 and 191, as candidates which could provide a structural basis for the A/B polymorphism. Subsequent molecular genetic and nucleotide sequencing studies by the La Du and Furlong groups (76, 78) showed that the Arg/Gln polymorphism which is observed at residue 191 follows exactly the A/B phenotype of human PON1. No influence on the enzyme has yet been observed of the Met/Leu polymorphism commonly observed at residue 54. It should be pointed out that PON1 displays no sequence homology with any known proteins.

Cloning of PON1 was followed by use of protein engineering techniques to study structure-function relationships. Two principal issues were addressed in these studies: **1.** Identification of functional amino acid residues, in which site-directed mutagenesis was complemented by chemical modification and fluorescence spectroscopy (79, 80); **2.** Study of the structural elements involved in interaction with lipoproteins (81).

Both site-directed mutagenesis and chemical modification were used to provide evidence that several histidine residues are involved in catalytic activity (79, 80), as well as at least one glutamate, one aspartate and one tryptophan. Whether most of these residues are directly involved in substrate binding or catalysis remains to be established. However, one tryptophan, Trp280, may be involved in the Ca^{++} -binding site required for catalytic activity (80). Generation of the Cys284Ala mutant showed that the free cysteine at that position is not required for either organophosphatase or arylesterase activity (82); it is, however, required for the protective action(s) of PON1 against oxidized LDL (83). In the course of such protection experiments, PON1 undergoes partial inactivation, and this inactivation appears to be, at least partly, due to modification of Cys284. Thus the protective activity of PON1 is not accurately predicted by its hydrolytic activity, and may, indeed, be oxidative or peroxidative rather than hydrolytic; and the active centers for the two types of catalytic activity, although similar, appear not to be identical.

Human PON1 is HDL-associated. Since the mature protein retains its leader sequence, the possibility was raised that it is the leader sequence which is responsible for this association (81). This was tested by mutation of two bulky residues to alanine, viz. generation of the His19Ala/Gln20Ala double mutant. As a result of the double mutation, the leader sequence was, indeed, cleaved, and the modified PON1 so generated lacked the capacity to bind to either apolipoproteins or to phospholipids. Nevertheless, the modified enzyme retains its capability to protect LDL from copper-ion induced oxidative damage in an *in vitro* assay, demonstrating that the N-terminus is not required for this function.

RESULTS

***Torpedo californica* Acetylcholinesterase**

a) 3D structures of non-aged and aged conjugates

As described in the Background Section, and in our previous Annual Report, we earlier reported the 3D structures of conjugates with *TcAChE* of soman, sarin and DFP (49). All three structures represented aged conjugates. It was, therefore, of interest to determine the structure of a conjugate with VX, both because of its overall importance, and as a representative non-aged structure. The fact that VX-AChE conjugates age, albeit very slowly, raised the possibility of obtaining homologous aged and non-aged conjugates whose 3D structures could be compared directly.

The experimental approach used was to reaction VX with *TcAChE* in solution to yield a non-aged conjugate. The conjugate was then used to grow trigonal crystals as for the native enzyme (39). The crystals of the conjugate were, indeed, isomorphous with the native crystals. If such crystals were allowed to remain for as long as five months at 4° C, they might be expected to undergo aging. Thus data collection was carried on freshly prepared crystals of the conjugate and on crystals which had been stored under the conditions just mentioned. It was thus possible to collect data sets to 2.2 Å and 2.4 Å, respectively, for the non-aged and aged VX-*TcAChE* conjugates. Data were collected at 100 K with synchrotron radiation at Elettra, Trieste, for the non-aged conjugate (PDB IDcode 1vxr), and at the NSLS at Brookhaven National Laboratory for the aged conjugate (PDB IDcode 1vx0).

Not unexpectedly, the 3D structure of the aged adduct is essentially identical to those solved previously for sarin and soman (49), since the OP substituent is identical in all three (Fig. 1c). However, the 3D structure of the pro-aged conjugate revealed a disruption of the Ser200-His440-Glu327 catalytic triad due to movement of His440. Whereas in the aged conjugate, as in the native structure (Figs. 1A,C) His440N δ is within H-bonding distance of Glu327O ϵ , the equivalent distance is 4.5 Å in the non-aged conjugate, in which the same nitrogen is within H-bonding distance (2.7 Å) of Glu199O ϵ (Fig. 1B). The observed uncoupling of the catalytic triad may explain the slow, often negligible, spontaneous reactivation of OP-AChE adducts. It is important to emphasize, however, that the movement of the imidazole in the non-aged conjugate is reversible. This is because the catalytic triad could be restored by either: (1) dephosphorylation with a nucleophile (reactivation); or (2) dealkylation of the VX *O*-ethyl group (aging). To confirm that active enzyme could be regenerated from the alternate conformation, VX-*TcAChE* crystals were dissolved in phosphate buffer (pH 7.5), incubated for 20 hr with 10 mM pralidoxime, and AChE activity was measured by the Ellman method (84). Oxime-reactivated VX-*TcAChE* was indistinguishable from native enzyme with respect to substrate kinetics, corroborating that the His440 movement caused by phosphorylation was reversed upon dephosphorylation.

It was earlier proposed that the histidine within the catalytic triad of serine hydrolases may be mobile during catalytic function (85, 86). Furthermore, Quinn and colleagues suggested that AChE may use a "cryptic catalytic mechanism" for certain less-reactive carboxyl ester substrates that relies upon Glu199 (87). In addition, the Glu199Gln mutation was found to reduce k_{cat}/K_m for hydrolysis of optimal ester substrates by more than 10-fold (43, 44). Although we do not know yet if the mobility of His440 extends to substrates other than phosphate esters, the widely conserved presence of the Glu327-His440-Glu199 array in divergent cholinesterases is consistent with a role in carboxyl ester catalysis.

Thus the VX-*Tc*AChE structures demonstrate that two buried acids in an active-site quartet (Ser-His(-Glu)-Glu) modulate the catalytic imidazole position during reaction with a rapid OP "hemi-substrate." Structural flexibility may underlie the biological persistence of the catalytic triad motif, and it offers a new hypothesis for how AChE hydrolyzes such a wide range of substrates, including bulky carboxyl esters, amides, carbamates and, to a limited extent, OPs, in a sterically-congested and buried active site.

b) Galanthamine-AChE complex

According to the 'cholinergic hypothesis', Alzheimer's disease (AD) is associated with cholinergic insufficiency (88-90). This serves as the rationale for use of cholinergic agonists (91, 92) and cholinesterase inhibitors (93, 94) for the symptomatic treatment of AD in its early stages. Indeed, cholinesterase inhibitors are the only drugs so far approved for treatment of AD. These drugs include natural substances, such as the alkaloids, physostigmine (95) and huperzine A (HupA) (96), and synthetic compounds, such as tacrine, under its trade name, Cognex® (97), SDZ ENA-713, also known as Exelon® (98), metrifonate (99) and E2020, under its trade name, Aricept® (40, 100).

Galanthamine (4a,5,9,10,11,12-Hexahydro-3-methoxy-11-methyl-6H-benzofuro[3a,3,2-ef][2]-benzazepin-6-ol; GAL; see Fig. 2) is an alkaloid found in the bulbs and flowers of the common snowdrop (*Galanthus nivalis*). As a natural compound, GAL has since been tested for use in anesthesiology (101), and for treatment of many human ailments, from facial nerve paralysis to schizophrenia and various dementia (102-104). It is marketed as Reminyl™.

GAL displays 53-fold selectivity for human erythrocyte AChE over BChE, with IC_{50} values of 0.35 μ M for erythrocyte AChE and 18.6 mM for plasma BChE (105). An IC_{50} of 652 nM has been recorded for *Tc*AChE (T. Lewis and C. Personeni, unpublished results). Interestingly, it displays 10-fold lower potency towards human brain AChE than towards the erythrocyte enzyme (106). In addition to serving as a cholinesterase inhibitor, GAL is also a nicotinic activator, acting both on ganglionic and muscle receptors (107, 108), and on nicotinic receptors in the brain (109). Nicotinic modulation represents a new and promising approach in Alzheimer research (110-115). Indeed, a recent report suggests that stimulation of nicotinic receptors may be associated with diminished appearance of amyloid plaques, one of the hallmarks of AD (116). The double action of GAL, as both an anticholinesterase and a nicotinic activator, has rendered it

a promising candidate drug for the treatment of AD. Indeed, Phase III clinical trials in Europe for the treatment of AD were recently completed (117), although approval has not yet been granted.

Structure-based drug design is an important tool in the development of second-generation candidate drugs based on a lead compound (113, 118-120). Although computerized docking programs are becoming increasingly sophisticated, the X-ray analysis of a ligand-protein structure often yields crucial information. Indeed, in the case of AChE, determination of the 3D structures of the appropriate ligand-AChE complexes was a prerequisite for making correct structural assignments for HupA (39) and E2020 (40), as well as for the snake venom toxin, fasciculin (24). In the case of GAL, too, docking protocols suggest more than one possible orientation (Fletcher, R., Viner, R., Lewis, T., unpublished results). Determination of the 3D structure of a GAL-AChE complex would obviously resolve the issue. Furthermore, knowledge of the structure of the complex would also allow us to rationalize results of recent synthetic modifications (121) aimed at improving binding characteristics of GAL to AChE.

GAL was soaked into native *TcAChE* crystals by our commonly employed procedures for reversible ligands (19, 39). A 2.3 Å data set was collected at 100 K, in-house at the Weizmann Institute of Science, using a Rigaku RAXIS IIC imaging plate system mounted on a Rigaku FR-C rotating anode.

The overall mode of binding of GAL to *TcAChE* is shown in Fig. 3 (122). The inhibitor binds at the base of the active-site gorge, spanning the acyl-binding pocket and the choline-binding site, viz. the indole ring of Trp84. There appear to be two classic hydrogen bonds formed with protein atoms (Fig. 4). One is between the hydroxyl group of the inhibitor and Glu199O^{e1} (2.7Å). The second possible hydrogen bond to a protein atom involves the hydroxyl group of Ser200, whose hydrogen may be bifurcated between His440N^{e2} and the oxygen of the O-methyl group of the inhibitor. There may also be a non-classical hydrogen bond between the N-methyl group of the inhibitor and Asp72 O^{δ2} (3.4Å), since the methyl group is expected to carry some of the positive charge of the amine. The rest of the interactions between the inhibitor and the protein appear to be non-polar. This is particularly noteworthy, since the protonated tertiary amine group does not interact with Trp84 or Phe330 analogously to the interaction which is believed to occur between the quaternary amine of the natural substrate (acetylcholine) and the enzyme, and has been observed for a number of inhibitors (19, 20, 39).

Initial inspection of the GAL-*TcAChE* complex does not reveal any specific interactions which could account for the tight binding observed. GAL is not a transition state analogue, which, of all the structures on the reaction coordinate, bind most tightly to the enzyme (123). Nor are there any charge-charge interactions between the inhibitor and the enzyme. In fact, the only charged group in the inhibitor interacts rather indirectly with residues of the protein (through a solvent molecule to Phe330, possibly via a methyl hydrogen to Asp72, and via a methylene hydrogen with the π system of Trp84). It must be assumed that the binding energy for GAL comes from a number of smaller enthalpic contributions, coupled to an unusually small entropic penalty. This latter point arises from the rigidity of the molecule, which allows the numerous

interactions to occur with minimal loss of entropy. A similar concept is utilized in the tight binding of multisubstrate analogues (124, 125).

Another AD drug, HupA (39, 126), shares common binding characteristics with GAL (Fig. 5). Both molecules have a bent hinge shape, and, in both cases, the hinge is oriented similarly when the ligand is bound to *TcAChE*. Both molecules pack against the face of Trp84, and make few direct hydrogen bonds to the protein. Nevertheless, there are several major differences in their binding modes. Thus, GAL does not induce a main chain conformational change at Gly117 as does HupA. Moreover, the orientation of the side chain of Phe330 differs in the two complexes. Furthermore, the primary amino group of HupA interacts much more closely with the indole ring of Trp84 than does the tertiary amine of GAL. Finally, GAL does not exhibit the slow binding kinetics observed for HupA (127). A partial answer to the question of why GAL binds with a tightness comparable to HupA, despite apparent lack of direct interaction between the amine group and Trp84, may lie in the fact that GAL fills more of the active site volume, since it also binds in the acyl binding pocket. Furthermore, one of the direct hydrogen bonds with the protein involves a charged residue (Glu199), which is not the case for HupA.

c) Specific chemical damage to proteins produced by synchrotron radiation

Although radiation damage is an inherent problem in X-ray crystallography, it has not, so far, been widely investigated. It is usually presumed to be non-specific, and to be manifested as a gradual decay in the overall quality of data obtained for a given crystal as data collection proceeds (128-130). Data collection at cryogenic temperatures (131, 132) has been used to reduce radiation damage, but data collection at powerful synchrotron sources, especially on large structures, has shown that radiation damage is still a problem to be overcome. In order to do so, it is imperative that we come to understand the mechanism of radiation damage and its detailed consequences.

In a study performed in preparation for time-resolved measurements on *TcAChE* (133), we observed, in addition to the loss of diffractive power of the crystal and a general increase in atomic B-factors, highly specific effects of X-ray irradiation. These included, in particular, breakage of disulfide bonds and loss of definition of the carboxyl groups of acidic residues. Very similar specific radiation damage was observed in studies of a second enzyme, hen egg white lysozyme, suggesting the generality of the observed phenomenon. Our studies have direct practical implications for macromolecular crystallographers using bright synchrotron sources, both with regard to data collection and to interpretation of the structures obtained. Finally, they show that radiochemistry of macromolecules exposed to synchrotron radiation can be monitored at a detailed structural level, and may thus supplement and augment data obtained by use of existing techniques used in radiation research, such as electron spin resonance and electron-nuclear double-resonance spectroscopy (134, 135). Exposure to ionizing radiation is a risk factor for both the civilian and military communities. For the civilian community, this means possible effects of constant exposure to low levels of radiation, various therapeutic treatments, industrial use of radioactive isotopes, and possible nuclear power station mishaps. For the military it means

the handling of nuclear weapons and fuel, and possible protection against nuclear attack. Both military and civilian space programs must take into account exposure to much higher radiation levels than on earth. Obviously, development of protective pharmacological agents demands a thorough knowledge of the molecular events that occur upon exposure to ionizing radiation (see <http://www.afrr.usuhs.mil/>). The results presented below show that X-ray crystallography can provide direct information concerning the susceptible groups in proteins and, presumably, in nucleic acids.

In this study, we carried out a detailed comparison of a series of nine consecutive data sets collected on the same *TcAChE* crystal, under cryogenic conditions, on a powerful undulator beamline at the 3rd generation synchrotron source of the ESRF in Grenoble. Each data set was collected over a period of 19 min. Upon comparison of the refined structures, the most striking change observed was a time-dependent change in electron density in the region corresponding to the intrachain disulfide bridge between Cys254 and Cys265 (Fig. 6). The other two intrachain disulfides, Cys402-Cys521 (Fig. 7) and Cys67-Cys94, appear substantially more stable over the same period of time.

Detailed inspection of the 9 temporal steps for the Cys254-Cys265 bond reveals that already in the first data set (Fig. 6b-A) some reduction of density is observed for Cys265S γ relative to that of Cys254S γ , with disappearance of any linking density already apparent in the second data set. Subsequently, it appears as if Cys265S γ is **detached**, *i.e.* moves away from Cys254S γ (Fig. 6b-C), and then disappears. Although Cys254S γ does not appear to move, its electron density gradually diminishes, and by the 8th step (Fig. 6b-H) it is no longer visible.

Comparison of the overall structures does not reveal any major change in backbone conformation occurring concomitantly with disulfide bond cleavage. B-factors do change as a function of time, but not uniformly throughout the protein. Specifically, the B-factors for Cys, Asp and Glu side chains increase much more than those for other amino acids (Fig. 8). Examination of individual amino acids shows that the rate of increase in B-factor for the side chain of Cys265, for the first three data sets, is the highest in the whole protein; that for the side chain of Cys254 is only exceeded by that for the side chain of the exposed glutamic acid residue, Glu306. The side chain of the glutamic acid in the catalytic triad, Glu327, also shows a marked increase in B-factor of 50% in the second (B) compared to the first (A) data set. Although the B-factors for histidine residues in general do not increase remarkably (Fig. 8), that for the catalytic triad residue, His440, increases by 34%.

Our observation of specific radiation damage, including cleavage of disulfide bridges and loss of definition of carboxyl groups of acidic residues, was, indeed, unexpected. To our knowledge, ours is the first report of such a phenomenon for X-ray data collection under cryogenic conditions. Under our experimental conditions, we reproducibly observe a specific order of cleavage, with the Cys254-Cys265 bond being the most susceptible in *TcAChE*. Breakage of the homologous disulfide, Cys292-Cys302, in the X-ray structure of *DmAChE* (136, 137), was observed in a data set collected on a second-generation synchrotron source (NSLS at Brookhaven National Laboratory).

From the histogram of increases in B-factors for *TcAChE* presented in Fig. 8, one can see that the residues most affected by synchrotron radiation, apart from the cysteines, are the acidic residues, glutamate and aspartate. One residue which is particularly affected is the AChE surface residue, Glu306; another is Glu327, which is a member of the catalytic triad characteristic of serine hydrolases. The increases in B-factors could be either a consequence of increased mobility, or decarboxylation, a known effect of ionizing radiation (138). Acidic residues are often seen in active sites of enzymes, as is the case for both enzymes in the present study. An important consequence of our experiments is the realization that any unusually large B-factor, *i.e.* apparent mobility, seen for such residues, might not be of functional significance, but simply the result of specific radiation damage during structure determination.

Among the 14 histidine residues in *TcAChE*, the catalytic triad residue His440 is the most affected by X-ray irradiation, as shown by the marked increase in its B-factor. This could be related to the observations of Faraggi and coworkers (139), who showed that pulsed radiolysis affected primarily histidine residues at active sites. However, the increase in B-factor may also be coupled to the increase in B-factor noted above for the acidic member of the catalytic triad, Glu327. Our observation that active-site residues are among the most radiation-sensitive residues, suggests that, like disulfide bonds, active site conformations constitute 'weak links' or 'strained' configurations in protein structures.

An important issue which arises is whether the specific structural changes which we observe are a consequence of "primary" interaction, *i.e.* between the X-rays and the moieties that suffer specific damage, or "secondary", *i.e.* mediated by free radicals generated by the X-rays either within the protein ("direct" damage) or within the solvent ("indirect" damage). The extent to which radiation damage to proteins and nucleic acids is "direct" or "indirect" is indeed the subject of controversy (see, for example, the review (140)). "Primary" damage might affect sulphur atoms preferentially since, at the wavelength utilized, they have a significantly higher absorption cross section than carbons, oxygens or nitrogens. Disulfide bonds were earlier shown, in pulse radiolysis studies, to be sensitive to radicals (141) and, therefore, to "secondary" damage. X-ray irradiation of water molecules in the solvent area releases highly reactive species, including hydrogen and hydroxyl radicals, and hydrated electrons (138, 139). These species should be capable of attacking the protein even under cryogenic conditions (142). There does, indeed, seem to be a correlation between solvent accessibility and susceptibility of disulfides to X-ray damage. Thus Cys254-Cys265 in *TcAChE*, and Cys6-Cys127 in HEWL, are the most susceptible disulfides in their respective proteins, and both seem to have the largest solvent accessible surface of the disulfides in that protein. Irradiation has, however, also been shown to cleave disulfide bridges in dry proteins (138). Thus possible involvement of "direct" radiation damage (140, 143) in generating the specific structural changes that we observe must also be taken into consideration.

Our findings have significant practical implications with respect to X-ray data collection using bright synchrotron sources. Figs. 6aA - 6aC and 6bA - 6bC clearly show that specific damage occurs from the very onset of exposure of the crystal to the X-ray beam. Yet, the

resolution of these first three data sets is virtually identical, although some decay in the signal-to-noise ratio for the higher resolution reflections was observed. These data sets were all complete. However, the redundancy was low as a result of the minimization of the data collection time. Thus, during standard data collection at brilliant undulator beamlines at third generation synchrotron sources, which aims at high redundancy, specific radiation damage of the type that we report is very likely to occur (142). Following the trends in Figs. 6 and 7, it is clear that each data set represents the average of a temporal ensemble, which might require extrapolation to zero time. We, ourselves, earlier observed a broken disulfide bond (Cys254-Cys265) in *TcAChE* using a data set that was collected on a second-generation source wiggler beamline at the NSLS of Brookhaven National Laboratory.

In some fields of synchrotron-related research, the free radicals generated by the X-rays have actually been utilized for studying biological systems in solution (144). For example, folding of an RNA molecule has been followed on a 10 ms timescale by monitoring its hydroxyl radical-accessible surface (145). We anticipate that, once the mechanism(s) underlying radiation damage in single crystal protein crystallography are better understood, it should be possible to utilize the wealth of sequential information generated as a valuable tool in radiation chemistry and biology. As mentioned above, this could be a valuable tool in developing approaches to protection against ionizing radiation for both military and civilian purposes.

3D Structure of *Drosophila melanogaster* AChE

Our structural studies on *TcAChE* and hAChE, as well as studies on mouse and *Electrophorus* AChEs, showed, as might be expected from the high degree of sequence homology, that they all possessed a very similar 3D structure. It was obvious, however, both from the diversion in sequences (Fig. 9) and from available biochemical data, that substantial structural differences might be expected between the invertebrate and vertebrate enzymes. Solution of the 3D structure of an insect enzyme would thus be expected to yield structural information which would be valuable for insecticide design. However, knowledge of differences in the 3D structures of the human and insect enzymes would also, obviously, be of great importance in the context of exposure of civilians or military personnel to insecticides or to other pesticides targeted toward AChE. Crop spraying with insecticides exposes agricultural workers to high levels of pesticides, and the WHO estimates that this leads to 220,000 deaths annually from single short-term exposure (146). An insect structure would also be relevant in the context of recent findings concerning possible synergistic action of multiple anticholinesterases in relation to the Gulf War Syndrome (147). Taken in conjunction with our knowledge of the structures of the complexes of *TcAChE* with a variety of AChE inhibitors (19, 20), and our recently reported solution of the 3D structure of the complex of hAChE with the snake venom toxin, fasciculin (23), an insect structure could provide a rational basis for improving the selectivity of new insecticides and, thereby, reducing their toxicity towards humans and other vertebrates.

We have now crystallized *DmAChE*, and solved the structure of the native enzyme, as well as of its complexes with two putative insecticides, all three at 2.7Å resolution. This work was done in close collaboration with the laboratories of Dr. Terry Rosenberry (Mayo Clinic, Jacksonville, FL) and Dr. Terry Lewis (Zeneca Agrochemicals, Jealott's Hill, UK).

For this purpose, Dr. Rosenberry constructed a secreted disulfide-linked dimeric form of *DmAChE*, which he transfected into *Drosophila* Schneider Line 2 cells (148). By subsequent expression, followed by purification of the secreted enzyme by affinity chromatography, he was able to supply us with batches each of which contained several milligrams of highly purified *DmAChE*.

DmAChE crystals were grown by the hanging drop method at 19°C from a medium whose composition was 13% MPEG 2000 (monomethyl ether)/0.1M ammonium sulfate/0.03M leucine/0.1M acetate, pH 4.6. Crystals grew in 4-5 days as trigonal prisms, 0.2mm in size, space group $P4_32_12$. Isomorphous crystals were obtained by cocrystallization with two putative insecticides which are analogs of tacrine (Fig. 10). A single suitable heavy atom derivative was found by immersing a native *DmAChE* crystal in a chamber containing gaseous xenon at 5 bar pressure for 1 min, as described by Sauer and coworkers (149). X-ray data for the native crystal, for the Xe derivative, and for the ZAI complex were collected at the Elettra synchrotron in Trieste, at 100K. Data for the ZA-*DmAChE* complex (Fig. 10) were collected at the NSLS (Brookhaven National Laboratory), also at 100K,

It turned out that the 3D structure of the *Dm*AChE is sufficiently different from that of the vertebrate enzymes to preclude solution by molecular replacement on the basis of the *Tc*AChE structure. In fact, as already mentioned, a heavy atom derivative was required to obtain experimental phases of sufficiently high quality to yield electron density maps which permitted tracing of the backbone of *Dm*AChE.

In the structure obtained, the packing in spacegroup $P4_32_12$ reveals the familiar AChE dimer (16), with a disulfide bridge between the COOH-terminal Cys577 residues. Residues 1-2, 104-135, 575-586 in the native *Dm*AChE structure, residues 103-135, 574-586 in the ZAI complex structure, and 1-2, 103-136, 574-586 in the ZA complex, do not lie in any significant electron density. The largest insert in the *Dm*AChE sequence, relative to *Tc*AChE, is residues 104-140 (Fig. 9). No electron density is observed for this insert, except for 4 residues at its C terminus. The atomic coordinates and structure factors for the native structure, and for the complexes with ZAI and ZA, have been deposited at the PDB, and have ID codes 1qo9, 1qon, and 1dx4, respectively.

The refined structure of *Dm*AChE is similar to that of vertebrate AChEs, e.g., human, mouse and fish, in its overall fold, charge distribution and deep active-site gorge, but some of the surface loops deviate by up to 8 Å from their position in the vertebrate structures, and the C-terminal helix is shifted substantially (Fig. 11). While the lower part of the active-site gorges of the insect enzyme and that of *Tc*AChE are very similar (Figs. 12 & 13), the upper part of the active-site gorge of the insect enzyme is more constricted than that of the vertebrate enzymes, due to the larger size of the side-chains of certain amino acids lining it (Fig. 14). Upon binding of either of the two inhibitors, nine aromatic side chains within the active-site gorge change their conformation so as to interact with the inhibitors (Fig. 15).

Comparison of the 3D structures of *Dm*AChE and the vertebrate AChE structures indeed suggest candidate residues which can be taken into account in attempting to achieve inhibitor selectivity. The primary candidates for achieving this selectivity are the 8 residues clustered near the opening of the gorge, which differ in the insect and vertebrate sequences. The largest differences, which are potential targets for inhibitor selectivity, are in Tyr71, Tyr73, Glu80 and Asp375 (*Dm*AChE numbering), which are Asp, Gln, Ser and Gly, respectively, in vertebrates. However, differences in residues which do not line the gorge, but interact with gorge residues (i.e., second shell), may play a role in influencing selectivity, as discussed below.

One of the known differences between vertebrate and insect AChEs is the latter's ability to hydrolyze substrates with larger acyl moieties, e.g. butyrylcholine (150). A possible reason for this difference is that in the vertebrate acyl binding pocket, the residues equivalent to Leu328 and Phe371 in *Dm*AChE (Phe288 and Phe331 in *Tc*AChE) are both phenylalanines, and form a rigid π - π stacking pair. Since residue 328 in *Dm*AChE is a leucine, the rigid π - π stacking is lost (though the total aromatic nature of the pocket is maintained by the 'gain' of Phe440). The loss of rigid stacking renders Phe371 more mobile, thus enabling the insect acyl binding pocket to accommodate larger moieties. Furthermore, mutagenesis of the same residue in hAChE, i.e. Phe295Leu, increased the substrate specificity of this enzyme for butyrylcholine relative to that

for ACh by more than 100-fold (32, 38). Hence, we predict that a Leu328Phe mutation in *DmAChE* should reduce its capacity to hydrolyze butyrylcholine. This prediction will be tested by site-directed mutagenesis.

Four natural mutations have been identified in insect AChEs (151, 152) which confer resistance to insecticides in both *Drosophila* and in houseflies: Gly265Ala, Phe330Tyr, Ile161Val and Phe77Ser. Our 3D structure can rationalize the effects of these mutations; (1) Gly265 is conserved across both insects and vertebrates (see Fig. 9). The Gly265Ala mutation is not in the active-site gorge, but in a second shell. We propose that the additional methyl group points toward the active-site Ser238 and thus affects catalysis. (2) The Phe330Tyr mutation is in the array of aromatics lining the acyl pocket. It is also conserved throughout other invertebrates as well as vertebrates. The additional OH of Tyr330 would be lodged in the acyl binding pocket, reduce its size and hence, its binding specificity. (3) The Ile161Val mutation is also in the second shell. Valine is found in this position in vertebrates (see Fig. 9). Residue 161 has some interactions with the key 'anionic' site residue, Trp83. Comparison of the *DmAChE* structure with the vertebrate structures shows that the isoleucine is in somewhat closer contact than the valine with Trp83 (3.8Å vs. 4.0Å). This may affect either the mobility of Trp83 or its electrostatic properties. (4) Phe77, another residue conserved across species, is also in the second shell. It forms an end-on π - π interaction with the active-site gorge residue Trp472; mutation to serine eliminates this interaction and, apparently, causes serious alteration of the active-site gorge.

Studies on Human Paraoxonase

Human paraoxonase/arylesterase (PON1) is an esterase with broad substrate specificity. It catalyzes the hydrolysis of paraoxon, and a number of other OPs, and of esters such as phenylacetate. OPs are widely used as insecticides and nerve gases, and are lethal for many species, including humans, due to their inhibition of the synaptic enzyme, AChE, as well as of other esterases and proteases. It has been shown that serum paraoxonase plays a significant role in the detoxification of a variety of OPs in mammals. Furthermore, correlations have been found between the levels of serum paraoxonase and systemic diseases, such as systemic amyloidosis (see Background Section). The enzyme does not correspond to any of the protein sequences in the Swiss-Prot data base or in the protein sequences derived from the GENE BANK database; thus it is difficult to infer any structural information from proteins found in the Protein Data Bank (PDB) (153). Although PON1 may be involved in breakdown of oxidized lipids (see Background Section), its physiological role and natural substrate remain to be clearly defined. Structural data may shed light on this issue, and may also offer a new structural motif.

Expression of PON1 has been achieved, both in human 293 kidney cells and in CHO-K1 cells. These expression systems were utilized, in conjunction with site-directed mutagenesis, to obtain evidence for a role in the catalytic action of PON1 of various candidate amino acids, and in an attempt to increase its catalytic efficacy (82, 154). In order to obtain the large quantities of

pure protein necessary for X-ray crystallographic studies, both of wild type PON1 and of pertinent mutant forms of the enzyme, we have chosen the Baculovirus expression vector system (BEVS) in insect cells. This expression system has proved itself in recent years as an extremely versatile and cost-effective tool for large-scale production of many eukaryotic proteins, with yields of as much as 50mg/l of culture medium (155). A scan of the PDB retrieved almost 100 structures of proteins which had been expressed using the BEVS expression system (<http://www.rcsb.org>). The BEVS system has also been successfully used in expression of both wild-type and selenomethionyl variants of human choriogonadotropin (156). The production of selenomethionyl variants of a particular protein is an extremely powerful tool which permits determination of a structure by multiple anomalous diffraction (MAD) techniques (157). This technique requires only a single crystal, with the phase problem being solved by varying the wavelength during data collection. This is in contrast to multiple isomorphous replacement methods, which require crystals that are isomorphous to the native ones with heavy atoms soaked in.

The BEVS is a eukaryotic expression system; it thus uses many of the protein modification, processing, and transport systems present in higher eukaryotic cells. Baculovirii are large, enveloped double-stranded DNA virii that infect arthropods. The viral genome is large (130 kbp); hence it can accommodate large segments of foreign DNA. Virii enter the cell by adsorptive endocytosis and move to the nucleus, where their DNA is released. Two types of viral progeny are produced: extracellular virus is released from the cell by budding, starting ~12 hr postinfection, and is produced at a logarithmic rate until 20 hr postinfection, after which production falls off. Polyhedra-derived virus appears in the nucleus at ~18 hr postinfection, and continues to accumulate as late as 72 hr postinfection, or until the cells lyse. Occluded viral particles are embedded in proteinaceous viral occlusions called polyhedra within the nuclei of infected cells. The polyhedrin protein (29 kDa) is the major protein component of the occlusion bodies.

The BEVS expression system takes advantage of several properties of the polyhedrin protein: (1) It is expressed at very high levels in infected cells, constituting more than half of the total cellular protein late in the infectious cycle; (2) It is not essential for infection or replication of the virus; (3) Virii lacking the polyhedrin gene have a plaque morphology distinct from that of viruses containing the gene. Thus the recombinant baculovirus is engineered to express the desired protein by replacing the polyhedrin gene with a foreign gene coding for this protein through homologous recombination. This is achieved by cotransfecting a linearized baculovirus genome with a transfer vector containing the gene of interest. This transfer vector, besides the elements needed for amplification in *E. coli*, contains a multiple cloning site for the insertion of the target gene, a promoter for the polyhedrin gene and a large tract of baculovirus genome flanking the cloning region to facilitate homologous recombination. Subsequently, recombinant viruses in which expression of polyhedrin has been replaced by the target protein can be selected by several screening methods. Many commercial improvements to this basic protocol, that report

increased efficiency in the production of recombinant virus, are available on the market, thus minimizing the time needed for production of a suitable virus.

We have received, from the laboratory of Prof. Bert La Du (Department of Pharmacology, University of Michigan), with whom we are collaborating, the PON1Q allelic variant of the PON1 gene in which residues His19 and Gln20 have both been mutated to alanine, which is, therefore, designated as AA PON1Q. This construct permits secretion of PON1Q into the medium, by enabling the cell machinery to cleave the N-terminal signal peptide (158). While the resulting product was reported to display reduced activity, its solubility properties were greatly enhanced, and we felt that it should constitute a suitable candidate for structural studies.

We have amplified the AA PON1Q clone, received from the La Du laboratory, via PCR, in a BlueScript[®] shuttle vector, with primers designed to contain the appropriate restriction sites for unidirectional cloning in the transfer vector. A region coding for six histidine residues (His-tag) was included in the 3' primer, in order to permit purification of the expressed protein on a nickel column (159). The product was sequenced to confirm the integrity of the coding sequence, and to check whether PCR had introduced any errors. The gene fragment was then isolated by digestion with the appropriate restriction enzymes, purified and cloned in an appropriate transfer vector for the BEVS, *viz.* AcNPV (160). The cloning strategy employed is shown schematically in Fig. 16.

Production of recombinant virus was successfully achieved after 4 days. Initial small-scale experiments in which the recombinant virus was used to infect *Spodoptera frugifera* sf9 cells resulted in successful expression and in secretion of active AA PON1Q into the culture medium. Presence of AA PON1Q was verified by Western blotting employing both antibodies against a C-terminal His₆-tag, and anti-PON antibodies provided by the La Du laboratory. They recognize the same polypeptide, with an apparent molecular weight of 40 kDa, which is 2.5-5 kDa lower than that of native PON1Q, due to cleavage of the N-terminal signal peptide. Arylesterase (ArE) activity measurements confirmed that the recombinant AA PON1Q is properly folded and enzymatically active, as shown in Table 1.

ArE activity in the crude extract was 6.2 U/ml, higher than previously reported for a AA PON1Q (77). Thus we were not able to confirm the earlier report that ArE activity is severely reduced in the double mutant (81). The units of specific activity are μ moles of phenylacetate hydrolyzed per min per mg of protein (77). Sorenson and coworkers expressed both WT PON1Q and AA PON1Q in 293 mammalian cells (81), and reported obtaining 0.2 U/ml in the medium for both recombinant enzymes.

We then proceeded to scale up production of the enzyme in order to obtain the quantities necessary for crystallization. Toward this objective we amplified the recombinant virus by infection of fresh sf9 cells. Amplification yielded a high titer virus preparation ($1-2 \times 10^8$ per ml) that was used to infect fresh sf9 cells. Our initial production yielded quantities of around 0.05mg/ml, which are more than sufficient to establish the quality of the expressed protein and adequate to begin crystallization trials. A crucial bottleneck in the production of diffraction grade crystals is the production of a highly pure, concentrated and monodisperse solution. Our preparation in sf9 cells was made using culture medium containing 15% fetal calf serum, which

introduces into the medium a large amount of foreign proteins (and proteases) that can affect both the stability and the purification of the target protein. In order to overcome this problem we infected a cell line, H5, that had been adapted to serum-free conditions. As with the sf9 cells, the infected H5 cells were found to release active AA PON1Q into the extracellular medium without the need for lysis, and in more than sufficient quantities to perform initial screening tests (0.1mg/ml). Purification of recombinant AA PON1Q was achieved by affinity chromatography on a Ni-NTA column that selectively binds the C-terminal His₆-tag. After elution from the column, purified PON was dialysed against the appropriate buffer, to eliminate any trace of detergent or heavy metals that might affect its stability. As can be seen from the SDS-PAGE in Fig. 17 and Western blot in Fig. 18, AA PON1Q can be purified to ~80% on just this first pass.

The results obtained so far are very promising. We have succeeded in obtaining high quantities of properly folded and active AA PON1Q, that can be easily extracted from the culture media to 80% purity in one step of affinity chromatography and, most likely, can be brought to a purity level acceptable for crystallization trials with only one more purification step. Further purification of the protein will take into consideration methods to ensure long-term stability of the enzyme and monodispersity of the solution, which are key requirements for obtaining X-ray grade crystals.

TABLES

Table 1. Expression parameters of PON1.

Comparison between expression parameters of PON1 in different phases of expression and purification, and human serum PON1(type Q).

Step	Yield (mg/ml)	ArE Activity (U/ml)	Specific Activity (U/mg)
Expression	0.05- 0.1	6.17	61.7 - 123.4 ^a
Nickel resin purification	0.15	12.3	82
Dialysis	0.22	25.44	115.6
Human serum PON1 ^b			1.26
Purified serum PON1 ^b			845

^a value varied between different batches of expression.

^b from Smolen et al. (77).

FIGURES

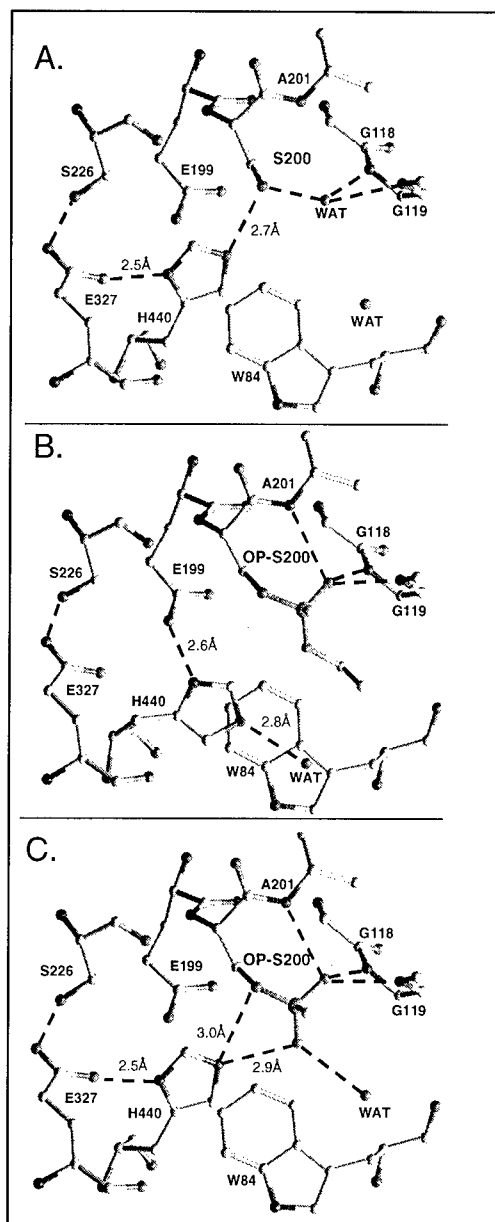


Fig. 1. Structural kinetics of VX inhibition of *TcAChE* by X-ray crystallography.

Structural kinetic of VX inhibition of *TcAChE* by X-ray crystallography at pH 6.0. The active site of *TcAChE* is depicted with possible H-bonds involving the catalytic triad and OP moiety (broken lines). Panel A (native structure) shows the active site, including the catalytic triad (Ser200-His440-Glu327) and the oxanion hole (-NH of Gly118, Gly119, and Ala201). Note that two water molecules (WAT) are displaced by the OP. (Panel B, pro-aged structure): Phosphorylation triggers a conformational change for His440 that disrupts the H-bond to Glu327; this may be caused by steric crowding in the pentavalent phosphorus transition state, or by re-distribution of charge on the His440 imidazolium during phosphorylation. Glu199 and a water (WAT) apparently stabilize the alternate conformation of His440. Subsequently, the His440 imidazole catalyzes either dealkylation (aging), or spontaneous reactivation (Scheme 1). For reaction of AChE with VX and most phosphonates, aging predominates, and dealkylation results in movement of His440 to the negatively charged pocket formed by Glu327O⁻, Ser200O⁻ and one anionic oxygen of the dealkylated OP (Panel C, aged structure).

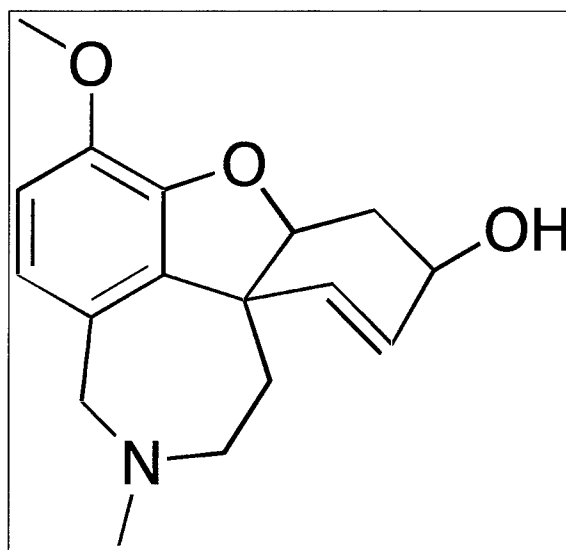


Fig. 2. Galanthamine (GAL).

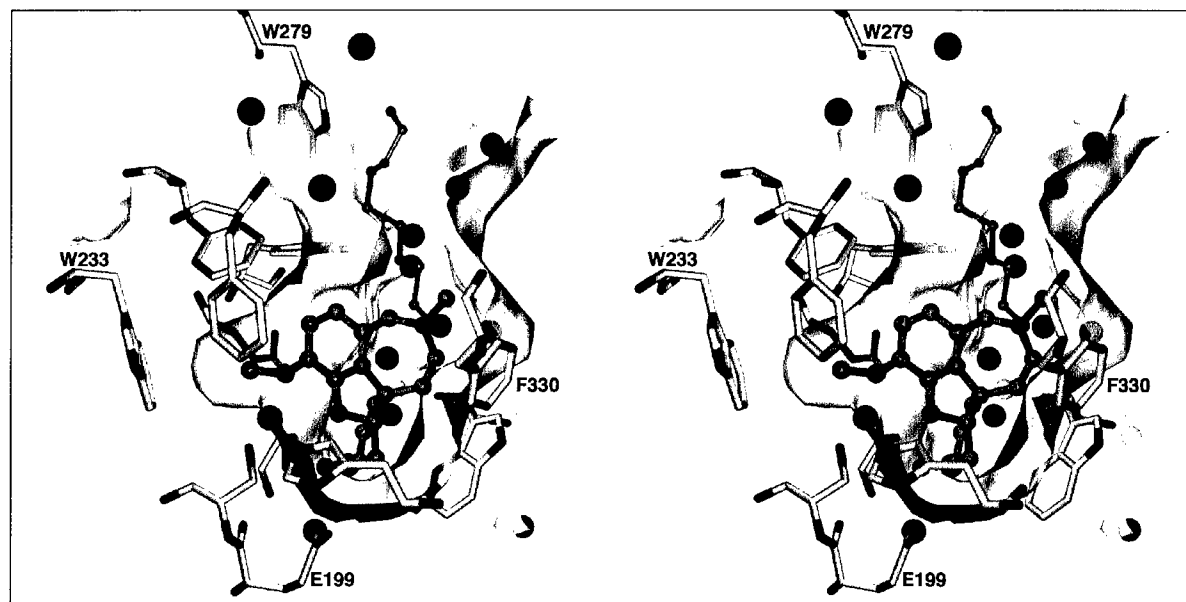


Fig. 3. Stereo view of binding of GAL in the active site gorge of *TcAChE*.

The solvent accessible surface of the protein (without waters and without ligands) was calculated by use of the program MSMS (161) with a probe radius of 1.4Å. Only those parts of the surface within 9.0Å of the bound inhibitor are visible, and the surface is 30% transparent, allowing visualization of some of the underlying protein residues. The surface has also been clipped to reveal the interior side, and has been color-coded such that blue indicates those parts of the surface whose underlying atoms are between 4.0 and 3.0Å from any atom of the inhibitor, and pink indicates distances of less than 3.0Å from the protein atoms to the inhibitor. Only a small portion of pink surface is visible in this orientation, located below the O-methyl group of the inhibitor, in the acyl-binding pocket. GAL has been rendered as a ball-and-stick model whose carbon atoms are colored green. Selected protein residues are shown as stick models with yellow carbon atoms. Water molecules are red spheres, and the PEG200 trimer/tetramer is rendered as a ball-and-stick model whose carbon atoms are colored pink.

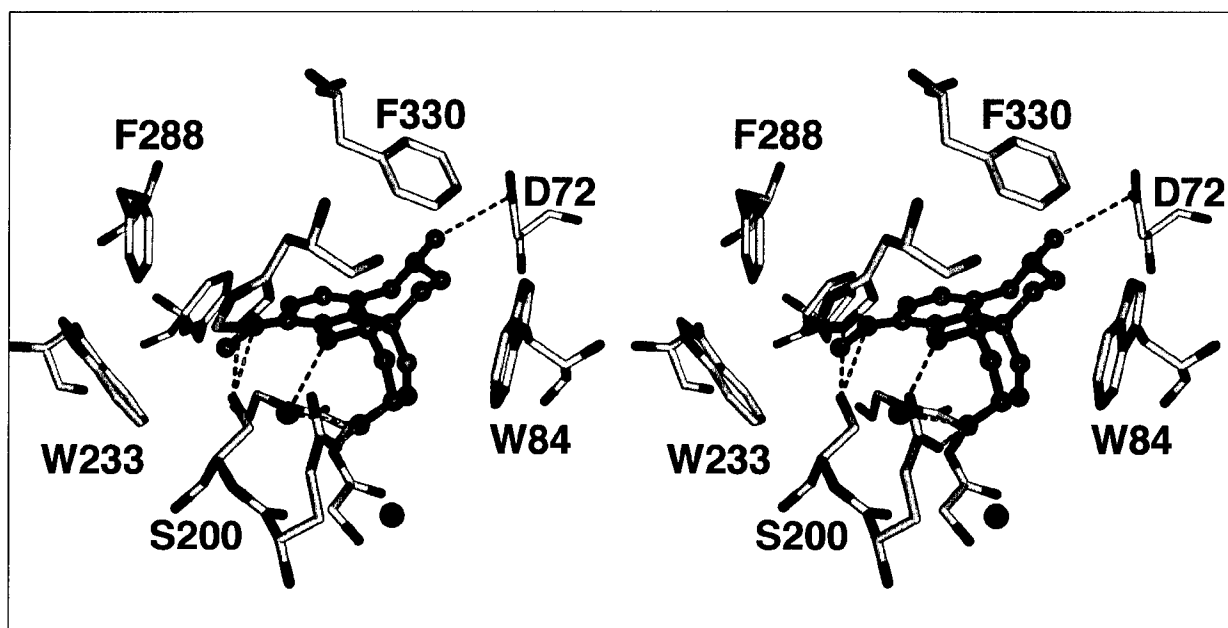


Fig. 4. Stereo view of possible hydrogen bonds between GAL and *TcAChE*.

The inhibitor is displayed as a ball-and-stick model, with green carbon atoms. The protein residues are rendered as stick models with yellow carbon atoms..

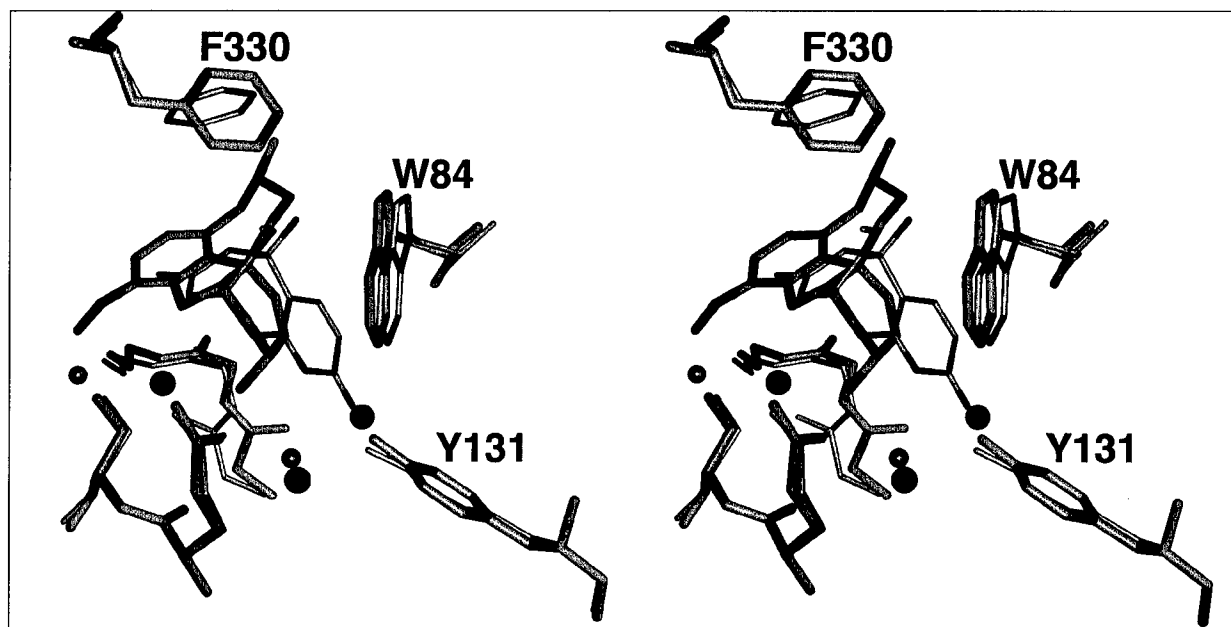


Fig. 5. Comparison of GAL vs HupA binding to the active site of *TcAChE*.

Stereo view comparing binding of GAL and HupA in the active site of *TcAChE*, showing the main-chain conformational change (Gly117) associated with binding of HupA. GAL and associated protein residues are rendered as green stick models, while HupA and associated protein residues are rendered as thin pink stick models. Water molecules associated with the GAL structure are shown as red spheres, while those from the HupA structure are displayed as smaller pink spheres.

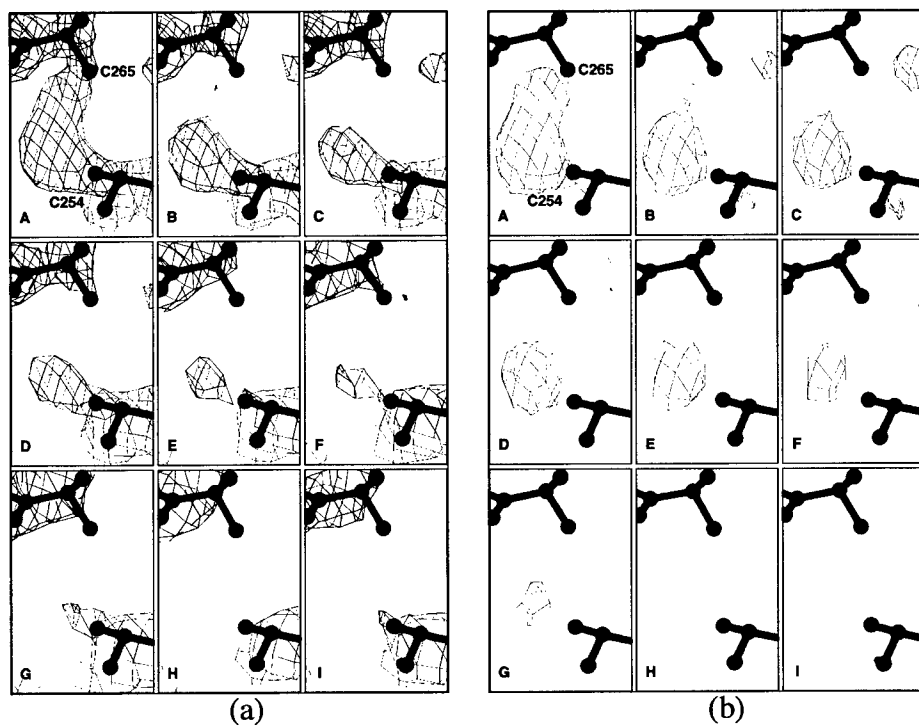


Fig. 6. Time course of cleavage of disulfide bond Cys254-Cys265 in *TcAChE*.

Sequential Fourier maps showing the time course of cleavage of the Cys254-Cys265 disulfide bond in *TcAChE*. Cysteine residues were refined as alanine residues to avoid model bias. (a) 3Fo-2Fc maps, contoured at 1.5 σ ; (b) Fo-Fc maps, contoured at 3 σ .

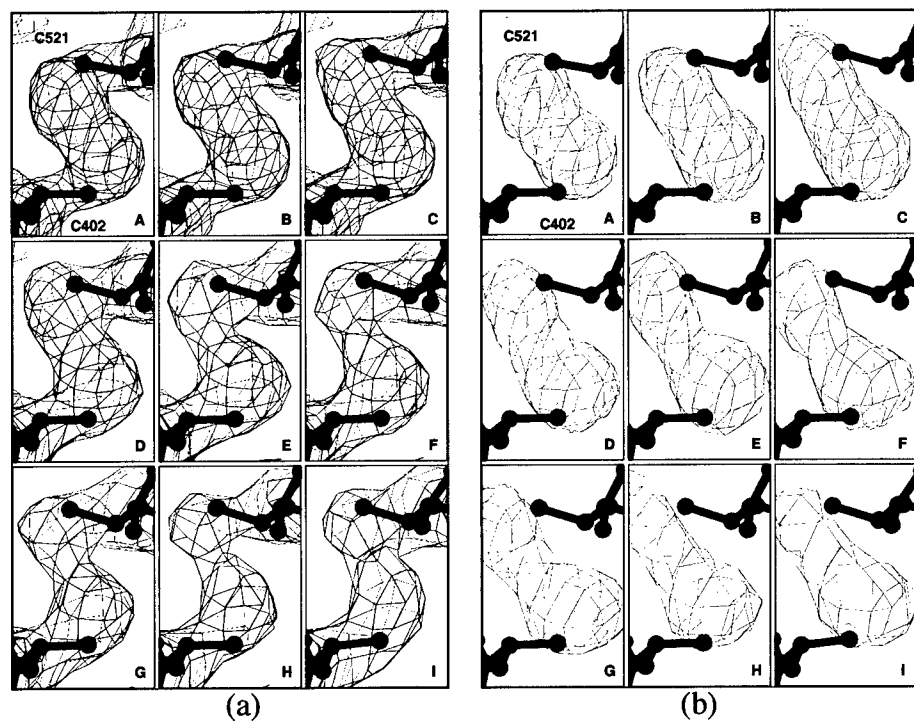


Fig. 7. Time course of cleavage of disulfide bond Cys402-Cys521 in *TcAChE*.

Sequential Fourier maps showing the time course of structural changes in the Cys402-Cys521 disulfide bond in *TcAChE*. Data collection, refinement and map contouring as in Fig. 1. (a) 3Fo-2Fc maps; (b) Fo-Fc maps.

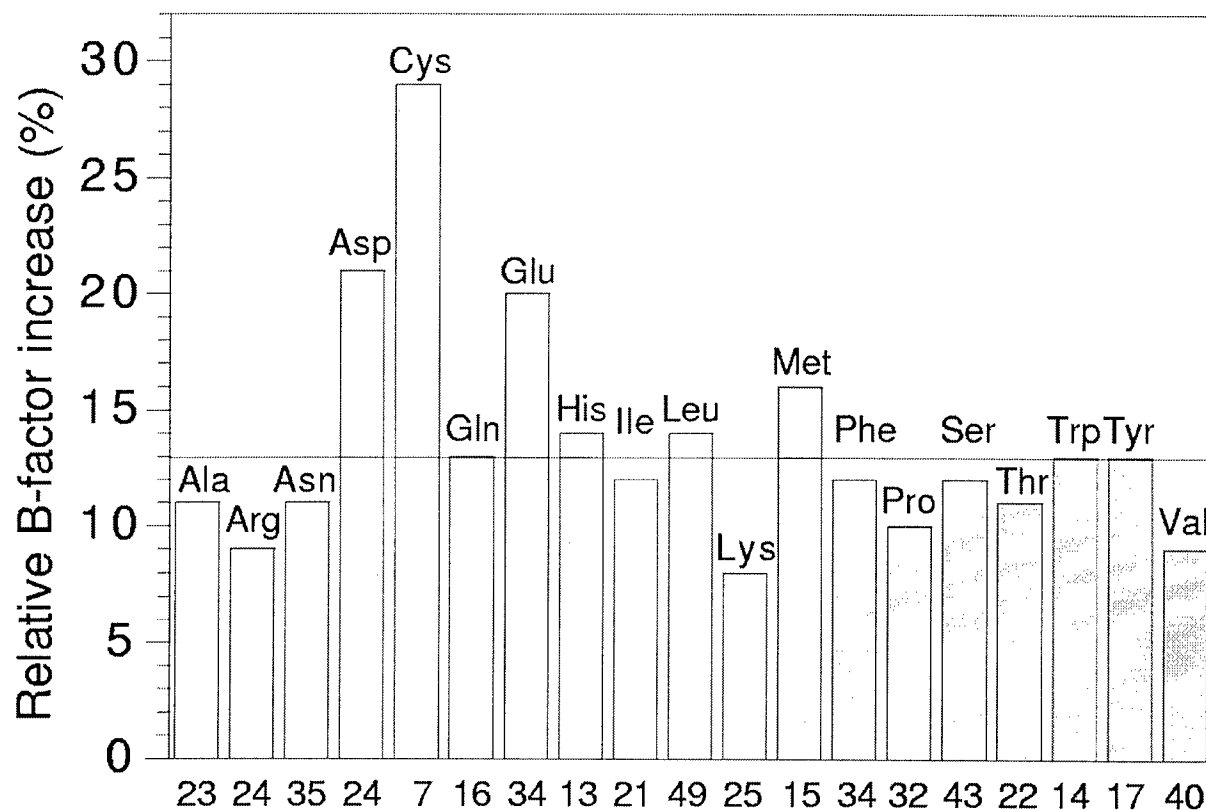


Fig. 8. Change in *TcAChE* B-factors due to synchrotron irradiation.

Histogram showing the increase in B-factors for the side chains of the different types of amino acid in *TcAChE* as a consequence of synchrotron irradiation. The horizontal line indicates the mean increase in side chain B-factors. The numbers along the x-axis show the number of occurrences of each type of amino acid in *TcAChE*. The individual bars show the average increase in B-factor for each type of amino acid for the 2nd data set (B), as compared to the 1st data set (A), viz. $(B\text{-factor}_B - B\text{-factor}_A) / B\text{-factor}_A$. Data in this figure, as well as values for increases in B-factors mentioned in the text, are derived from models in which the six Sγ atoms of cysteine residues participating in intrachain disulfide linkages were included in the refinement.

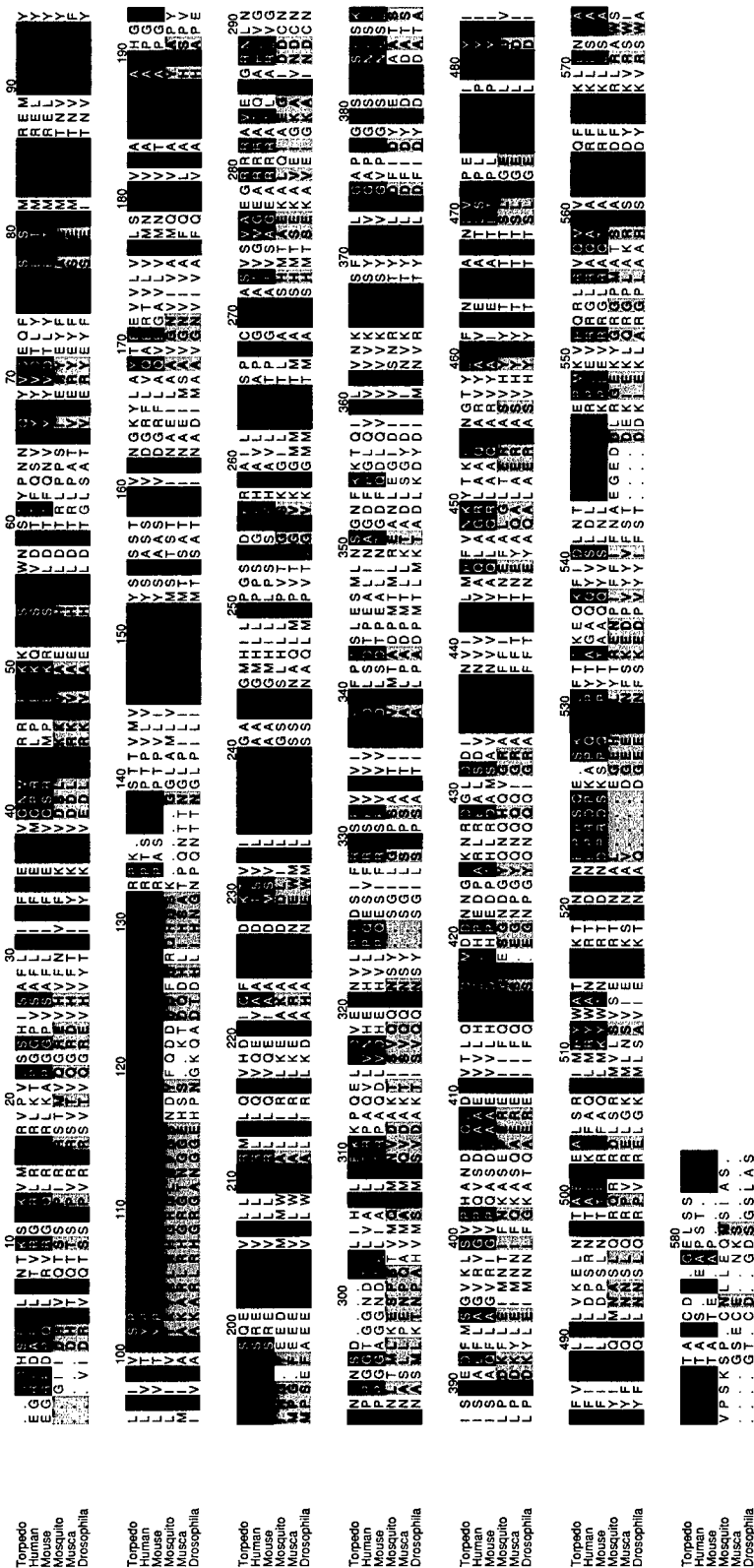
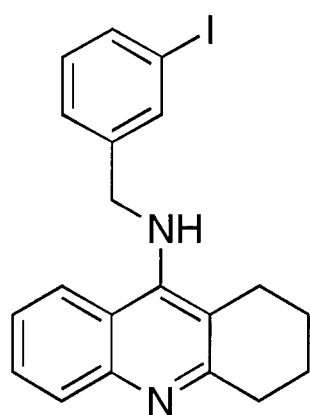
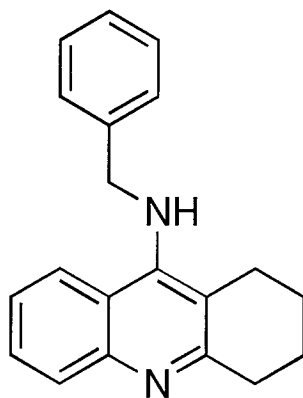


Fig. 9. Alignment of three vertebrate and three insect AChE sequences.

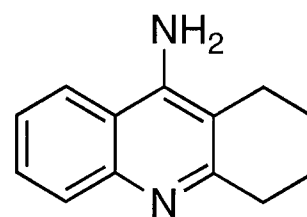
Red: insect/vertebrate identity; yellow: insect/vertebrate similarity; blue: vertebrate only identity or similarity; green: insect only identity or similarity; *DmAChE* numbering.



ZAI



ZAI



Tacrine

Fig. 10. Chemical formulae of reversible AChE inhibitors: ZAI, ZA and tacrine.

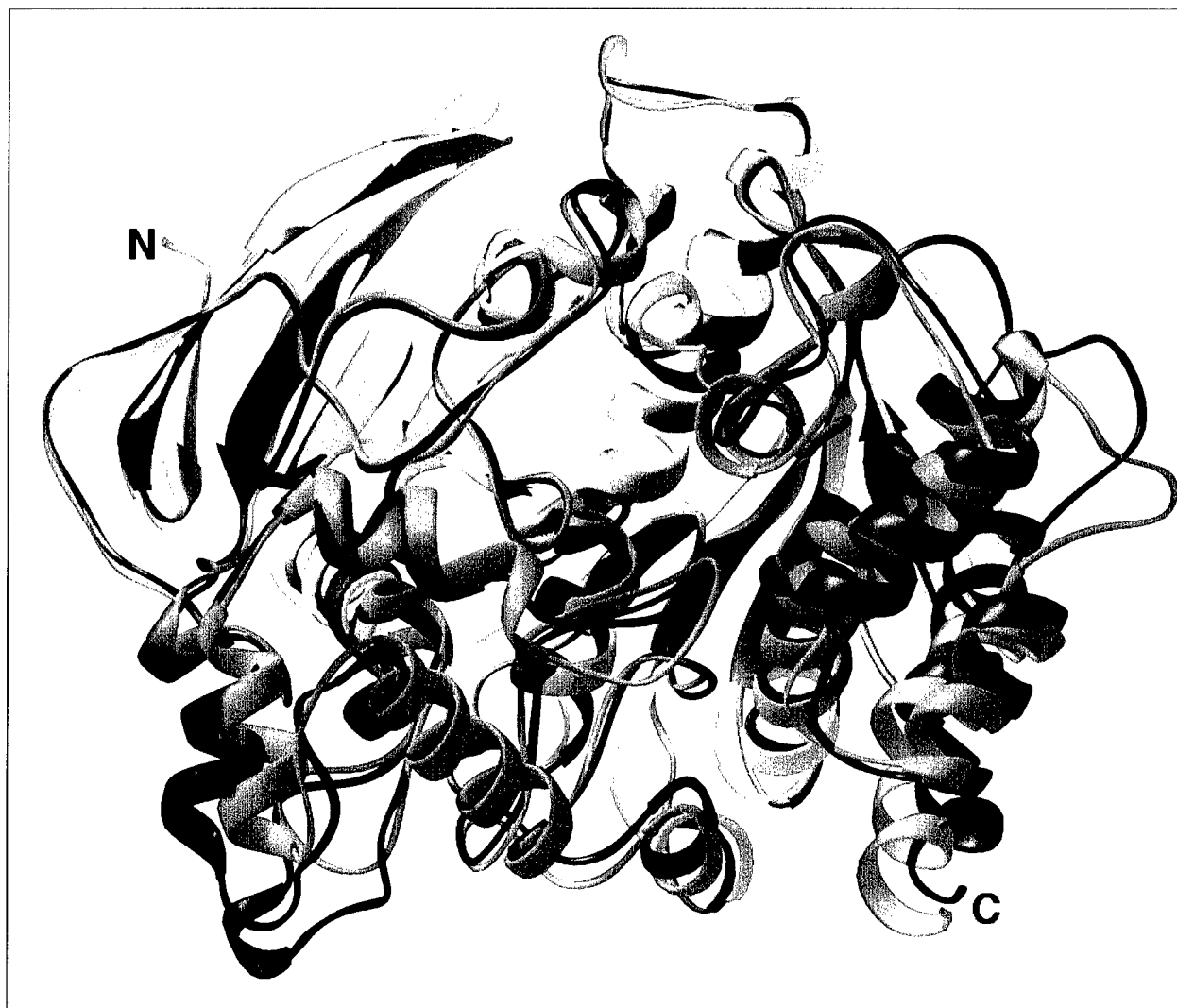


Fig. 11. Overall comparison of 3D structures of *Dm*AChE and *Tc*AChE.
Overlap of *Dm*AChE (red) and *Tc*AChE (green) C α traces.

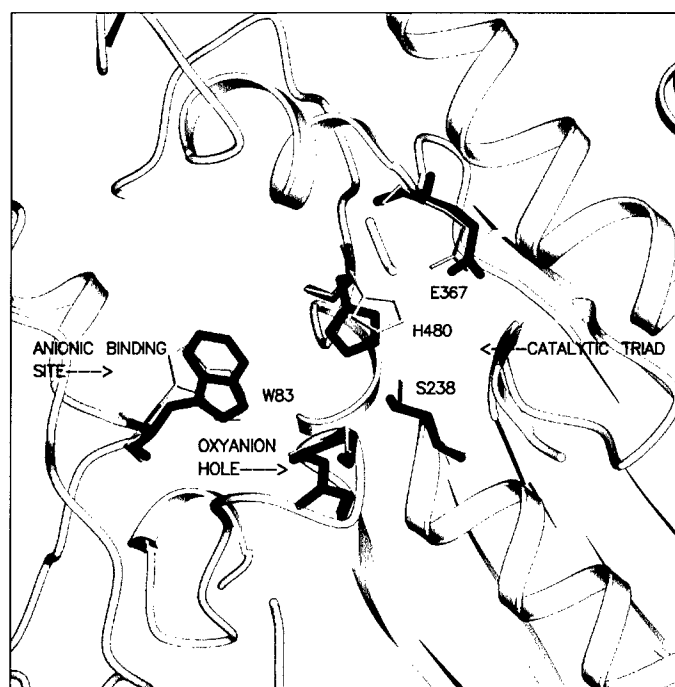


Fig. 12. Comparison of catalytic triads in 3D structures of *DmAChE* and *TcAChE*.

Overlap of *DmAChE* (red) and *TcAChE* (green) catalytic triad, oxyanion hole residues and anionic binding site residue Trp 83 (*DmAChE* numbering).

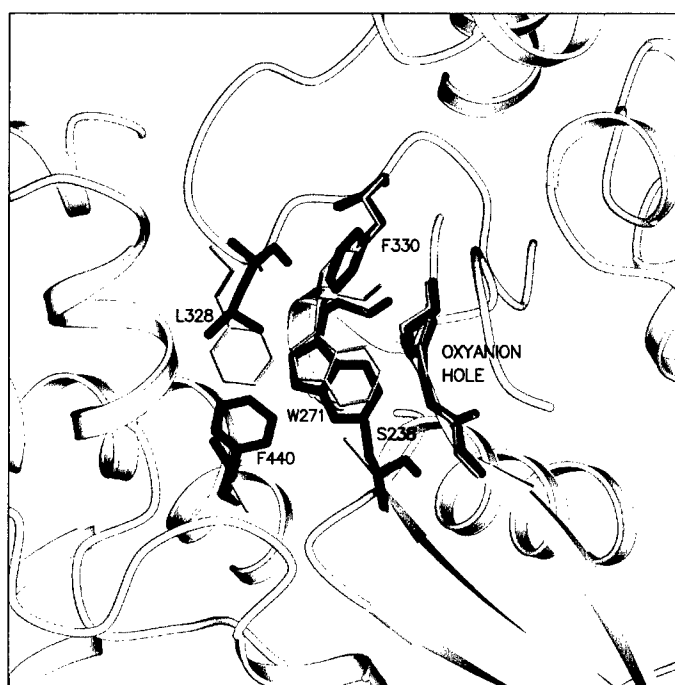


Fig. 13. Comparison of acyl pockets in 3D structures of *DmAChE* and *TcAChE*.

Overlap of *DmAChE* (red) and *TcAChE* (green) acyl pocket residues, oxyanion hole and active-site serine.

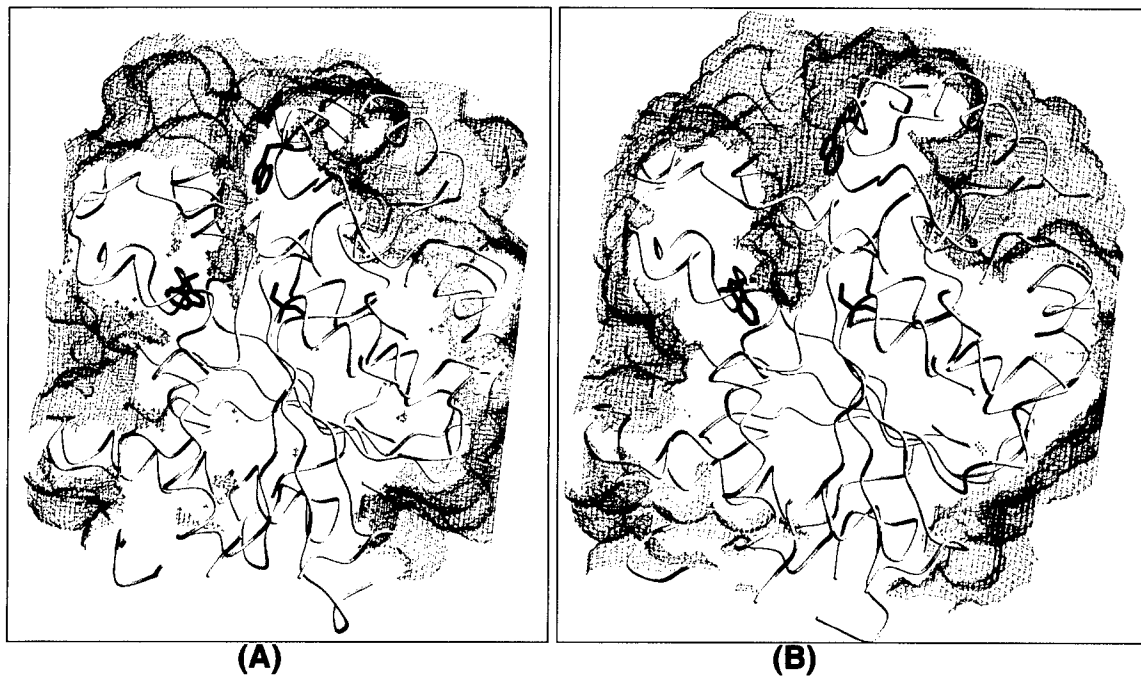


Fig. 14. Solvent-accessible area in *DmAChE* and *TcAChE*.

A: *DmAChE*; **B:** *TcAChE*. Key active-site gorge flanking residues are shown in red.

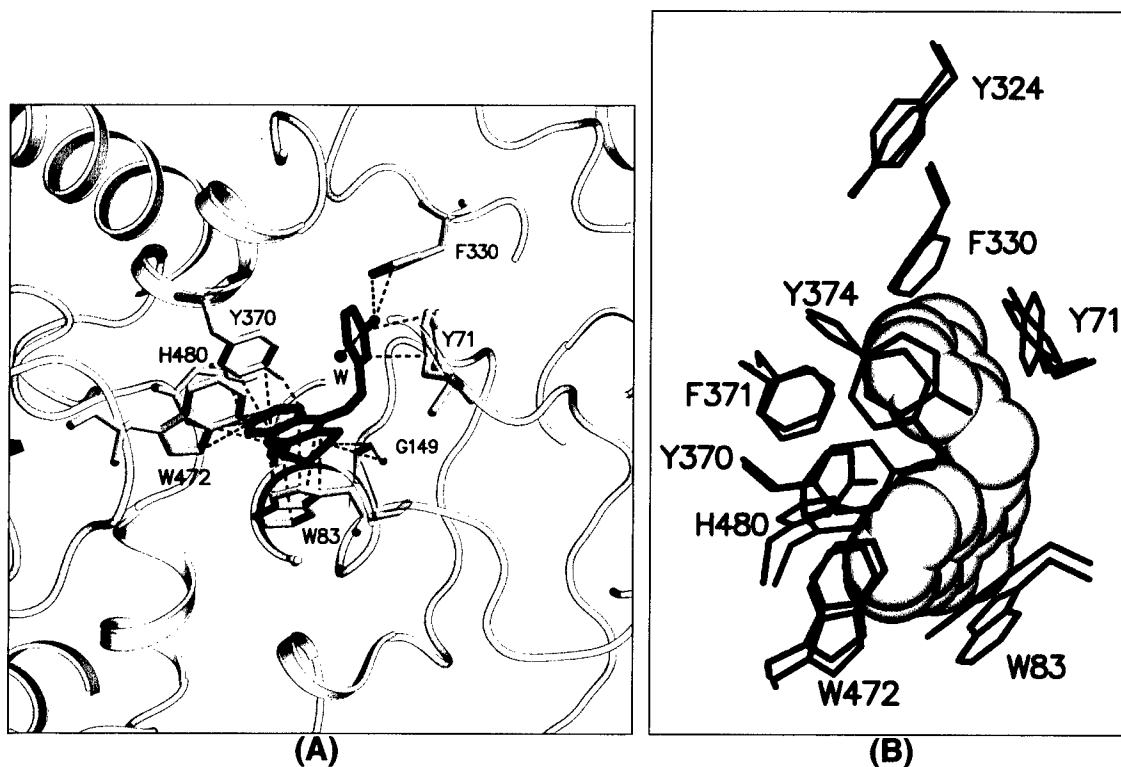


Fig. 15. ZAI/*DmAChE* interactions.

A: *DmAChE* residues (turquoise) interacting with ZAI (red) with distances $<3.8\text{\AA}$. **B:** Nine aromatic residues in native *DmAChE* (black) change their conformation when ZAI (red) shown with its van der Waals surface, binds to *DmAChE*.

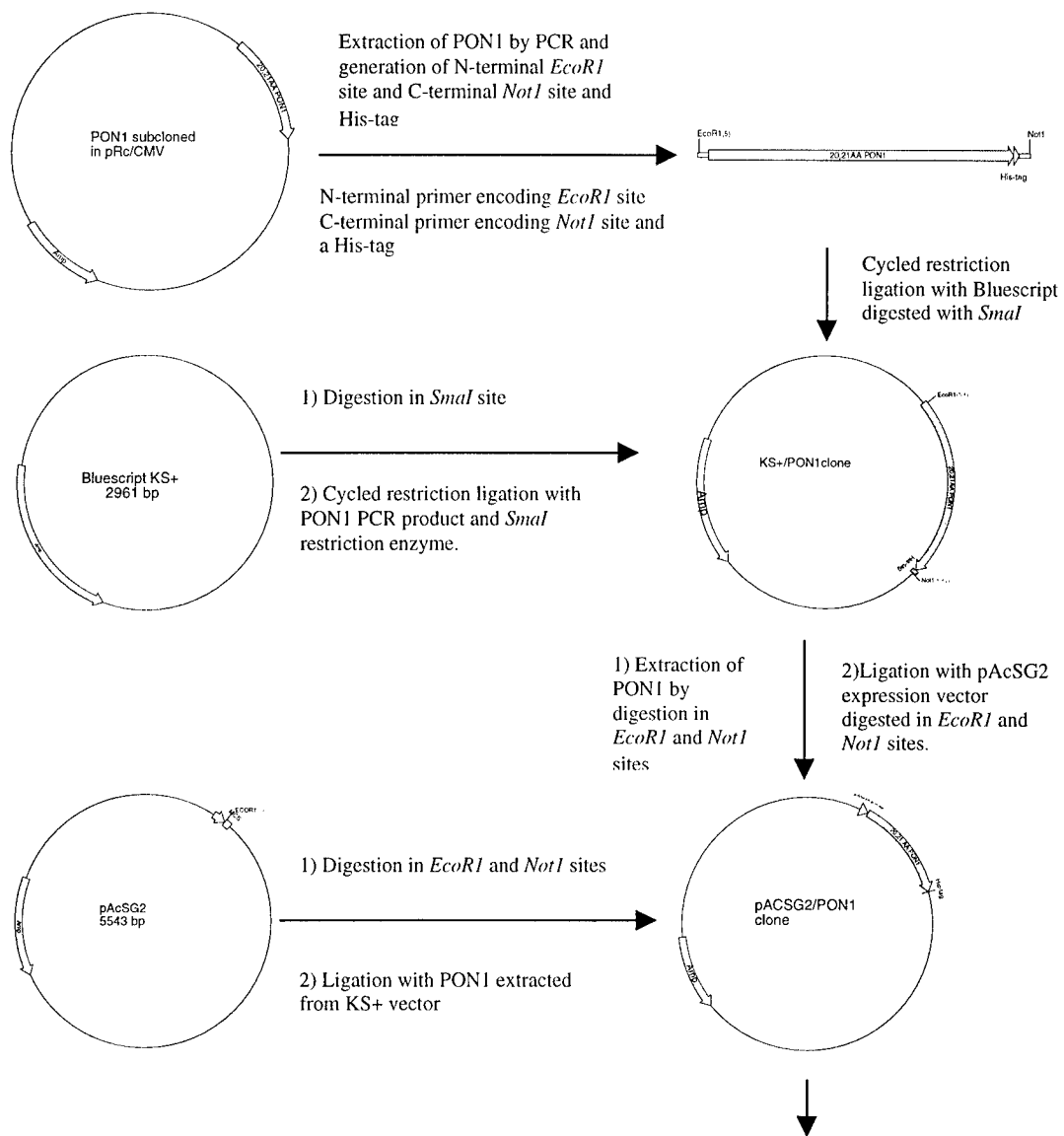


Fig. 16. PON cloning scheme.

Cloning scheme of AA PON1Q from the initial clone received to the expression clone ready to transfect into insect cells.

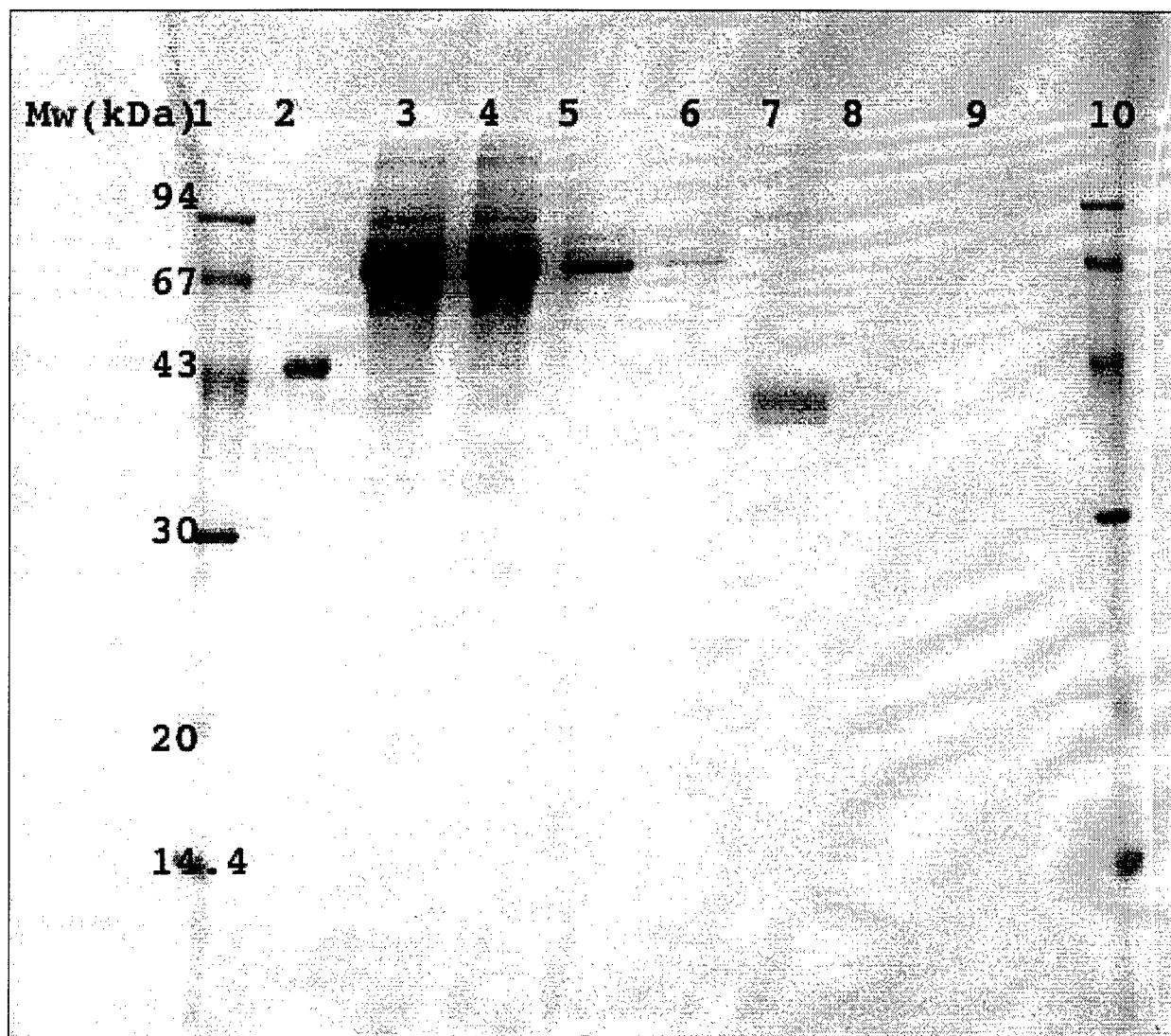


Fig. 17. Results of Ni-NTA purification of recombinant AA PON1Q.

SDS-PAGE shows molecular weight markers in lanes 1 and 10, PON1 purified from human serum in lane 2 at a molecular weight of ca 43 kDa, crude culture medium from sf9 cells expressing recombinant AA PON1Q in lanes 3 and 4, wash fractions from the Ni-NTA column in lanes 5 and 6, and purified AA PON1Q, at a molecular weight of ca. 40 kDa, in the eluate fraction from the Ni-NTA column in lane 7. Lanes 8 and 9 are subsequent elution fractions in which the concentration of AA PON1Q is below the threshold of detection of the staining method employed.

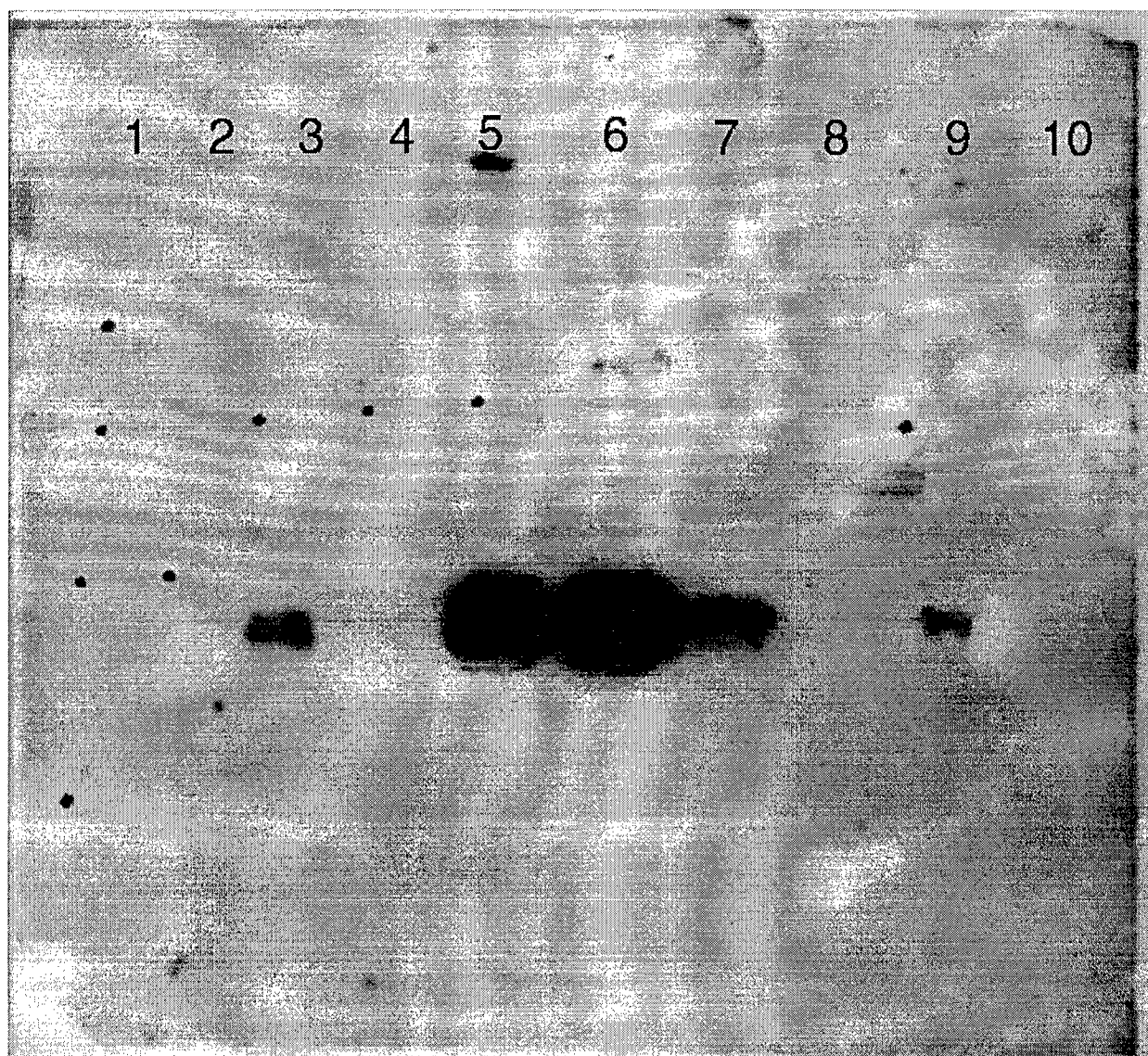


Fig. 18. Western blot showing recombinant AA PON1Q.

Western Blot showing recombinant AA PON1Q in the crude culture medium from sf9 cells (lane 3) and in the elution fractions from the Ni-NTA column (lanes 5-7).

REFERENCES

1. Neuromuscular transmission - enzymatic destruction of acetylcholine (1974), Barnard, E. A., In *The Peripheral Nervous System* (J.I. Hubbard, Eds.), pp. 201-224, Plenum, New York.
2. Acetylcholinesterase: enzyme structure, reaction dynamics, and virtual transition states (1987), Quinn, D. M., *Chem. Rev.*, **87**, 955-975.
3. Kinetics of acetylthiocholine binding to electric eel acetylcholinesterase in glycerol/water solvents of increased viscosity. Evidence for a diffusion-controlled reaction (1982), Hasinoff, B. B., *Biochim. Biophys. Acta*, **704**, 52-58.
4. Fractional diffusion-limited component of reactions catalyzed by acetylcholinesterase (1986), Bazelyansky, M., Robey, C. and Kirsch, J. F., *Biochemistry*, **25**, 125-130.
5. *Cholinesterases and Anticholinesterase Agents* (1963), Koelle, G. B., Eds., Springer-Verlag, Heidelberg.
6. Anticholinesterases: medical applications of neurochemical principles (1995), Millard, C. B. and Broomfield, C. A., *J. Neurochem.*, **64**, 1909-1918.
7. *Enzyme Inhibitors as Substrates: Interactions of Esterases with Esters of Organophosphorus and Carbamic Acids* (1972), Aldridge, W. N. and Reiner, E., North-Holland Publishing, Amsterdam.
8. Anticholinesterase agents (1990), Taylor, P., In *The Pharmacological Basis of Therapeutics*, 5th edition (A.G. Gilman, A.S. Nies, T.W. Rall and P. Taylor, Eds.), pp. 131-150, MacMillan, New York.
9. *Alzheimer Disease: Therapeutic Strategies* (1994), Giacobini, E. and Becker, R., Eds., Birkhäuser, Boston.
10. Tacrine: an overview of efficacy in two parallel group studies (1994), Gracon, S. I. and Knapp, M. J., In *Alzheimer Disease: Therapeutic Strategies* (E. Giacobini and R. Becker, Eds.), pp. 145-149, Birkhäuser, Boston.
11. Donepezil approved for treatment of Alzheimer's disease (1997), Nightingale, S. L., *JAMA*, **277**, 10.

12. Golden age of insecticide research: past, present, or future? (1998), Casida, J. E. and Quistad, G. B., *Annu. Rev. Entomol.*, **43**, 1-16.
13. Acetylcholine binding by a synthetic receptor: implications for biological recognition (1990), Dougherty, D. A. and Stauffer, D. A., *Science*, **250**, 1558-1560.
14. Acetylcholinesterase: structure and use as a model for specific cation-protein interactions (1992), Sussman, J. L. and Silman, I., *Curr. Opin. Struct. Biol.*, **2**, 721-729.
15. Nicotinic acetylcholine receptor at 9 Å resolution (1993), Unwin, N., *J. Mol. Biol.*, **229**, 1101-1124.
16. Atomic structure of acetylcholinesterase from *Torpedo californica*: a prototypic acetylcholine-binding protein (1991), Sussman, J. L., Harel, M., Frolow, F., Oefner, C., Goldman, A., Toker, L. and Silman, I., *Science*, **253**, 872-879.
17. Structure and dynamics of the active site gorge of acetylcholinesterase: synergistic use of molecular dynamics simulation and X-ray crystallography (1994), Axelsen, P. H., Harel, M., Silman, I. and Sussman, J. L., *Protein Sci.*, **3**, 188-197.
18. Effective charge on acetylcholinesterase active sites determined from the ionic strength dependence of association rate constants with cationic ligands (1980), Nolte, H.-J., Rosenberry, T. L. and Neumann, E., *Biochemistry*, **19**, 3705-3711.
19. Quaternary ligand binding to aromatic residues in the active-site gorge of acetylcholinesterase (1993), Harel, M., Schalk, I., Ehret-Sabatier, L., Bouet, F., Goeldner, M., Hirth, C., Axelsen, P., Silman, I. and Sussman, J. L., *Proc. Natl. Acad. Sci. USA*, **90**, 9031-9035.
20. The X-ray structure of a transition state analog complex reveals the molecular origins of the catalytic power and substrate specificity of acetylcholinesterase (1996), Harel, M., Quinn, D. M., Nair, H. K., Silman, I. and Sussman, J. L., *J. Am. Chem. Soc.*, **118**, 2340-2346.
21. Anionic subsites of the acetylcholinesterase from *Torpedo californica*: affinity labelling with the cationic reagent *N,N*-dimethyl-2-phenyl-aziridinium (1990), Weise, C., Kreienkamp, H.-J., Raba, R., Pedak, A., Aaviksaar, A. and Hucho, F., *EMBO J.*, **9**, 3885-3888.
22. Acetylcholinesterase inhibition by fasciculin: crystal structure of the complex (1995), Bourne, Y., Taylor, P. and Marchot, P., *Cell*, **83**, 503-512.

23. 3D Structure at 2.7Å resolution of native and E202Q mutant human acetylcholinesterase complexed with fasciculin-II (1998), Kryger, G., Giles, K., Harel, M., Toker, L., Velan, B., Lazar, A., Kronman, C., Barak, D., Ariel, N., Shafferman, A., Silman, I. and Sussman, J. L., In *Structure and Function of Cholinesterases and Related Proteins* (B.P. Doctor, P. Taylor, D.M. Quinn, R.L. Rotundo and M.K. Gentry, Eds.), pp. 323-326, Plenum, New York.
24. Crystal structure of an acetylcholinesterase-fasciculin complex: interaction of a three-fingered toxin from snake venom with its target (1995), Harel, M., Kleywegt, G. J., Ravelli, R. B. G., Silman, I. and Sussman, J. L., *Structure*, **3**, 1355-1366.
25. Alignment of amino acid sequences of acetylcholinesterases and butyrylcholinesterases (1991), Gentry, M. K. and Doctor, B. P., In *Cholinesterases: Structure, Function, Mechanism, Genetics and Cell Biology* (J. Massoulié, F. Bacou, E. Barnard, A. Chatonnet, B.P. Doctor and D.M. Quinn, Eds.), pp. 394-398, American Chemical Society, Washington, DC.
26. Conversion of acetylcholinesterase to butyrylcholinesterase: modeling and mutagenesis (1992), Harel, M., Sussman, J. L., Krejci, E., Bon, S., Chanal, P., Massoulié, J. and Silman, I., *Proc. Natl. Acad. Sci. USA*, **89**, 10827-10831.
27. The inhibitory effect of stilbamidine, curare and related compounds and its relationship to the active groups of acetylcholine esterase. Action of stilbamidine upon nerve impulse conduction (1950), Bergmann, F., Wilson, I. B. and Nachmansohn, D., *Biochim. Biophys. Acta*, **6**, 217-224.
28. Ligand binding properties of acetylcholinesterase determined with fluorescent probes (1974), Mooser, G. and Sigman, D. S., *Biochemistry*, **13**, 2299-2307.
29. Interaction of fluorescence probes with acetylcholinesterase. The site and specificity of propidium binding (1975), Taylor, P. and Lappi, S., *Biochemistry*, **14**, 1989-1997.
30. Role of the peripheral anionic site on acetylcholinesterase: inhibition by substrates and coumarin derivatives (1991), Radic, Z., Reiner, E. and Taylor, P., *Mol. Pharmacol.*, **39**, 98-104.
31. Three distinct domains in the cholinesterase molecule confer selectivity for acetyl- and butyrylcholinesterase inhibitors (1993), Radic, Z., Pickering, N. A., Vellom, D. C., Camp, S. and Taylor, P., *Biochemistry*, **32**, 12074-12084.
32. Dissection of the human acetylcholinesterase active center - determinants of substrate specificity - identification of residues constituting the anionic site, the hydrophobic site, and the

acyl pocket (1993), Ordentlich, A., Barak, D., Kronman, C., Flashner, Y., Leitner, M., Segall, Y., Ariel, N., Cohen, S., Velan, B. and Shafferman, A., *J. Biol. Chem.*, **268**, 17083-17095.

33. Differential effects of "peripheral" site ligands on *Torpedo* and chicken acetylcholinesterase (1994), Eichler, J., Anselmet, A., Sussman, J. L., Massoulié, J. and Silman, I., *Mol. Pharmacol.*, **45**, 335-340.

34. Substrate inhibition of acetylcholinesterase: residues affecting signal transduction from the surface to the catalytic center (1992), Shafferman, A., Velan, B., Ordentlich, A., Kronman, C., Grosfeld, H., Leitner, M., Flashner, Y., Cohen, S., Barak, D. and Ariel, N., *EMBO J.*, **11**, 3561-3568.

35. Modelling and mutagenesis of butyrylcholinesterase based on the X-ray structure of acetylcholinesterase (1992), Silman, I., Harel, M., Krejci, E., Bon, S., Chanal, P., Sussman, J. L. and Massoulié, J., In *Membrane Proteins: Structures, Interactions and Models* (A. Pullman, J. Jortner and B. Pullman, Eds.), **25**, pp. 177-184, Kluwer Academic Publishers, Dordrecht, Holland.

36. External and internal electrostatic potentials of cholinesterase models (1997), Felder, C. E., Silman, I., Lifson, S., Botti, S. A. and Sussman, J. L., *J. Molec. Graphics & Modelling*, **15**, 318-327.

37. Three distinct domains distinguish between acetylcholinesterase and butyrylcholinesterase substrate and inhibitor specificities (1993), Radic, Z., Pickering, N., Vellom, D. C., Camp, S. and Taylor, P., *Biochemistry*, **32**, 12074-12084.

38. Amino acid residues controlling acetylcholinesterase and butyrylcholinesterase specificity (1993), Vellom, D. C., Radic, Z., Li, Y., Pickering, N. A., Camp, S. and Taylor, P., *Biochemistry*, **32**, 12-17.

39. 3D structure of acetylcholinesterase complexed with the nootropic alkaloid, (-)-huperzine A (1997), Raves, M. L., Harel, M., Pang, Y.-P., Silman, I., Kozikowski, A. P. and Sussman, J. L., *Nature Struct. Biol.*, **4**, 57-63.

40. Structure of acetylcholinesterase complexed with E2020 (Aricept®): implications for the design of new anti-Alzheimer drugs (1999), Kryger, G., Silman, I. and Sussman, J. L., *Structure*, **7**, 297-307.

41. Improvements in scavenger protection against organophosphorus agents by modification of cholinesterases (1999), Maxwell, D. M., Saxena, A., Gordon, R. K. and Doctor, B. P., *Chem. Biol. Interactions*, **119-120**, 419-428.
42. Protein engineering of a human enzyme that hydrolyzes V and G nerve agents: design, construction and characterization (1999), Broomfield, C. A., Lockridge, O. and Millard, C. B., *Chem. Biol. Interactions*, **119-120**, 413-418.
43. Engineering resistance to 'aging' of phosphylated human acetylcholinesterase: role of the hydrogen bond network in the active center (1993), Ordentlich, A., Kronman, C., Barak, D., Stein, D., Ariel, N., Marcus, D., Velan, B. and Shafferman, A., *FEBS Lett.*, **334**, 215-220.
44. The role of glutamate-199 in the aging of cholinesterase (1993), Saxena, A., Doctor, B. P., Maxwell, D. M., Lenz, D. E., Radic, Z. and Taylor, P., *Biochem. Biophys. Res. Commun.*, **197**, 343-349.
45. Mutant acetylcholinesterases as potential detoxification agents for organophosphate poisoning (1997), Saxena, A., Maxwell, D. M., Quinn, D. M., Radic, Z., Taylor, P. and Doctor, B. P., *Biochem. Pharmacol.*, **54**, 269-274.
46. Design and expression of organophosphorus acid anhydride hydrolase activity in human butyrylcholinesterase. (1995), Millard, C. B., Lockridge, O. and Broomfield, C. A., *Biochemistry*, **36**, 786-795.
47. A single amino acid substitution, Gly117His, confers phosphotriesterase (organophosphorus acid anhydride hydrolase) activity on human butyrylcholinesterase (1997), Lockridge, O., Blong, R. M., Masson, P., Froment, M.-T., Millard, C. B. and Broomfield, C. A., *Biochemistry*, **36**, 786-795.
48. Organophosphorus acid anhydride hydrolase activity in human butyrylcholinesterase: synergy results in a somanase (1998), Millard, C. B., Lockridge, O. and Broomfield, C. A., *Biochemistry*, **37**, 237-247.
49. Crystal structure of "aged" phosphylated *Torpedo* acetylcholinesterase: nerve agent reaction products at the atomic level (1999), Millard, C., Kryger, G., Ordentlich, A., Harel, M., Raves, M., Greenblatt, H. M., Segall, Y., Barak, D., Shafferman, A., Silman, I. and Sussman, J. L., *Biochemistry*, **38**, 7032-7039.

50. Reaction products of acetylcholinesterase and VX reveal a mobile histidine in the catalytic triad (1999), Millard, C. B., Koellner, G., Ordentlich, A., Shafferman, A., Silman, I. and Sussman, J. L., *J. Am. Chem. Soc.*, **121**, 9883-9884.
51. Refined crystal structures of "aged" and "non-aged" organophosphoryl conjugates of γ -chymotrypsin (1991), Harel, M., Su, C. T., Frolow, F., Ashani, Y., Silman, I. and Sussman, J. L., *J. Mol. Biol.*, **221**, 909-918.
52. *Esterases Reacting with Organophosphorus Compounds. Proc. 3rd Internat. Meeting, Dubrovnik, 1998. Chemical Biological Interactions Vols. 119-120* (1999), Reiner, E., Simeon-Rudolf, V., Doctor, B. P., Furlong, C. E., Johnson, M. K., Lotti, M., Silman, I. and Taylor, P., Eds.,
53. Rational design of organophosphorus hydrolase for altered substrate specificities (1999), Di Sioudi, B. S., Miller, C. E., Lai, K., Grimsley, J. K. and Wild, J. R., *Chem. Biol. Interactions*, **119-120**, 211-223.
54. Stereochemical preferences for chiral substrates by the bacterial phosphotriesterase (1999), Hong, S. B. and Raushel, F. M., *Chem. Biol. Interactions*, **119-120**, 225-234.
55. Organophosphorus acid anhydrolase in slime mold, duckweed and mung bean: a continuing search for a physiological role and a natural substrate (1999), Hoskin, F. C., Walker, J. E. and Mello, C. M., *Chem. Biol. Interactions*, **119-120**, 399-404.
56. Serum esterases II. An enzyme hydrolysing diethyl *p*-nitrophenyl acetate (E600) and its identity with the A-esterase of mammalian sera (1953), Aldridge, W. N., *Biochem. J.*, **53**, 117-124.
57. Paraoxon hydrolysis vs. covalent binding in the elimination of paraoxon in the rabbit (1986), Butler, E. G., Eckerson, H. W. and La Du, B. N., *Drug Metab. Dispos.*, **13**, 640-645.
58. Paraoxonase prevents accumulation of lipoperoxides in low-density lipoprotein (1991), Mackness, M. I., Arrol, S. and Durrington, P. N., *FEBS Lett.*, **286**, 152-154.
59. On the physiological role(s) of the paraoxonases (1999), La Du, B. N., Aviram, M., Billecke, S., Navab, M., Primo-Parmo, S., Sorenson, R. C. and Standiford, T. J., *Chem. Biol. Interactions*, **119-120**, 379-388.
60. Low serum paraoxonase: a risk factor for atherosclerotic disease? (1999), Mackness, M. I., Durrington, P. N., Ayub, A. and Mackness, B., *Chem. Biol. Interactions*, **119-120**, 389-397.

61. Mice lacking serum paraoxonase are susceptible to organophosphate toxicity and atherosclerosis (1998), Shih, D. M., Gu, L., Xia, Y. R., Navab, M., Li, W. F., Hama, S., Castellani, L. W., Furlong, C. E., Costa, L. G., Fogelman, A. M. and Lusis, A. J., *Nature*, **394**, 284-287.
62. *Enzymes Hydrolyzing Organophosphorus Compounds* (1989), Reiner, E., Aldridge, W. N. and Hoskin, F. C. G., Eds., Ellis Horwood, Chichester.
63. *Enzymes Interacting with Organophosphorus Compounds* (1993), Reiner, E. and Lotti, M., Eds., Elsevier, Shannon.
64. Purification of a DFP-hydrolyzing enzyme from squid head ganglion (1972), Hoskin, F. C. G. and Long, R. J., *Arch. Biochem. Biophys.*, **150**, 548-555.
65. Purification and properties of the phosphotriesterase from *Pseudomonas diminuta* (1989), Dumas, D. P., Caldwell, S. R., Wild, J. R. and Raushel, F. M., *J. Biol. Chem.*, **264**, 19659-19665.
66. Human serum paraoxonase/arylesterase (1992), La Du, B. N., In *Genetic Factors Influencing the Metabolism of Foreign Compounds* (W. Kalow, Eds.), pp. 51-91, Pergamon, New York.
67. Three-dimensional structure of phosphotriesterase: an enzyme capable of detoxifying organophosphate nerve agents (1994), Benning, M. M., Kuo, J. M., Raushel, F. M. and Holden, H. M., *Biochemistry*, **33**, 15001-15007.
68. Three-dimensional structure of the binuclear metal center of phosphotriesterase (1995), Benning, M. M., Kuo, J. M., Raushel, F. M. and Holden, H. M., *Biochemistry*, **34**, 7973-7978.
69. Characterization of the zinc binding site of bacterial phosphotriesterase (1992), Omburo, G. A., Kuo, J. M., Mullins, L. S. and Raushel, F. M., *J. Biol. Chem.*, **267**, 13278-13283.
70. Structural characterization of the divalent cation sites of bacterial phosphotriesterase by ^{113}Cd NMR spectroscopy (1993), Omburo, G. A., Mullins, L. S. and Raushel, F. M., *Biochemistry*, **32**, 9148-9155.
71. The human serum paraoxonase/arylesterase polymorphism (1983), Eckerson, H. W., Wyte, C. M. and La Du, B. N., *Am. J. Hum. Genet.*, **35**, 1126-1138.

72. The human serum paraoxonase/arylesterase gene (PON1) is one member of a multigene family (1996), Primo-Parmo, S. L., Sorenson, R. C., Teiber, J. and La Du, B. N., *Genomics*, **33**, 498-507.
73. Serum paraoxonase status: a major factor in determining resistance to organophosphates (1993), Li, W. F., Costa, L. G. and Furlong, C. E., *J. Toxicol. Environ. Health*, **40**, 337-346.
74. Purification of human serum paraoxonase/arylesterase: evidence for one esterase catalyzing both activities (1991), Gan, K. N., Smolen, A., Eckerson, H. W. and La Du, B. N., *Drug Metab. Dispos.*, **19**, 100-106.
75. Molecular basis for the polymorphic forms of human serum paraoxonase/arylesterase: glutamine or arginine at position 191, for the respective A or B allozymes (1993), Adkins, S., Gan, K. N., Mody, M. and La Du, B. N., *Am. J. Hum. Genet.*, **52**, 598-608.
76. The molecular basis of the human serum paraoxonase activity polymorphism (1993), Humbert, R., Adler, D. A., Disteché, C. M., Hassett, C., Omiecinski, C. J. and Furlong, C. E., *Nature Genet.*, **3**, 73-76.
77. Characteristics of the genetically determined polymorphic forms of human serum paraoxonase/arylesterase (1991), Smolen, A., Eckerson, H. W., Gan, K., Hailat, N. and La Du, B. N., *Drug Metab. Dispos.*, **19**, 107-112.
78. Studies on human serum paraoxonase/arylesterase (1993), La Du, B. N., Adkins, S., Kuo, C.-L. and Lipsig, D., *Chem. Biol. Interactions*, **87**, 25-34.
79. Evidence that several conserved histidine residues are required for hydrolytic activity of human paraoxonase/arylesterase (1999), Doorn, J. A., Sorenson, R. C., Billecke, S. S., Hsu, C. and La Du, B. N., *Chem. Biol. Interactions*, **119-120**, 235-241.
80. Identification of residues essential for human paraoxonase (PON1) arylesterase/organophosphatase activities (1999), Josse, D., Xie, W., Renault, F., Rochu, D., Schopfer, L. M., Masson, P. and Lockridge, O., *Biochemistry*, **38**, 2816-2825.
81. Properties of the retained N-terminal hydrophobic leader sequence in human serum paraoxonase/arylesterase (1999), Sorenson, R. C., Aviram, M., Bisgaier, C. L., Billecke, S., Hsu, C. and La Du, B. N., *Chem. Biol. Interactions*, **119-120**, 243-249.

82. Reconsideration of the catalytic center and mechanism of mammalian paraoxonase/arylesterase (1995), Sorenson, R. C., Primo-Parmo, S. G., Kuo, C.-L., Adkins, S., Lockridge, O. and La Du, B. N., *Proc. Natl. Acad. Sci. USA*, **92**, 7187-7191.
83. Paraoxonase inhibits high-density lipoprotein oxidation and preserves its functions. A possible peroxidative role for paraoxonase (1998), Aviram, M., Rosenblat, M., Bisgaier, C. L., Newton, R. S., Primo-Parmo, S. L. and La Du, B. N., *J. Clin. Invest.*, **101**, 1581-1590.
84. A new and rapid colorimetric determination of acetylcholinesterase activity (1961), Ellman, G. L., Courtney, K. D., Andres, V., Jr. and Featherstone, R. M., *Biochem. Pharmacol.*, **7**, 88-95.
85. The mechanism of the aminolysis of acetate esters (1974), Satterthwait, A. C. and Jencks, W. P., *J. Am. Chem. Soc.*, **96**, 7018-7031.
86. ¹⁵N NMR spectroscopy of hydrogen-bonding interactions in the active site of serine proteases: evidence for a moving histidine mechanism (1986), Bachovchin, W. W., *Biochemistry*, **25**, 7751-7759.
87. Parallel mechanisms in acetylcholinesterase-catalyzed hydrolysis of choline esters (1993), Selwood, T., Feaster, S. R., States, M. J., Pryor, A. N. and Quinn, D. M., *J. Am. Chem. Soc.*, **115**, 10477-10482.
88. The cholinergic hypothesis of geriatric memory dysfunction (1982), Bartus, R. T., Dean, R. L., Beer, B. and Lippa, A. S., *Science*, **217**, 408-414.
89. Role of forebrain cholinergic systems in learning and memory: relevance to the cognitive deficits of aging and Alzheimer's dementia (1993), Dunnett, S. B. and Fibiger, H. C., *Prog. Brain Res.*, **98**, 413-420.
90. Possible role of the cholinergic system and disease models (1997), Weinstock, M., *J. Neural Transm. Suppl.*, **49**, 93-102.
91. In vitro muscarinic activity of spiromuscarones and related analogs (1995), Wu, E. S., Griffith, R. C., Loch, J. T. r., Kover, A., Murray, R. J., Mullen, G. B., Blosser, J. C., Machulskis, A. C. and McCreedy, S. A., *J. Med. Chem.*, **38**, 1558-1570.
92. Reversal of age-related cognitive impairments by an M1 cholinergic agonist, AF102B (1990), Brandeis, R., Dachir, S., Sapir, M., Levy, A. and Fisher, A., *Pharmacol. Biochem. Behavior*, **36**, 89-95.

93. Brain selective inhibition of acetylcholinesterase: a novel approach to therapy for Alzheimer's disease (1993), Enz, A., Amstutz, R., Boddeke, H., Gmelin, G. and Malanowski, J., *Prog. Brain Res.*, **98**, 431-438.
94. The pharmacotherapy of Alzheimer's disease based on the cholinergic hypothesis: an update (1995), Weinstock, M., *Neurodegeneration*, **4**, 349-356.
95. Oral physostigmine treatment for patients with presenile and senile dementia of the Alzheimer's type: a double-blind placebo-controlled trial (1990), Jenike, M. A., Albert, M. S., Heller, H., Gunther, J. and Goff, D., *J. Clin. Psychiatry*, **51**, 3-7.
96. Drug evaluation of huperzine A in the treatment of senile memory disorders (1991), Zhang, R. W., Tang, X. C., Han, Y. Y., Sang, G. W., Zhang, Y. D., Ma, Y. X., Zhang, C. L. and Yang, R. M., *Acta Pharmacol. Sinica*, **12**, 250-252.
97. Tacrine (1995), Davis, K. L. and Powchik, P., *Lancet*, **345**, 625-630.
98. Pharmacological evaluation of phenyl-carbamates as CNS-selective acetylcholinesterase inhibitors (1994), Weinstock, M., Razin, M., Chorev, M. and Enz, A., *J. Neural Transm. Suppl.*, **43**, 219-225.
99. Metrifonate for Alzheimer's disease: Is the next cholinesterase inhibitor better? (1998), Knopman, D. S., *Neurology*, **50**, 1203-1205.
100. The rationale for E2020 as a potent acetylcholinesterase inhibitor (1996), Kawakami, Y., Inoue, A., Kawai, T., Wakita, M., Sugimoto, H. and Hopfinger, A. J., *Bioorg. Med. Chem. Lett.*, **4**, 1429-1446.
101. Clinical trials of a new anticholinesterase agent, galanthamine, in anesthesiology (1965), Bretagne, M. and Valletta, J., *Anesth. Analg. (Paris)*, **22**, 285-292.
102. The pharmacology of galanthamine and its analogues (1995), Harvey, A. L., *Pharmacol. Ther.*, **68**, 113-128.
103. Trials in the treatment of facial nerve paralysis using nivaline (1969), Bystrzanowska, T., *Wiad Lek.*, **22**, 1233-1239.
104. Nivalin in the treatment of residual post-polio paralysis and pseudo-hypertrophic muscular dystrophy (1965), Gujral, V. V., *Indian Pediatr.*, **2**, 89-93.

105. Selective inhibition of human acetylcholinesterase by galanthamine *in vitro* and *in vivo* (1990), Thomsen, T. and Kewitz, H., *Life Sci.*, **46**, 1553-1558.
106. Inhibition of acetylcholinesterase activity in human brain tissue and erythrocytes by galanthamine, physostigmine and tacrine (1991), Thomsen, T., Kaden, B., Fischer, J. P., Bickel, U., Barz, H., Gusztory, G., Cervos-Navarro, J. and Kewitz, H., *Eur. J. Clin. Chem. Clin. Biochem.*, **29**, 487-492.
107. Agonist responses of neuronal nicotinic acetylcholine receptors are potentiated by a novel class of allosterically acting ligands. (1996), Schrattenholz, A., Pereira, E. F., Roth, U., Weber, K. H., Albuquerque, E. X. and Maelicke, A., *Mol. Pharmacol.*, **49**, 1-6.
108. Physostigmine, galanthamine and codeine act as 'noncompetitive nicotinic receptor agonists' on clonal rat pheochromocytoma cells (1995), Storch, A., Schrattenholz, A., Cooper, J. C., Abdel Ghani, E. M., Gutbrod, O., Weber, K. H., Reinhardt, S., Lobron, C., Hermsen, B., Soskic, V., Pereira, E. F. R., Albuquerque, E. X., Methfessel, C. and Maelicke, A., *Eur. J. Biochem.*, **290**, 207-219.
109. Identification and functional characterization of a new agonist site on nicotinic acetylcholine receptors of cultured hippocampal neurons (1993), Pereira, E. F., Reinhardt-Maelicke, S., Schrattenholz, A., Maelicke, A. and Albuquerque, E. X., *J. Pharmacol. Exp. Ther.*, **265**, 1474-1491.
110. Central nicotinic receptor agonists ABT-418, ABT-089, and (-)-nicotine reduce distractibility in adult monkeys (1998), Prendergast, M. A., Jackson, W. J., Terry, A. V., Decker, M. W., Arneric, S. P. and Buccafusco, J. J., *Psychopharmacol. (Berlin)*, **136**, 50-58.
111. Improved learning and memory in aged rats with chronic administration of the nicotinic receptor agonist GTS-21 (1995), Arendash, G. W., Sengstock, G. J., Sanberg, P. R. and Kem, W. R., *Brain Res.*, **674**, 252-259.
112. Modulation of acetylcholine release by nicotinic receptors in the rat brain (1989), De Sarno, P. and Giacobini, E., *J. Neurosci. Res.*, **22**, 194-200.
113. Alzheimer's drug design based upon an invertebrate toxin (anabaseine) which is a potent nicotinic receptor agonist. (1997), Kem, W. R., *Invert. Neurosci.*, **3**, 251-259.
114. The potential of subtype-selective neuronal nicotinic acetylcholine receptor agonists as therapeutic agents (1998), Lloyd, G. K., Menzaghi, F., Bontempi, B., Suto, C., Siegel, R.,

Akong, M., Stauderman, K., Velicelebi, G., Johnson, E., Harpold, M. M., Rao, T. S., Sacca, A. I., Chavez-Noriega, L. E., Washburn, M. S., Vernier, J. M., Cosford, N. D. and McDonald, L. A., *Life Sci.*, **62**, 1601-1606.

115. Nicotinic system involvement in Alzheimer's and Parkinson's diseases. Implications for therapeutics (1997), Newhouse, P. A., Potter, A. and Levin, E. D., *Drugs Aging*, **11**, 206-228.

116. Expression of nicotinic acetylcholine receptor subunits in the cerebral cortex in Alzheimer's disease: histotopographical correlation with amyloid plaques and hyperphosphorylated-tau protein (1999), Wevers, A., Monteggia, L., Nowacki, S., Bloch, W., Schutz, U., Lindstrom, J., Pereira, E. F., Eisenberg, H., Giacobini, E., De Vos, R. A., Steur, E. N., Maelicke, A., Albuquerque, E. X. and Schroder, H., *Eur. J. Neurosci.*, **11**, 2551-2565.

117. Cholinesterase inhibitors in the treatment of Alzheimer's disease: a comparison of tolerability and pharmacology (1998), Nordberg, A. and Svensson, A. L., *Drug Saf.*, **19**, 465-480.

118. Science commentary: rational drug design for Alzheimer's disease (1999), Berger, A., *BMJ*, **318**, 639.

119. Chance favors the prepared mind - from serendipity to rational drug design (1999), Kubinyi, H., *J. Recept. Signal Transduct. Res.*, **19**, 15-39.

120. Structure-based drug design (1998), Amzel, L. M., *Curr. Opin. Biotechnol.*, **9**, 366-369.

121. Potent acetylcholinesterase inhibitors: design, synthesis, and structure-activity relationships of bis-interacting ligands in the galanthamine series (1998), Mary, A., Renko, D. Z., Guillou, C. and Thal, C., *Bioorg. Med. Chem. Lett.*, **6**, 1835-1850.

122. Structure of acetylcholinesterase complexed with (-)-galanthamine at 2.3 Å resolution (1999), Greenblatt, H. M., Kryger, G., Lewis, T., Silman, I. and Sussman, J., *FEBS Lett.*, **463**, 321-326.

123. Enzymatic catalysis and transition-state theory (1973), Lienhard, G. E., *Science*, **180**, 149-154.

124. Aspartate transcarbamylase. Interaction with the transition state analogue N-(phosphonacetyl)-L-aspartate. (1971), Collins, K. D. and Stark, G. R., *J. Biol. Chem.*, **246**, 6599-6605.

125. *Enzyme Structure and Mechanism* (1977), Fersht, A. R., W. H. Freeman, Reading and San Francisco.
126. The Structures of huperzine A and B, two new alkaloids exhibiting marked anticholinesterase activity (1986), Liu, J.-S., Zhu, Y.-L., Yu, C.-M., Zhou, Y.-Z., Han, Y.-Y., Wu, F.-W. and Qi, B.-F., *Can. J. Chem*, **64**, 837-839.
127. Mechanism of inhibition of cholinesterases by huperzine A (1992), Ashani, Y., Peggins, J. O., III and Doctor, B. P., *Biochem. Biophys. Res. Commun.*, **184**, 719-726.
128. *Protein Crystallography* (1976), Blundell, T. L. and Johnson, L. N., Academic Press, New York.
129. Sequential radiation damage in protein crystallography. (1988), Sygusch, J. and Allaire, M., *Acta Cryst.*, **A44**, 443-448.
130. Radiation damage in protein crystals at low temperature (1994), Gonzalez, A. and Nave, C., *Acta Cryst.*, **D50**, 874-877.
131. Cryocrystallography of biological macromolecules: a generally applicable method (1988), Hope, H., *Acta Cryst.*, **B44**, 22-26.
132. Macromolecular cryocrystallography (1997), Garman, E. F. and Schneider, T. R., *J. Appl. Cryst.*, **29**, 211-237.
133. Static Laue diffraction studies on acetylcholinesterase (1998), Ravelli, R. B. G., Raves, M. L., Ren, Z., Bourgeois, D., Roth, M., Kroon, J., Silman, I. and Sussman, J. L., *Acta Cryst.*, **D54**, 1359-1366.
134. An electron spin resonance study of gamma-irradiated frozen aqueous solutions containing dipeptides. Mechanism of radical reaction (1979), Sevilla, M. D., D'Arcy, J. B. and Morehouse, K. M., *J. Phys. Chem.*, **83**, 2887-2892.
135. Biochemical and biophysical applications of electron spin resonance (1983), Swartz, H. M. and Swartz, S. M., *Methods Biochem. Anal.*, **29**, 207-323.
136. 3D structure of *Drosophila* acetylcholinesterase: implications for insecticide design (1999), Harel, M., Kryger, G., Sussman, J. L., Silman, I., Rosenberry, T. L., Mallender, W. D., Lewis, T., Fletcher, R. J. and Guss, M., *Abstracts IUCr XVIII World Crystallography Congress*, P09.04.023.

137. 3D Structure of *Drosophila Melanogaster* acetylcholinesterase and of its complexes with putative insecticides (2000), Harel, M., Kryger, G., Rosenberry, T. L., Mallender, W. D., Lewis, T., Fletcher, R. J., Guss, J. M., Silman, I. and Sussman, J. L., (submitted).
138. Effects of ionizing radiations on biological macromolecules (1967), Alexander, P. and Lett, J. T., In *Comprehensive Biochemistry* (M. Florkin and E. Stotz, Eds.), **27**, pp. 267-356, Elsevier, Amsterdam.
139. Radiolysis of proteins and model compounds (1995), Faraggi, M., Ferradini, C., Houee-Levin, C. and Klapper, M. H., In *Radiation Research 1895-1995* (U. Hagen, D. Harder, H. Jung and C. Streffer, Eds.), **2**, pp. 241-248, Universitätsdruckerei H. Sturtz AG, Würzburg.
140. Electron spin resonance studies of radiation damage to DNA and to proteins (1995), Symons, M. C. R., *Radiat. Phys. Chem.*, **45**, 837-845.
141. *The Chemical Basis of Radiation Biology. 1. Radiobiology* (1987), von Sonntag, C., Taylor & Francis (Printers) Ltd,
142. Influence of electron scavengers on the radical formation in thymidine-5'-monophosphate and DNA in frozen aqueous solution and glasses (1995), Lange, M., Weiland, B. and Huttermann, J., *Int. J. Radiat. Biol.*, **68**, 475-486.
143. Structure and mobility of electron gain and loss centres in proteins (1987), Jones, G. D., Lea, J. S., Symons, M. C. and Taiwo, F. A., *Nature*, **330**, 772-773.
144. Free radical mediated x-ray damage of model membranes (1996), Cheng, A. and Caffrey, M., *Biophys. J.*, **70**, 2212-2222.
145. RNA folding at millisecond intervals by synchrotron hydroxyl radical footprinting (1998), Sclavi, B., Sullivan, M., Chance, M. R., Brenowitz, M. and Woodson, S. A., *Science*, **279**, 1940-1943.
146. *Our Planet, Our Health* (1992), Veil, S., World Health Organization, New York.
147. Increased neurotoxicity following concurrent exposure to pyridostigmine bromide, DEET, and chlorpyrifos (1996), Abou-Donia, M. B., Wilmarth, K. R., Abdel-Rahman, A. A., Jensen, K. F., Oehme, F. W. and Kurt, T. L., *Fundam. Appl. Toxicol.*, **34**, 201-222.

148. Construction and characterization of secreted and chimeric transmembrane forms of *Drosophila* acetylcholinesterase: a large truncation of the C-terminal signal peptide does not eliminate glycoinositol phospholipid anchoring (1996), Incardona, J. P. and Rosenberry, T. L., *Mol. Biol. Cell*, **7**, 595-611.
149. Freeze-trapping isomorphous xenon derivatives of protein crystals (1997), Sauer, O., Schmidt, A. and Kratky, C., *J. Appl. Cryst.*, **30**, 476-486.
150. Isolation and characterization of acetylcholinesterase from *Drosophila* (1987), Gnagey, A. L., Forte, M. and Rosenberry, T. L., *J. Biol. Chem.*, **262**, 13290-13298.
151. *Drosophila* acetylcholinesterase: mechanisms of resistance to organophosphates (1993), Fournier, D., Mutero, A., Pralavorio, M. and Bride, J.-M., *Chem. Biol. Interactions*, **87**, 233-238.
152. Characterization of the acetylcholinesterase gene from insecticide-resistant houseflies (*Musca domestica*) (1997), Yao, H., Chuanling, Q., Williamson, M. S. and Devonshire, A. L., *Chin. J. Biotechnol.*, **13**, 177-183.
153. Protein Data Bank (PDB): a database of 3D structural information of biological macromolecules (1998), Sussman, J. L., Lin, D., Jiang, J., Manning, N. O., Prilusky, J., Ritter, O. and Abola, E. E., *Acta Cryst.*, **D54**, 1078-1084.
154. Enzymes hydrolyzing organophosphates as potential catalytic scavengers against organophosphate poisoning (1998), Masson, P., Josse, D., Lockridge, O., Viguié, N., Taupin, C. and Buhler, C., *J. Physiol. (Paris)*, **92**, 357-362.
155. Production of human secretory component with dimeric IgA binding capacity using viral expression systems (1995), Rindisbacher, L., Cottet, S., Wittek, R., Kraehenbuhl, J.-P. and Corthésy, B., *J. Biol. Chem.*, **270**, 14220-14228.
156. Recombinant carbohydrate and selenomethionyl variants of human choriogonadotropin (1991), Chen, W. and Bahl, O. P., *J. Biol. Chem.*, **266**, 8192-8197.
157. Determination of macromolecular structures from anomalous diffraction of synchrotron radiation (1991), Hendrickson, W. A., *Science*, **254**, 51-58.
158. Properties of the retained N-terminal hydrophobic leader sequence in human serum paraoxonase/arylesterase (1998), Sorenson, R. C., Aviram, M., Bisgaier, C. L., Billecke, S., Hsu, C. and La Du, B. N., *Abstracts of Third International Meeting on Esterases Reacting with Organophosphorus Compounds*, P21.

159. Purification and characterization of recombinant histidine-tagged human platelet 12-lipoxygenase expressed in a baculovirus/insect cell system (1993), Chen, X. S., Brash, A. R. and Funk, C. D., *Eur. J. Biochem.*, **214**, 845-852.

160. *Baculovirus Expression Vector System manual* (1998), Crossen, R. and Gruenwald, S., Pharmingen, San Diego.

161. Reduced surface: an efficient way to compute molecular surfaces (1996), Sanner, M. F., Olson, A. J. and Spehner, J. C., *Biopolymers*, **38**, 305-320.

List of Publications
2nd Annual Report for US Army Cooperative Agreement No. DAMD17-97-2-7022
Profs. Joel L. Sussman and Israel Silman
Weizmann Institute of Science
Rehovot, ISRAEL
January 2000

1. Felder, C. E., Silman, I., Lifson, S., Botti, S. & Sussman, J. L. (1997). "External and Internal Electrostatic Potentials of Cholinesterase Models". *J. Comput.-Aided Mol. Design*, **15**, 318-327.
2. Botti, S., Felder, C. E., Sussman, J. L. & Silman, I. (1998). "Electrotactins: A Class of Adhesion Proteins with Conserved Electrostatic and Structural Motifs". *Protein Eng.* **11**, 415-420.
3. Kryger, G., Silman, I. & Sussman, J. (1998). "Three-dimensional Structure of a Complex of E2020 with Acetylcholinesterase from *Torpedo californica*". *J. Physiol. (Paris)* **92**, 191-194.
4. Silman, I., Harel, M., Raves, M. & Sussman, J. L. (1998). "Crystallographic Studies on Complexes of Acetylcholinesterase with the Natural Cholinesterase Inhibitors Fasciculin and Huperzine A". in *Progress in Alzheimer's and Parkinson's Diseases* (Fisher, A., Yoshida, M. & Hanin, I., eds.), Plenum Press, New York, pp. 523-530.
5. Millard, C.B., Kryger, G., Ordentlich, A., Harel, M., Raves, M., Greenblatt, H. M., Segall, Y., Barak, D., Shafferman, A., Silman, I. & Sussman, J. L. (1998). "Crystal Structure of "Aged" Phosphorylated and Phosphonylated *Torpedo californica* Acetylcholinesterase". in *Structure and Function of Cholinesterases and Related Proteins* (Doctor, B. P., Quinn, D. M., Rotundo, R. L. & Taylor, P., eds.), Plenum, New York, pp. 425-431.
6. Kryger, G., Giles, K., Harel, M., Toker, L., Velan, B., Lazar, A., Kronman, C., Barak, D., Ariel, N., Shafferman, A., Silman, I. & Sussman, J. L. (1998). "3D Structure at 2.7Å Resolution of Native and E202Q Mutant Human Acetylcholinesterase Complexed with Fasciculin-II". in *Structure and Function of Cholinesterases and Related Proteins* (Doctor, B. P., Quinn, D. M., Rotundo, R. L. & Taylor, P., eds.), Plenum, New York, pp. 323-326.
7. Kryger, G., Silman, I. & Sussman, J. L. (1998). "3D Structure of a Complex of the Anti-Alzheimer Drug, E2020, with Acetylcholinesterase at 2.5Å Resolution". in *Structure and Function of Cholinesterases and Related Proteins* (Doctor, B. P., Quinn, D. M., Rotundo, R. L. & Taylor, P., eds.), Plenum, New York, pp. 469-476.
8. Raves, M., Giles, K., Schrag, J. D., Schmid, M. F., Phillips, G. N., Jr., Chiu, W., Howard, A., Silman, I. & Sussman, J. L. (1998). "Quaternary Structure of Tetrameric Acetylcholinesterase". in *Structure and Function of Cholinesterases and Related Proteins* (Doctor, B. P., Quinn, D. M., Rotundo, R. L. & Taylor, P., eds.), Plenum, New York, pp. 351-356.
9. Silman, I. & Sussman, J. L. (1998). "Structural and Functional Studies on Acetylcholinesterase: A Perspective". in *Structure and Function of Cholinesterases and Related Proteins* (Doctor, B. P., Quinn, D. M., Rotundo, R. L. & Taylor, P., eds.), Plenum, New York, pp. 25-33.
10. Silman, I., Millard, C. B., Ordentlich, A., Greenblatt, H. M., Harel, M., Barak, D., Shafferman, A. & Sussman, J. L. (1999). "A Preliminary Comparison of Structural Models for Catalytic Intermediates of Acetylcholinesterase". *Chem. Biol. Interactions* **119-120**, 43-52.

11. Kryger, G., Silman, I. & Sussman, J. L. (1999). "Structure of Acetylcholinesterase Complexed with E2020 (Aricept®): Implications for the Design of New Anti-Alzheimer Drugs". *Structure* **7**, 297-307.
12. Morel, N., Bon, S., Greenblatt, H., Wodak, S., Sussman, J., Massoulié, J. and Silman, I. (1999) "Effect of Mutations in the Peripheral Anionic Site on the Stability of Acetylcholinesterase" *Mol. Pharm.* **55**, 982-992.
13. Millard, C. B., Kryger, G., Ordentlich, A., Harel, M., Raves, M., Greenblatt, H. M., Segall, Y., Barak, D., Shafferman, A., Silman, I. & Sussman, J. L. (1999). "Crystal Structure of "Aged" Phosphylated *Torpedo* Acetylcholinesterase: Nerve Agent Reaction Products at the Atomic Level". *Biochemistry* **22**, 7032-7039.
14. Botti, S. A., Felder, C., Lifson, S., Sussman, J. L. & Silman, I. (1999). "A Modular Treatment of Molecular Traffic Through the Active Site of Cholinesterases" *Biophys. J.* **77**, 2430-2450.
15. Millard, C. B., Koellner, G., Ordentlich, A., Shafferman, A., Silman, I. & Sussman, J. L. (1999). "Reaction Products of Acetylcholinesterase and VX Reveal a Mobile Histidine in the Catalytic Triad". *J. Am. Chem. Soc.* **121**, 9883-9994.
16. Greenblatt, H. M., Kryger, G., Lewis, T., Silman, I. & Sussman, J. (1999). "Structure of Acetylcholinesterase Complexed with (-)-Galanthamine at 2.3Å Resolution". *FEBS Lett.* **463**, 321-326.
17. Weik, M., Ravelli, R. B. G., Kryger, G., McSweeney, S., Raves, M., Harel, M., Gros, P., Silman, I., Kroon, J. & Sussman, J. L. (2000). "Synchrotron X-ray Radiation Produces Specific Chemical and Structural Damage to Protein Structures". *Proc. Natl. Acad. Sci. USA* **97**, in press.

Specific chemical and structural damage to proteins produced by synchrotron radiation

Martin Weik^{*,†}, Raimond B. G. Ravelli^{*,†}, Gitay Kryger[‡], Sean McSweeney[‡], Maria L. Raves[§], Michal Harel[§], Piet Gros^{*}, Israel Silman^{||}, Jan Kroon^{*}, and Joel L. Sussman^{§***††}

Departments of ^{*}Crystal and Structural Chemistry and [†]NMR Spectroscopy, Bijvoet Center for Biomolecular Research, Utrecht University, Utrecht, NL-3584 CH, The Netherlands; [‡]European Molecular Biology Laboratory Outstation, Grenoble, 38042 France; Departments of [§]Structural Biology and ^{||}Neurobiology, Weizmann Institute of Science, Rehovot, 76100 Israel; and ^{**}Biology Department, Brookhaven National Laboratory, Upton, NY 11973

Communicated by F. William Studier, Brookhaven National Laboratory, Upton, NY, November 16, 1999 (received for review October 6, 1999)

Radiation damage is an inherent problem in x-ray crystallography. It usually is presumed to be nonspecific and manifested as a gradual decay in the overall quality of data obtained for a given crystal as data collection proceeds. Based on third-generation synchrotron x-ray data, collected at cryogenic temperatures, we show for the enzymes *Torpedo californica* acetylcholinesterase and hen egg white lysozyme that synchrotron radiation also can cause highly specific damage. Disulfide bridges break, and carboxyl groups of acidic residues lose their definition. Highly exposed carboxyls, and those in the active site of both enzymes, appear particularly susceptible. The catalytic triad residue, His-440, in acetylcholinesterase, also appears to be much more sensitive to radiation damage than other histidine residues. Our findings have direct practical implications for routine x-ray data collection at high-energy synchrotron sources. Furthermore, they provide a direct approach for studying the radiation chemistry of proteins and nucleic acids at a detailed, structural level and also may yield information concerning putative "weak links" in a given biological macromolecule, which may be of structural and functional significance.

Although radiation damage is an inherent problem in x-ray crystallography, it has not, so far, been widely investigated. It usually is presumed to be nonspecific and to be manifested as a gradual decay in the overall quality of data obtained for a given crystal as data collection proceeds (1–3). The macromolecular crystallographic community has responded to the reality of radiation damage by implementing cryo-techniques (4, 5). However, even during data collection at cryogenic temperatures, using moderate-intensity synchrotron radiation facilities, substantial damage, in terms of loss of resolution, was repetitively observed for large structures like the ribosome (6), as well as for globular proteins (7). At third-generation sources, it is not uncommon for insertion device beamlines to attenuate or defocus the beam (8) simply to lower the available flux density, which is too high even for globular proteins and nucleic acids. To make optimal use of bright synchrotron sources, it is imperative that we come to understand the mechanism of radiation damage and its detailed consequences.

In the following, we present a study on two proteins that provides a description of the molecular consequences of radiation damage at cryogenic temperatures. The initial study, performed in preparation for time-resolved measurements on *Torpedo californica* acetylcholinesterase (TcAChE) (9), showed, in addition to the loss of diffractive power of the crystal and a general increase in atomic B factors, highly specific effects of x-ray irradiation. These included, in particular, breakage of disulfide bonds and loss of definition of the carboxyl groups of acidic residues. Very similar specific radiation damage was observed in studies of a second enzyme, hen egg white lysozyme (HEWL), suggesting the generality of the observed phenomenon. Our studies have direct practical implications for macromolecular crystallographers using bright synchrotron sources, both with regard to data collection and interpretation of the

structures obtained. Furthermore, they have served as a starting point for more detailed studies of the mechanism of radiation damage using insertion device x-ray sources at a third-generation synchrotron (R.B.G.R. and S.M., unpublished work). Finally, they show that radiochemistry of macromolecules exposed to synchrotron radiation can be monitored at a detailed structural level and thus may supplement and augment data obtained by use of existing techniques used in radiation research, such as electron spin resonance and electron-nuclear double-resonance spectroscopy (10, 11).

Methods

Materials. TcAChE is a glycoprotein of subunit molecular weight 65,000. It contains three intramolecular disulfide bonds and an intermolecular disulfide at the C terminus, which participates in dimer formation. TcAChE was purified, subsequent to solubilization with phosphatidylinositol-specific phospholipase C, by affinity chromatography, as described (12). Trigonal crystals of space group P3₁21 were grown from 34% polyethyleneglycol 200/0.3 M morpholino-ethanesulfonic acid, pH 5.8, at 4°C (13).

HEWL is a monomeric protein of molecular weight 15,000, containing four intrachain disulfide bonds. It was obtained from Appligene (Illkirch, France). Tetragonal crystals, of space group P4₃2₁2, were grown from 2–6% NaCl/0.2 M Na acetate, pH 4.7 (14).

Data Collection and Processing. TcAChE. Crystals were transferred into mineral oil and flash-cooled by using an Oxford Cryosystem (Oxford Cryosystems) operating at 100 K. On a single crystal, a series of nine complete data sets (A–I) were collected on the undulator beamline, ID14-EH4, at the European Synchrotron Radiation Facility in Grenoble. The unattenuated beam was used at a wavelength of 0.931 Å. For each data set, 70 frames were collected, with an oscillation range of 0.5° and an exposure time of 3 sec per frame, at a starting angle determined by use of the STRATEGY program (15). The entire duration of collection of each data set was 19 min. Data were processed by using DENZO and SCALEPACK (16) (see Table 1). The resolution limit, as determined by $\langle I \rangle / \langle \sigma I \rangle$ and R_{merge} in the highest resolution shell, was 2.0–2.1 Å for the first three data sets (A–C) and gradually decreased to 3.0 Å for the last data set (I).

Abbreviations: AChE, acetylcholinesterase; TcAChE, *Torpedo californica* AChE; HEWL, hen egg white lysozyme.

Data deposition: The nine structures of AChE and the structure of HEWL, collected at 100 K, have been deposited at the Protein Data Bank, www.rcsb.org (PDB ID codes 1QID, 1QIE, 1QIF, 1QIG, 1QIH, 1QII, 1QIJ, 1QIK, and 1QIM and 1QIO, respectively).

*M.W. and R.B.G.R. contributed equally to this study.

††To whom reprint requests should be addressed at: Department of Structural Biology, Weizmann Institute of Science, Rehovot 76100, Israel. E-mail: Joel.Sussman@weizmann.ac.il.

The publication costs of this article were defrayed in part by page charge payment. This article must therefore be hereby marked "advertisement" in accordance with 18 U.S.C. §1734 solely to indicate this fact.

PNAS • 2000 • vol. 97 • no. • •

Oxford Cryosystems cooling apparatus
Oxford Cryosystems, Oxford, UK

Table 1. Diffraction data statistics AChE

Data set	A	B	C	D	E	F	G	H	I
Resolution, Å	40–2.05	40–2.1	40–2.1	40–2.3	40–2.5	40–2.65	40–2.8	40–2.9	40–3.0
No unique reflections	62,401	56,543	58,334	44,671	34,910	29,417	25,004	21,801	20,415
Redundancy	2.1	1.8	1.8	2.1	2.1	2.1	2.1	1.8	2.1
$\langle I \rangle / \langle \sigma(I) \rangle^*$	16.4 (2.8)	13.1 (1.9)	13.8 (1.6)	14.2 (1.9)	13.4 (1.8)	12.2 (1.7)	10.7 (1.7)	8.8 (1.8)	9.0 (1.9)
Completeness (%) [*]	99.0 (99.3)	96.1 (96.9)	99.0 (99.2)	99.1 (99.4)	99.0 (99.4)	99.0 (99.1)	98.9 (99.2)	95.5 (98.6)	98.8 (99.2)
R_{merge} , % [†]	4.7	5.1	5.2	5.4	5.8	6.5	7.1	9.4	8.6

*Numbers in parentheses indicate statistics for highest resolution shells.

[†] $R_{\text{merge}} = \sum |I - \langle I \rangle| / \sum I$.

HEWL. As part of a longer time series, three data sets were collected on the same undulator beamline, at the same wavelength as for TcAChE, but with an attenuated (ca. 15-fold) beam. The exposure time was 1 sec, and the oscillation range was 0.5° per frame. Total time to collect one data set was 14 min. The attenuated beam had to be used to prevent serious overloads of the low-resolution reflections. Between the second and the third data sets (B and C), the crystal was exposed for 132 sec to the unattenuated beam. The crystal diffracted to better than 1.2 Å for all three data sets, and data processing was carried out as described for TcAChE (see above) (see Table 2).

Dose Calculations. A typical flux at the sample position of the utilized beamline is 5×10^{12} photons/sec through a collimator 0.15 mm in diameter. As determined by the crystal size and a calculated absorption coefficient, 1.2% and 2.1% of the photons were absorbed by the crystals of TcAChE and HEWL, respectively, resulting in deposited energies of the order of magnitude of 10^7 Gy per data set for TcAChE and 10^5 Gy per data set for HEWL. Between the second and third data sets collected on the HEWL crystal, it was exposed to a total absorbed dose of the order of 10^7 Gy.

Table 2. Diffraction data statistics HEWL

Data set	A	B	C
Resolution, Å	25–1.2	25–1.2	25–1.2
No. unique reflections	34,095	34,062	34,143
Redundancy	3.93	3.92	3.94
$\langle I \rangle / \langle \sigma(I) \rangle^*$	23.7 (4.3)	23.6 (4.2)	22.8 (2.6)
Completeness (%) [*]	95.3	95.2	95.1
	(99.9, 69.2) [*]	(99.9, 68.9) [*]	(100, 67.8) [*]
R_{merge} , % [‡]	6.1	5.9	6.1

*Numbers in parentheses indicate statistics for resolution shell 1.24–1.2 Å.

[†]Data sets are complete up to 1.4 Å, but incomplete between 1.4 and 1.2 Å because these reflections were measured in the edges of the squared detector.

*Numbers in parentheses indicate statistics for resolution shells 1.51–1.42 Å and 1.24–1.2 Å, respectively.

[‡] $R_{\text{merge}} = \sum |I - \langle I \rangle| / \sum I$.

Table 3. Refinement statistics AChE

Data set	A	B	C	D	E	F	G	H	I
R factor, %	21.6	21.4	21.2	20.3	19.9	19.8	19.4	19.9	19.1
R_{free} , %	22.9	23.0	22.7	22.0	21.6	21.9	22.3	22.6	21.6
No. protein atoms	4,239	4,239	4,239	4,239	4,239	4,239	4,239	4,239	4,239
No. solvent molecules	333	320	314	335	325	297	293	284	260
Average B factor, Å ²	30.5	33.9	39.1	41.1	43.9	46.1	46.4	43.0	46.1
rmsd bond length, Å	0.007	0.007	0.007	0.008	0.008	0.008	0.009	0.008	0.009
rmsd bond angle, °	1.4	1.4	1.4	1.4	1.4	1.4	1.4	1.4	1.4

rmsd, rms deviation.

Structure Refinement and Analysis. For both proteins, all data, up to the high-resolution limit, were used for refinement. For TcAChE, electron density maps were obtained for each data set by routine refinement, using the program CNS (17), starting from the model of native TcAChE, namely Protein Data Bank (PDB) ID code 2ACE (13), with minor adjustments obtained from the higher-resolution structure, PDB ID code 1VXR (18) (see Table 3). All six cysteine residues participating in intrachain disulfide linkages were refined as alanines, to avoid any potential bias in the electron density maps (the interchain disulfide was not observed; ref. 19). The programs MOLSCRIPT (20), BOBSCRIPT (20, 21), and RASTER3D (22) were used to produce illustrations showing the time course of occurrence of specific structural damage, using electron densities calculated by the program CNS (17), and displayed with o (23). For HEWL, structures were refined by using SHELXL (24) based on the model of HEWL, namely PDB ID code 194L (●●● Vaney, ●●● Maignan, ●●● Ries-Kautt, and ●●● Ducruix, personal communication) (see Table 4).

Results

Comparison of the series sequence of refined structures for TcAChE reveals specific and time-dependent changes in electron density in the region corresponding to the disulfide bridge between Cys-254 and Cys-265 (Fig. 1a). To be certain that there was no model bias in these maps, all six cysteine residues taking part in intrachain disulfide linkages were refined as alanines. This permitted unequivocal visualization of the S_y atoms in difference Fourier maps (Fig. 1b). The other two disulfide bonds, Cys-402–Cys-521 (Fig. 2) and Cys-67–Cys-94 (data not shown), appear substantially more stable over the same period of time. Similar cleavage of S–S bonds has been noted in a number of other x-ray crystallographic measurements on TcAChE using ID14-EH4, in which the cryogenic temperature was varied, and both shorter and longer exposure times were used (data not shown).

Detailed inspection of the nine temporal steps for the Cys-254–Cys-265 bond reveals that already in the first data set (Fig. 1bA) some reduction of density is observed for Cys-265S_y relative to that of Cys-254S_y, with disappearance of any linking

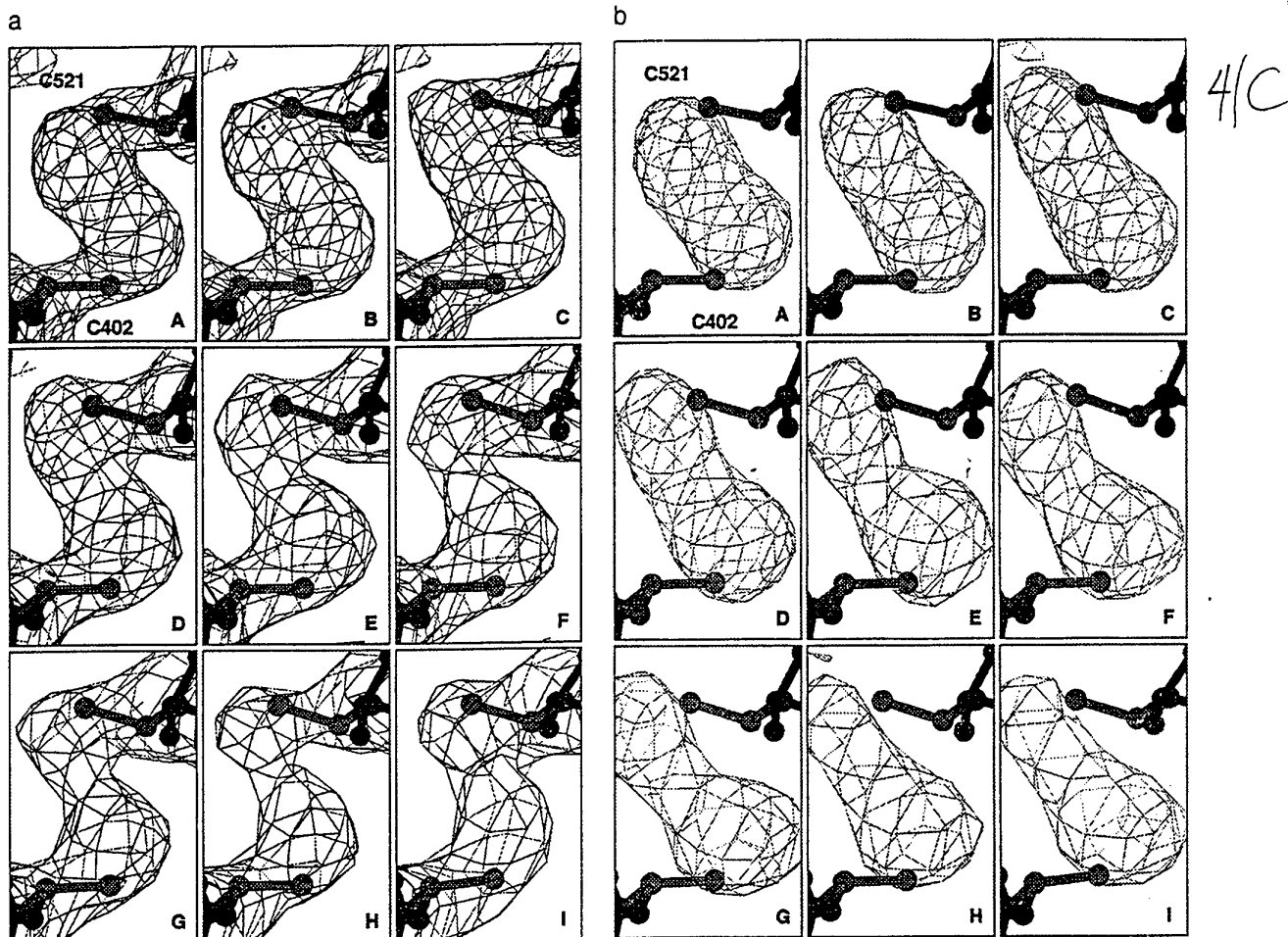


Fig. 2. Sequential Fourier maps showing the time course of structural changes in the Cys-402-Cys-521 disulfide bond in TcAChE. Data collection and refinement were as in Fig. 1. (a) 3Fo-2Fc maps, contoured at 1.5 σ . (b) Fo-Fc maps, contoured at 3 σ .

the crystal to the unattenuated beam, shows clear peaks in the sequential Fourier difference map, indicating significant reduction in electron density of both S- γ atoms in the third data set as compared with the second (Fig. 4C).

Discussion and Conclusions

The design and construction of increasingly brilliant x-ray sources have brought us to a point at which the number of photons a crystal can absorb before its crystalline diffraction disappears is reached rather fast, even at cryogenic temperatures. This finding is in agreement with predictions made by Gonzalez and Nave (3), which were based on extrapolation of radiation damage occurring during experiments at a second-generation source making use of a polychromatic beam. In the series of data sets collected on a single crystal of TcAChE at the undulator beamline, ID14-EH4, of the third-generation synchrotron source at the European Synchrotron Radiation Facility, the resolution decreased from 2.0 Å for the first to 3.0 Å for the ninth consecutive data set. The observed decay is not unexpected, because our calculations show that the dose of energy absorbed per data set for TcAChE was of the order of 10^7 Gy, i.e., similar to the value of 2×10^7 Gy that Henderson (25) calculated to be required to totally eradicate crystalline diffraction of proteins.

Our observation of specific radiation damage, including cleavage of disulfide bridges and loss of definition of carboxyl groups

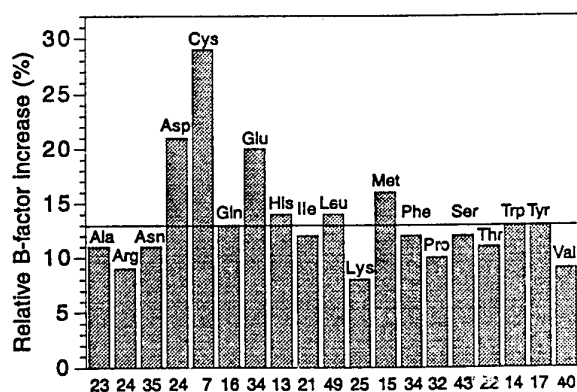


Fig. 3. Histogram showing the increase in B factors for the side chains of the different types of amino acid in TcAChE as a consequence of synchrotron irradiation. The horizontal line indicates the mean increase in side-chain B factors. The numbers along the x-axis show the number of occurrences of each type of amino acid in TcAChE. The individual bars show the average increase in B factor for each type of amino acid for the second data set (B), as compared with the first data set (A), namely $(B \text{ factor}_B - B \text{ factor}_A) / B \text{ factor}_A$.

Data in this figure, as well as values for increases in B factors mentioned in the text, are derived from models in which the six S- γ atoms of cysteine residues participating in intrachain disulfide linkages were included in the refinement.

Subsequently, it appears as if Cys-265 γ first moves away from Cys-254 γ (Figs. 1bB and 1bC), then is detached and finally disappears

Table 4. Refinement statistics HEWL

Data set	A	B	C
R factor, %	14.1	14.5	14.6
R _{free} , %	18.7	19.1	19.0
No. protein atoms	1,026	1,021	1,021
No. solvent molecules	189	184	184
No. heterogen atoms	3	3	3
Average B factor, Å ²	16.9	16.4	17.5
rmsd bond length, Å	0.013	0.013	0.013
rmsd angle distance, Å	0.031	0.030	0.020
rmsd, rms deviation.			0.029

density already apparent in the second data set. Subsequently, it appears as if Cys-265 γ is detached, i.e., moves away from Cys-254 γ (Fig. 1bC), and then disappears. Although Cys-254 γ does not appear to move, its electron density gradually diminishes, and by the eighth step (Fig. 1bH) it is no longer visible.

Comparison of the overall structures does not reveal any major change in backbone conformation occurring concomitantly with disulfide bond cleavage. B factors do change as a function of time, but not uniformly throughout the protein. Specifically, the B factors for Cys, Asp, and Glu side chains increase much more than those for other amino acids (Fig. 3). Examination of

individual amino acids shows that the rate of increase in B factor for the side chain of Cys-265, for the first three data sets, is the highest in the whole protein and that for the side chain of Cys-254 is only exceeded by that for the side chain of the exposed glutamic acid residue, Glu-306. The side chain of the glutamic acid in the catalytic triad, Glu-327, also shows a marked increase in B factor of 50% in the second (B) compared with the first (A) data set. Although the B factors for histidine residues in general do not increase remarkably (Fig. 3), that for the catalytic triad residue, His-440, increases by 34%.

For HEWL, exposure to the unattenuated x-ray beam produced chemical damage similar to that observed for TcAChE. Disulfide bond breakage was the most noteworthy effect. Cys-6-Cys-127 is the most susceptible disulfide bond. The Cys-76-Cys-94 bond is partially cleaved, with an alternative rotamer position for Cys-94 γ clearly visible. The Cys-30-Cys-115 (Fig. 4A) and Cys-64-Cys-80 bonds appear to be the least susceptible. B factors for aspartic acid residues, and for the two glutamates present in lysozyme, increase more than those for other amino acids. By using the attenuated beam, it was possible to mitigate bond breakage substantially. Specifically, comparison of the first two data sets, collected with the attenuator in place, shows no apparent difference in the electron density maps for the Cys-30-Cys-115 bond (Fig. 4B). However, comparison of the second data set to a third data set collected similarly, but after exposing

F4

BIOPHYSICS

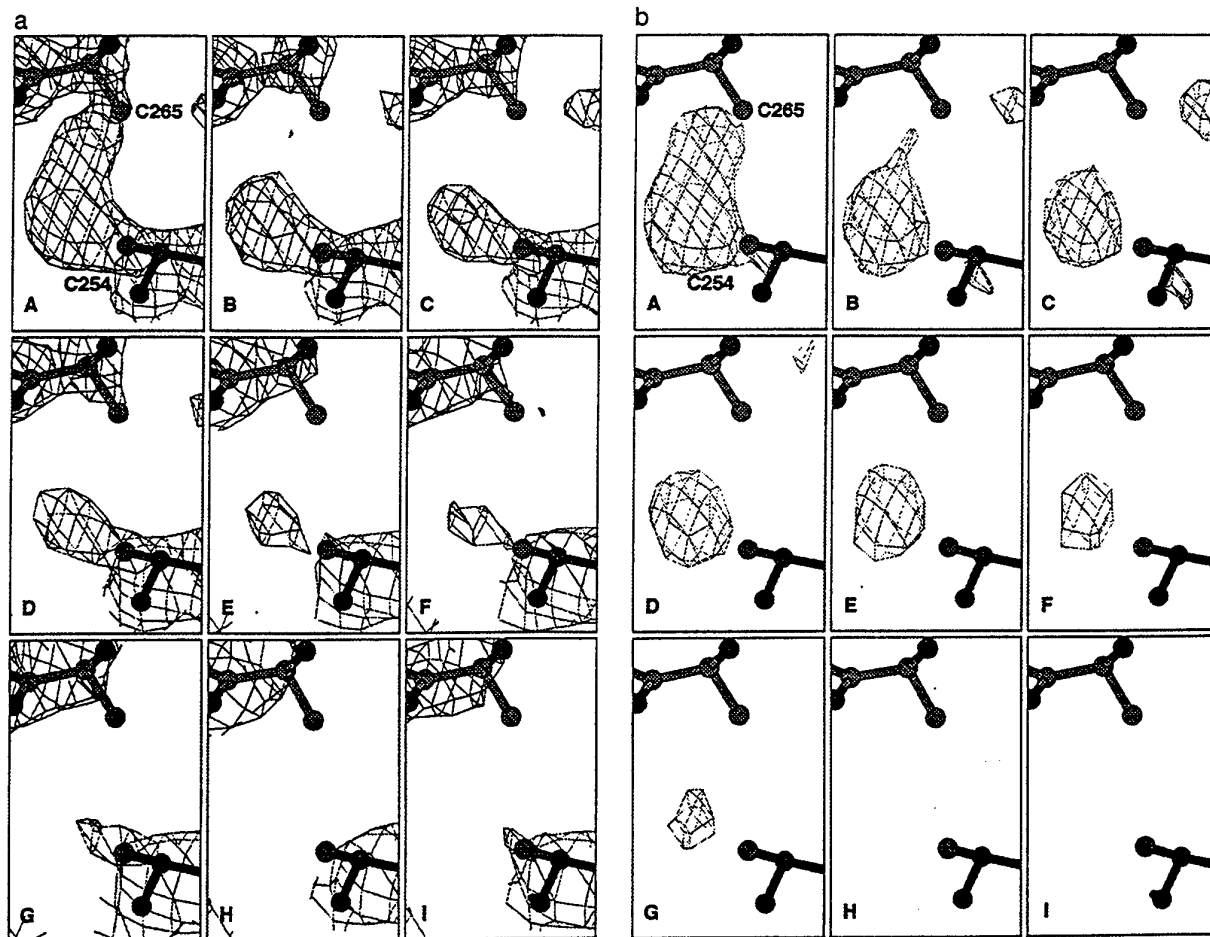


Fig. 1. Sequential Fourier maps showing the time course of cleavage of the Cys-254-Cys-265 disulfide bond in TcAChE. Cysteine residues were refined as alanine residues to avoid model bias. (a) 3Fo-2Fc maps, contoured at 1.5 σ . (b) Fo-Fc maps, contoured at 3 σ .

1

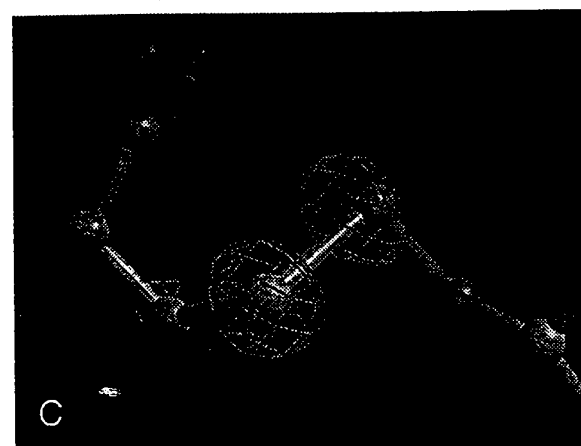
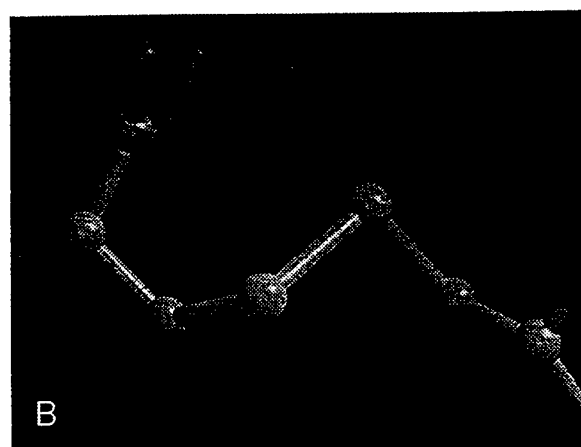
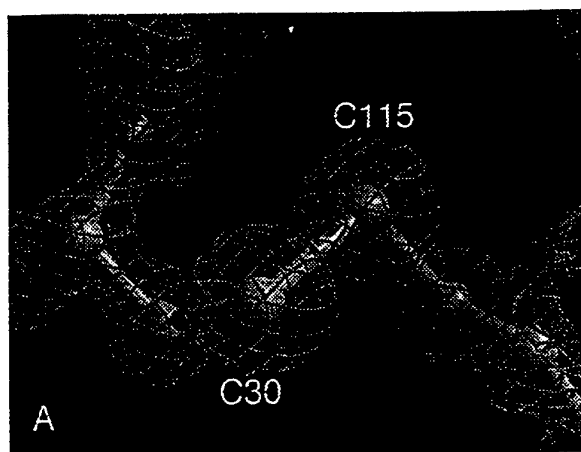


Fig. 4. Sequential Fourier maps and difference Fourier maps showing cleavage of the Cys-30-Cys-115 disulfide bond in HEWL as a function of x-ray dose at 1.2-Å resolution. (A) Initial 2Fo-Fc map, contoured at 1.5 σ . (B) Difference Fourier map, $wF_A - wF_B$, for two successive data sets collected using an attenuator, contoured at 5 σ (the w refers to SIGMAA weighting (39)). (C) Difference Fourier map, $wF_A - wF_C$, for two successive data sets, between which the crystal was exposed to the unattenuated beam, contoured at 6 σ .

of acidic residues, was, however, unexpected. Disulfide bond cleavage by ionizing radiation has been described in a variety of studies in solution (see ref. 26 and references therein). Helliwell (27) reported disulfide bond cleavage in crystalline des-pentapeptide insulin under conditions of synchrotron radiation at room temperature, and Burley, Petsko, and Ringe (personal communication) made similar observations for ribonuclease by using a conventional x-ray source. Under our experimental (cryogenic) conditions, we reproducibly observe a specific order of cleavage, with the Cys-254-Cys-265 bond being the most susceptible in TcAChE and Cys6-Cys127 the most susceptible in HEWL. Breakage of the homologous disulfide, Cys-292-Cys-302, in the x-ray structure of *Drosophila melanogaster* AChE (M.H., unpublished results), was observed in a data set collected on a second-generation synchrotron source (NSLS-X12c at Brookhaven National Laboratory). Selective cleavage of the Cys-6-Cys-127 disulfide bond in lysozyme was earlier observed in a steady-state radiolysis study in solution (28).

From the histogram of increases in B factors for TcAChE presented in Fig. 3, one can see that the residues most affected by synchrotron radiation, apart from the cysteines, are the acidic residues, glutamate and aspartate. One residue that is particularly affected is the AChE surface residue, Glu-306; another is Glu-327, which is a member of the catalytic triad characteristic of serine hydrolases. In lysozyme, both acidic residues in the active site, namely Glu-35 and Asp-52, are affected, together with the surface residues, Glu-7 and Asp-87. The increases in B factors could be either a consequence of increased mobility or decarboxylation, a known effect of ionizing radiation (29). Acidic residues often are seen in active sites of enzymes, as is the case for both enzymes in the present study. An important consequence of our experiments is the realization that any unusually large B factor, i.e., apparent mobility, seen for such residues, might not be of functional significance, but simply the result of specific radiation damage during structure determination.

Among all the 14 histidine residues in TcAChE, the catalytic triad residue His-440 is the most affected by x-ray irradiation, as shown by the marked increase in its B factor. This finding could be related to the observations of Faraggi and coworkers (28), who showed that pulsed radiolysis affected primarily histidine residues at active sites. However, the increase in B factor also may be coupled to the increase in B factor noted above for the acidic member of the catalytic triad, Glu-327. Our observation that active-site residues are among the most radiation-sensitive residues, suggests that, like disulfide bonds, active site conformations constitute "weak links" or "strained" configurations in protein structures.

An important issue that arises is whether the specific structural changes that we observe are a consequence of "primary" interaction, i.e., between the x-rays and the moieties that suffer specific damage, or "secondary", i.e., mediated by free radicals generated by the x-rays either within the protein ("direct" damage) or within the solvent ("indirect" damage). The extent to which radiation damage to proteins and nucleic acids is direct or indirect is indeed the subject of controversy (see, for example, the review in ref. 30). Primary damage might affect sulfur atoms preferentially because, at the wavelength used, they have a significantly higher absorption cross section than carbons, oxygens, or nitrogens. Disulfide bonds were earlier shown, in pulse radiolysis studies, to be sensitive to radicals (26) and, therefore, to secondary damage. X-ray irradiation of water molecules in the solvent area releases highly reactive species, including hydrogen and hydroxyl radicals, and hydrated electrons (28, 29). These species should be capable of attacking the protein even under cryogenic conditions (31). There does, indeed, seem to be a correlation between solvent accessibility and susceptibility of disulfides to x-ray damage. Thus Cys-254-Cys-265 in TcAChE,

M ✓
yes
we
have
perm
sion
to
cite
(Le Her
attal

BIOPHYSICS

PV

and Cys-6-Cys-127 in HEWL, are the most susceptible disulfides in their respective proteins, and both seem to have the largest solvent accessible surface of the disulfides in that protein. Irradiation has, however, also been shown to cleave disulfide bridges in dry proteins (29). Thus possible involvement of direct radiation damage (30, 32) in generating the specific structural changes that we observe also must be taken into consideration.

Our findings have significant practical implications with respect to x-ray data collection using bright synchrotron sources. Fig. 1 *aA*, *aC*, *bA*, and *bC* clearly show that specific damage occurs from the very onset of exposure of the crystal to the x-ray beam. Yet, the resolution of these first three data sets is virtually identical, although some decay in the signal-to-noise ratio for the higher-resolution reflections was observed. These data sets were all complete. However, the redundancy was low as a result of the minimization of the data collection time. Thus, during standard data collection at brilliant undulator beamlines at third-generation synchrotron sources, which aims at high redundancy, the specific radiation damage of the type that we report is very likely to occur (31). Following the trends in Figs. 1 and 2, it is clear that each data set represents the average of a temporal ensemble, which might require extrapolation to zero time. We observed earlier a broken disulfide bond (Cys-254-Cys-265) in TcAChE using a data set that was collected on a second-generation source wiggler beamline (NSLS-X25 at Brookhaven National Laboratory). The Protein Data Bank (33) may contain a substantial number of structures (see e.g., refs. 34 and 35) with broken disulfide bonds: it would be useful if validation programs could help to clarify whether these structures had been affected by radiation damage. Obviously, these programs would benefit

from serious investigation of the chemistry and physics underlying radiation damage to protein crystals at powerful synchrotron sources.

The radiation damage we have observed also may explain why collection of multiwavelength anomalous dispersion (MAD) data (36) has been problematic at third-generation synchrotron sources. It is noteworthy that virtually all strong third-generation undulator MAD beamlines make routine use of attenuators (8).

In some fields of synchrotron-related research, the free radicals generated by the x-rays actually have been used for studying biological systems in solution (37). For example, folding of an RNA molecule has been followed on a 10-ms time scale by monitoring its hydroxyl radical-accessible surface (38). We anticipate that once the mechanism(s) underlying radiation damage in single crystal protein crystallography is better understood it should be possible to use the wealth of sequential information generated as a valuable tool in radiation chemistry and biology.

We thank Arthur Grollman, Lev Weiner, and Martin Caffrey for valuable discussions and Deborah Fass for critical and constructive reading of the manuscript. This work was supported by the U.S. Army Medical and Materiel Command under Contract No. DAMD17-97-2-7022, the European Union 4th Framework Program in Biotechnology, the Kimmelman Center for Biomolecular Structure and Assembly (Rehovot, Israel), and the Dana Foundation. The generous support of Mrs. Tania Friedman is gratefully acknowledged. R.B.G.R. acknowledges support from the ~~●●●~~ TMR Access to Large Scale Facilities Contract ERBFMGECT980133 to the European Molecular Biology Laboratory Grenoble Outstation, and I.S. is Bernstein-Mason Professor of Neurochemistry.

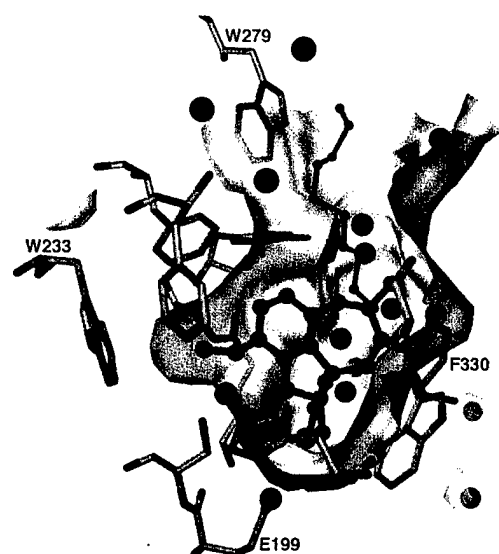
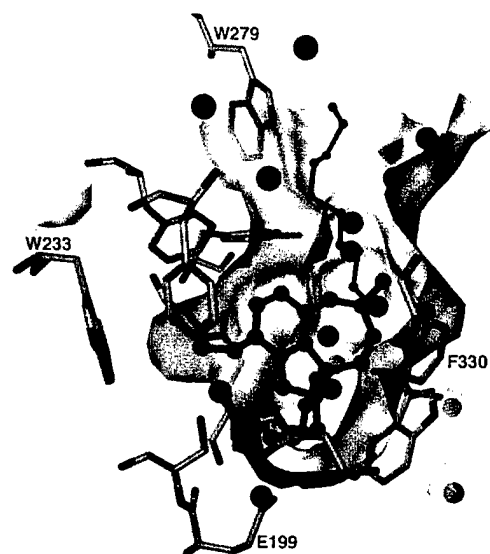
Training and Mobility of Researchers

1. Blundell, T. L. & Johnson, L. N. (1976) *Protein Crystallography* (Academic, New York).
2. Sygusch, J. & Allaire, M. (1988) *Acta Crystallogr. A* 44, 443-448.
3. Gonzalez, A. & Nave, C. (1994) *Acta Crystallogr. D* 50, 874-877.
4. Hope, H. (1988) *Acta Crystallogr. B* 44, 22-26.
5. Garman, E. F. & Schneider, T. R. (1997) *J. Appl. Crystallogr.* 29, 211-237.
6. Yonath, A., Harms, J., Hansen, H. A., Bashan, A., Schlunzen, F., Levin, I., Koelln, L., Tocilj, A., Agmon, I., Peretz, M., et al. (1998) *Acta Crystallogr. A* 54, 945-955.
7. Owen, D. J., Noble, M. E., Garman, E. F., Papageorgiou, A. C. & Johnson, L. N. (1995) *Structure (London)* 3, 467-482.
8. Walsh, M. A., Dementieva, I., Evans, G., Sanishvili, R. & Joachimiak, A. (1999) *Acta Crystallogr. D* 55, 1168-1173.
9. Ravelli, R. B. G., Ravess, M. L., Ren, Z., Bourgeois, D., Roth, M., Kroon, J., Silman, I. & Sussman, J. L. (1998) *Acta Crystallogr. D* 54, 1359-1366.
10. Sevilla, M. D., D'Arcy, J. B. & Morehouse, K. M. (1979) *J. Phys. Chem.* 83, 2887-2892.
11. Swartz, H. M. & Swartz, S. M. (1983) *Methods Biochem. Anal.* 29, 207-323.
12. Sussman, J. L., Harel, M., Frolow, F., Varon, L., Toker, L., Futerman, A. H. & Silman, I. (1988) *J. Mol. Biol.* 203, 821-823.
13. Ravess, M. L., Harel, M., Pang, Y.-P., Silman, I., Kozikowski, A. P. & Sussman, J. L. (1997) *Nat. Struct. Biol.* 4, 57-63.
14. Drenth, J. (1994) *Principles of Protein X-ray Crystallography* (Springer, Berlin).
15. Ravelli, R. B. G., Sweet, R. M., Skinner, J. M., Duisenberg, A. J. M. & Kroon, J. (1997) *J. Appl. Crystallogr.* 30, 551-554.
16. Otwinowski, Z. (1993) in *Proceedings of the CCP4 Study Weekend: Data Collection and Processing, 29-30 January, 1993*, eds. Sawyer, L., Isaacs, N. & Bailey, S. (Science and Engineering Research Council Daresbury Laboratory, Daresbury, U.K.), pp. 56-62.
17. Brünger, A. T., Adams, P. D., Clore, G. M., DeLano, W. L., Gros, P., Grosse-Kunstleve, R. W., Jiang, J. S., Kuszewski, J., Nilges, M., Pannu, N. S., et al. (1998) *Acta Crystallogr. D* 54, 905-921.
18. Millard, C. B., Koellner, G., Ordentlich, A., Shafferman, A., Silman, I. & Sussman, J. L. (1999) *J. Am. Chem. Soc.*, in press 121, 9883-9884.
19. Sussman, J. L., Harel, M., Frolow, F., Oefner, C., Goldman, A., Toker, L. & Silman, I. (1991) *Science* 253, 872-879.
20. Kraulis, P. (1991) *J. Appl. Crystallogr.* 24, 946-950.
21. Esnouf, R. M. (1999) *Acta Crystallogr. D* 55, 938-940.
22. Merritt, E. A. & Murphy, M. E. P. (1994) *Acta Crystallogr. D* 50, 869-873.
23. Jones, T. A., Zou, J.-Y., Cowan, S. W. & Kjeldgaard, M. (1991) *Acta Crystallogr. A* 47, 110-119.
24. Sheldrick, G. M. (1997) in *Recent Advances in Phasing: Proceedings of the CCP4 Study Weekend*, eds. Wilson, K. S., Davies, G., Ashton, W. & Bailey, S. (Daresbury Laboratory, Daresbury, U.K.), pp. 147-157.
25. Henderson, R. (1990) *Proc. R. Soc. London Ser. B* 248, 6-8.
26. von Sonntag, C. (1987) *The Chemical Basis of Radiation Biology: Radiobiology* (Taylor & Francis, ~~●●●~~ London, UK).
27. Helliwell, J. R. (1988) *J. Crystallogr. Growth* 90, 259-272.
28. Faraggi, M., Ferradini, C., Houee-Levin, C. & Klapper, M. H. (1995) in *Radiation Research 1895-1995*, eds. Hagen, U., Harder, D., Jung, H. & Streffer, C. (Universitätsdruckerei H. Sturtz AG, Würzburg, Germany), Vol. 2, pp. 241-248.
29. Alexander, P. & Lett, J. T. (1967) in *Comprehensive Biochemistry*, eds. Florkin, M. & Stotz, E. (~~●●●~~), Vol. 27, pp. 267-356.
30. Symons, M. C. R. (1995) *Radiat. Phys. Chem.* 45, 837-845.
31. Lange, M., Weiland, B. & Huttermann, J. (1995) *Int. J. Radiat. Biol.* 68, 475-486.
32. Jones, G. D., Lea, J. S., Symons, M. C. & Taiwo, F. A. (1987) *Nature (London)* 330, 772-773.
33. Sussman, J. L., Lin, D., Jiang, J., Manning, N. O., Prilusky, J., Ritter, O. & Abola, E. E. (1998) *Acta Crystallogr. D* 54, 1078-1084.
34. Burmeister, W. P., Gastinel, L. N., Simister, N. E., Blum, M. L. & Bjorkman, P. J. (1994) *Nature (London)* 372, 336-343.
35. Burling, F. T., Weis, W. I., Flaheley, K. M. & Brünger, A. T. (1996) *Science* 271, 72-77.
36. Hendrickson, W. A. (1991) *Science* 254, 51-58.
37. Cheng, A. & Caffrey, M. (1996) *Biophys. J.* 70, 2212-2222.
38. Slavi, B., Sullivan, M., Chance, M. R., Brenowitz, M. & Woodson, S. A. (1998) *Science* 279, 1940-1943.
39. Read, R. J. (1986) *Acta Crystallogr. A* 42, 140-149.

Elsevier, Amsterdam,
Holland

FEBS *Letters*

An international journal
for the rapid publication
of short reports in
biochemistry, biophysics
and molecular cell
biology



Published by Elsevier
on behalf of the
Federation of European
Biochemical Societies
ISSN 0 014 5793

Last number of this volume
Volume 463
Number 3
17 December 1999

Structure of acetylcholinesterase complexed with (–)-galanthamine at 2.3 Å resolution

H.M. Greenblatt^a, G. Kryger^a, T. Lewis^b, I. Silman^c, J.L. Sussman^{a,*}

^aDepartment of Structural Biology, Weizmann Institute of Science, Rehovot 76100, Israel

^bZeneca Agrochemicals, Jealott's Hill Research Station, Bracknell, Berkshire RG12 6EY, UK

^cDepartment of Neurobiology, Weizmann Institute of Science, Rehovot 76100, Israel

Received 8 November 1999

Edited by Shmuel Shaltiel

Abstract (–)-Galanthamine (GAL), an alkaloid from the flower, the common snowdrop (*Galanthus nivalis*), shows anticholinesterase activity. This property has made GAL the target of research as to its effectiveness in the treatment of Alzheimer's disease. We have solved the X-ray crystal structure of GAL bound in the active site of *Torpedo californica* acetylcholinesterase (TcAChE) to 2.3 Å resolution. The inhibitor binds at the base of the active site gorge of TcAChE, interacting with both the choline-binding site (Trp-84) and the acyl-binding pocket (Phe-288, Phe-290). The tertiary amine group of GAL does not interact closely with Trp-84; rather, the double bond of its cyclohexene ring stacks against the indole ring. The tertiary amine appears to make a non-conventional hydrogen bond, via its N-methyl group, to Asp-72, near the top of the gorge. The hydroxyl group of the inhibitor makes a strong hydrogen bond (2.7 Å) with Glu-199. The relatively tight binding of GAL to TcAChE appears to arise from a number of moderate to weak interactions with the protein, coupled to a low entropy cost for binding due to the rigid nature of the inhibitor.

© 1999 Federation of European Biochemical Societies.

Key words: Cholinesterase; Alzheimer's disease; Natural product; Herbal medicine; Galanthamine

1. Introduction

According to the 'cholinergic hypothesis', Alzheimer's disease (AD) is associated with cholinergic insufficiency [1–3]. This serves as the rationale for use of cholinergic agonists [4,5] and cholinesterase inhibitors [6,7] for the symptomatic treatment of AD in its early stages. Indeed, cholinesterase inhibitors are the only drugs so far approved for treatment of AD. These drugs include natural substances, such as the alkaloids, physostigmine [8] and huperzine A [9], and synthetic compounds, such as tacrine, under its trade name, Cognex[®] [10], SDZ ENA-713, also known as Exelon[®] [11], metrifonate [12] and E2020, under its trade name, Aricept[®] [13,14].

Galanthamine (4a,5,9,10,11,12-hexahydro-3-methoxy-11-methyl-6H-benzofuro[3a,3,2-ef][2]-benzazepin-6-ol; GAL; see Fig. 1) is an alkaloid found in the bulbs and flowers of the common snowdrop (*Galanthus nivalis*) and of several other

members of the *Amaryllidaceae* family. The active ingredient was discovered accidentally by a Bulgarian pharmacologist in wild Caucasian snowdrops in the early 1950s [15]. The plant extracts were used initially to treat nerve pain and poliomyelitis. As a natural compound, GAL has since been tested for use in anesthesiology [16] and for treatment of many human ailments, from facial nerve paralysis to schizophrenia and various dementia [17–19]. It is marketed as a hydrobromide salt under the name Reminyl[®].

GAL displays 53-fold selectivity for human erythrocyte acetylcholinesterase (AChE) over butyrylcholinesterase (BChE), with IC₅₀ values of 0.35 µM for erythrocyte AChE and 18.6 mM for plasma BChE [20]. An IC₅₀ of 652 nM has been recorded for *Torpedo californica* AChE (TcAChE) (T. Lewis and C. Personeni, unpublished results). Interestingly, it displays 10-fold lower potency towards human brain AChE than towards the erythrocyte enzyme [21]. In addition to serving as a cholinesterase inhibitor, GAL is also a nicotinic activator, acting both on ganglionic and muscle receptors [22,23] and on nicotinic receptors in the brain [24]. Nicotinic modulation represents a new and promising approach in Alzheimer research [25–30]. A recent report suggests that stimulation of nicotinic receptors may be associated with diminished appearance of amyloid plaques, one of the hallmarks of AD [31]. The double action of GAL, as both an anticholinesterase and a nicotinic activator, has rendered it a promising candidate drug for the treatment of AD. Indeed, phase III clinical trials in Europe for the treatment of AD were recently completed [32], although approval has not yet been granted.

Structure-based drug design is an important tool in the development of second-generation candidate drugs based on a lead compound [28,33–35]. Although computerized docking programs are becoming increasingly sophisticated, the X-ray analysis of a ligand-protein structure often yields crucial information. Indeed, in the case of AChE, determination of the three-dimensional (3D) structures of the appropriate ligand-AChE complexes was a prerequisite for making correct structural assignments for huperzine A [36] and E2020 [14], as well as for the snake venom toxin, fasciculin [37]. In the case of GAL, too, docking protocols suggest more than one possible orientation (Fletcher, R., Viner, R., Lewis, T., unpublished results). Determination of the 3D structure of a GAL-AChE complex would obviously resolve the issue. Furthermore, knowledge of the structure of the complex would also allow us to rationalize results of recent synthetic modifications [38] aimed at improving binding characteristics of GAL to AChE. In the following, we present the X-ray crystal structure, at 2.3 Å resolution, of the GAL-TcAChE complex.

*Corresponding author. Fax: (972)-8-934 4159.
E-mail: joel.sussman@weizmann.ac.il

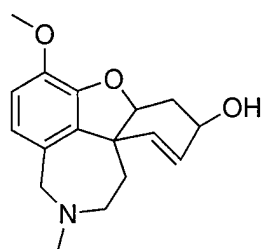


Fig. 1. GAL.

2. Materials and methods

2.1. Crystallization and data collection

TcAChE was purified and crystallized as described [36]. GAL was purchased from Sigma (G1160, lot # 56H0191, hydrobromide form). Three crystals of *TcAChE* were harvested and transferred to a drop containing mother liquor and 10 mM GAL. After 2 days, they were transferred to a second solution of mother liquor containing 20 mM GAL. All work was done at 4°C. After 2 more days, a crystal was transferred to oil, mounted in a cryo-loop, placed on the goniostat and flash-cooled to 100 K in an Oxford Systems Cryostream. The X-ray source was a Rigaku FR-C rotating anode running at 50 KV/100 mA. Images were collected with a Rigaku RAXIS-IIC. Data collection statistics are summarized in Table 1. Data processing was carried out with DENZO/SCALEPACK [39]. Data were truncated with the CCP4 [40] program TRUNCATE, and a list of randomly generated test reflections was added from a master list for the trigonal crystal form of *TcAChE* using CAD and FREERFLAG. Reflections were output with MTZ2VARIOUS to a format suitable for CNS.

2.2. Refinement

The protein was refined in CNS [41], initially by use of rigid body refinement. Subsequently, difference maps (Fo–Fc) and 2Fo–Fc maps were used to fit the GAL molecule, two carbohydrate moieties and 93 water molecules (to 4.5σ). The initial electron density for the inhibitor was unambiguous, as seen in Fig. 2. The program XtalView [42] was used for all model building. The model used for GAL was taken from the crystal structure [43]; CSD code SIBHAM) of the neutral compound. Individual B-refinement was carried out, followed by simulated annealing (torsion dynamics mode [44]), followed again by individual B-factor refinement. Inspection of positive peaks in difference maps to 4σ showed an additional 51 water molecules, as well as a continuous stretch of density near the top of the active site gorge which was modeled as a PEG trimer. Inspection of the entire protein resulted in a few minor changes to side chain positions outside the area of the active site. The model was further refined by positional maximum-likelihood minimization and by individual B-factor refinement. The results are summarized in Table 2.

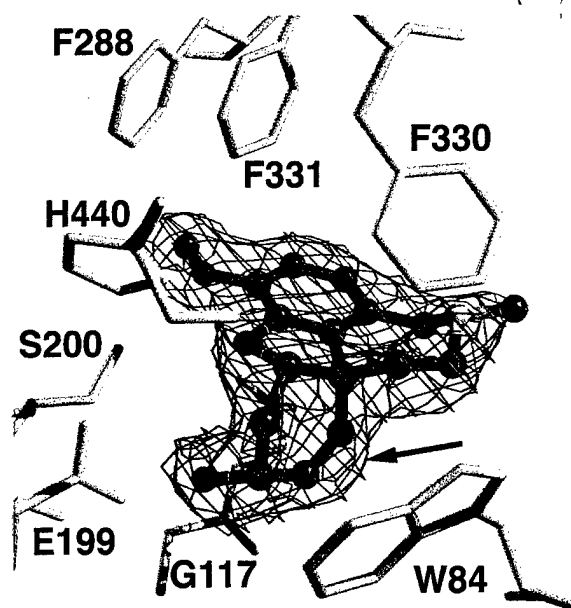


Fig. 2. Electron density map (Fo–Fc) from the GAL-*TcAChE* complex after rigid body refinement. The map shows unambiguous density for GAL bound in the active site of the enzyme. Contouring level is at 3σ, shown in thin blue lines. Only contours within 2.0 Å of the inhibitor are shown. GAL is rendered as a ball-and-stick model, with carbon atoms colored green. Selected protein residues are rendered as sticks, with carbon atoms colored yellow and labeled appropriately. The double bond of the cyclohexene ring in GAL is indicated by the arrow (picture made with Xfit [42] and Raster3d [54]).

3. Results

The overall mode of binding of GAL to *TcAChE* is shown in Fig. 3. The inhibitor binds at the base of the active site gorge, spanning the acyl-binding pocket and the choline-binding site, viz. the indole ring of Trp-84. There appear to be two classic hydrogen bonds formed with protein atoms (Fig. 4). One is between the hydroxyl group of the inhibitor and Glu-199 O^{E1} (2.7 Å). The hydroxyl group also interacts with two water molecules. One water molecule (3.1 Å) is that which is bound in the oxyanion hole by the three NH groups of Gly-118, Gly-119 and Ala201. It is also bifurcated with the oxygen atom of the dihydrofuran ring of the inhibitor (3.1 Å). A second water molecule is 3.3 Å away and interacts also with Tyr-130 O^N and Gly-117 N. The second possible hydrogen bond to a protein atom involves the hydroxyl group of Ser-200, whose hydrogen may be bifurcated between His-440 N^{E2}

Table 1
Collection and processing statistics

Oscillation angle	0.5°
Total number of frames	72
Total number of reflections	215 846
Resolution range	30–2.3 Å
Number of unique reflections	43 422
Redundancy	0
% Reflection	1.3
Average redundancy (weighted)	3.1
Overall completeness	98.7%
Completeness in highest resolution shell	97.1%
Overall R_{merge}	7.7%
R_{merge} in highest resolution shell	39%
(2.38–2.30 Å)	

Table 2
Refinement results

Resolution range	30.0–2.3 Å
Number of protein atoms	4211
Number of non-protein atoms	
Solvent (water, PEG)	144, 10
Carbohydrate atoms	28
Inhibitor	21
R_{work}	21.3%
R_{free} (5% of reflections)	25.0%
rms bond deviations	0.017 Å
rms angle deviations	1.8°

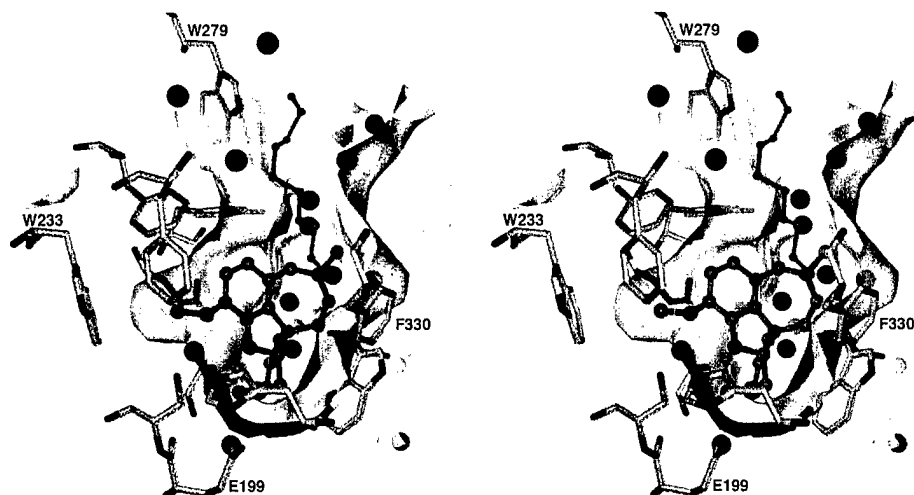


Fig. 3. Stereo view of binding of GAL in the active site gorge of *TcAChE*. The solvent accessible surface of the protein (without waters and without ligands) was calculated by use of the program MSMS [55] with a probe radius of 1.4 Å. Only those parts of the surface within 9.0 Å of the bound inhibitor are visible, and the surface is 30% transparent, allowing visualization of some of the underlying protein residues. The surface has also been clipped to reveal the interior side, and has been color-coded such that blue indicates those parts of the surface whose underlying atoms are between 4.0 and 3.0 Å from any atom of the inhibitor, and pink indicates distances of less than 3.0 Å from the protein atoms to the inhibitor. Only a small portion of pink surface is visible in this orientation, located below the O-methyl group of the inhibitor, in the acyl-binding pocket. GAL has been rendered as a ball-and-stick model whose carbon atoms are colored green. Selected protein residues are shown as stick models with yellow carbon atoms. Water molecules are red spheres, and the PEG200 trimer/tetramer is rendered as a ball-and-stick model whose carbon atoms are colored pink (picture made with DINO [56] and rendered in POV-ray® [57]).

and the oxygen of the O-methyl group of the inhibitor. There may also be a non-classical hydrogen bond between the N-methyl group of the inhibitor and Asp-72 O^{δ2} (3.4 Å), since the methyl group is expected to carry some of the positive charge of the amine. The unexpected presence of a PEG molecule in the active site gorge gives rise to an interesting interaction between the terminal hydroxyl group of the PEG molecule and the tertiary amine of GAL (2.8 Å). The terminal hydroxyl group, in turn, forms an aromatic hydrogen bond [45,46] with Phe-330. A water molecule could presumably fulfil the same role in the absence of PEG. The rest of the interactions between the inhibitor and the protein appear to be non-polar. This is particularly noteworthy, since the protonated tertiary amine group does not interact with Trp-84 or Phe-330 analogously to the interaction which is believed to

occur between the quaternary amine of the natural substrate (acetylcholine) and the enzyme, and has been observed for a number of inhibitors [36,47,48]. In fact, the nitrogen and its three substituents are quite removed from Trp-84, the closest approach being between C11 of the inhibitor and C^γ (3.6 Å) and C^{δ1} (3.7 Å) of the indole ring. The next methylene group in the tetrahydroazepine ring (C12) makes three contacts with the indole ring, and the rest of the interactions with Trp-84 involve the cyclohexene ring of GAL. The double bond in the cyclohexene ring stacks against the π system of the indole ring of Trp-84. Saturation of this double bond (to give lycoramine) greatly reduces the binding affinity of the inhibitor (T. Lewis, C. Personeni, unpublished results). On the opposite side of the gorge, the O-methoxy group of GAL occupies the acyl-binding pocket, contacting Phe-288 and Phe-290.

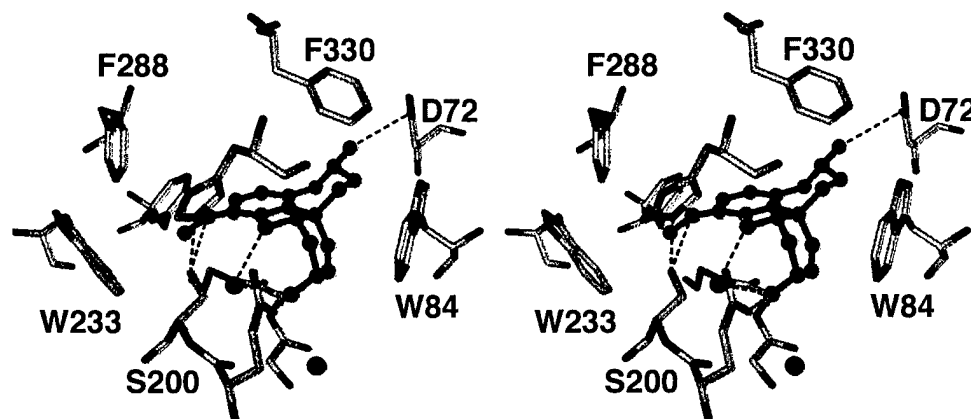


Fig. 4. Stereo view of possible hydrogen bonds between GAL and *TcAChE*. The inhibitor is displayed as a ball-and-stick model, with green carbon atoms. The protein residues are rendered as stick models with yellow carbon atoms (DINO/POV-ray).

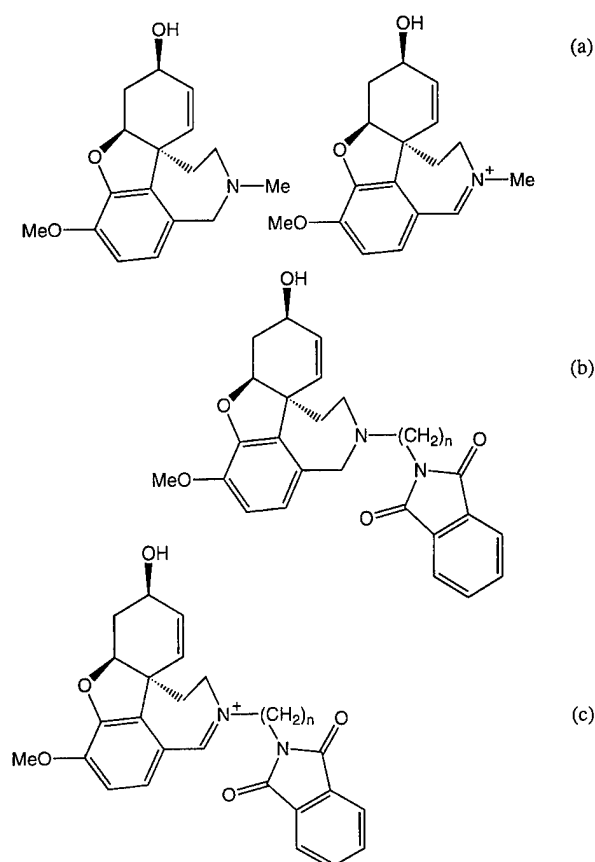


Fig. 5. (a) Comparison of GAL (left) with its iminium derivative (right). This is the same structure as in Fig. 1, but drawn here to show some of the stereochemistry. (b) GAL with N-linked phthalimide group using variable length alkyl chain. (c) Iminium derivative of GAL with N-linked phthalimide group, as in (b).

4. Discussion

Initial inspection of the GAL-*TcAChE* complex does not reveal any specific interactions which could account for the tight binding observed. GAL is not a transition state ana-

logue, which, of all the structures on the reaction coordinate, bind most tightly to the enzyme [49]. Nor are there any charge-charge interactions between the inhibitor and the enzyme. In fact, the only charged group in the inhibitor interacts rather indirectly with residues of the protein (through a solvent molecule to Phe-330, possibly via a methyl hydrogen to Asp-72, and via a methylene hydrogen with the π system of Trp-84). It must be assumed that the binding energy for GAL comes from a number of smaller enthalpic contributions, coupled to an unusually small entropic penalty. This latter point arises from the rigidity of the molecule, which allows the numerous interactions to occur with minimal loss of entropy. A similar concept is utilized in the tight binding of multisubstrate analogues ([50], see Fersht [51]).

Recent attempts to produce synthetic derivatives of GAL with higher binding affinities [38] showed that conversion of the tertiary amine to an iminium ion (See Fig. 5a) increased the affinity for electric eel AChE (*EeAChE*) by 4.5-fold. In an attempt to produce bifunctional ligands which would interact with Trp-279 at the top of the gorge, a phthalimido group was attached to the nitrogen (Fig. 5b), via alkyl spacers of varying lengths. This had only a moderate effect on the IC_{50} , with a maximal decrease of 5.6-fold (four-carbon spacer), and a maximal increase of only 1.3-fold (eight-carbon spacer), relative to GAL. Interestingly, a molecule combining both the iminium and phthalimido (eight-carbon spacer) modifications (Fig. 5c) showed a 36-fold increase in affinity. The crystal structure of GAL bound in the active site of *TcAChE* justifies the above rationale for creating bis-interacting derivatives, since the nitrogen atom is oriented up the gorge. This is in contrast to the results obtained when attachment of the alkyl-phthalimido functionality was via the hydroxyl group of GAL. The compounds so obtained inhibit AChE approximately two orders of magnitude more weakly than GAL itself. Since the observed binding mode of GAL places the hydroxyl group in an area of restricted volume, additions to this part of the molecule would presumably force GAL to bind in a different fashion. What is not apparent is why the iminium derivative should be a better inhibitor than native GAL, since the latter is presumably protonated at pH 5.6. One possibility is that the

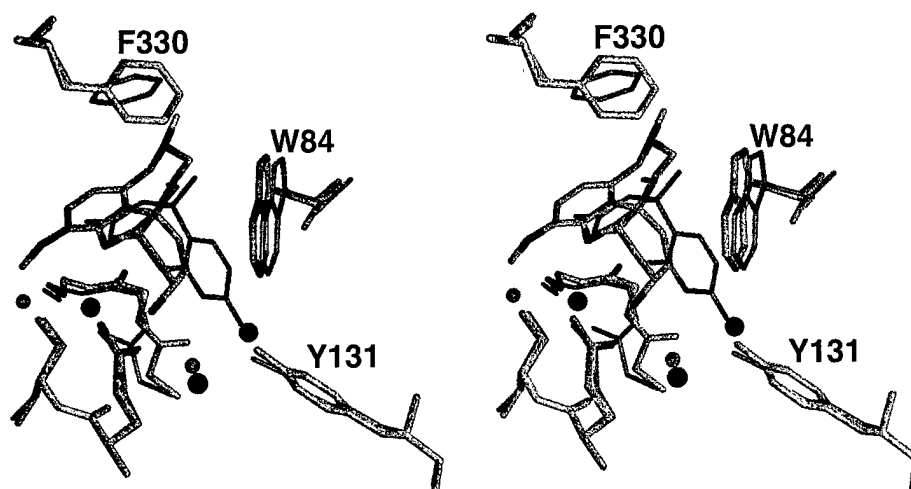


Fig. 6. Stereo view comparing binding of GAL and huperzine A in the active site of *TcAChE*, showing the main chain conformational change (Gly-117) associated with binding of huperzine A. GAL and associated protein residues are rendered as green stick models, while huperzine and associated protein residues are rendered as thin pink stick models. Water molecules associated with the GAL structure are shown as red spheres, while those from the huperzine structure are displayed as smaller pink spheres (DINO/POV-ray).

planar geometry of the nitrogen atom allows closer interaction of the N-methyl group with Asp-72, resulting in a stronger hydrogen bond.

Another AD drug, huperzine A [36,52], shares common binding characteristics with GAL (Fig. 6). Both molecules have a bent hinge shape and, in both cases, the hinge is oriented similarly when the ligand is bound to *TcAChE*. Both molecules pack against the face of Trp-84 and make few direct hydrogen bonds to the protein. Nevertheless, there are several major differences in their binding modes. Thus, GAL does not induce a main chain conformational change at Gly-117 as does huperzine A. Moreover, the orientation of the side chain of Phe-330 differs in the two complexes. Furthermore, the primary amino group of huperzine A interacts much more closely with the indole ring of Trp-84 than does the tertiary amine of GAL. Finally, GAL does not exhibit the slow binding kinetics observed for huperzine A [53]. A partial answer to the question of why GAL binds with a tightness comparable to huperzine A, despite apparent lack of direct interaction between the amine group and Trp-84, may lie in the fact that GAL fills more of the active site volume, since it also binds in the acyl-binding pocket. Furthermore, one of the direct hydrogen bonds with the protein involves a charged residue (Glu-199), which is not the case for huperzine A.

5. Conclusions

The structure of the complex of GAL and *TcAChE* shows that GAL binds at the base of the gorge interacting with both the acyl-binding pocket and the principal quaternary ammonium-binding site, the indole ring of Trp-84. The high affinity displayed by the inhibitor for *AChE* appears to come from a number of moderate to weak interactions accompanied by a low entropic cost owing to its rigid structure.

Acknowledgements: This work was supported by the U.S. Army Medical and Materiel Command under Contract No. DAMD17-97-2-7022, the EU 4th Framework Program in Biotechnology, the Kimmelman Center for Biomolecular Structure and Assembly (Rehovot, Israel), and the Dana Foundation. The generous support of Mrs. Tania Friedman is gratefully acknowledged. I.S. is a Bernstein-Mason Professor of Neurochemistry.

References

- [1] Bartus, R.T., Dean, R.L., Beer, B. and Lipka, A.S. (1982) *Science* 217, 408–414.
- [2] Dunnett, S.B. and Fibiger, H.C. (1993) *Prog. Brain Res.* 98, 413–420.
- [3] Weinstock, M. (1997) *J. Neural Transm.* 49, 93–102.
- [4] Wu, E.S., Griffith, R.C., Loch, J.T., Kover, A., Murray, R.J., Mullen, G.B., Blosser, J.C., Machulski, A.C. and McCreedy, S.A. (1995) *J. Med. Chem.* 38, 1558–1570.
- [5] Brandeis, R., Dachir, S., Sapir, M., Levy, A. and Fisher, A. (1990) *Pharmacol. Biochem. Behav.* 36, 89–95.
- [6] Enz, A., Amstutz, R., Boddeke, H., Gmelin, G. and Malanowski, J. (1993) *Prog. Brain Res.* 98, 431–438.
- [7] Weinstock, M. (1995) *Neurodegeneration* 4, 349–356.
- [8] Jenike, M.A., Albert, M.S., Heller, H., Gunther, J. and Goff, D. (1990) *J. Clin. Psychiatr.* 51, 3–7.
- [9] Zhang, R.W., Tang, X.C., Han, Y.Y., Sang, G.W., Zhang, Y.D., Ma, Y.X., Zhang, C.L. and Yang, R.M. (1991) *Acta Pharmacol. Sin.* 12, 250–252.
- [10] Davis, K.L. and Powchik, P. (1995) *Lancet* 345, 625–630.
- [11] Weinstock, M., Razin, M., Chorev, M. and Enz, A. (1994) *J. Neural Transm.* 43, 219–225.
- [12] Knopman, D.S. (1998) *Neurology* 50, 1203–1206.
- [13] Kawakami, Y., Inoue, A., Kawai, T., Wakita, M., Sugimoto, H. and Hopfinger, A.J. (1996) *Bioorg. Med. Chem.* 4, 1429–1446.
- [14] Kryger, G., Silman, I. and Sussman, J.L. (1999) *Structure* 7, 297–307.
- [15] As reported on the Sanochemia web site, under the information concerning galanthamine, <http://www.sanochemia.at/>.
- [16] Bretagne, M. and Valletta, J. (1965) *Anesth. Analg. (Paris)* 22, 285–292.
- [17] Harvey, A.L. (1995) *Pharmacol. Ther.* 68, 113–128.
- [18] Bystrzanowska, T. (1969) *Wiad Lek* 22, 1233–1239.
- [19] Gujral, V.V. (1965) *Indian Pediatr.* 2, 89–93.
- [20] Thomsen, T. and Kewitz, H. (1990) *Life Sci.* 46, 1553–1558.
- [21] Thomsen, T., Kaden, B., Fischer, J.P., Bickel, U., Barz, H., Gusztony, G., Cervos-Navarro, J. and Kewitz, H. (1991) *Eur. J. Clin. Chem. Clin. Biochem.* 29, 487–492.
- [22] Schrattenholz, A., Pereira, E.F., Roth, U., Weber, K.H., Albuquerque, E.X. and Maelicke, A. (1996) *Mol. Pharmacol.* 49, 1–6.
- [23] Storch, A., Schrattenholz, A., Cooper, J.C., Abdel Ghani, E.M., Gutbrod, O., Weber, K.H., Reinhardt, S., Lobron, C., Hermesen, B., Soskić, V., Pereira, E.F.R., Albuquerque, E.X., Methfessel, C. and Maelicke, A. (1995) *Eur. J. Pharmacol.* 290, 207–219.
- [24] Pereira, E.F., Reinhardt-Maelicke, S., Schrattenholz, A., Maelicke, A. and Albuquerque, E.X. (1993) *J. Pharmacol. Exp. Ther.* 265, 1474–1491.
- [25] Prendergast, M.A., Jackson, W.J., Terry Jr., A.V., Decker, M.W., Arneric, S.P. and Buccafusco, J.J. (1998) *Psychopharmacology (Berl.)* 136, 50–58.
- [26] Arendash, G.W., Sengstock, G.J., Sanberg, P.R. and Kem, W.R. (1995) *Brain Res.* 674, 252–259.
- [27] De Sarno, P. and Giacobini, E. (1989) *J. Neurosci. Res.* 22, 194–200.
- [28] Kem, W.R. (1997) *Invert. Neurosci.* 3, 251–259.
- [29] Lloyd, G.K., Menzaghi, F., Bontempi, B., Suto, C., Siegel, R., Akong, M., Stauderman, K., Velicelebi, G., Johnson, E., Harpold, M.M., Rao, T.S., Sacca, A.I., Chavez-Noriega, L.E., Washburn, M.S., Vernier, J.M., Cosford, N.D. and McDonald, L.A. (1998) *Life Sci.* 62, 1601–1606.
- [30] Newhouse, P.A., Potter, A. and Levin, E.D. (1997) *Drugs Aging* 11, 206–228.
- [31] Wevers, A., Monteggia, L., Nowacki, S., Bloch, W., Schutz, U., Lindstrom, J., Pereira, E.F., Eisenberg, H., Giacobini, E., De Vos, R.A., Steur, E.N., Maelicke, A., Albuquerque, E.X. and Schroder, H. (1999) *Eur. J. Neurosci.* 11, 2551–2565.
- [32] Stein, K. (1996) *Inpharma* 4, 1019.
- [33] Berger, A. (1999) *BMJ* 318, 639.
- [34] Kubinyi, H. (1999) *J. Recept. Signal Transduct. Res.* 19, 15–39.
- [35] Amzel, L.M. (1998) *Curr. Opin. Biotechnol.* 9, 366–369.
- [36] Raves, M.L., Harel, M., Pang, Y.P., Silman, I., Kozikowski, A.P. and Sussman, J.L. (1997) *Nat. Struct. Biol.* 4, 57–63.
- [37] Harel, M., Kleywegt, G.J., Ravelli, R.B., Silman, I. and Sussman, J.L. (1995) *Structure* 3, 1355–1366.
- [38] Mary, A., Renko, D.Z., Guillou, C. and Thal, C. (1998) *Bioorg. Med. Chem.* 6, 1835–1850.
- [39] Otwinowski, Z. (1993) in: *Data Collection and Processing* (Sawyer, L., Isaacs, N. and Bailey, S., Eds.), *Proceedings of the CCP4 Study Weekend 29–30 January 1993*, pp. 56–62, SERC, Daresbury.
- [40] Collaborative Computational Project, Number 4 (1994) *Acta Crystallogr. Sect. D Biol. Crystallogr.* 50, pp. 760–763.
- [41] Brunger, A.T., Adams, P.D., Clore, G.M., DeLano, W.L., Gros, P., Grosse-Kunstleve, R.W., Jiang, J.S., Kuszewski, J., Nilges, M., Pannu, N.S., Read, R.J., Rice, L.M., Simonson, T. and Warren, G.L. (1998) *Acta Crystallogr. D Biol. Crystallogr.* 54, 905–921.
- [42] McRee, D.E. (1999) *J. Struct. Biol.* 125, 156–165.
- [43] Carroll, P., Furst, G.T., Han, S.Y. and Joullie, M. (1990) *Bull. Soc. Chim. Fr.* 127, 769–780.
- [44] Brunger, A.T., Adams, P.D. and Rice, L.M. (1999) *Prog. Biophys. Mol. Biol.* 72, 135–155.
- [45] Burley, S.K. and Petsko, G.A. (1986) *FEBS Lett.* 203, 139–143.
- [46] Levitt, M. and Perutz, M.F. (1988) *J. Mol. Biol.* 201, 751–754.
- [47] Harel, M., Schalk, I., Ehret Sabatier, L., Bouet, F., Goeldner,

- M., Hirth, C., Axelsen, P.H., Silman, I. and Sussman, J.L. (1993) Proc. Natl. Acad. Sci. USA 90, 9031–9035.
- [48] Harel, M., Quinn, D., Nair, H., Silman, I. and Sussman, J. (1996) J. Am. Chem. Soc. 118, 2340–2346.
- [49] Lienhard, G.E. (1973) Science 180, 149–154.
- [50] Collins, K.D. and Stark, G.R. (1971) J. Biol. Chem. 246, 6599–6605.
- [51] Fersht, A.R. (1977) Enzyme Structure and Mechanism, W.H. Freeman, Reading.
- [52] Liu, J.-S., Zhu, Y.-L., Yu, C.-M., Zhou, Y.-Z., Han, Y.-Y., Wu, F.-W. and Qi, B.-F. (1986) Can. J. Chem. 64, 837–839.
- [53] Ashani, Y., Peggins, J.O. and Doctor, B.P. (1992) Biochem. Biophys. Res. Commun. 184, 719–726.
- [54] Merritt, E.A. and Bacon, D.J. (1997) Methods Enzymol. 277, 505–524.
- [55] Sanner, M.F., Olson, A.J. and Spehner, J.C. (1996) Biopolymers 38, 305–320.
- [56] Phillippsen, A. (1999) DINO: Visualizing Structural Biology, <http://www.bioz.unibas.ch/~xray/dino>.
- [57] POV-ray-Team® (1998) POV-ray, www.povray.org.

Reaction Products of Acetylcholinesterase and VX Reveal a Mobile Histidine in the Catalytic Triad

Charles B. Millard,* Gertraud Koellner,[†] Arie Ordentlich,[‡] Avigdor Shafferman,[‡] Israel Silman, and Joel L. Sussman

Departments of Structural Biology and Neurobiology
The Weizmann Institute of Science
Rehovot 76100 Israel, Israel Institute for Biological Research
Ness Ziona 70450 Israel

Received July 30, 1999

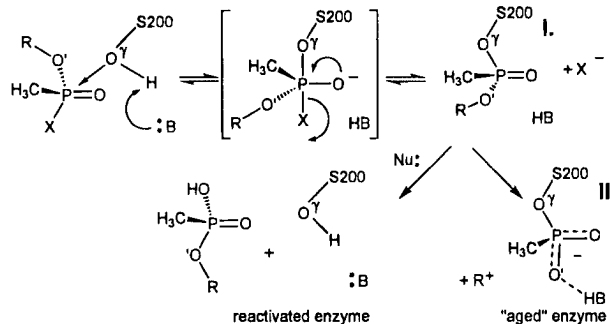
The presence of a precisely aligned active-site triad (Ser-His-Asp/Glu) in the three-dimensional structures of widely different hydrolytic enzymes has generated intense interest in the chemical *modus operandi* of this catalytic motif.¹ One hypothesis, which has not received wide acceptance, proposes that the imidazole of the catalytic His is mobile during enzyme function.² We solved the structures of the phosphorylation and dealkylation (“aging”) reaction products of acetylcholinesterase (AChE; EC 3.1.1.7) and an organophosphorus (OP) inhibitor, *O*-ethyl-S-[2-bis(1-methylethyl)amino]ethyl methylphosphonothioate (VX) by X-ray crystallography. The structures clearly demonstrate reversible movement of the catalytic His. Moreover, the conformational change apparently involves a hydrogen (H—) bond with a glutamate (E199) which had been implicated previously in OP and substrate reactions.

Most serine hydrolases, including AChE, use a catalytic triad and a dipolar oxyanion hole in tandem to catalyze substrate hydrolysis via an acylation–deacylation mechanism.³ This two-step mechanism is also a weakness, however, because it renders the enzyme susceptible to stoichiometric inhibition by “hemi-substrates” which react to form stable analogues of natural reaction intermediates. Following phosphorylation of the active-site Ser O γ , some OP–enzyme adducts undergo further post-inhibitory reactions, including dealkylation, which result in truly irreversible enzyme inhibition (collectively called “aging”) (Scheme 1).

Structures of the reaction products of *Torpedo californica* (Tc) AChE with DFP, sarin or soman⁴ after aging reveal that the OP undergoes dealkylation to yield a stable anionic phosphonyl adduct.⁵ As reported previously for aged OP–serine proteases,⁶ the catalytic imidazole (H440) of TcAChE is positioned to form H-bonds with its normal carboxylic acid partner (E327), and with one oxygen of the negatively charged phosphonyl moiety. Such structures are limited, however, because they reveal only the final product (II) of the OP reaction. To overcome this limitation, we employed VX. Although phosphorylation of AChE with VX is rapid ($>10^7$ M⁻¹ min⁻¹), the ethyl group of VX dealkylates slowly, thus allowing us to solve the structures of both (I) and (II) by conventional X-ray crystallography to 2.2 and 2.4 Å resolution, respectively.⁷

The most striking feature of the pro-aged VX–AChE structure (I) was disruption of the catalytic triad due to movement of H440. The H440 N δ was 4.5 Å away from its resting state partner, E327

Scheme 1. OP Reaction with Serine Hydrolases^a



^a The OP undergoes nucleophilic attack by a reactive Ser (represented here by S200 O γ of TcAChE) assisted by a general base (probably H440 N ϵ 2 for TcAChE) in the enzyme active site; the leaving group, X, is expelled, and a stable tetrahedral adduct (I) is formed. The adduct can undergo further reactions (“aging”); R is an alkyl group that departs during aging with some OPs, perhaps via a carbonium ion (R⁺). Prior to aging, a properly positioned nucleophile (Nu⁻), such as an hydroxyl ion or oxime, can catalyze slow dephosphorylation of I to regenerate free enzyme (reactivation).

O ϵ , and within H-bond distance (2.7 Å) of E199 O ϵ (Figure 1). The observed uncoupling of the catalytic triad offers a new explanation for the slow, often negligible spontaneous reactivation of the VX–AChE adduct. Movement of the imidazole was reversible, however, because the catalytic triad could be restored by either: (1) dephosphorylation with a nucleophile (reactivation) or (2) dealkylation of the VX *O*-ethyl group (aging). To confirm that active enzyme could be regenerated from the alternate conformation, VX–TcAChE crystals were dissolved in phosphate buffer (pH 7.5), incubated for 20 h with 10 mM pralidoxime, and AChE activity then measured.⁸ Oxime-reactivated VX–TcAChE was indistinguishable from native enzyme with respect to substrate kinetics, corroborating that the H440 movement caused by phosphorylation was reversed upon dephosphorylation.

Alternatively, if crystalline VX–TcAChE was allowed to age completely (II), the H440 imidazole moved to a position close to that found in native TcAChE. The aged adduct was essentially identical to those solved previously for sarin or soman,⁵ and the catalytic H440–E327 pair had reverted to its native conformation (Figure 1).

Functional Significance for the Glu327–His440–Glu199 Array in AChE. Site-specific replacement of E199 with Q reduces the rate constant for aging approximately 100-fold.⁹ Furthermore, the pH dependence of OP–AChE aging follows an asymmetric bell curve with a maximum rate at pH 6, and three apparent pK_a's which implicate two carboxylic acids (4.0–4.9) and an imidazole (5.2–6.6).¹⁰ Mechanistic hypotheses of the aging reaction, therefore, have centered upon the role of E199.¹¹

The VX–TcAChE structures, obtained near the optimal pH for aging, provide the first evidence that H440 is mobile in

* Author for correspondence. E-mail: limill@sgjs8.weizmann.ac.il. Present address: U.S. Army Medical Research Institute of Infectious Diseases, 1425 Porter Street, Fort Detrick, MD 21702-5011.

[†] Present address: Free University of Berlin, Takustrasse 6, D-14195, Berlin, Germany.

[‡] Israel Institute for Biological Research.

(1) Reviewed in Dodson, G.; Wlodawer, A. *Trends Biochem. Sci.* **1998**, *23*, 347–352.

(2) (a) Satterthwait, A. C.; Jencks, W. P. *J. Am. Chem. Soc.* **1974**, *96*, 7018–7031. (b) Bachovchin, W. W. *Biochemistry* **1986**, *25*, 7751–7759.

(3) Kraut, J. *Annu. Rev. Biochem.* **1977**, *46*, 331–358.

(4) DFP, diisopropylphosphorofluoridate; sarin, *O*-isopropylmethylphosphonofluoridate; soman, *O*-pinacolyl methylphosphonofluoridate.

(5) Millard, C. B.; Kryger, G.; Ordentlich, A.; Greenblatt, H. M.; Harel, M.; Raves, M. L.; Segall, Y.; Barak, D.; Shafferman, A.; Silman, I.; Sussman, J. *Biochemistry* **1999**, *38*, 7032–7039.

(6) Kossiakoff, A. A.; Spencer, S. A. *Nature* **1980**, *288*, 414–416.

(7) Coordinates and details of data collection and refinement are available from the Protein Databank under accession codes 1vxr (pro-aged adduct) and 1vxo (aged adduct). Briefly, crystals of space group P3₁21 were prepared in PEG-200, pH 6.0, and data were collected at 100 K with synchrotron radiation at Elettra, Trieste (1vxr) or Brookhaven National Laboratory, NY (1vxo). All crystals were isomorphous with native TcAChE (2ace); see ref 5 and Sussman, J. L.; Harel, M.; Frolow, F.; Oefner, C.; Goldman, A.; Tokar, L.; and Silman, I. *Science* **1991**, *253*, 872–879. The final *R*-factors were 18.9% (1vxr) and 19.4% (1vxo), and the free-*R*-factors were 23.0% (1vxr) and 23.4% (1vxo).

(8) The substrate was acetylthiocholine and enzyme activity was measured by the method of Ellman, G. L.; Courtney, K. D.; Andres, V.; Featherstone, R. M. *Biochem. Pharmacol.* **1961**, *7*, 88–95.

(9) (a) Ordentlich, A.; Kronman, C.; Barak, D.; Stein, D.; Ariel, N.; Marcus, D.; Velan, B.; Shafferman, A. *FEBS Lett.* **1993**, *334*, 215–220. (b) Saxena, A.; Doctor, B. P.; Maxwell, D. M.; Lenz, D. E.; Radic, Z.; Taylor, P. *Biochem. Biophys. Res. Commun.* **1993**, *197*, 343–349.

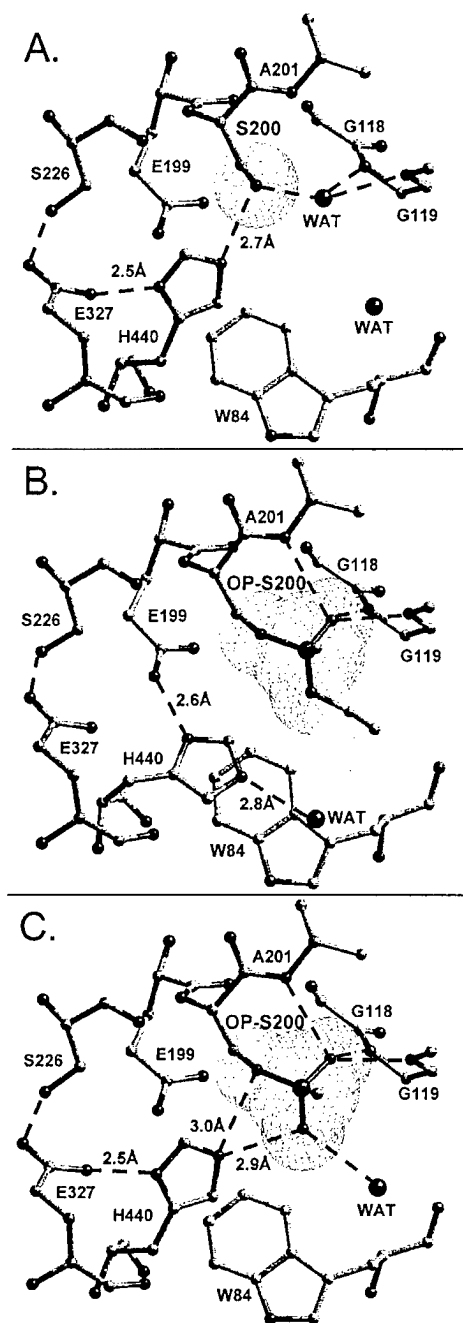


Figure 1. Structural kinetic of VX inhibition of *TcAChE* by X-ray crystallography at pH 6.0. The active site of *TcAChE* is depicted with possible H-bonds involving the catalytic triad and the OP moiety (broken lines). Panel A (native structure) shows the active site, including the catalytic triad (S200–H440–E327) and the oxanion hole (–NH of G118, G119, and A201). Note that two water molecules (WAT) are displaced by the OP. Panel B (pro-aged structure): Phosphorylation triggers a conformational change for H440 that disrupts the H-bond to E327; this may be caused by steric crowding in the pentavalent phosphorus transition state, or by re-distribution of charge on the H440 imidazolium during phosphorylation. Note that E199 and a water (WAT) apparently stabilize the alternate conformation of H440. Subsequently, the H440 imidazole catalyzes either dealkylation (aging), or spontaneous reactivation (Scheme 1). Panel C (aged structure): For reaction of AChE with VX and most phosphonates, aging predominates, and dealkylation results in movement of H440 to the negatively charged pocket formed by E327 O ϵ , S200 O γ , and one anionic oxygen of the dealkylated OP.

phosphonate adducts of AChE and strongly suggest a cooperative role for E199. It appears that the side chain of H440 rotates around

its χ^1 - and χ^2 -angles to move between the carboxylic acids of E327 and E199 (Figure 1). A tripartite array, E327–H440–E199, probably persists through much of the span of this motion; this array may be a structural device for orienting the imidazole according to the steric and electrostatic features of the ligand bound to S200. Thus, we propose that the two VX–*TcAChE* structures (pro-aged and aged) reveal the H440 imidazole trapped in the extreme positions of a continuous, reversible path.

The AChE E199Q mutation was found to reduce k_{cat}/K_m for hydrolysis of optimal ester substrates by 10- to 100-fold,⁹ and recent Brownian dynamics simulations have attributed this effect partly to electrostatic stabilization of H440 by E199 during acylation.¹² In addition, Quinn and colleagues proposed a “cryptic catalytic mechanism” that relies upon E199 during hydrolysis of certain relatively slow-reacting carboxyl ester substrates.¹³ Although we do not know yet if the mobility of H440 extends to substrate reactions, the widely conserved presence of the E327–H440–E199 array in divergent cholinesterases is consistent with a role in carboxyl ester catalysis.

Comparison with Serine Proteases. The possibility of a mobile catalytic histidine in selected serine protease reactions has been demonstrated and discussed previously.^{2b,14} The crystal structure of diethoxyphosphorylated chymotrypsin (analogous to **I** in Scheme 1) showed no movement of the catalytic His,¹⁵ but reaction of α -lytic protease with a more selective phosphonate substrate analogue showed a large movement of H57.¹⁴ Nevertheless, the prevailing view remains that the His–Asp/Glu pair is H-bonded throughout catalysis, and most structures of serine hydrolases bound to transition state analogue inhibitors support this conclusion.

Structural differences in the active-site suggest to us that *TcAChE* H440 has greater mobility than does the catalytic His found in many serine proteases: (1) flexibility of the longer Glu side chains in the E327–H440–E199 array of AChE should facilitate a larger span of motion for the imidazole than is possible with the Asp residue in the catalytic triad of serine proteases; (2) the handedness of the serine protease triad is opposite to that of AChE, which places the Asp analogous to *TcAChE* E199 on the opposite side of the OP and too far away to interact with the catalytic His;^{11a} and (3) interatomic distances in the crystal structures imply that many serine proteases possess a stabilizing H-bond between the catalytic His C ϵ 1 and a nearby main-chain carbonyl oxygen,¹⁶ but this distance is consistently too long for an optimal H-bond in *TcAChE*.

The VX–*TcAChE* structures demonstrate that two buried acids in an active-site quartet (Ser–His(–Glu)–Glu) modulate the catalytic imidazole position during reaction with a rapid OP “hemi-substrate.” Structural flexibility may underlie the biological persistence of the catalytic triad motif, and offers a new hypothesis for how AChE hydrolyzes such a wide range of substrates, including bulky carboxyl esters, amides, carbamates and, to a limited extent, OPs, in a sterically congested and buried active site.

Acknowledgment. The work was supported by the U.S. Army (agreements DAMD17-97-2-7022 and 17-96-C-6088) and Minerva Foundation, Munich.

JA9927041

(10) Saxena, A.; Viragh, C.; Frazier, D. S.; Kovach, I. M.; Maxwell, D. M.; Lockridge, O.; Doctor, B. P. *Biochemistry* **1998**, *37*, 15086–15096.

(11) (a) Bencsura, A.; Enyedy, I. Y.; Kovach, I. M. *J. Am. Chem. Soc.* **1996**, *118*, 8531–8541. (b) Shafferman, A.; Ordentlich, A.; Barak, D.; Stein, D.; Ariel, N.; Velan, B. *Biochem. J.* **1996**, *318*, 833–840.

(12) Wlodek, S. T.; Antosiewicz, J.; Briggs, J. M. *J. Am. Chem. Soc.* **1997**, *119*, 8159–8165.

(13) Selwood, T.; Feaster, S. R.; States, M. J.; Pryor, A. N.; Quinn, D. M. *J. Am. Chem. Soc.* **1993**, *115*, 10477–10482.

(14) Bone, R.; Sampson, N. S.; Bartlett, P. A.; Agard, D. A. *Biochemistry* **1991**, *30*, 2263–2272.

(15) Harel, M.; Su, C.-T.; Frolov, F.; Ashani, Y.; Silman, I.; Sussman, J. L. *J. Mol. Biol.* **1991**, *221*, 909–918.

(16) Derewenda, Z. S.; Derewenda, U.; Kobos, P. M. *J. Mol. Biol.* **1994**, *241*, 83–93.

A Modular Treatment of Molecular Traffic Through the Active Site of Cholinesterase

Simone A. Botti^{*#}, Clifford E. Felder^{*}, Shneior Lifson[§], Joel L. Sussman^{*} and Israel Silman[#]

Departments of ^{*}Structural Biology, [#]Neurobiology, and [§]Chemical Physics Weizmann Institute of Science, Rehovot 76100, Israel

ABSTRACT We present a model for the molecular traffic of ligands, substrates, and products through the active site of cholinesterases (ChEs). First, we describe a common treatment of the diffusion to a buried active site of cationic and neutral species. We then explain the specificity of ChEs for cationic ligands and substrates by introducing two additional components to this common treatment. The first module is a surface trap for cationic species at the entrance to the active-site gorge that operates through local, short-range electrostatic interactions and is independent of ionic strength. The second module is an ionic-strength-dependent steering mechanism generated by long-range electrostatic interactions arising from the overall distribution of charges in ChEs. Our calculations show that diffusion of charged ligands relative to neutral isosteric analogs is enhanced ~ 10 -fold by the surface trap, while electrostatic steering contributes only a 1.5- to 2-fold rate enhancement at physiological salt concentration. We model clearance of cationic products from the active-site gorge as analogous to the escape of a particle from a one-dimensional well in the presence of a linear electrostatic potential. We evaluate the potential inside the gorge and provide evidence that while contributing to the steering of cationic species toward the active site, it does not appreciably retard their clearance. This optimal fine-tuning of global and local electrostatic interactions endows ChEs with maximum catalytic efficiency and specificity for a positively charged substrate, while at the same time not hindering clearance of the positively charged products.

INTRODUCTION

Cholinesterases (ChEs) are a family of enzymes that fall broadly into two types: acetylcholinesterase (AChE) and butyrylcholinesterase (BChE). They are distinguished primarily by their substrate specificity: AChE hydrolyzes the natural neurotransmitter acetylcholine (ACh) faster than choline esters with bulkier acyl chains; thus it is much less active on the synthetic substrate, butyrylcholine (BCh). In contrast, BChE displays similar activity toward the two substrates (Chatonnet and Lockridge, 1989).

Vertebrates contain both AChE and BChE, which probably originate from the duplication of a single ChE gene (Massoulié et al., 1993). Insects possess a single ChE gene coding for an enzyme with a specificity intermediate between those of AChE and BChE (Massoulié et al., 1993; Taylor and Radic, 1994), while in certain nematode species, up to four ChE genes have been identified (Grauso et al., 1998). The principal physiological function of AChE has long been known to be termination of impulse transmission at cholinergic synapses by rapid hydrolysis of ACh, but the biological role of BChE is still an open question (Chatonnet and Lockridge, 1989).

ChEs are able to catalyze the rapid breakdown of a variety of esters, both cationic and neutral (Quinn, 1987). The highest catalytic rate is displayed by AChE hydrolysis of ACh, at a rate approaching the diffusion-controlled limit

(Rosenberry, 1975b; Hasinoff, 1982; Bazelyansky et al., 1986). This efficiency is a common characteristic of ChEs. A tally of the bimolecular rate constants (k_{cat}/K_M) among ChEs for their best substrates shows a spread of less than an order of magnitude. Values range from $1.6 \times 10^8 \text{ M}^{-1} \text{ s}^{-1}$, for hydrolysis of ACh by *Electrophorus electricus* AChE (EeAChE) (Rosenberry, 1975a), to $4.0 \times 10^7 \text{ M}^{-1} \text{ s}^{-1}$ for BChE hydrolysis of both ACh and BCh (Vellom et al., 1993).

Catalytic efficiency of ChEs for neutral substrates is also very high. Values of k_{cat}/K_M for hydrolysis by AChE of ACh and of its neutral isoster 3,3-dimethylbutylacetate (DBA) do differ by ~ 40 -fold at physiological salt concentration (Hasan et al., 1981), but there is evidence that the hydrolysis of the thio analog of DBA is also diffusion-controlled (Bazelyansky et al., 1986). Moreover, it has been shown that BChE turns over *o*-nitrophenyl butyrate (*o*-NPB) faster than it breaks down butyrylthiocholine (Masson et al., 1997).

Studies of the pH and charge dependence of catalytic hydrolysis of substrates and of binding of reversible inhibitors suggested that the active site of ChEs contains two major subsites, the "esteratic" and the "anionic" (Wilson and Bergmann, 1950), corresponding, respectively, to the catalytic machinery and the choline-binding pocket (Froede and Wilson, 1971). The high bimolecular association constants for cationic ligands and their ionic strength dependence suggested a high charge density in the active site. This led to the prediction that up to nine negative charges were present in the "anionic" site (Rosenberry and Neumann, 1977; Nolte et al., 1980). A second "anionic" site, which became known as the "peripheral" anionic site (PAS), was proposed based on binding of bis-quaternary

Received for publication 4 September 1998 and in final form 23 July 1999.

Address reprint requests to Dr. Simone A. Botti, Department of Structural Biology, Weizmann Institute of Science, 76100 Rehovot, Israel. Tel.: 972-8-934-3759; Fax: 972-8-934-4159; E-mail: simone.botti@weizmann.ac.il.

© 1999 by the Biophysical Society

0006-3495/99/11/2430/21 \$2.00

ammonium compounds (Bergmann et al., 1950). Binding of ligands to the peripheral anionic site causes inactivation of the enzyme, though the mechanism of inhibition is not clear. It has been speculated that the PAS is involved in the phenomenon of substrate inhibition and activation through binding of a second substrate molecule. Its function may involve either allosteric modification of the active site (Radic et al., 1991; Shafferman et al., 1992; Barak et al., 1995) or alteration of the traffic of substrate and products by blocking access to the catalytic machinery (Berman and Nowak, 1992; Haas et al., 1992; Schalk et al., 1992). In addition, there is evidence for an involvement of the PAS in functions distinct from catalysis. Recent studies have presented evidence for a role of the PAS of AChE in neurite regeneration and outgrowth (Layer et al., 1993; Willbold and Layer, 1994; Jones et al., 1995; Srivatsan and Peretz, 1997) and in the growth and differentiation of spinal motor neurons (Bataillé et al., 1998).

Catalysis by ChEs occurs by a mechanism similar to that of the serine proteases, via an acyl-enzyme intermediate. It is assumed to involve a tetrahedral transition state produced by nucleophilic attack on the substrate by a serine, followed by general-base catalysis assisted by a histidine. The transition state subsequently collapses to the acyl-enzyme by general-acid-catalyzed expulsion of choline (Quinn, 1987). Solution of the three-dimensional (3D) structure of AChE from *Torpedo californica* (TcAChE) (Sussman et al., 1991) was followed by determination of the crystal structures of several complexes of AChE with specific inhibitors (Harel et al., 1993, 1995, 1996). Analysis of these structures, taken together with systematic site-directed mutagenesis studies (Radic et al., 1991, 1993; Shafferman et al., 1992; Barak et al., 1995), has permitted identification of the key functional residues in the active site and contributed to clarification of their role in recognition of substrates and inhibitors. (A comprehensive and updated list of references for cholinesterase mutants can be obtained through the ESTHER server, <http://meleze.ensam.inra.fr/cholinesterase> (Cousin et al., 1997).) It has thus been possible to construct a picture of the structural factors governing both the mechanism and specificity of ChEs. At the same time the data obtained have given rise to a new set of still unanswered questions.

The structure/function relationships that have emerged over the past seven years paint a picture of a family of rapid enzymes specific for cationic substrates that have evolved to very high catalytic efficiency by adopting some rather counterintuitive solutions. The active-site serine of TcAChE, S200, was unexpectedly found to be located near the bottom of a 24-Å-deep gorge, ~4.4 Å wide at its narrowest point and 8.0 Å wide at its mouth. This serine forms a catalytic triad with H440 and E327. [Residue numbers follow the guidelines established at the 1992 OHOLO meeting, Eilat (Massoulié et al., 1993). The numbering used is that of the sequence of TcAChE. When species-specific numbers are employed, the homologous position in TcAChE will follow, printed in italics and appearing in parentheses.] Contrary to the assumption of a concentration of negative charges

within the active site (Nolte et al., 1980), no more than two formal negative charges were found near the active site serine (E199 and E443). In fact, the walls of the gorge were found to be lined by the side-chains of 14 conserved aromatic residues (Sussman et al., 1991). In analogy to studies of ACh binding to model hosts (Dougherty and Stauffer, 1990), it was suggested that the binding of ACh to the sites within the gorge involved in substrate recognition is stabilized by interactions between the quaternary ammonium group of ACh and the π electrons of some of the conserved aromatic residues of AChE. This hypothesis was confirmed by inspection of the structures of complexes of AChE with various quaternary inhibitors (Harel et al., 1993). Analysis of the 3D structure of the complex of AChE with the transition-state analog, *m*-trimethylammonium trifluoroacetophenone (TFK⁺), has highlighted the specific intermolecular interactions between the substrate and the active site that are responsible for the catalytic efficacy of AChE. These structural data suggest that the particular active-site configuration of AChE allows the enzyme to efficiently sequester the acylation transition state in a preorganized polar environment formed by the oxyanion hole, consisting of the main-chain N-H dipoles, G118, G119, and A201, and the side chains of key aromatic residues such as W84 and F330 (Harel et al., 1996). This environment is able to stabilize the catalytic transition state by providing it with larger electrostatic stabilization than in the solvent and is the basis of the catalytic power of the ChEs (Fuxeiter and Warshel, 1998).

Inspection of the overall 3D structure of TcAChE revealed a marked asymmetrical surface distribution of charged residues. These residues were shown to segregate roughly into a "northern" negative hemisphere, considering the mouth of the gorge as the north pole, and a "southern" positive one, giving rise to a large "dipole moment" roughly oriented along the axis of the active-site gorge (Ripoll et al., 1993; Tan et al., 1993; Antosiewicz et al., 1994; Felder et al., 1997). The magnitude of this "dipole moment" was estimated, by electrooptical measurements on *Bungarus fasciatus* AChE (BfAChE), to be ~1000 Debyes (Porschke et al., 1996). The biological significance of these unusual electrostatic properties has been the subject of much controversy. It has been suggested that the "macro-dipole" might act to steer cationic ligands to the mouth of the gorge (Sussman et al., 1991; Tan et al., 1993), where they would bind to the aromatic residues lining it and subsequently be committed to moving down the gorge, toward the active site, in a fashion similar to that of an affinity column (Sussman et al., 1991). Calculations of the rates of encounter of charged ligands and substrates based on Brownian dynamics (BD) simulations predicted that the electrostatic properties of AChE would be responsible for a rate enhancement of up to 240-fold (Zhou et al., 1996). The possibility of a large electrostatic steering effect on positively charged substrates has raised the question of the route of clearance of choline (Ch), the cationic product of enzy-

matic hydrolysis, which would seem to be trapped at the bottom of the gorge by a strong electric field.

Molecular dynamics (MD) simulations have suggested that an alternative route of access to the active site might open via the concerted movement of residues W84, V129, and G441 (Gilson et al., 1994), while a more recent MD study has identified a number of "side entrances" to the gorge, all involving concerted movements of a number of side chains in the Ω loop (C67–C92) of AChE (Wlodek et al., 1997b). As yet, no simple and predictive model for the clearance of the products of hydrolysis of ACh or BCh has been introduced into the treatment of the molecular traffic of substrates and ligands through the active site of ChEs.

The importance of electrostatic interactions in the steering of cationic substrates to the active site of ChEs was challenged by a study of a series of mutants of human recombinant AChE (hAChE), in which up to seven negative residues around the outer rim of the gorge were neutralized, thus substantially reducing the magnitude of the "macro-dipole," without producing large changes in the second-order hydrolysis rate constant (Shafferman et al., 1994). The contradiction between data documenting the electrostatic properties of ChEs and the apparent lack of correlation between their experimental modification and a major catalytic effect has been the topic of various studies. Antosiewicz and co-workers (Antosiewicz et al., 1994, 1995a,b, 1996; Antosiewicz and McCammon, 1995) have attempted to correlate the electrostatic properties of AChE with the on rates for charged ligands and the second-order hydrolysis rate constants. The picture emerging from their work supports the existence of an electrostatic steering effect in ChEs. Moreover, calculations performed by the same group, on structural models of the mutants analyzed kinetically by Shafferman et al. (1994), account for the small changes in catalytic rates observed. This reconciles the hypothesis of a role for electrostatics in accelerating the encounter between the enzyme and reactive species with experimental data that seemed to argue against it (Antosiewicz et al., 1995b). Nevertheless, these studies were unable to strongly correlate experimental results with any one particular aspect of the electrostatic properties of the ChEs, since neither the total charge nor the dipole moment fully accounted for the electrostatic steering of ligand to the active site.

Calculations of the potential gradient along the axis of the gorge and of its dependence on salt concentration have been performed both for wild-type (WT) AChE of different species and for a series of surface and active-site mutants (Antosiewicz et al., 1995b; Wlodek et al., 1997a; Felder et al., 1997). These calculations have revealed that AChEs display a similar negative potential gradient, beginning several angstroms outside the gorge entrance, and continuing down the gorge toward the active site. This potential is not correlated with ChE surface charge distribution, but is due to a combined effect of the overall charge distribution in the ChE molecule, including the effect of several α -helix dipoles. The results of these studies suggest the existence of a

long-range electrostatic interaction, attributable to this potential gradient, that contributes to both the enhancement of encounter rates between cationic ligands and the catalytic machinery buried at the bottom of the active-site gorge of ChEs. Radic et al. (1997) have performed a detailed analysis of the influence of electrostatics on the kinetics of ligand binding to AChE. This study focused on the ionic-strength dependence of the binding of reversible inhibitors to AChE after neutralization, by site-directed mutagenesis, of anionic side chains in the surface area around the entrance to the active-site gorge, in the PAS and in the active center. Comparison of the experimental data to BD simulations of the on rates of the ligands revealed good agreement for surface mutants, while predictions were less accurate when some key residues in the PAS were neutralized. The results were interpreted in the framework of two distinct types of electrostatic interactions: the first, dependent on salt concentration, causing acceleration of the initial encounter rates of cationic ligands with the enzyme, and the second, independent of salt concentration, resulting in trapping of these ligands by specific residues in the PAS or within the active site. The presence of a trap for cationic ligands in AChE and BChE has been proposed in several other studies (Rosenberry and Neumann, 1977; Hasinoff, 1982; Hosea et al., 1996; Masson et al., 1996, 1997), but no analytical and quantitative treatment of the effect of a trapping surface on the encounter rate of cationic ligands with the ChEs has been advanced until now.

In the following sections we will present a model for the molecular traffic of neutral and cationic ligands, substrates, and products through the active site of ChEs, and we will evaluate the contributions of electrostatic interactions to the traffic of cationic species.

First, we will illustrate a common treatment for the diffusion of both neutral and cationic ligands toward an enzyme characterized by a buried active site. Subsequently, we will show how the specificity of ChEs for cationic ligands and substrates can be treated by introducing two additional modules to this common treatment:

1. A module that incorporates the effects of short-range and ionic strength *independent* interactions between key residues in the area of the entrance to the active-site gorge and the quaternary ammonium moiety of cationic substrates and ligands. This local module will be shown to describe the effects of a putative trapping mechanism for cationic species. The effect of this surface trap on the enhancement of encounter rates between cationic ligands and ChEs will be analyzed quantitatively by correlating the electrostatic potentials in the area surrounding the entrance to the active-site gorge with the experimentally measured encounter rates of cationic ligands with ChEs.
2. A module that incorporates the effects of long-range and ionic-strength *dependent* interactions. This global module, which is shown to describe the steering of cationic substrates and ligands to the gorge floor, can be analyzed quantitatively by evaluating the overall electric potential

around the entrance and within the active-site gorge and its dependence on ionic strength.

The clearance of positively charged products and ligands from the active-site gorge will be considered as analogous to the Brownian migration of a charged particle out of a one-dimensional box against an electrostatic potential linear in distance along the length of the box. For neutral molecules, the value of this potential will be set to zero, while for charged species we will introduce values of the gorge potential either derived from experimental data or calculated with the Poisson-Boltzmann equation (PB).

This modular approach will enable us to rationalize the apparent paradox of electric fields, which act to steer cationic species toward the active site while at the same time not hindering the clearance of positively charged products. The results obtained will be used to discuss the mechanisms involved in the emergence of the specificity of ChEs for cationic substrates from the framework of an already very efficient catalytic machinery for the hydrolysis of small esters.

METHODS: ELECTROSTATIC CALCULATIONS AND HOMOLGY MODELS

We calculated the electrostatic potential along the active-site gorge of ChEs, by solving the PB equation, to study the influence on gorge electrostatic potentials of salt concentration and of the neutralization of a number of key residues in the area of the surface cationic trap and in the active-site gorge. The electrostatic calculations were performed on the following enzymes (where crystallographic coordinates are available, the PDB ID code will follow in parentheses): AChE from the following species: *Torpedo californica* (TcAChE-PDB ID: 2ACE), mouse (mAChE-PDB ID 1MAH), *Bungarus fasciatus* (BfAChE), *Drosophila melanogaster* (DmAChE), and human (hAChE); and human BChE (hBChE). Where the crystallographic coordinates were not available, homology models were constructed. The residues to be mutated were chosen on the basis of their presumed involvement in the recognition of cationic substrates and in the contribution to the steering of cationic ligands toward the active site of ChEs (Shafferman et al., 1992, 1994; Radic et al., 1993, 1995; Barak et al., 1995; Masson et al., 1996; Ordentlich et al., 1996). Three classes of mAChE mutants, as shown in Table 1, were generated by homology modeling from the respective WT structures. The positions of these mutations on the 3D fold of ChE are illustrated in Fig. 1. In the first class, based on the studies of Shafferman et al. (1994) and Radic et al. (1997), we generated five mutant structures in which up to seven acidic residues on the enzyme surface near the gorge entrance were neutralized. In the second and third classes, the mutations focused on the modification of residues in the area of the cationic trap and at the bottom of the gorge, respectively, to analyze the correlation between local and overall electrostatic potentials and the encounter rates of cationic ligands and substrates.

Construction of homology models

In brief, models were constructed by use of the automated knowledge-based model-building tool resident on the Swiss-Model Server (Peitsch, 1996) (http://www.expasy.ch/swissmod/SWISS_MODEL.html), employing 3D structures of TcAChE (PDB ID 2ACE, 1ACJ, 1FSS) and mAChE (PDB ID 1MAH) as templates. The automatic procedure involved alignment of the sequence to be modeled with the template sequences, by application of the BLAST algorithm (Altschul et al., 1990). Regions of sequence similarity were automatically selected and employed to build a framework for the model structure. Missing loops were automatically

TABLE 1 List of mAChE mutants employed in this study

mAChE surface mutants	
D275V (D280V)	
D275V/D278N (D280V/D283N)	
E82Q/E89Q/D275V/D278N (E84Q/E91Q/D280V/D283N)	
E82Q/E89Q/D275V/D278N/D365N (E84Q/E91Q/D280V/D283N/E372N)	
E82Q/E89Q/D275V/D278N/E285Q/D365N (E84Q/E91Q/D280V/D283N/E292Q/E372N)	
mAChE trap mutants	
D72N (D74N)	
D72N/D275V/D278N (D74N/D280V/D283N)	
mAChE gorge mutant	
E199Q (E202Q)	

TcAChE numbering is employed. The mAChE numbering follows in parentheses and italics.

constructed by searching the PDB database, employing either the best fitting fragment corresponding to the sequence or a framework constructed by the average of the five best fragments. The last step of the procedure involved automated rebuilding of side chains, verification of the quality of the model, and refinement of the final structure by energy minimization and molecular dynamics. The models were then checked again manually, and any missing part that was not successfully built automatically was added manually as described previously (Felder et al., 1997).

Calculation of electrostatic potentials along the active-site gorge

The electrostatic potential along the active-site gorge was calculated by generating a string of dummy atoms at 1-Å intervals along the gorge axis (Fig. 1) and evaluating the electric potential for the position of each dummy atom. The axis of the active-site gorge in the structures examined was defined as extending from atom I444-CD (gorge bottom) to the center of mass of atoms E73-CA, N280-CB, D285-CG, and L333-O (gorge entrance) (Antosiewicz and McCammon, 1995). The portion of the gorge extending from the bottom to S200-OG was defined as the binding region (~4 Å long), and the remainder as the transit region (~20 Å long). The width of the gorge mouth was measured by taking the average of the values of gorge radii originating from the center of mass of atoms E73-CA, N280-CB, D285-CG, and L333-O and intersecting the gorge rim at the CB atoms of residues D72, W279, D273, and D365. To study the local electrostatic potentials generated in the gorge by the residues involved in the cationic trap, we defined a region of the gorge extending from its mouth (as defined above) to a depth of 6 Å. The value of the electrostatic potential along this portion of the axis was then averaged and taken as a measure of the local potential in the trap region.

The PB equation was solved by the finite-difference method (Warwicker and Watson, 1982), using the QDIFFXS algorithm of version 3.0 of DelPhi (Gilson and Honig, 1988; Honig and Nicholls, 1995). A grid of up to 90 Å³ was used. Calculations were performed, using an initial coarser grid with a 35-Å border and 1.45-Å grid spacing and subsequently focusing onto a second grid with a 10-Å border and 0.89-Å spacing. The internal and external dielectric constants were fixed at values of 2 and 80, respectively. Calculations were performed for salt concentrations of 5, 145, and 670 mM. The Stern ion exclusion layer was set at 2 Å, and the dielectric boundary between protein and solvent was constructed using a probe radius of 1.4 Å. Calculations were performed at 298.15 K and pH 7.0, using the Parse partial atomic charge and radius set (Sitkoff et al., 1994). The protonation states of the ionizable amino acids were assigned by examination of the solvent accessibility of their side chains in the 3D structure.

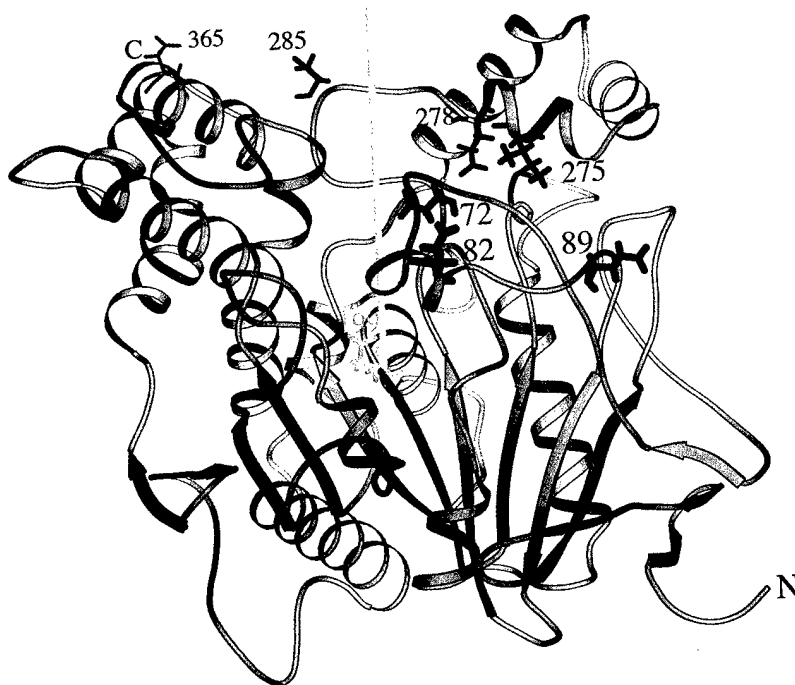


FIGURE 1 Ribbon diagram of AChE showing the relative positions of the mutated residues. The axis of the gorge is indicated by the yellow bar; the side chains of the surface mutants are colored in red; E199, at the bottom of the gorge, is in green; and D72, the main component of the cationic trap, is in purple.

On the basis of this analysis, all Glu, Asp, Lys, and Arg residues were set to be fully ionized, and the average charge on the active-site H440 and on all other histidines was set to zero (M. K. Gilson, personal communication). Potential values are expressed in kT/e units ($1 kT/e = 25.6 \text{ mV} = 0.593 \text{ kcal/mol/e}$).

RESULTS AND DISCUSSION

Because our study focuses on providing a model for the diffusive and binding events occurring before and after the bond rearrangement and cleavage steps of catalysis, the experimental parameters best suited for comparison with our model are the on rates and binding constants (k_{on} and K_i) of transition-state analogs, whose magnitudes are dependent only on the processes of diffusion and binding to the active site of ChEs. The contributions of both long- and short-range electrostatic interactions to the stability of the complex formed between a charged transition-state analog and AChE (or BChE) and to the on rate of the ligand can be evaluated by comparing the values of K_i and k_{on} for the charged species with those for a neutral isosteric ligand. These results can then be used to segregate the contributions of electrostatic interactions to molecular traffic from their effect on the chemical steps of catalysis.

Peptidyl trifluoromethyl ketones have been used extensively as transition-state analogs of various serine hydrolases (Imperiali and Abeles, 1986; Takahashi et al., 1988; Allen and Abeles, 1989b; Brady et al., 1989). In particular, they have been employed to assess the role of global electrostatic interactions in the stabilization of the catalytic transition state of subtilisin BPN' (Jackson and Fersht, 1993). A large body of kinetic evidence demonstrates that

another series of trifluoromethyl ketones serves as transition-state analogs of ChEs (Allen and Abeles, 1989a; Nair et al., 1993, 1994). The structure of the complex of the phenyl trifluoromethyl ketone, TFK^+ , with $TcAChE$ has been solved by x-ray crystallography, illustrating in detail the structural interactions responsible for the tight binding of this particular transition-state analog (Harel et al., 1996). The effect of salt concentration and of the mutation of residues D72, E199, and several negatively charged surface residues on the K_i of both TFK^+ and its isosteric neutral analog, *m*-tertbutyltrifluoroacetophenone (TFK^0) (Quinn et al., 1995; Radic et al., 1995, 1997; Hosea et al., 1996), have been measured.

Accordingly, the results of our calculations, presented in the following sections, will be compared to experimental data collected for TFK^+ , TFK^0 , and another ligand, *N*-methylacridinium (NMA), which has been employed to study the role of electrostatic properties in ChE catalysis (Nolte et al., 1980).

Part I: Molecular traffic—diffusion

A common treatment for the diffusion of cationic and neutral isosteric ligands to a buried active site points toward two different limits for diffusion to the active site of ChEs

In treating the diffusion of ligands and substrates toward ChEs, we will employ the model described by Samson and Deutch (1978). In this model, the enzyme is approximated as a sphere, and the active site by a spherical cap. It focuses on the effect of burying a reactive site on the inside of an

enzyme, away from the surface and at the bottom of a conical duct. The rest of the spherical surface, including the walls of the duct, is considered to be inert. The relationship between the actual 3D structure of AChE and the model is shown in Fig. 2. The entrance to the active-site gorge constitutes a cap on the surface of a sphere of radius R . The gorge is modeled as a conical duct, characterized by an opening angle, ϑ . The bottom of this duct is delimited by a spherical cap of radius ρ , the surface of which includes the catalytic machinery of the enzyme. We will ignore complications arising from hydrodynamic interactions and dynamic conformational changes of the enzyme. BD simulations of the diffusion of a ligand to the active site of AChE indicate that the influence of these effects on the diffusive process is not very significant (Antosiewicz et al., 1995a; Antosiewicz and McCammon, 1995).

The following expressions should permit evaluation of the upper limit for the encounter rates of charged and neutral ligands without postulating any special diffusive mechanism for cationic species. According to Samson and Deutch (1978), the rate constant for the encounter of a ligand with the active site buried at the bottom of the conical duct can be expressed as

$$k(\vartheta, s) = 4\pi DR \frac{1}{2} [1 - \cos \vartheta] \left[\left(\frac{1-s}{s} \right) + \eta(\cos \vartheta) \right]^{-1} \quad (1)$$

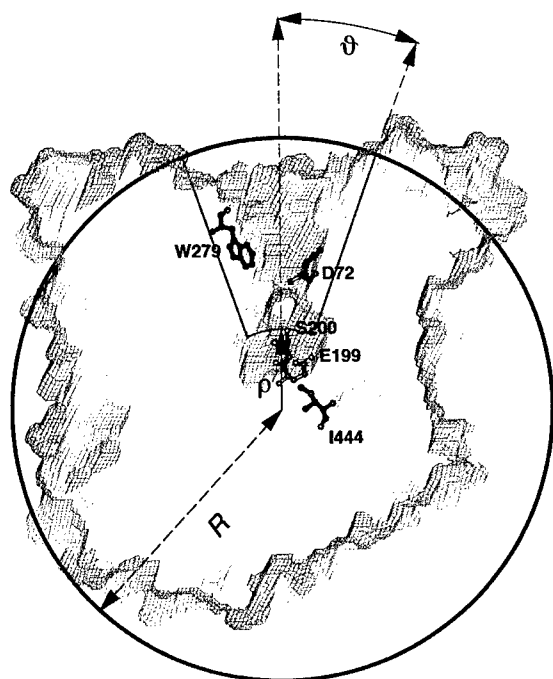


FIGURE 2 Schematic diagram of the model for diffusion of neutral and cationic ligands and substrates to the active site of ChE. The spherical model is superimposed on a slab view of TcAChE showing the active-site gorge and the positions of D72 and of the catalytic serine, S200. The inner and outer spherical caps are colored in red. The inner cap includes the catalytic machinery of AChE, as can be seen by the position of S200.

where s is given by ρ/R , D is the diffusion coefficient of the ligand, and the function $\eta(\cos \vartheta)$ is given by the following expression:

$$\eta(x) = \frac{1}{2} \left[(1-x) + \sum_{l=1}^{\infty} \frac{P_{l-1}(x) - P_{l+1}(x)}{l+1} \right] \quad (2)$$

where P_l is the Legendre polynomial of order l .

Let us then introduce numerical values for diffusion to the active site of AChE of TFK⁺, of TFK⁰, and of NMA, a charged ligand characterized by essentially the same diffusion coefficient as TFK⁺ and TFK⁰ (Fig. 3 A).

A value of 32 Å for the hydrodynamic radius, R , of AChE is taken from the study of Antosiewicz et al. (1995a). The value of ρ can be estimated by subtracting the transit region of the gorge (as defined in Methods) from the value of R , and the value of ϑ can be estimated by taking arctan (r/g), where r is the radius of the gorge mouth as defined in Methods, and g is the total gorge length. Inspection of the crystallographic 3D structure of TcAChE and mAChE yields values of 8 Å for r and 24 Å for g (of which 4 Å constitute the binding region and 20 Å the transit region). These figures result in a value of $\sim 18^\circ$ for ϑ and 0.38 for s (for an active site buried ~ 20 Å deep in the center of a protein of 32-Å radius). If we assume that TFK⁺, TFK⁰, and NMA are characterized by diffusion constants similar to that of ACh, we can employ the value of $D = 61.2 \times 10^{-7} \text{ cm}^2 \text{ s}^{-1}$ (Antosiewicz et al., 1995a).

Introducing the values for R , ρ , ϑ , s , and D into Eq. 1 yields a value of $k = 0.21 \times 10^9 \text{ M}^{-1} \text{ s}^{-1}$ for diffusion of these ligands to the active site of AChE buried $\sim 60\%$ ($\rho/R = s = 0.38$) of the way down a conical duct of aperture $\vartheta = 20^\circ$. Values for k were calculated using the program MATLAB (Version 5.1, 1998, Mathworks, Inc.). The values tabulated in Table 2 reveal a good agreement with experimental values gathered for TFK⁰; but values for the charged ligands, TFK⁺ and NMA, are between 10- and 80-fold larger (depending on whether the data were collected at very high or very low ionic strength, respectively).

Our guiding assumption for explaining the faster diffusion of cationic species relative to their isosteric counterparts is that positively charged ligands and substrates will diffuse in 3D until they reach a negatively charged area at the entrance to the active-site gorge. This area will act as a perfect sink for positively charged ligands, which will undergo a reduction in dimensionality of diffusion from 3D to 1D (Adam and Delbrück, 1968) and be committed to travel to the bottom of the gorge by a negative potential gradient. Because each encounter with this trap will be productive, in effect "raising" the buried active site to the surface, it can be modeled as a spherical patch on the surface of the enzyme. In the case of neutral isosteric ligands, which should neither interact with the trapping surface nor be influenced by the gorge potential gradient, an encounter will be considered productive only if the ligand hits the spherical cap at the

A

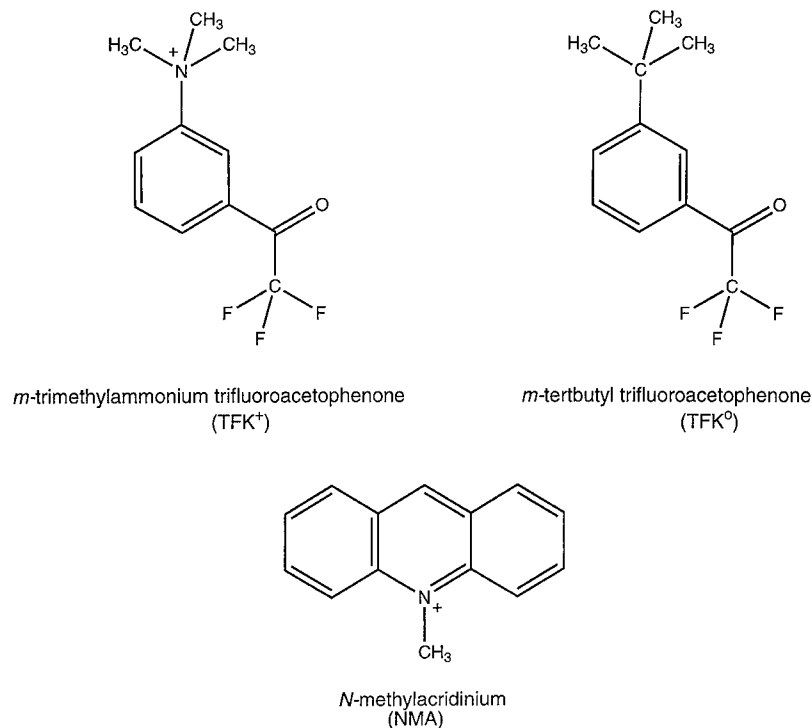
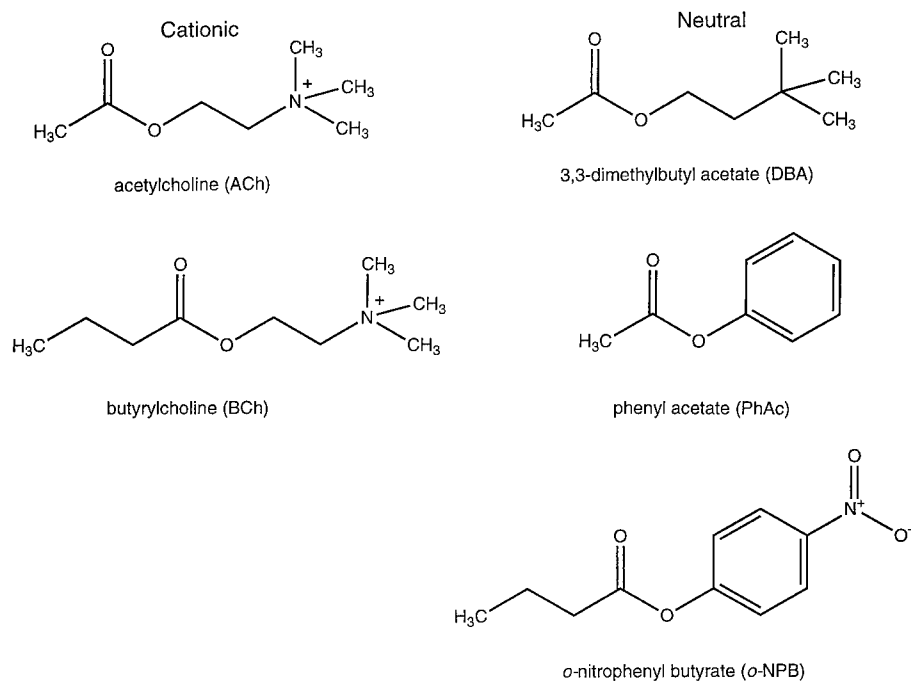


FIGURE 3 (A) Molecular structure of the transition-state analogs, TFK⁺ and TFK⁰, and of NMA. (B) Molecular structures of ACh, BCh, and some neutral substrates of the ChEs.

B



bottom of the gorge. Thus, even though the gorge may restrict the mobility of neutral species, they can effectively be considered to be searching for the buried active site as if diffusion were taking place in 3D, because their diffusion is not facilitated by a surface trap or by the negative potential gradient.

If we then assume a surface trap around the gorge area of

a ChE molecule for cationic ligands, $s = 1$, and the model gives the following expression for the rate constant:

$$k(\vartheta) = 4\pi DR \frac{1}{2} [1 - \cos \vartheta] / \eta(\cos \vartheta) \quad (3)$$

Introducing the appropriate numerical values, we get $1.5 \times 10^9 \text{ M}^{-1} \text{ s}^{-1}$ as the limit of diffusion for TFK⁺ (or

TABLE 2 Experimental inhibition constants and on rates of TFK⁺, TFK⁰, and NMA and comparison with theoretical values

Enzyme	K_i^0 (10^{-12} M ⁻¹)	K_i^H (10^{-12} M ⁻¹)	k_{on}^0 (10^9 M ⁻¹ s ⁻¹)	k_{on}^H (10^9 M ⁻¹ s ⁻¹)	$k_{on}^{H\text{ theor}}$ (10^9 M ⁻¹ s ⁻¹)
TFK⁺					
WT TcAChE [#]	0.002 ($I = 5$ mM)	0.033 ($I = 600$ mM)	80 ($I = 5$ mM)	3.9 ($I = 600$ mM) 6.0 ($I = 125$ mM)	1.5
WT mAChE [§]	0.001 ($I = 0$ mM)	0.01 ($I = 670$ mM)	16 ($I = 0$ mM)	2.1 ($I = 670$ mM)	1.5
(D74N) mAChE [§]	0.14 ($I = 0$ mM)	1.0 ($I = 670$ mM)	0.65 ($I = 0$ mM)	0.10 ($I = 670$ mM)	0.21*
NMA					
WT EeAChE [‡]	1200 ($I = 1$ mM)	26000 ($I = 125$ mM)	6.3 ($I = 1$ mM)	0.80 ($I = 125$ mM)	1.5
TFK⁰					
WT TcAChE [#]	—	3.6 ($I = 250$ mM)	—	0.30 ($I = 250$ mM)	0.21
WT EeAChE	—	1.9 ($I = 250$ mM)	—	0.12 ($I = 250$ mM)	0.21
WT mAChE [§]	6.8 ($I = 0$ mM)	3.1 ($I = 670$ mM)	0.05 ($I = 0$ mM)	0.08 ($I = 670$ mM)	0.21
(D74N) mAChE [§]	5.6 ($I = 0$ mM)	5.6 ($I = 670$ mM)	0.07 ($I = 0$ mM)	0.10 ($I = 670$ mM)	0.21

The superscripts ⁰ and ^H refer, respectively, to measurements performed at low and high salt concentrations. The superscript ^{theor} refers to theoretical values.

*Because neutralization of the charge on residue D72 results in abolition of the surface trap, the theoretical value is assumed to be one derived from Eq. (3).

[#]Quinn et al. (1995).

[§]Radic et al. (1997).

[‡]Nolte et al. (1980).

^{||}Nair et al. (1995).

NMA) toward a molecule of AChE characterized by a surface trap with $\vartheta = 20^\circ$. As can be seen by comparing this result with the values in Table 2, agreement with experimental data is very good for on rates measured at high ionic strength. The additional acceleration of diffusion that is observed at very low ionic strengths is best explained by a steering mechanism produced by long-range electrostatic interactions arising from the global asymmetrical distribution of surface charges in ChEs (Ripoll et al., 1993; Antosiewicz et al., 1996; Felder et al., 1997).

On the basis of these observations, we can conclude that there are two separate limits for the diffusion toward ChEs of neutral and charged isosteric ligands. In the absence of a steering mechanism generated by long-range electrostatic interactions (as is the case when on rates for ligands are measured at high salt concentration), cationic substrates are characterized by a diffusion limit about one order of magnitude larger than that for neutral isosters, and this effect is achieved by means of a trapping surface at the entrance to the gorge. As can be seen from the data in Table 2, at physiological salt concentration steering effects contribute only a 1.5–2-fold acceleration. Significant steering is present only at very low salt concentrations, when long-range contributions are strongest. Even then, the steering effect is responsible for an additional increase in encounter rates for cationic ligands of only one order of magnitude, which is much lower than the 240-fold enhancement calculated on the basis of BD simulations (Zhou et al., 1996).

We can extend this treatment to the diffusion of cationic and neutral isosteric substrates (Fig. 3 B). At high salt concentration, in the absence of any steering effect, the k_{cat}/K_M values for ACh and BCh are 10–15-fold larger than those for the neutral substrates, DBA, phenyl acetate (PhAC), and *o*-NPB (Tables 3 and 4, column 6), and both are about one order of magnitude smaller than the respective upper diffusion limits for cationic and neutral ligands. If we take the values of k_{cat}/K_M as reflecting the catalytic effi-

ciency of ChEs toward these two classes of substrates, we can say that the hydrolysis of both cationic and neutral substrates approaches their specific limits of diffusion.

These findings lead us to conclude that ChEs are as efficient in catalyzing the hydrolysis of neutral substrates as they are in catalyzing the hydrolysis of their isosteric cationic counterparts. The emergence of specificity for cationic substrates thus seems to arise via a mechanism geared to speed up the diffusion of positively charged substrates toward an already optimally efficient catalytic active site. This enhancement of diffusion is accomplished primarily via a surface trap whose effectiveness is independent of salt concentration, and secondarily through a salt-dependent steering effect. The manner in which they operate will be the subject of the following sections.

Module I: a surface trap for cationic species operating via short-range local interactions

Experimental evidence for the presence of a trapping surface on ChEs and for a reduction in the dimensionality of diffusion for charged reactive species comes also from a study of the influence of viscosity on the catalytic efficiency of EeAChE (Hasinoff, 1982), in which the dependence of k_{cat}/K_M on $\eta^{2/3}$ was interpreted as evidence for a reaction governed by nonspecific binding of ACh to the enzyme, followed by surface diffusion to the active site. A measure of the radius of the trapping surface can be calculated by introducing the value for the on rate of a ligand into the following equation (Hasinoff, 1982):

$$k_{on} = 4\pi NDR_{eff}/1000 \quad (4)$$

where R_{eff} is the effective trap radius, N is Avogadro's number, and D is the diffusion coefficient of the ligand.

If we introduce into Eq. 4 the value for the diffusion coefficient of TFK⁺ or NMA, and the on rates measured for

TABLE 3 Experimental kinetic constants for cationic substrates at high and low salt concentrations

Enzyme	K_M^0 (10^{-6} M $^{-1}$)	K_M^H (10^{-6} M $^{-1}$)	k_{cat}^0 (10^5 s $^{-1}$)	k_{cat}^H (10^5 s $^{-1}$)	k_{cat}/K_M^0 (10^8 M $^{-1}$ s $^{-1}$)	k_{cat}/K_M^H (10^8 M $^{-1}$ s $^{-1}$)
ACh						
WT <i>EeAChE</i> *	—	—	—	—	—	0.11 ± 0.2 (glycerol)
WT <i>EeAChE</i> *	—	—	—	—	—	0.17 ± 0.5 (sucrose)
WT <i>TcAChE</i> #	23 (<i>I</i> = 1 mM)	121 (<i>I</i> = 500 mM)	0.20 (<i>I</i> = 1 mM)	0.58 (<i>I</i> = 500 mM)	0.98 (<i>I</i> = 1 mM)	0.48 (<i>I</i> = 500 mM)
WT <i>hAChE</i> §	80 ± 10 (<i>I</i> = 5 mM)	120 ± 20 (<i>I</i> = 125 mM)	0.76 ± 0.11 (<i>I</i> = 5 mM)	0.83 ± 0.12 (<i>I</i> = 125 mM)	0.87 ± 0.12 (<i>I</i> = 5 mM)	0.48 ± 0.08 (<i>I</i> = 125 mM)
WT <i>mAChE</i> ¶	—	—	—	—	4.1 ± 0.4 (2 mM)	0.25 ± 0.03 (<i>I</i> = 670 mM)
(D74N) <i>hAChE</i> §	—	500 ± 200 (<i>I</i> = 145 mM)	—	0.04 ± 0.02 (<i>I</i> = 145 mM)	—	0.07 ± 0.02 (<i>I</i> = 145 mM)
(D74G) <i>hAChE</i> §	—	630 ± 200 (<i>I</i> = 145 mM)	—	0.06 ± 0.02 (<i>I</i> = 145 mM)	—	0.09 ± 0.02 (<i>I</i> = 145 mM)
(D74N) <i>mAChE</i> ¶	—	1300 (<i>I</i> = 145 mM)	—	0.01 ± 0.002 (<i>I</i> = 145 mM)	—	0.01 (<i>I</i> = 145 mM)
BCh						
WT <i>hBChE</i>	—	18 (<i>I</i> = 145 mM)	—	0.04 ± 0.01 (<i>I</i> = 145 mM)	—	0.22 (<i>I</i> = 145 mM)
(D70G) <i>hBChE</i>	—	150 (<i>I</i> = 145 mM)	—	0.04 ± 0.01 (<i>I</i> = 145 mM)	—	0.02 (<i>I</i> = 145 mM)

The superscripts ⁰ and ^H refer, respectively, to measurements performed at low and high salt concentrations.

*Bazelyansky et al. (1986).

#Berman and Nowak (1992).

§Shafferman et al. (1992).

¶Radic et al. (1997).

||Masson et al. (1997).

TABLE 4 Experimental kinetic constants for neutral substrates at high and low salt concentrations

Enzyme	K_M^0 (10^{-6} M $^{-1}$)	K_M^H (10^{-6} M $^{-1}$)	k_{cat}^0 (10^5 s $^{-1}$)	k_{cat}^H (10^5 s $^{-1}$)	k_{cat}/K_M^0 (10^8 M $^{-1}$ s $^{-1}$)	k_{cat}/K_M^H (10^8 M $^{-1}$ s $^{-1}$)
DBA						
WT <i>EeAChE</i> *	—	—	—	—	—	0.01 (glycerol)
WT <i>EeAChE</i> *	—	—	—	—	—	0.01 (sucrose)
WT <i>EeAChE</i> #	—	260 ± 30 (200 mM)	—	0.31 (<i>I</i> = 200 mM)	—	0.01 (<i>I</i> = 200 mM)
WT <i>TcAChE</i> §	—	—	—	0.19 (<i>I</i> = 250 mM)	—	0.07 (<i>I</i> = 250 mM)
WT <i>hAChE</i> ¶	280 ± 40 (<i>I</i> = 5 mM)	260 ± 30 (<i>I</i> = 125 mM)	0.76 ± 0.11 (<i>I</i> = 5 mM)	0.83 ± 0.12 (<i>I</i> = 125 mM)	0.02 (<i>I</i> = 5 mM)	0.02 (<i>I</i> = 125 mM)
<i>o</i> -NPB						
WT <i>hBChE</i>	—	125 ± 20 (<i>I</i> = 145 mM)	—	0.06 ± 0.005 (<i>I</i> = 145 mM)	—	0.05 (<i>I</i> = 145 mM)
(D70G) <i>hBChE</i>	—	12 ± 20 (<i>I</i> = 145 mM)	—	0.06 ± 0.02 (<i>I</i> = 145 mM)	—	0.05 (<i>I</i> = 145 mM)

The superscripts ⁰ and ^H refer, respectively, to measurements performed at low and high salt concentrations.

*Bazelyansky et al. (1986).

#Hasan et al. (1981).

§Nair et al. (1995).

¶Shafferman et al. (1992).

||Masson et al. (1997).

these ligands and AChE from various species at high salt concentration, we get an average value for the trap radius of ~ 7.5 Å, which is similar both to the mean radius of ~ 9 Å estimated in recent MD studies (Wlodek et al., 1997b) and to our own estimate of ~ 8 Å derived from the crystallographically determined structure of *TcAChE* (Sussman et al., 1991).

Recent studies have suggested that a particular residue, D72 (D74 in mAChE and hAChE, D70 in hBChE), might contribute to the specificity of ChEs for cationic ligands by a trapping mechanism (Hosea et al., 1996; Masson et al., 1996, 1997). This residue is strategically placed near the top of the active-site gorge (Fig. 1) and was identified as a crucial component of the PAS (Shafferman et al., 1992; Barak et al., 1995). Strong evidence in support of our model comes from the observation that in mutant enzymes in which the putative cationic trap has been removed by neutralizing the charge on D72, on-rate values for cationic ligands fall to the theoretical values for neutral ones (Table 2). In addition, at physiological salt concentration, k_{cat}/K_M values for cationic substrates closely approach the values for neutral substrates when the negative charge on the side chain of residue D72 is neutralized (Table 3, column 6). These findings point to D72 as the major component of a cation-specific trap at the entrance to the active-site gorge of ChEs. Previous calculations comparing the D72N mutant to WT AChE revealed a small contribution of the negative charge of the side chain of D72 to the overall potential gradient within the active-site gorge (Felder et al., 1997). This small contribution does not correlate with the drastic reductions in both catalytic efficiency and in on rates for cationic ligands produced by mutations in this position. BD simulations of the on rates of cationic ligands have been found to be in good agreement with experimental data, but their predictions were significantly less accurate when residue D72 was neutralized (Radic et al., 1997). However, we find a good correlation between on rates for TFK^+ and the average potential in the gorge region corresponding to the cationic trap, both for WT AChE and for a series of mutants in which the charge on D72 was neutralized along with the charges on a number of surface residues, particularly D82 and D278 (Radic et al., 1997) (Fig. 4 A). Moreover, we also find a good correlation between on rates for TFK^+ and overall gorge potentials for surface mutants and for the E199Q mutant, whose side chain is shown to contribute significantly to the overall gorge potential (Felder et al., 1997; Wlodek et al., 1997a) (Fig. 4 B). These findings provide supporting evidence for our treatment of the acceleration of diffusion of cationic species as being composed of the additive effects of a surface trap operating through local short-range interactions, constituted by the side chains of a few key residues, primarily D72, D82, and D278, and of a long-range steering effect generated by the overall gorge potential.

If we want to uncouple the effects of local short-range interactions from the effect produced by long-range interactions on diffusion rates, we must resort to systems in

which the mechanism necessary for the recognition of positively charged substrates is maintained, while the contribution of the negative charge on D72 to the gorge potential has been eliminated. It so happens that in all insect species studied so far, the amino acid at the position equivalent to residue 72 in *TcAChE* is a tyrosine (Toutant, 1989; Anthony et al., 1995; Zhu and Clark, 1995). Site-directed mutagenesis studies on *DmAChE* in which Y109 (equivalent to D72 in *TcAChE*) was mutated to a glycine or a lysine showed that such a mutation increased the K_M for ACh by 10- and 100-fold, respectively, whereas mutation to glutamate had no effect on K_M (Mutero et al., 1992). We interpret these results as evidence for a trapping mechanism for cationic substrates and ligands mediated, in insect ChEs, by the aromatic side chain of Y109 via local cation- π interactions. The predictions made by our model are supported by a comparison of the 3D structure of *DmAChE*, recently solved in our laboratory (Harel et al., 1999) and that of *TcAChE*, which shows the position of residue Y109 to be almost identical to that of D72. We thus predict that the D72Y mutant in *Torpedo* or other vertebrate ChEs should retain most of its catalytic efficiency, and that any reduction in catalytic efficiency resulting from the D72Y mutation should be correlated with the corresponding small decrease in gorge potential. Our assumption that an aromatic residue can be as efficient as a negatively charged one in the recognition of cations is corroborated by the following data:

1. Cation- π interactions are predominantly electrostatic, involving the interaction of the cation with the large, permanent quadrupole moment of the aromatic ring (Dougherty, 1996).
2. Gas-phase measurements of binding energy of cations to benzene and to toluene have shown that in this phase a cation would preferentially bind to an aromatic compound rather than to water (Sunner et al., 1981).
3. In an aqueous environment, a pocket lined with the side chains of amino acids such as Trp, Phe, and Tyr can efficiently compete with full water solvation for the stabilization of a positive charge, because of the sizable quadrupole moment of the rings of aromatic residues (Luhmer et al., 1994). The importance of cation- π interactions in the catalytic function of ChEs has been confirmed by a large body of structural (Sussman et al., 1991; Harel et al., 1993, 1996) and kinetic (Ordentlich et al., 1993; Radic et al., 1993; Nair et al., 1994; Barak et al., 1995) data.

Modeling of the D72Y mutant of *TcAChE* shows that the hydroxyl moiety of the tyrosine at position 72 is capable of forming a hydrogen bond with Y121. It has been hypothesized that the hydrogen bond between Y121 and D72 in WT AChE is required for maintaining the "functional cross-talk" postulated for the transduction of allosteric signals from the PAS to the catalytic center (Shafferman et al., 1992; Barak et al., 1995). These considerations also provide us with a rather straightforward test for the presence of such

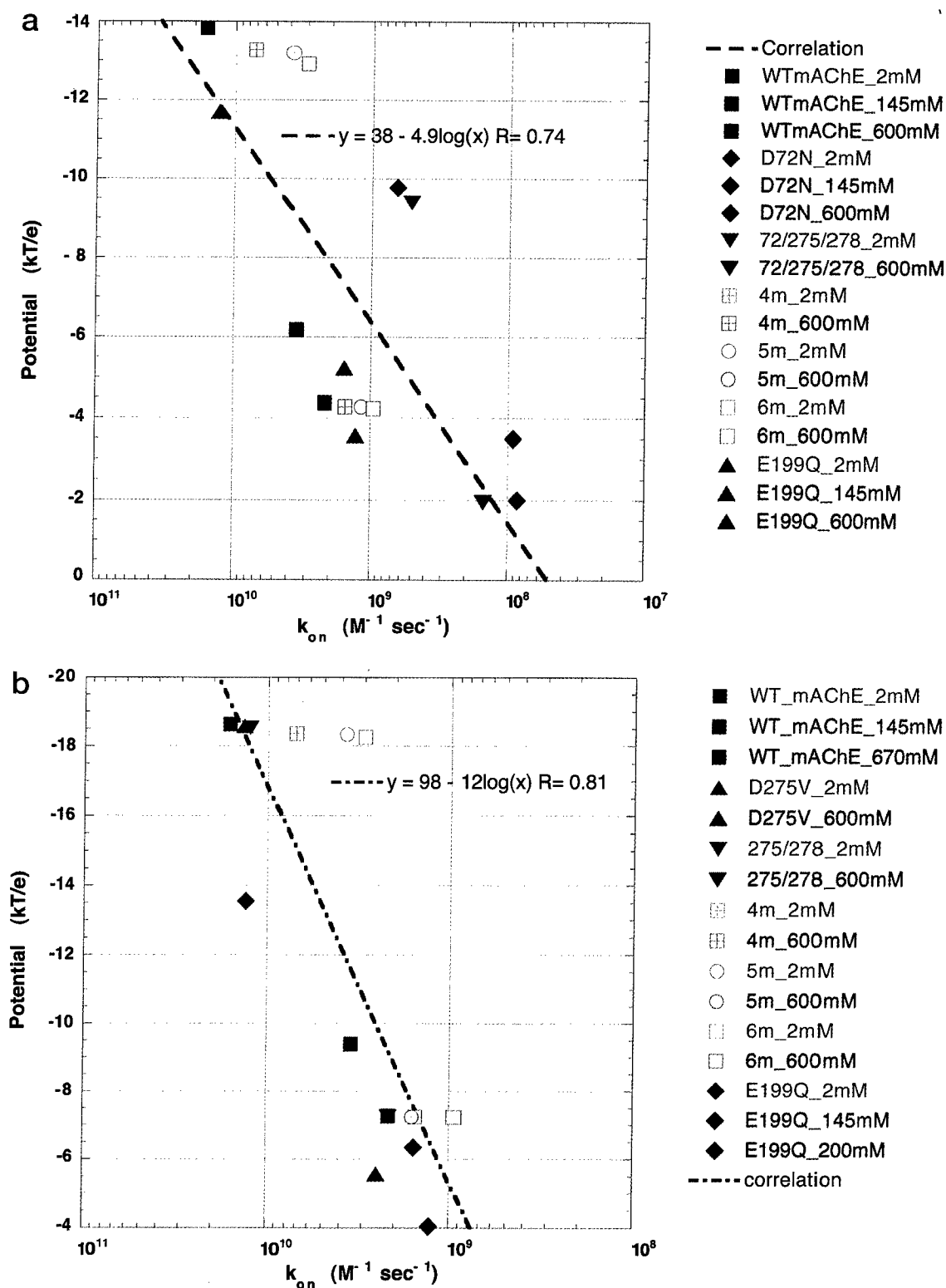


FIGURE 4 (A) Correlation between average potentials in the trap region and encounter rates for TFK⁺ at high (600 mM), physiological (145 mM), and low (2 mM) salt concentrations. The potential values are calculated for WT mAChE and for the following mutants (the abbreviations used in the list on the right of the figure are given in parentheses): D72N (D72N); D72N/D275V/D278N (72/275/278); E82Q/E89Q/D275V/D278N (4m); E82Q/E89Q/D275V/D278N/D365N (5m); E82Q/E89Q/D275V/D278N/E285Q/D365N (6m). (B) Correlation between overall gorge potential and encounter rates for TFK⁺ at high (600 mM), physiological (145 mM), and low (2 mM) salt concentrations. The potential values are calculated for WT mAChE and for the following mutants (the abbreviations used in the list on the right of the figure are given in parentheses): D275V (D275V); D275V/D278N (275/278); E82Q/E89Q/D275V/D278N (4m); E82Q/E89Q/D275V/D278N/D365N (5m); E82Q/E89Q/D275V/D278N/E285Q/D365N (6m); E199Q (E199Q).

cross-talk, because replacing tyrosine with phenylalanine, i.e., generating the D72F mutant, should have a disruptive effect on signal transduction and reduce catalytic efficiency significantly. Analysis of the kinetic properties of these mutants is under way, and preliminary results show that the K_M values of both D72Y and D72F mutants of *TcAChE* are not significantly different from those of WT-*TcAChE*, thus providing strong supportive evidence for our hypothesis. A complete analysis of the catalytic properties of these mutants, along with other mutants generated to study the role of aromatic and charged residues inside the active-site gorge of ChEs, is currently under way (S. A. Botti, E. Krejci, S. Bon, D. M. Quinn, J. L. Sussman, I. Silman, and J. Massoulié, manuscript in preparation).

Module II: the potential gradient along the active-site gorge is responsible for steering cationic species to the active site of ChE

We now turn our attention to the second module of our treatment: the long-range electrostatic steering effect. We will discuss how this effect arises from the potential gradient along the gorge axis, which arises from the combined effect of the overall charge distribution in the ChE molecule and the contribution of several α -helix dipoles. Kinetic studies have revealed both a marked reduction in the affinity of AChE for cationic substrates and inhibitors (Mendel and Rudney, 1943) and an increase in k_{cat} (Nolte et al., 1980; Smissaert, 1981; Hofer et al., 1984), upon the addition of inorganic salts such as sodium or magnesium chloride. The dependence upon salt concentration has been ascribed to the binding of inorganic cations to anionic sites (Taylor and Lappi, 1975; Smissaert, 1981), to conformational changes resulting from occupation of the PAS by metal ions (Changeux, 1966), and to the screening of favorable electrostatic interactions between the cationic substrate and the "anionic" subsite in the active site of the enzyme (Dawson and Crone, 1973; Nolte et al., 1980; Hofer et al., 1984). Comparison of the effects of monovalent and divalent ions on the activity of AChE suggests a general screening effect of monovalent cations, while it has been proposed that divalent cations interact specifically with carboxylate groups present in the active site (Hofer et al., 1984). The identification of a putative binding site for Zn^{2+} in hBChE (Bhanumathy and Balasubramanian, 1996) supports the notion of specific binding sites for divalent cations in ChEs.

The potential gradient along the gorge axis and its dependence on salt concentration have been calculated both for WT *TcAChE* and for a series of surface and active-site mutant models (Antosiewicz et al., 1995b; Felder et al., 1997; Wlodek et al., 1997a). On the basis of these results, it has been suggested that enhancement of encounter rates between cationic ligands and the catalytic machinery buried near the bottom of the active-site gorge is due to long-range electrostatic interactions, attributable to the potential drop along the length of the active-site gorge. Radic et al. (1997)

recently analyzed in detail the influence of electrostatics on the kinetics of ligand binding to AChE. Their study focused on the ionic-strength dependence of the binding of ligands to AChE after neutralization, through site-directed mutagenesis, of the negative charges of residues in the active site, in the PAS, and within a surface area around the entrance to the gorge. Comparison of experimental on rates for TFK^+ gathered on the surface and active-site mutants revealed good agreement with BD simulations. However, prediction of on rates after neutralization of the negative charge of D72, which is considered to be a major component of the PAS, was considerably less accurate. Radic et al. (1997) interpreted their results by assuming two distinct types of electrostatic interaction: one interaction, dependent on salt concentration, brings about acceleration of the initial encounter rates of cationic ligands with the enzyme, and a second one, independent of salt concentration, results in trapping of these ligands by specific residues within the PAS.

Fig. 5 shows that the ionic-strength-dependent decrease in electrostatic potential inside (and outside) the active-site gorge is rather well correlated with the corresponding decrease in encounter rates of both NMA and TFK^+ with *EeAChE*, *TcAChE*, and *mAChE* (Nolte et al., 1980; Berman et al., 1991). It thus seems reasonable to argue that this correlation corresponds to the contribution to molecular traffic of salt-dependent long-range interactions arising from the global asymmetrical distribution of charges in ChEs.

This argument is reinforced by the observation that neutralization of seven negatively charged residues around the entrance to the active-site gorge has only a small effect on the potential gradient within the active-site gorge (Felder et al., 1997), and that this small change is strongly correlated with a concomitant small reduction in catalytic efficiency (Shafferman et al., 1994). The overall potential difference along the axis of the active-site gorge is similar for AChE of different species and is $\sim 20\%$ smaller for hBChE, as shown in Fig. 6. In this figure, it is interesting to note that the slope of the potential gradient displays an inflection ~ 14 Å from the bottom of the gorge, in the neighborhood of D72, D82, and D278. Antosiewicz et al. (1995b) pointed out that the profile of rate constant versus depth of penetration inside the gorge suggests a "choke point" in the same region, beyond which the reactive species becomes committed to a productive encounter. In *DmAChE*, where the residue homologous to D72 is a tyrosine (Y109), the inflection in gorge potential is less pronounced than for vertebrate AChEs. Our hypothesis is that this smaller inflection is due to the contribution of conserved negatively charged residues in *DmAChE* (Felder et al., 1997), homologous to D82 and D278, which constitute the secondary components of the cationic surface trap. These considerations strengthen the case for a major role of D72, and secondarily of D82 and D278, in the recognition of cationic substrates.

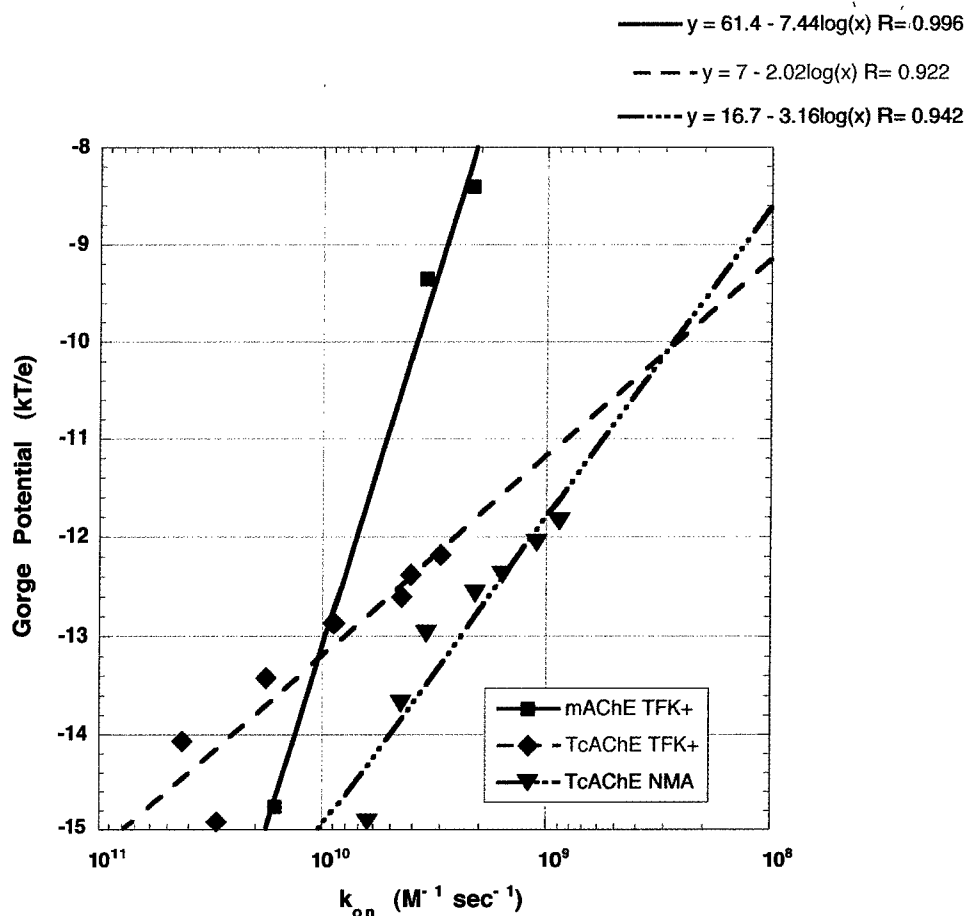


FIGURE 5 Correlation between overall gorge potentials of WT AChEs and encounter rates of TFK⁺ and NMA as a function of salt concentration. The potential values were calculated for TcAChE for salt concentration values varying from 2 to 600 mM.

Part II: quantitative treatment of the electrostatic forces underlying ChE-ligand binding interactions

Contribution of electrostatic interactions to the binding of transition-state analogs to ChEs

In the previous sections we showed that diffusion of cationic species toward the active site of ChEs is enhanced both by a cationic trap, which operates through local short-range electrostatic interactions, and by a steering effect that emerges from the global asymmetrical spatial distribution of charges in the ChE molecule. In this section we analyze the contribution of a single positive charge to the stabilization of the binding of transition-state analogs to ChEs, with a treatment analogous to the one used in the previous sections. Binding experiments have revealed a strong dependence upon ionic strength of the K_i of TFK⁺, which is not observed for TFK⁰ (Radic et al., 1997). Mutation studies have shown that stabilization of the binding of both TFK⁺ and TFK⁰ is primarily due to short-range interactions between W84 and the quaternary ammonium (*tert*-butyl) moiety of TFK⁺ (TFK⁰) (Radic et al., 1995, 1997), which take the form of cation- π interactions in the case of TFK⁺ and of short-range London dispersion forces in the case of TFK⁰ (Nair et al., 1994). These studies show that binding of TFK⁺ to the W86A (W84A) mutant of mAChE is ~1500-fold weaker than binding to WT mAChE. In contrast, mu-

tation of E199 or E443 (near the gorge floor) results in only a ~10-fold decrease in binding strength, and neutralization of the negative charge on D72 (at the top of the gorge) in only a 20-fold decrease. Moreover, only the mutation of W84 affects the binding strength of TFK⁰ to AChE (Radic et al., 1995, 1997; Hosea et al., 1996). The primary role of W84 in the binding of these transition-state analogs has been confirmed by the solution of the 3D structure of the complex of TFK⁺ and TcAChE (Harel et al., 1996), and we can reasonably assume that the neutral analog, TFK⁰, would bind in an analogous fashion.

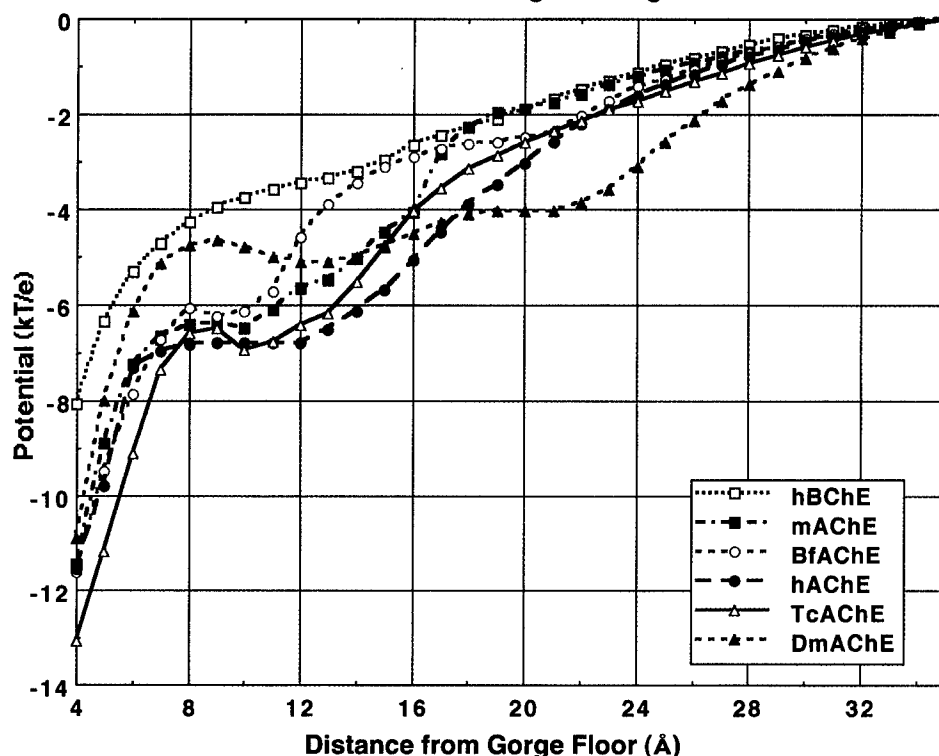
Consequently, we can consider the overall "charge effect," i.e., the added stabilization to the binding energy of cationic transition state analogs for ChEs relative to their neutral isosteric counterparts, to be composed of two independent contributions, both electrostatic:

1. A global term arising from long-range electrostatic contributions that are screened at high salt concentrations.
2. A local term that can be identified with cation- π and local, short-range electrostatic interactions between the charged substrates and key binding residues, such as W84, in the active-site gorge.

The difference in binding between TFK⁺ and TFK⁰ due to the positive charge, which we shall term $\Delta\Delta G_{charge}$, can

Electrostatic Potentials Along the Gorge Axis of ChEs

FIGURE 6 Electrostatic potentials along the gorge axis for ChEs. The potentials were calculated for TcAChE, mAChE, hAChE, DmAChE, BfAChE, and hBChE.



be calculated from the experimentally determined dissociation constants measured for WT mAChE and can be defined as

$$\Delta\Delta G_{\text{charge}} = \Delta G_{\text{TFK}^+} - \Delta G_{\text{TFK}^0} \quad (5)$$

With $\Delta G_{\text{TFK}^+} = -RT \ln K_{i\text{TFK}^+}$ and $\Delta G_{\text{TFK}^0} = -RT \ln K_{i\text{TFK}^0}$ it follows that

$$\Delta\Delta G_{\text{charge}} = RT \ln (K_{i\text{TFK}^0}/K_{i\text{TFK}^+}) \quad (6)$$

If we assume $\Delta\Delta G_{\text{charge}}$ to be the sum of all local interactions between the quaternary ammonium (*tert*-butyl) moiety of TFK⁺ (TFK⁰) and the aromatic side chains in the acyl binding pocket, and of global electrostatic interactions due to the potential gradient within the active-site gorge, we can express $\Delta\Delta G_{\text{charge}}$ as

$$\Delta\Delta G_{\text{charge}} = \Delta\Delta G_L + \Delta\Delta G_G \quad (7)$$

in which

$$\Delta\Delta G_L = \Delta G_{L\text{TFK}^+} - \Delta G_{L\text{TFK}^0} \quad (8)$$

and

$$\Delta\Delta G_G = \Delta G_{G\text{TFK}^+} - \Delta G_{G\text{TFK}^0} \quad (9)$$

If we consider the major contribution to the local term to be due to interaction of TFK⁺ and TFK⁰ with W84, we can isolate the contribution to the global term by considering the change in K_i between WT AChE and the W84A. Although it is possible that the W84A mutation may produce structural rearrangements, these should affect binding of both

TFK⁺ and TFK⁰ similarly, so that the only effect measured will be that produced by the difference in charge of the two inhibitors.

In this case,

$$\begin{aligned} \Delta\Delta G_G &= \Delta G_{W84A\text{TFK}^+} - \Delta G_{W84A\text{TFK}^0} \\ &= RT \ln (K_{iW84A\text{TFK}^0}/K_{iW84A\text{TFK}^+}) \end{aligned} \quad (10)$$

The value of the contribution to the local term can similarly be isolated and assessed by examining the difference in binding energy between TFK⁺ and TFK⁰ at very high salt concentrations, where the steering effect should be completely screened. In this case,

$$\begin{aligned} \Delta\Delta G_L &= \Delta G_{\text{highTFK}^+} - \Delta G_{\text{highTFK}^0} \\ &= RT \ln (K_{i\text{highTFK}^+}/K_{i\text{highTFK}^0}) \end{aligned} \quad (11)$$

We can safely assume the value of $K_{i\text{TFK}^0}$ to be independent of salt concentration because global electrostatic forces should have little effect on TFK⁰ (Quinn et al., 1995; Radic et al., 1997).

If our assumptions are correct, the experimental data gathered for these systems should yield values for $\Delta\Delta G_L$ and $\Delta\Delta G_G$ which, when summed, should give back the experimentally measured value for $\Delta\Delta G_{\text{charge}}$.

The validity of our assumption is shown in Table 5. Substituting in Eqs. 5, 10, and 11 the appropriate experimental K_i values for TFK⁺ and TFK⁰, tabulated in column 1 of Table 5, yields values for $\Delta\Delta G_L$ of ~ 3.4 kcal/mol and for $\Delta\Delta G_G$ of 0.4 kcal/mol for $I = 0.145$ mM and of 1.4

TABLE 5 Experimental values of K_i for TFK⁺ and TFK⁰ employed in the calculation of $\Delta\Delta G_{\text{charge}}$, $\Delta\Delta G_L$, and $\Delta\Delta G_g$

Enzyme	K_i TFK ⁺ (10^{-12} M)	K_i TFK ⁰ (10^{-12} M)	$\Delta\Delta G$ (kcal M ⁻¹)
WT TcAChE*	0.002 ($I = 2$ mM)	3.6 ($I = 2$ mM)	4.3 (total)
WT TcAChE [#]	0.003 ($I = 600$ mM)	3.6 ($I = 600$ mM)	2.9 (local)
WT mAChE [#]	0.001 ($I = 2$ mM)	3.6 ($I = 2$ mM)	4.7 (total)
WT mAChE [§]	0.005 ($I = 145$ mM)	3.7 ($I = 145$ mM)	3.8 (total)
WT mAChE [#]	0.012 ($I = 670$ mM)	3.6 ($I = 670$ mM)	3.4 (local)
(W84A) mAChE [§]	7.7	78	1.4–0.4 (global)

*Quinn et al. (1995).

[#]Radic et al. (1997).[§]Radic et al. (1995).

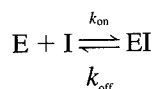
kcal/mol for $I = 0.02$ mM. Substitution of these values in Eq. 7 yields values for $\Delta\Delta G_{\text{charge}}$ of 3.8 kcal/mol and 4.8 kcal/mol, at physiological and low salt concentrations, respectively, thus supporting our hypothesis.

Calculation of the potential inside the active-site gorge of AChE from $\Delta\Delta G^\ddagger$ values for the activated complex of AChE with TFK⁺ and TFK⁰

Having established that measurement of the difference in K_i between TFK⁺ and TFK⁰ provides a powerful tool for calculating the contributions of electrostatic interactions, one can ask if the same tool can be employed to measure the electrostatic potential within the active site, and if values so obtained will be in agreement with the ones calculated by solving the PB equation for the system in question.

In a recent study (Stauffer and Karlin, 1994), the electrostatic potential of ACh binding sites in the nicotinic ACh receptor (nAChR) was measured by analyzing the rate constants for the reactions of charged and neutral methanethiosulfonates with binding-site cysteines within the nAChR in terms of absolute rate theory and Debye-Huckel theory, which, together, can be used to obtain rate constants as a function of the electrostatic potential, the charges of the reactants, and the ionic strength of the solution (Laidler, 1965).

This treatment was applied to our system in an analogous fashion. TFK⁺ and TFK⁰ bind to ChEs by forming a hemiketal adduct with the active-site serine, S200. Reaction of either TFK⁺ or TFK⁰ with AChE (Quinn et al., 1995) can be considered to take place according to the following scheme:



Formation of the hemiketal adduct can be considered as proceeding through a short-lived activated complex, EI^\ddagger . Transition state theory provides the relationship between rate constants and free energies of the enzyme, the inhibitor, their complex, and the activated binding state (Glasstone et al., 1941):

$$k_{\text{on TFK}} = \nu \exp(-\Delta G_{\text{on}}^\ddagger/RT) \quad (12.1)$$

$$k_{\text{off TFK}} = \nu \exp(-\Delta G_{\text{off}}^\ddagger/RT) \quad (12.2)$$

where ν is the vibrational frequency of the activated complex in the degree of freedom leading to its decomposition, and

$$\Delta G_{\text{on}}^\ddagger = G_{\text{EI}^\ddagger}^0 - G_E^0 + G_I^0 \quad (13.1)$$

$$\Delta G_{\text{off}}^\ddagger = G_{\text{EI}^\ddagger}^0 - G_{\text{EI}}^0 \quad (13.2)$$

We can then apply the reasoning used in the previous section to determine the contribution of global and local terms to $\Delta\Delta G_{\text{charge}}$, and consider the global contribution of long-range interactions separately from all other contributions, including nonelectrostatic interactions, which we will bundle into the local term. In this case,

$$\Delta G_{\text{on}}^\ddagger = \Delta G_{\text{onL}}^\ddagger + \Delta G_{\text{onG}}^\ddagger \quad (14)$$

The change in electrostatic energy due to the global term can be expressed as the sum of the energies associated with uncharging of the ionic atmospheres of the reactants, and with charging of the ionic atmosphere of the activated binding complex, so that

$$\Delta G_{\text{onG}}^\ddagger = z_{\text{TFK}} F \psi_E + RT \ln(\gamma_{\text{EI}^\ddagger}/(\gamma_E \gamma_I)) \quad (15)$$

where ψ_E , expressed in volts, is the electrostatic potential due to E at the reaction radius at zero ionic strength; z_{TFK} is the charge of TFK; γ_E , γ_I , and $\gamma_{\text{EI}^\ddagger}$ are, respectively, the molar activity coefficients of enzyme, inhibitor, and activated complex; and F is the Faraday constant. The first term on the right is the electrostatic free energy for formation of the activated complex in the absence of ionic atmospheres, and the second term on the right is the difference in the free energies of charging of the ionic atmospheres of the complex and of the reactants.

Combining Eqs. 12, 14, and 15, we obtain, for TFK⁺,

$$\ln(k_{\text{on TFK}^+}) = \ln(k_L) - F/RT(z_{\text{TFK}^+} \psi_E + \ln(\gamma_{\text{EI}^\ddagger}/\gamma_E \gamma_I)) \quad (16)$$

where $k_{\text{on TFK}^+} = \nu \exp(\Delta G_{\text{onL}}^\ddagger/RT)$.

If we take the ratios between the on rates of TFK⁺ and TFK⁰, we get the following expression:

$$\ln(k_{\text{on TFK}^+}/k_{\text{on TFK}^0}) = \ln(k_{\text{L TFK}^+}/k_{\text{L TFK}^0}) - F/RT(z_{\text{TFK}^+} \psi_E + \ln(\gamma_{\text{EI}^\ddagger}/\gamma_E \gamma_I)) \quad (17)$$

OR

$$RT \ln(k_{\text{on TFK}^+}/k_{\text{on TFK}^0}) = -\Delta\Delta G_{\text{on L}}^\ddagger - F(z_{\text{TFK}^+}\psi_E + \ln(\gamma_{+EI}/\gamma_E \gamma_I)) \quad (18)$$

where the long-range term will be contributed only by TFK^+ , because TFK^0 binding is not dependent on long-range electrostatic interactions.

Using an approach analogous to that used to calculate $\Delta\Delta G_L$ in the previous section, we can calculate $\Delta\Delta G_{\text{on L}}^\ddagger$ from the ratio of on rates for TFK^+ and TFK^0 at very high salt concentrations, where, as may be recalled, the global interactions should be completely screened and the long-range term for TFK^+ can be considered negligibly small:

$$\Delta\Delta G_{\text{on L}}^\ddagger = -RT \ln(k_{\text{on high TFK}^+}/k_{\text{on high TFK}^0}) \quad (19)$$

Substituting Eq. 19 into Eq. 18, we get the following expression:

$$RT \ln(k_{\text{on TFK}^+}/k_{\text{on TFK}^0}) = RT \ln(k_{\text{on high TFK}^+}/k_{\text{on high TFK}^0}) - F(z_{\text{TFK}^+}\psi_E + \ln(\gamma_{EI}/\gamma_E \gamma_I)) \quad (20)$$

The dependence of the rate constant of TFK^+ on the electric potential is free of geometric assumptions. Its dependence on ionic strength, however, is derived with a number of simplifying assumptions, including spherically symmetrical ions. Subject to these assumptions, and at the limit of low ionic strength, we can express

$$\log(\gamma) = -Qz^2I^{1/2} \quad (21)$$

where $Q = 1.826 \times 10^6/(\epsilon T)^{3/2}$, ϵ is the dielectric constant, and I is the ionic strength. At 25°C in water ($\epsilon = 80$), $Q = 0.51 \text{ M}^{-1/2}$, thus combining Eqs. 20 and 21 and dividing by RT , we get

$$\log(k_{\text{on TFK}^+}/k_{\text{on TFK}^0}) = RT \log(k_{\text{on high TFK}^+}/k_{\text{on high TFK}^0}) - 0.434F/RT(z_{\text{TFK}^+}\psi_E + z_{\text{TFK}^+}I^{1/2}) \quad (22)$$

for very low ionic strength the term $z_{\text{TFK}^+}I^{1/2}$ becomes negligible, and we get (at 298.15K, $0.434 F/RT = 17$)

$$\log(k_{\text{on TFK}^+}^0/k_{\text{on TFK}^0}^0) = \log(k_{\text{on high TFK}^+}/k_{\text{on high TFK}^0}) - 17z_{\text{TFK}^+}\psi_E \quad (23)$$

which expresses the ratio of the on rates for TFK^+ and TFK^0 at very low ionic strength as a function of the electrostatic potential in the gorge of AChE. As can be calculated by taking the appropriate values from column 4 of Table 2, the electrostatic potentials inside the gorges of TcAChE and mAChE are -80.4 mV and -71.2 mV , respectively. These values constitute the upper limit of the overall gorge potential at zero ionic strength and give a value for $\Delta\Delta G_{\text{on G}}^\ddagger$ of $\sim 1.6 \text{ kcal/mol}$, which can be considered to be the maximum contribution of global electrostatic

interactions to the stabilization of the activated binding state.

Potential values obtained by solving the PB equation exceed the ones calculated from the above experimental data by approximately fourfold (Felder et al., 1997; Wlodek et al., 1997b). While both methods involve several approximations, we are inclined to think that the methods using the PB equation might overestimate the potential inside the active-site gorge due to the inherent error involved in calculating the field within very tight crevices such as the active-site gorge, where the environment can be considered neither fully solvated nor completely devoid of water molecules.

Part III: product clearance from the active-site gorge

The electrostatic potential gradient inside the active-site gorge of ChEs does not retard clearance of positively charged products

One of the open questions concerning the mechanism of molecular traffic through the active-site gorge of ChEs is whether the effect of the electrostatic potential on the positively charged product of catalysis, choline (Ch), might be so strong as to impede its exit and, if so, whether there might be an alternative route for product traffic. The clearance of the other products of ACh hydrolysis has not attracted as much attention as that of their positively charged partner. In the case of acetate and acetic acid, the anionic and neutral nature of these molecules argues against an electrostatic impediment to clearance through the gorge. In the case of the proton, its clearance probably occurs either via water molecules present in the gorge or via coupling to the acetate ion (D. van Belle and S. Wodak, personal communication), and no hindrance from the gorge potential to its release has been suggested.

To establish whether the magnitude of the electrostatic potential inside the gorge is sufficient to sensibly retard the clearance of cationic species from the active site, we chose to describe this process by treating the exit of Ch from the gorge as a 1D escape from a well in the presence of a linear potential (Fig. 7). Accordingly, Ch will be modeled as a spherical particle with a single positive charge, and interactions with the walls of the gorge will be ignored. The gorge will be considered as a one-dimensional box, 20 \AA long, filled with water (Fig. 7). The effect of an electrostatic potential gradient on the rate of migration of a cationic ligand can be modeled by calculating the mean escape time $\langle t \rangle$ of a particle in a 1D potential well. The value of $\langle t \rangle$ can be derived as (Lifson and Jackson, 1962)

$$\nabla \cdot (e^\phi \nabla \langle t \rangle) = -e^\phi/D \quad (24)$$

where D is the diffusion constant of the ligand, and $\phi = -\psi(e/kT)$ is a reduced dimensionless electrostatic potential, where ψ is expressed in units of kT/e . Although not strictly correct, we can assume for the present purpose the potential

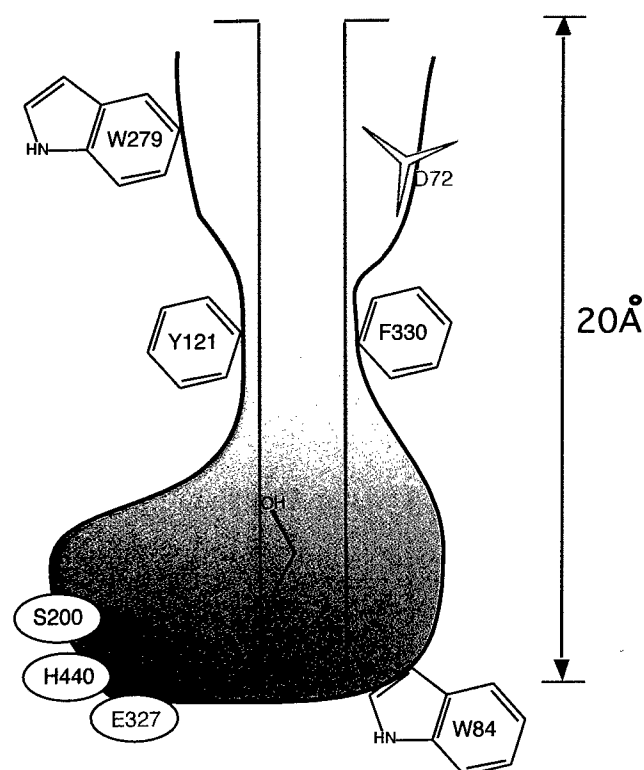


FIGURE 7 Schematic of the active-site gorge of AChE and model for the escape of choline from a one-dimensional potential well. The potential well is delimited by the green lines, and the bottleneck formed by F330 and Y121 is indicated by the benzene rings midway up the gorge.

gradient inside the gorge to be linear in distance. Accordingly, if L is the length of the gorge, the solution to Eq. (23) is

$$\langle t \rangle = (e^{\phi L} - 1 - \phi L) / D\phi^2 \quad (25)$$

In the special case of $\phi = 0$, and assuming a value of the diffusion constant, D , for Ch equal to that of ACh ($6.1 \times 10^{-6} \text{ cm}^2 \text{ s}^{-1}$), we get

$$\begin{aligned} \langle t \rangle &= L^2 / 2D = (2.0 \times 10^{-7} \text{ cm})^2 / 2 \cdot (6.1 \times 10^{-6} \text{ cm}^2 \text{ s}^{-1}) \\ &= 3.3 \times 10^{-9} \text{ s} \end{aligned} \quad (26)$$

In the case of the value that we calculated for the potential ψ at the bottom of the active-site gorge of 80 mV (which

is $\sim 3kT/e$), Eq. 24 yields the following escape time:

$$\begin{aligned} \langle t \rangle &= (L^2 / 2D)(2e^{\phi} / \phi^2) = (3.3 \times 10^{-9} \text{ s}) \times 2\exp(3) / 3^2 \\ &= 1.5 \times 10^{-8} \text{ s} \end{aligned} \quad (27)$$

This is ~ 4.5 -fold slower than the calculated escape time in the absence of the field. If it is assumed that varying the field does not affect any chemical step in the enzymatic hydrolysis, we can check the validity of our assumption by inspecting the variation of k_{cat} for ACh with salt concentration. It can be seen that at very low salt concentration, where the steering effect should be felt most strongly, turnover is just ~ 5 times slower than at $I = 600 \text{ mM}$, when the effect of the field should be completely screened by salt effects (Table 6). Because the strength of the field inside the active site gorge drops logarithmically with increasing ionic strength, its influence at physiological salt concentrations will be even less significant. From this result it can be seen that the presence of an electrostatic steering mechanism does not greatly influence the clearance of products from the gorge.

We are aware that the model we are employing is approximate, and that a more detailed treatment should include the effect of a gate midway through the gorge, constituted by residues F330 and Y121. Nonetheless, the presence of F330 as a bottleneck in *TcAChE* (Y337 in *hAChE* and *mAChE*) does not detract from our treatment, because this residue is known to be flexible (Harel et al., 1993). Moreover, in a recent MD study it was calculated that even if a putative gate made by F330 and Y121 is open for only 2.4% of the time, the transit of ACh will be slowed by no more than twofold (Zhou et al., 1998). In addition, we suggest that the aromatic side chain of F330 might play a more active role in assisting the clearance of cationic products from the gorge. In the F330A mutant, while k_{cat} for ACh is reduced, it is actually increased for its neutral analog, DBA (Ordentlich et al., 1993). A possible explanation for this observation is that substitution of a smaller side chain at position 330 widens the gorge, thus permitting faster traffic of the neutral product of DBA hydrolysis. In the case of Ch, however, removal of the aromatic side chain of F330 might destroy a shuttle-like mechanism for molecular traffic mediated by cation- π interactions between Ch and F330, thus reducing the rate of product clearance.

Our analysis of the contribution of long-range interactions to the binding of transition-state analogs of AChE

TABLE 6 Dependence on salt concentration of k_{cat} and comparison with calculated escape times

Theoretical		Experimental	
Potential (ϕ)	$\langle t \rangle$ (s)	k_{cat} (s^{-1})	
$0 \text{ kT}/e = 0 \text{ mV}$	$t_{\text{min}} = 3.3 \times 10^{-9}$	$k_{\text{max}} 1.06 \times 10^6 (I = 300 \text{ mM})^*$	$k_{\text{max}} 0.58 \times 10^6 (I = 500 \text{ mM})^{\#}$
$3.5 \text{ kT}/e = -80 \text{ mV}$	$t_{\text{max}} = 13 \times 10^{-9}$	$k_{\text{min}} 0.69 \times 10^6 (I = 2 \text{ mM})^*$	$k_{\text{min}} 0.20 \times 10^6 (I = 5 \text{ mM})$
Ratio	$t_{\text{max}}/t_{\text{min}} = 3.9$	$k_{\text{max}}/k_{\text{min}} = 4.3$	$k_{\text{max}}/k_{\text{min}} = 2.9$

*Nolte et al. (1980).

[#]Berman and Nowak (1992).

permits us to estimate whether the magnitude of these contributions might be sufficient to hinder the exit of Ch. The value of ~ 0.4 kcal/mol at $I = 145$ mM contributed by long-range electrostatic forces is close to the value of kT at 298.15K. Thus, it seems improbable that such a value would drastically impede Ch from drifting out of the active-site gorge by thermal diffusion. Ch is a noncompetitive inhibitor, with $K_i \approx 1.5$ mM at physiological salt concentration (Wilson and Alexander, 1962; Krupka, 1963; Eriksson and Augustinsson, 1979), and we can estimate the dissociation rate constant, k_{off} , from $K_i = k_{\text{off}}/k_{\text{on}}$. If k_{on} for Ch is comparable to the values for TFK⁺ and NMA, which are around $10^9 \text{ M}^{-1} \text{ s}^{-1}$ for TcAChE, then k_{off} will be $\sim 10^6 \text{ s}^{-1}$. Thus, k_{off} for Ch is larger than k_{cat} (of which k_{off} is a component), which is in the range of $0.5\text{--}1 \times 10^4 \text{ s}^{-1}$, by two orders of magnitude. Moreover, at low salt concentrations, k_{cat} values are decreased only by a fewfold, indicating that the binding strength of Ch is not significantly increased (Nolte et al., 1980; Hofer et al., 1984).

More evidence for the hypothesis that the potential gradient inside the active-site gorge of ChEs does not appreciably retard the clearance of positively charged products comes from studies of the ionic strength dependence of binding of TFK⁺ (Quinn et al., 1995; Radic et al., 1997). These studies showed that k_{off} for TFK⁺ is not dependent on salt concentration. This finding can be viewed in light of the fact that k_{on} and $1/K_i$, which are influenced by salt concentration, depend, respectively, on the free energy difference between the E + I state and the EI[‡] state, and between the E + I and the EI state. However, k_{off} depends on the energy difference between the EI and the EI[‡] states. Inspection of the free energy diagram displayed in Fig. 8 shows that if the effect of the electric field on the energies of EI and EI[‡] is of the same magnitude, the free energy barrier for release of the inhibitor will not be affected by the field. Hence, masking of the field by increasing salt concentration will have little influence on k_{off} .

There is some evidence pointing to the existence of alternative pathways for molecular traffic of substrates and products. A conformation for an open "back door" was suggested by molecular dynamics calculations (Gilson et al., 1994). However, a series of site-directed mutagenesis studies challenged this hypothesis by showing that mutations engineered to close the "back door" had little or no effect on the catalytic activity of AChE (Kronman et al., 1994; Faerman et al., 1996). Nonetheless, recent MD studies have revealed a number of possible alternative passageways to and from the active site (Wlodek et al., 1997b), and a MD study of the clearance from the gorge of acetic acid and acetate has identified a passageway for their release competing with the main entrance to the gorge (Enyedy et al., 1998). Furthermore, inspection of the crystal structure of TcAChE carbamoylated by the physostigmine analog 8-(*cis*-2,6-dimethylmorpholino)octylcarbamoyleseroline has provided indirect experimental evidence for a "back door" (Bartolucci et al., 1999). In addition, a study on the binding of TFK⁺ and TFK⁰ to the complex of AChE with the PAS

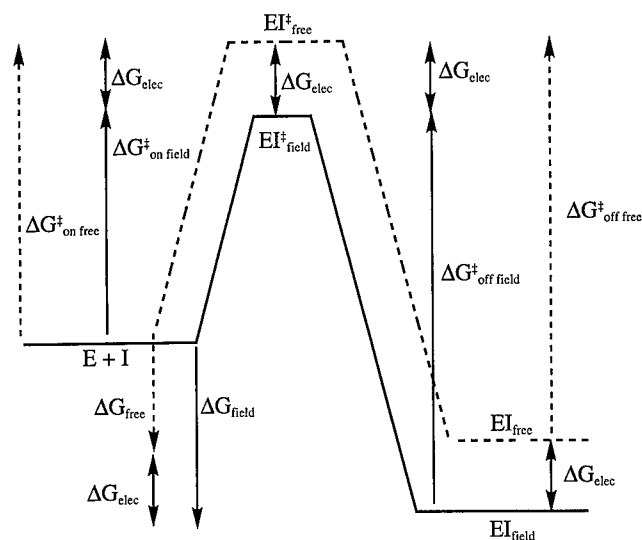


FIGURE 8 Free energy diagram for binding of TFK⁺ to AChE in the presence and absence of an electrostatic field in the active-site gorge. ΔG is the total free energy difference between the E + I state (free enzyme and inhibitor) and the EI complex. $\Delta G_{\text{on}}^{\ddagger}$ is the free energy difference between the E + I state and the activated binding state EI[‡], and $\Delta G_{\text{off}}^{\ddagger}$ is the free energy difference between the EI complex and activated binding state EI[‡]. The subscripts "field" and "free" refer, respectively, to the presence or absence of an electric field within the active-site gorge, and the difference in free energy due to this field is indicated by ΔG_{elec} . It can be seen that if ΔG_{elec} is the same for the EI[‡] state and for the EI complex, $\Delta G_{\text{off free}}^{\ddagger} = \Delta G_{\text{off field}}^{\ddagger}$. Consequently, k_{off} , which can be expressed as $k_{\text{off}} = \nu \exp(-\Delta G_{\text{off}}^{\ddagger}/RT)$, according to transition state theory, will not be affected by the presence of an electric field within the gorge (Quinn et al., 1995).

inhibitor fasciculin II (FAS), a three-fingered polypeptide toxin from the venom of the green mamba (Karlsson et al., 1984), showed an increase in on rates for both TFK⁺ and TFK⁰ but diminished inhibition when W84, whose side chain is assumed to form a major part of the "back door," was mutated to Y, F, or A (Radic et al., 1995). FAS has been shown to bind in a "cork-and-bottle fashion" to the entrance of the active-site gorge of AChE (Bourne et al., 1995; Harel et al., 1995). The surface complementarity between enzyme and inhibitor is very large; $\sim 2000 \text{ \AA}^2$ of accessible surface is buried upon binding, and analysis of the accessible surface of the FAS-AChE complex shows that the route to the bottom of the gorge is blocked even for a 1- \AA -radius probe.

From the above considerations, it can be concluded that side doors may exist in AChE, but rather than functioning as necessary exits for products, they might function as alternative routes for molecular traffic that are unmasked only when the principal pathway through the gorge is obstructed.

CONCLUSIONS

We have described a modular treatment for diffusion to and clearance from the active site of ChE and have estimated the contribution of a positive charge to the stabilization of the activated binding state of transition-state analogs for ChEs. Our model shows that diffusion of charged ligands relative

to neutral isosters is enhanced by ~ 10 -fold, because of a surface trap for cationic ligands. A steering mechanism contributes a maximum of 20-fold to rate enhancement at low salt concentration, but only about twofold at physiological salt concentration. We identify D72 as the primary component of the surface trap, and residues D82 and D278 as supplementary components. The maximum contribution of a positive charge to the binding energy is calculated to be ~ 4.7 kcal M^{-1} , of which ~ 1.3 kcal M^{-1} can be attributed to long-range electrostatic contributions, and ~ 3.5 kcal M^{-1} to short-range electrostatic interactions. Employing absolute rate reaction theory, we calculate the electrostatic potential at the binding-site to be ~ 80 mV at zero ionic strength. The clearance of cationic products from the active-site gorge is considered as analogous to the escape of a particle from a 1D well in the presence of a linear potential. Our calculations and experimental data show that clearance of Ch via the main entrance of the gorge is not hindered by the active-site potential, and while alternative routes to the active site may exist, they do not seem to be required for optimal catalytic function of ChEs.

These findings allow us to hypothesize that ChEs may have evolved from an ancestor whose efficiency for hydrolyzing esters already approached the theoretical limit, as this property is still evident in the very efficient cleavage of neutral esters. The optimal catalytic efficiency of this putative ancestor was possibly due to the burying of the transition state in the heart of the protein, providing it with a preorganized polar environment (Fuxreiter and Warshel, 1998). The penalty paid for this arrangement is that diffusion to the active site is not as fast as that to a shallow cleft on the surface of the protein.

Our contention is that acceleration of diffusion for cationic esters in ChEs arose by evolution of two additional modules. The first module is a surface trap for cationic substrates at the entrance to the gorge, operating through short-range electrostatic interactions, whose effect is to raise the theoretical limit of diffusion to a buried active site by an order of magnitude. The second module is a steering effect by means of long-range electrostatic interactions, giving charged substrates an added edge of about one additional order of magnitude, with minimum hindrance to the molecular traffic of substrate and products. Optimal flow of substrates and products is ensured by the aromatic residues lining the gorge, which constitute a series of binding sites for quaternary ammonium moieties. These binding sites provide a method of orientation and stabilization of the substrate in the active site and possibly a shuttle-like mechanism for the clearance of products. Molecular "traffic jams" are averted by the affinity of these binding sites, because the strength of the cation- π interaction is strongly dependent on the mutual orientation of the groups involved and decreases sharply with distance.

The work we have presented shows that, in ChEs, maximum catalytic efficiency and specificity for a positively charged substrate are achieved by an optimal fine-tuning of long- and short-range electrostatic interactions, while at the

same time striking a balance so that the electric potential inside the active site does not hinder the clearance of the positively charged product of the reaction.

The authors thank Drs. Charles Millard and Dan Quinn for valuable discussions. This work was supported by the U.S. Army Medical Research Acquisition Activity under Contract 17-97-2-7022; the Kimmelman Center for Biomolecular Structure and Assembly, Rehovot, Israel; and the Fourth Framework Program in Biotechnology of the European Union. IS is Bernstein-Mason Professor of Neurochemistry, and SAB is supported by the Theodore R. and Edlyn Racoosin Scholarship Fund.

REFERENCES

- Adam, G., and M. Delbrück. 1968. Reduction of dimensionality in biological diffusion processes. In *Structural Chemistry and Molecular Biology*. A. Rich and N. Davidson, editors. Freeman, San Francisco. 198–215.
- Allen, K. N., and R. H. Abeles. 1989a. Inhibition kinetics of acetylcholinesterase with fluoromethyl ketones. *Biochemistry*. 28:8466–8473.
- Allen, K. N., and R. H. Abeles. 1989b. Inhibition of pig liver esterase by trifluoromethyl ketones: modulators of the catalytic reaction after inhibition kinetics. *Biochemistry*. 28:135–140.
- Altschul, S. F., W. Gish, W. Miller, E. W. Myers, and D. J. Lipman. 1990. Basic local alignment search tool. *J. Mol. Biol.* 215:403–410.
- Anthony, N., T. Rocheleau, G. Mocelin, H. J. Lee, and R. Ffrench-Constant. 1995. Cloning, sequencing and functional expression of an acetylcholinesterase gene from the yellow fever mosquito *Aedes aegypti*. *FEBS Lett.* 368:461–465.
- Antosiewicz, J., M. K. Gilson, I. H. Lee, and J. A. McCammon. 1995a. Acetylcholinesterase: diffusional encounter rate constants for dumbbell models of ligand. *Biophys. J.* 68:62–68.
- Antosiewicz, J., M. K. Gilson, and A. McCammon. 1994. Acetylcholinesterase: effects of ionic strength and dimerization on the rate constants. *Isr. J. Chem.* 34:151–158.
- Antosiewicz, J., and J. A. McCammon. 1995. Electrostatic and hydrodynamic orientational steering effects in enzyme-substrate association. *Biophys. J.* 69:57–65.
- Antosiewicz, J., J. A. McCammon, S. T. Wlodek, and M. K. Gilson. 1995b. Simulation of charge-mutant acetylcholinesterases. *Biochemistry*. 34:4211–4219.
- Antosiewicz, J., S. T. Wlodek, and J. A. McCammon. 1996. Acetylcholinesterase: role of the enzyme's charge distribution in steering charged ligands toward the active site. *Biopolymers*. 39:85–94.
- Barak, D., A. Ordentlich, A. Bromberg, C. Kronman, D. Marcus, A. Lazar, N. Ariel, B. Velan, and A. Shafferman. 1995. Allosteric modulation of acetylcholinesterase activity by peripheral ligands involves a conformational transition of the anionic subsite. *Biochemistry*. 34:15444–15452.
- Bartolucci, C., E. Perola, L. Cellai, M. Brufani, and D. Lamba. 1999. "Back door" opening implied by the crystal structure of a carbamoylated acetylcholinesterase. *Biochemistry*. 38:5714–5719.
- Bataillé, S., P. Portalier, P. Coulon, and J. P. Ternaux. 1998. Influence of acetylcholinesterase on embryonic spinal rat motoneurons growth in culture: a quantitative morphometric study. *Eur. J. Neurosci.* 10:560–572.
- Bazelyansky, M., E. Robey, and J. F. Kirsch. 1986. Fractional diffusion-limited component of reactions catalyzed by acetylcholinesterase. *Biochemistry*. 25:125–130.
- Bergmann, F., I. B. Wilson, and D. Nachmansohn. 1950. The inhibitory effect of stilbamidine, curare and related compounds and its relationship to the active groups of acetylcholine esterase. *Biochim. Biophys. Acta*. 6:217–224.
- Berman, H. A., K. Leonard, and M. W. Nowak. 1991. Function of the peripheral anionic site of acetylcholinesterase. In *Cholinesterases: Structure, Function, Mechanism, Genetics and Cell Biology*. J. Massoulié, F. Bacou, E. Barnard, A. Chatonnet, B. P. Doctor, and D. M. Quinn, editors. American Chemical Society, Washington, DC. 229–234.
- Berman, H. A., and M. W. Nowak. 1992. Influence of the ionic composition of the medium on acetylcholinesterase. In *Multidisciplinary Ap-*

- proaches to Cholinesterase Functions. A. Shafferman and B. Velan, editors. Plenum Press, New York. 149–156.
- Bhanumathy, C. D., and A. S. Balasubramanian. 1996. Evidence for a Zn(2+)-binding site in human serum butyrylcholinesterase. *Biochem. J.* 315:127–131.
- Bourne, Y., P. Taylor, and P. Marchot. 1995. Acetylcholinesterase inhibition by fasciculin: crystal structure of the complex. *Cell.* 83:503–512.
- Brady, K., T. C. Liang, and R. H. Abeles. 1989. pH dependence of the inhibition of chymotrypsin by a peptidyl trifluoromethyl ketone. *Biochemistry.* 28:9066–9070.
- Changeux, J.-P. 1966. Responses of acetylcholinesterase from *Torpedo marmorata* to salts and curarizing drugs. *Mol. Pharmacol.* 2:369–392.
- Chatonnet, A., and O. Lockridge. 1989. Comparison of butyrylcholinesterase and acetylcholinesterase. *Biochem. J.* 260:625–634.
- Cousin, X., T. Hotelier, K. Giles, P. Lievin, J.-P. Toutant, and A. Chatonnet. 1997. The α/β fold family of proteins database and the cholinesterase genes server ESTHER. *Nucleic Acids Res.* 25:143–146.
- Dawson, R. M., and H. D. Crone. 1973. Inorganic ion effects on the kinetic parameters of acetylcholinesterase. *J. Neurochem.* 21:247–249.
- Dougherty, D. A. 1996. Cation- π interactions in chemistry and biology: a new view of benzene, Phe, Tyr and Trp. *Science.* 271:163–168.
- Dougherty, D. A., and D. A. Stauffer. 1990. Acetylcholine binding by a synthetic receptor: implications for biological recognition. *Science.* 250:1558–1560.
- Enyedy, I. J., I. M. Kovach, and B. R. Brooks. 1998. Alternate pathways for acetic acid and acetate ion release from acetylcholinesterase: a molecular dynamics study. *J. Am. Chem. Soc.* 120:8043–8050.
- Eriksson, H., and K. B. Augustinsson. 1979. A mechanistic model for butyrylcholinesterase. *Biochim. Biophys. Acta.* 567:161–173.
- Faerman, C., D. Ripoll, S. Bon, Y. Le Feuvre, N. Morel, J. Massoulié, J. L. Sussman, and I. Silman. 1996. Site-directed mutants designed to test back-door hypotheses of acetylcholinesterase function. *FEBS Lett.* 386:65–71.
- Felder, C. E., S. A. Botti, S. Lifson, I. Silman, and J. L. Sussman. 1997. External and internal electrostatic potentials of cholinesterase models. *J. Mol. Graph. Mod.* 15:318–327.
- Froede, H. C., and I. B. Wilson. 1971. Acetylcholinesterase. In *The Enzymes*. P. D. Boyer, editor. Academic Press, New York. 87–114.
- Fuxreiter, M., and A. Warshel. 1998. Origin of the catalytic power of acetylcholinesterase: computer simulation studies. *J. Am. Chem. Soc.* 120:183–194.
- Gilson, M. K., and B. Honig. 1988. Calculation of the total electrostatic energy of a macromolecular system: solvation energies, binding energies, and conformational analysis. *Proteins.* 4:7–18.
- Gilson, M. K., T. P. Straatsma, J. A. McCammon, D. R. Ripoll, C. H. Faerman, P. H. Axelsen, I. Silman, and J. L. Sussman. 1994. Open “back door” in a molecular dynamics simulation of acetylcholinesterase. *Science.* 263:1276–1278.
- Glasstone, S., K. J. Laidler, and H. Eyring. 1941. *The Theory of Rate Processes*. McGraw-Hill, New York.
- Grauso, M., E. Culetto, D. Combes, Y. Fedon, J. P. Toutant, and M. Arpagus. 1998. Existence of four acetylcholinesterase genes in the nematodes *Caenorhabditis elegans* and *Caenorhabditis briggsae*. *FEBS Lett.* 424:279–284.
- Haas, R., T. R. Marshall, and T. L. Rosenberry. 1992. Substrate-selective inhibition and peripheral site labeling of acetylcholinesterase by platinum(terpyridine)chloride. In *Multidisciplinary Approaches to Cholinesterase Functions*. A. Shafferman and B. Velan, editors. Plenum Press, New York. 131–140.
- Harel, M., G. J. Kleywegt, R. B. G. Ravelli, I. Silman, and J. L. Sussman. 1995. Crystal structure of an acetylcholinesterase-fasciculin complex: interaction of a three-fingered toxin from snake venom with its target. *Structure.* 3:1355–1366.
- Harel, M., D. M. Quinn, H. K. Nair, I. Silman, and J. L. Sussman. 1996. The x-ray structure of a transition state analog complex reveals the molecular origins of the catalytic power and substrate specificity of acetylcholinesterase. *J. Am. Chem. Soc.* 118:2340–2346.
- Harel, M., I. Schalk, L. Ehret-Sabatier, F. Bouet, M. Goeldner, C. Hirth, P. H. Axelsen, I. Silman, and J. L. Sussman. 1993. Quaternary ligand binding to aromatic residues in the active-site gorge of acetylcholinesterase. *Proc. Natl. Acad. Sci. USA.* 90:9031–9035.
- Harel, M., G. Kryger, J. L. Sussman, J. Silman, T. L. Rosenberry, W. D. Mallander, T. Lewis, R. J. Fletcher, and M. Guss. 1999. 3D structures of *Drosophila* acetylcholinesterase: implications for insecticide design. Abstracts IUCr XVII World Crystallography Congress, Glasgow, Scotland P09.04.023.
- Hasan, F. B., J. L. Elkind, S. G. Cohen, and J. B. Cohen. 1981. Cationic and uncharged substrates and reversible inhibitors in hydrolysis by acetylcholinesterase: the trimethyl subsite (EC 3.1.1.7). *J. Biol. Chem.* 256:7781–7785.
- Hasinoff, B. B. 1982. Kinetics of acetylthiocholine binding to electric eel acetylcholinesterase in glycerol/water solvents of increased viscosity. Evidence for a diffusion-controlled reaction. *Biochim. Biophys. Acta.* 704:52–58.
- Hofer, P., U. P. Fringeli, and W. H. Hopff. 1984. Activation of acetylcholinesterase by monovalent (Na^+ , K^+) and divalent (Ca^{2+} , Mg^{2+}) cations. *Biochemistry.* 23:2730–2734.
- Honig, B., and A. Nicholls. 1995. Classical electrostatics in biology and chemistry. *Science.* 268:1144–1149.
- Hosea, N. A., Z. Radic, I. Tsigelny, H. A. Berman, D. M. Quinn, and P. Taylor. 1996. Aspartate 74 as a primary determinant in acetylcholinesterase governing specificity to cationic organophosphonates. *Biochemistry.* 35:10995–11004.
- Imperiali, B., and R. H. Abeles. 1986. Inhibition of serine proteases by peptidyl fluoromethyl ketones. *Biochemistry.* 25:3760–3767.
- Inestrosa, N. C., A. Alvarez, C. A. Perez, R. D. Moreno, M. Vicente, C. Linker, O. I. Casanueva, C. Soto, and J. Garrido. 1996. Acetylcholinesterase accelerates assembly of amyloid beta-peptides into Alzheimer's fibrils: possible role of the peripheral site of the enzyme. *Neuron.* 16:881–891.
- Jackson, S. E., and A. R. Fersht. 1993. Contribution of long-range electrostatic interactions to the stabilization of the catalytic transition state of the serine protease subtilisin BPN'. *Biochemistry.* 32:13909–13916.
- Jones, S. A., C. Holmes, T. C. Budd, and S. A. Greenfield. 1995. The effect of acetylcholinesterase on outgrowth of dopaminergic neurons in organotypic slice culture of rat mid-brain. *Cell Tissue Res.* 279:323–330.
- Karlsson, E., P. M. Mbugua, and D. Rodriguez-Ithurralde. 1984. Fasciculins, anticholinesterase toxins from the venom of the green mamba *Dendroaspis angusticeps*. *J. Physiol. (Paris).* 79:232–240.
- Kortüm, G., and J. O. Bockris. 1951. *Textbook of Electrochemistry*. Elsevier Publishing, New York.
- Kronman, C., A. Ordentlich, D. Barak, B. Velan, and A. Shafferman. 1994. The “back door” hypothesis for product clearance in acetylcholinesterase challenged by site-directed mutagenesis. *J. Biol. Chem.* 269:27819–27822.
- Krupka, R. M. 1963. The mechanism of action of acetylcholinesterase: substrate inhibition and the binding of inhibitors. *Biochemistry.* 2:76–82.
- Laidler, K. J. 1965. *Chemical Kinetics*. McGraw-Hill, New York.
- Layer, P. G., T. Weikert, and R. Alber. 1993. Cholinesterases regulate neurite growth of chick nerve cells *in vitro* by means of a non-enzymatic mechanism. *Cell Tissue Res.* 273:219–226.
- Lifson, S., and J. Jackson. 1962. On the self diffusion of ions in a polyelectrolyte solution. *J. Chem. Phys.* 36:2410–2414.
- Luhmer, M., K. Bartik, A. Dejaegere, P. Bovy, and J. Reisse. 1994. The importance of quadrupolar interactions in molecular recognition processes involving a phenyl group. *Bull. Soc. Chim. Fr.* 131:603.
- Masson, P., M. T. Froment, C. F. Bartels, and O. Lockridge. 1996. Asp70 in the peripheral anionic site of human butyrylcholinesterase. *Eur. J. Biochem.* 235:36–48.
- Masson, P., P. Legrand, C. F. Bartels, M. T. Froment, L. M. Schopfer, and O. Lockridge. 1997. Role of aspartate 70 and tryptophan 82 in binding of succinylthiocholine to human butyrylcholinesterase. *Biochemistry.* 36:2266–2277.
- Massoulié, J., L. Pezzementi, S. Bon, E. Krejci, and F.-M. Vallette. 1993. Molecular and cellular biology of cholinesterases. *Prog. Neurobiol.* 41:31–91.
- Mendel, B., and H. Rudney. 1943. Studies on cholinesterase. I. Cholinesterase and pseudo-cholinesterase. *Biochem. J.* 37:59–63.

- Mutero, A., M. Pralavorio, V. Simeon, and D. Fournier. 1992. Catalytic properties of cholinesterases: importance of tyrosine 109 in *Drosophila* protein. *Neuroreport*. 3:39–42.
- Nair, H. K., K. Lee, and D. M. Quinn. 1993. *m*-(*N,N,N*,-Trimethylammonio)trifluoroacetophenone: a femtomolar inhibitor of acetylcholinesterase. *J. Am. Chem. Soc.* 115:9939–9941.
- Nair, H. K., J. Seravalli, T. Arbuckle, and D. M. Quinn. 1994. Molecular recognition in acetylcholinesterase catalysis: free-energy correlations for substrate turnover and inhibition by trifluoro ketone transition-state analogs. *Biochemistry*. 33:8566–8576.
- Nolte, H. J., T. L. Rosenberry, and E. Neumann. 1980. Effective charge on acetylcholinesterase active sites determined from the ionic strength dependence of association rate constants with cationic ligands. *Biochemistry*. 19:3705–3711.
- Ordentlich, A., D. Barak, C. Kronman, N. Ariel, Y. Segall, B. Velan, and A. Shafferman. 1996. The architecture of human acetylcholinesterase active center probed by interactions with selected organophosphate inhibitors. *J. Biol. Chem.* 271:11953–11962.
- Ordentlich, A., D. Barak, C. Kronman, Y. Flashner, M. Leitner, Y. Segall, N. Ariel, S. Cohen, B. Velan, and A. Shafferman. 1993. Dissection of the human acetylcholinesterase active center determinants of substrate specificity. Identification of residues constituting the anionic site, the hydrophobic site, and the acyl pocket. *J. Biol. Chem.* 268:17083–17095.
- Peitsch, M. C. 1996. ProMod and Swiss-Model: Internet-based tools for automated comparative protein modelling. *Biochem. Soc. Trans.* 24:274–279.
- Porschke, D., C. Créminon, X. Cousin, C. Bon, J. Sussman, and I. Silman. 1996. Electrooptical measurements demonstrate a large permanent dipole moment associated with acetylcholinesterase. *Biophys. J.* 70:1603–1608.
- Quinn, D. M. 1987. Acetylcholinesterase: enzyme structure, reaction dynamics, and virtual transition states. *Chem. Rev.* 87:955–979.
- Quinn, D. M., J. Serravalli, H. K. Nair, R. Medhekar, B. Hussein, Z. Radic, D. C. Vellom, N. Pickering, and P. Taylor. 1995. The function of electrostatics in acetylcholinesterase catalysis. In *Enzymes of the Cholinesterase Family*. D. M. Quinn, A. S. Balasubramanian, B. P. Doctor, and P. Taylor, editors. Plenum Press, New York. 203–207.
- Radic, Z., P. D. Kirchoff, D. M. Quinn, J. A. McCammon, and P. Taylor. 1997. Electrostatic influence on the kinetics of ligand binding to acetylcholinesterase. *J. Biol. Chem.* 272:23265–23277.
- Radic, Z., N. A. Pickering, D. C. Vellom, S. Camp, and P. Taylor. 1993. Three distinct domains in the cholinesterase molecule confer selectivity for acetyl- and butyrylcholinesterase inhibitors. *Biochemistry*. 32:12074–12084.
- Radic, Z., D. M. Quinn, D. C. Vellom, S. Camp, and P. Taylor. 1995. Allosteric control of acetylcholinesterase catalysis by fasciculin. *J. Biol. Chem.* 270:20391–20399.
- Radic, Z., E. Reiner, and P. Taylor. 1991. Role of the peripheral anionic site on acetylcholinesterase: inhibition by substrates and coumarin derivatives. *Mol. Pharmacol.* 39:98–104.
- Ripoll, D. R., C. H. Faerman, P. H. Axelsen, I. Silman, and J. L. Sussman. 1993. An electrostatic mechanism for substrate guidance down the aromatic gorge of acetylcholinesterase. *Proc. Natl. Acad. Sci. USA*. 90:5128–5132.
- Rosenberry, T. L. 1975a. Acetylcholinesterase. *Adv. Enzymol.* 43:103–218.
- Rosenberry, T. L. 1975b. Catalysis by acetylcholinesterase: evidence that the rate-limiting step by acetylation with certain substrate precedes general acid-base catalysis. *Proc. Natl. Acad. Sci. USA*. 72:3834–3838.
- Rosenberry, T. L., and E. Neumann. 1977. Interaction of ligands with acetylcholinesterase. Use of temperature-jump relaxation kinetics in the binding of specific fluorescent ligands. *Biochemistry*. 16:3870–3877.
- Samson, R., and J. M. Deutch. 1978. Diffusion-controlled reaction to a buried active site. *J. Chem. Phys.* 68:285–290.
- Schalk, I., L. Ehret-Sabatier, F. Bouet, M. Goeldner, and C. Hirth. 1992. Structural analysis of acetylcholinesterase ammonium binding sites. In *Multidisciplinary Approaches to Cholinesterase Functions*. A. Shafferman and B. Velan, editors. Plenum Press, New York. 117–120.
- Shafferman, A., A. Ordentlich, D. Barak, C. Kronman, R. Ber, T. Bino, N. Ariel, R. Osman, and B. Velan. 1994. Electrostatic attraction by surface charge does not contribute to the catalytic efficiency of acetylcholinesterase. *EMBO J.* 13:3448–3455.
- Shafferman, A., B. Velan, A. Ordentlich, C. Kronman, H. Grosfeld, M. Leitner, Y. Flashner, S. Cohen, D. Barak, and N. Ariel. 1992. Substrate inhibition of acetylcholinesterase: residues affecting signal transduction from the surface to the catalytic center. *EMBO J.* 11:3561–3568.
- Sitkoff, D., K. A. Sharp, and B. Honig. 1994. Accurate calculation of hydration free energies using macroscopic solvent models. *J. Phys. Chem.* 98:1978–1988.
- Smissaert, H. R. 1981. Acetylcholinesterase: evidence that sodium ion binding at the anionic site causes inhibition of the second-order hydrolysis of acetylcholine and a decrease of its pKa as well as of deacetylation. *Biochem. J.* 197:163–170.
- Srivatsan, M., and B. Peretz. 1997. Acetylcholinesterase promotes regeneration of neurites in cultured adult neurons of *Aplysia*. *Neuroscience*. 77:921–931.
- Stauffer, D. A., and A. Karlin. 1994. Electrostatic potential of the acetylcholine binding sites in the nicotinic receptor probed by reactions of binding-site cysteines with charged methanethiosulfonates. *Biochemistry*. 33:6840–6849.
- Sunner, J., K. Nishizawa, and P. Kebarle. 1981. Ion-solvent molecule interactions in the gas phase. *J. Phys. Chem.* 85:1815–1820.
- Sussman, J. L., M. Harel, F. Frolow, C. Oefner, A. Goldman, L. Toker, and I. Silman. 1991. Atomic structure of acetylcholinesterase from *Torpedo californica*: a prototypic acetylcholine-binding protein. *Science*. 253:872–879.
- Takahashi, L. H., R. Radhakrishnan, R. E. Rosenfield, Jr., E. F. Meyer, Jr., D. A. Trainor, and M. Stein. 1988. X-ray diffraction analysis of the inhibition of porcine pancreatic elastase by a peptidyl trifluoromethylketone. *J. Mol. Biol.* 201:423–428.
- Tan, R. C., T. N. Truong, J. A. McCammon, and J. L. Sussman. 1993. Acetylcholinesterase: electrostatic steering increases the rate of ligand binding. *Biochemistry*. 32:401–403.
- Taylor, P., and S. Lappi. 1975. Interaction of fluorescence probes with acetylcholinesterase. The site and specificity of propidium. *Biochemistry*. 14:1989–1997.
- Taylor, P., and Z. Radic. 1994. The cholinesterases: from genes to proteins. *Annu. Rev. Pharmacol. Toxicol.* 34:281–320.
- Toutant, J. P. 1989. Insect acetylcholinesterase: catalytic properties, tissue distribution and molecular forms. *Prog. Neurobiol.* 32:423–446.
- Vellom, D. C., Z. Radic, Y. Li, N. A. Pickering, S. Camp, and P. Taylor. 1993. Amino acid residues controlling acetylcholinesterase and butyrylcholinesterase specificity. *Biochemistry*. 32:12–17.
- Warwicker, J., and H. C. Watson. 1982. Calculation of the electric potential in the active site cleft due to alpha-helix dipoles. *J. Mol. Biol.* 157:671–679.
- Willbold, E., and P. G. Layer. 1994. Butyrylcholinesterase regulates laminar retinogenesis of the chick embryo *in vitro*. *Eur. J. Cell Biol.* 64:192–199.
- Wilson, I. B., and J. Alexander. 1962. Acetylcholinesterase: reversible inhibitors, substrate inhibition. *J. Biol. Chem.* 237:1323–1326.
- Wilson, I. B., and F. Bergmann. 1950. Studies on cholinesterase. VII. The active surface of acetylcholine esterase derived from effects of pH on inhibitors. *J. Biol. Chem.* 185:479–489.
- Wlodek, S. T., J. Antosiewicz, and J. M. Briggs. 1997a. On the mechanism of acetylcholinesterase action: the electrostatically induced acceleration of the catalytic step. *J. Am. Chem. Soc.* 119:8159–8165.
- Wlodek, T. S., T. W. Clark, L. R. Scott, and A. J. McCammon. 1997b. Molecular dynamics of acetylcholinesterase dimer complexed with tacrine. *J. Am. Chem. Soc.* 119:9513–9522.
- Zhou, H. X., J. M. Briggs, and J. A. McCammon. 1996. A 240-fold electrostatic rate enhancement for acetylcholinesterase substrate binding can be predicted by the potential within the active site. *J. Am. Chem. Soc.* 118:13069–13070.
- Zhou, H. X., S. T. Wlodek, and J. A. McCammon. 1998. Conformational gating as a mechanism for enzyme specificity. *Proc. Natl. Acad. Sci. USA*. 95:9280–9283.
- Zhu, K. Y., and J. M. Clark. 1995. Cloning and sequencing of a cDNA encoding acetylcholinesterase in Colorado potato beetle, *Leptinotarsa decemlineata* (Say). *Insect Biochem. Mol. Biol.* 25:1129–1138.

Crystal Structures of Aged Phosphonylated Acetylcholinesterase: Nerve Agent Reaction Products at the Atomic Level

**Charles B. Millard, Gitay Kryger, Arie Ordentlich,
Harry M. Greenblatt, Michal Harel, Mia L. Raves, Yoffi Segall,
Dov Barak, Avigdor Shafferman, Israel Silman, and
Joel L. Sussman**

Departments of Neurobiology and Structural Biology, Weizmann
Institute of Science, Rehovot 76100, Israel, and Israel Institute
for Biological Research, Ness Ziona 70450, Israel

Biochemistry[®]

Reprinted from
Volume 38, Number 22, Pages 7032-7039

Crystal Structures of Aged Phosphonylated Acetylcholinesterase: Nerve Agent Reaction Products at the Atomic Level^{†,‡}

Charles B. Millard,*[§] Gitay Kryger,^{||} Arie Ordentlich,[⊥] Harry M. Greenblatt,^{||} Michal Harel,^{||} Mia L. Raves,^{||,¶} Yoffi Segall,[⊥] Dov Barak,[⊥] Avigdor Shafferman,[⊥] Israel Silman,[▽] and Joel L. Sussman^{||,§}

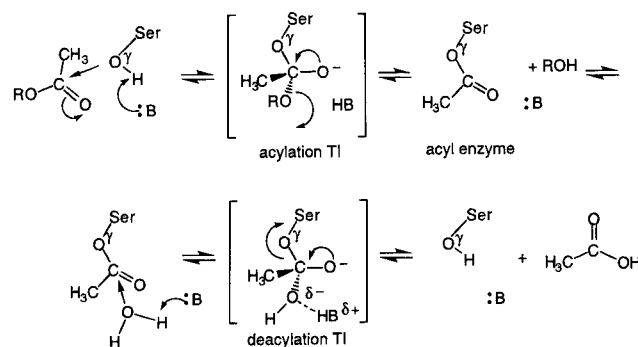
Departments of Neurobiology and Structural Biology, Weizmann Institute of Science, Rehovot 76100, Israel, and Israel Institute for Biological Research, Ness Ziona 70450, Israel

Received November 10, 1998; Revised Manuscript Received March 26, 1999

ABSTRACT: Organophosphorus acid anhydride (OP) nerve agents are potent inhibitors which rapidly phosphonylate acetylcholinesterase (AChE) and then may undergo an internal dealkylation reaction (called “aging”) to produce an OP-enzyme conjugate that cannot be reactivated. To understand the basis for irreversible inhibition, we solved the structures of aged conjugates obtained by reaction of *Torpedo californica* AChE (*TcAChE*) with diisopropylphosphorofluoridate (DFP), *O*-isopropylmethylphosphonofluoridate (sarin), or *O*-pinacolylmethylphosphonofluoridate (soman) by X-ray crystallography to 2.3, 2.6, or 2.2 Å resolution, respectively. The highest positive difference density peak corresponded to the OP phosphorus and was located within covalent bonding distance of the active-site serine (S200) in each structure. The OP-oxygen atoms were within hydrogen-bonding distance of four potential donors from catalytic subsites of the enzyme, suggesting that electrostatic forces significantly stabilize the aged enzyme. The active sites of aged sarin- and soman-*TcAChE* were essentially identical and provided structural models for the negatively charged, tetrahedral intermediate that occurs during deacylation with the natural substrate, acetylcholine. Phosphorylation with DFP caused an unexpected movement in the main chain of a loop that includes residues F288 and F290 of the *TcAChE* acyl pocket. This is the first major conformational change reported in the active site of any AChE–ligand complex, and it offers a structural explanation for the substrate selectivity of AChE.

Acetylcholinesterase (AChE¹) is an especially efficient serine hydrolase that catalyzes the breakdown of acetylcholine (ACh) at cholinergic synapses (reviewed in ref 1). The

Scheme 1: Reaction of AChE with a Natural Carboxyl Ester Substrate, Such as ACh^a



^a The scheme begins with the reversible enzyme–substrate complex and ends with free enzyme. The enzyme’s catalytic general base, probably Ne2 of His440, is depicted as :B, and the first product is depicted as ROH (choline in the case of ACh). The top panel shows acylation and the lower panel shows deacylation. For both reactions, the carbonyl carbon is expected to proceed from its planar geometry to a tetrahedral intermediate with an asymmetric negative charge distribution (depicted in brackets) during nucleophilic attack. Note that the theoretical deacylation TI for AChE is expected to resemble the aged OP-AChE conjugate (depicted in Scheme 2).

reaction of AChE with carboxyl ester substrates, including ACh, is believed to proceed through an unstable tetrahedral intermediate (TI) before collapsing to a short-lived ($t_{1/2} \sim 50 \mu\text{s}$) acetyl-enzyme (2) (Scheme 1). The acetyl-enzyme subsequently undergoes nucleophilic attack by water, passing through a second TI, and the regenerated enzyme is expelled as the leaving group (deacylation). The two-step catalytic

[†] The U.S. Army Medical Research & Materiel Command (agreements DAMD17-97-2-7022 and DAMD17-96-C-6088) and the U. S. Army Scientist/Engineer Exchange Program supported this project. The work was presented in preliminary form at the sixth International Meeting on Cholinesterases & Related Proteins, La Jolla, CA, 1998, and at the U.S. Army Bioscience Review, Hunt Valley, MD, 1998.

[‡] Coordinates for the solved crystal structures have been deposited in the Brookhaven Protein Data Bank, Biology Department, Brookhaven National Laboratory, Upton, NY 11973 under accession codes 1som (soman), 1cfj (sarin), and 2dfp (DFP).

* Corresponding author e-mail: limill@sgjs6.weizmann.ac.il.

[§] Visiting scientist at the Weizmann Institute from the U.S. Army Medical Research Institute of Chemical Defense, APG, MD 21010-5425.

^{||} Department of Structural Biology, The Weizmann Institute of Science.

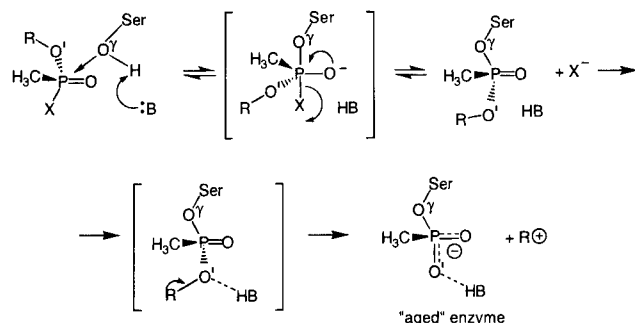
[⊥] Israel Institute for Biological Research.

[¶] Present address: Department of NMR Spectroscopy, Bijvoet Center for Biomolecular Research, Utrecht University, 3584 CH Utrecht, The Netherlands.

[▽] Department of Neurobiology, The Weizmann Institute of Science.

[§] Biology Department, Brookhaven National Laboratory, Upton, NY 11973.

¹ Abbreviations: ACh, acetylcholine; AChE, acetylcholinesterase (EC 3.1.1.7); ATCh, acetylthiocholine; BChE, butyrylcholinesterase (EC 3.1.1.8); BTCh, butyrylthiocholine; DFP, diisopropylphosphorofluoridate; Hu, human; MeP-, methylphosphonylated; MES, (2-[N-morpholino]ethanesulfonic acid); MiPrP-, monoisopropylphosphorylated; OP, organophosphorus acid anhydride; PDB, Protein Data Bank; PEG, poly(ethylene glycol); rmsd, root-mean-square deviation; *Tc*, *Torpedo californica*; TI, tetrahedral intermediate; TMTFA, *m*-(*N,N,N*-trimethylammonio)-2,2,2-trifluoroacetophenone.

Scheme 2: Reaction of AChE with a Phosphonate Nerve Agent^a

^a The scheme begins with the reversible enzyme-OP complex and ends with irreversibly inhibited aged enzyme. The phosphorylation leaving group is depicted as X (fluoride ion in the case of soman, sarin, or DFP); the enzyme's catalytic general base, probably Ne2 of His440, is depicted as :B; R is a branched alkyl group; and R+ is a hypothetical carbonium ion which reacts in water to yield primarily the alcohol product, ROH (9). The top panel shows phosphorylation, and the lower panel shows dealkylation (aging). Phosphorylation is expected to occur via a trigonal bipyramidal intermediate (depicted in brackets in the upper panel), or a transition state resembling such a structure, with inversion of stereochemistry at P. For reaction of AChE with DFP, an -O*i*Pr group replaces the -CH₃ bonded to P.

mechanism renders AChE susceptible to rapid, stoichiometric, and essentially irreversible inhibition by a class of organophosphorus acid anhydride (OP) inhibitors, typified by diisopropylphosphorofluoridate (DFP) and the phosphonate nerve agents, which can act as "hemisubstrates" to trap the enzyme in a structure that closely resembles the negatively charged deacylation TI (3) (Scheme 2).

Unlike the intermediates formed with carboxyl esters, the OP-enzyme persists for many hours or days (reviewed in ref 4). Slow hydrolysis has been explained by steric exclusion; the active-site histidine (H440) is not positioned to carry a water molecule to the correct face of the phosphorus required for nucleophilic attack (5, 6). It also has been proposed that H440 is rendered ineffective as a general base because the imidazolium forms an unproductive hydrogen bond with an oxygen atom of the OP (7).

After phosphorylation² of the active-site serine, some OP-AChE conjugates undergo post-inhibitory reactions, collectively called "aging", which result in truly irreversible enzyme inhibition (Scheme 2). The best-characterized aging reaction is that of AChE inhibited by DFP, *O*-isopropylmethylphosphonofluoridate (sarin), or *O*-pinacolylmethylphosphonofluoridate (soman). These inhibitors possess a branched alkyl group (Figure 1) which has been proposed to undergo dealkylation by a carbonium ion mechanism, thereby adding a formal negative charge to the active site of phosphylated AChE (8, 9).

The X-ray crystallographic structure of *Torpedo californica* (*Tc*) AChE (10) and computer-based homology models of human (Hu) AChE (11) and the closely related serum enzyme butyrylcholinesterase (BChE; refs 12, 13), combined with site-directed mutagenesis studies, have permitted tentative identification of the specific amino acid residues which constitute several catalytic subsites, including an "oxyanion hole" (14), a hydrophobic acyl pocket, and a trimethylam-

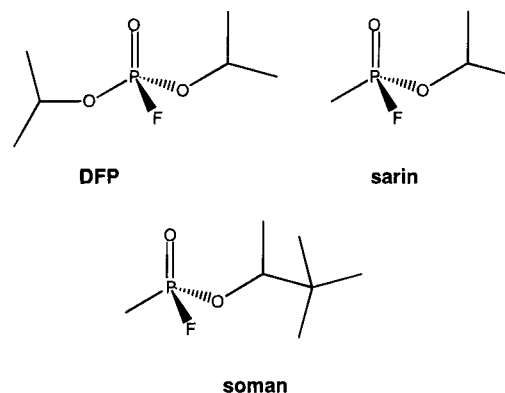


FIGURE 1: Chemical formulas of the OP inhibitors (non-hydrogen atoms).

monium (choline) binding site (reviewed in ref 15). Direct demonstration of these subsites with natural substrates has not been achieved because of the inherent instability of the intermediates that form during carboxyl ester hydrolysis. Our goal was to solve the three-dimensional structures of aged phosphylated *TcAChE* as a means of (1) understanding the forces that oppose reactivation (dephosphorylation) of the OP-enzyme, and (2) providing structural models for the deacylation TI of carboxyl ester hydrolysis which could validate the topography of the AChE active site.

MATERIALS AND METHODS

Enzyme Purification and Characterization. *TcAChE* was purified as described (16), and the steady-state constants for its reactions with acetylthiocholine (ATCh), butyrylthiocholine (BTCh), and DFP were measured using previously described methods (17, 18). Briefly, the catalytic activity was determined for substrates ATCh and BTCh by the spectrophotometric method of Ellman (19). Substrate Michaelis constants (K_m) and catalytic rate constants (k_{cat}) were derived from Lineweaver-Burk plots and from direct nonlinear curve fitting of the rate equation. The steady-state dissociation constant (K_d) and phosphorylation rate constant (k_2) for the reaction of DFP with *TcAChE* were measured by monitoring continuous inhibition curves in the presence of excess substrate (ATCh) (18, 20). All kinetic experiments were done in 50 mM phosphate buffer, pH 8.0, 24 °C.

Crystallization of OP-*TcAChE* Conjugates. Purified *TcAChE* was inhibited with DFP, sarin, or soman.³ DFP and sarin were used at 300-fold molar excess to enzyme, and soman was used at 2100-fold molar excess. The aging reaction proceeded to >95% completion; aliquots of the OP-*TcAChE* conjugates could not be reactivated by 20 h incubation with either 10 mM pyridine-2-aldoxime methiodide or 1,1'-trimethylene-bis(4-formylpyridinium bromide) dioxime. Unbound OP was removed by gel filtration before the crystallization experiments.

OP-*TcAChE* conjugates were crystallized in hanging drops by the vapor diffusion method. Protein crystallized at a concentration of 10 mg/mL from a precipitating solution of 35–40% w/v PEG-200 (Sigma Chemicals, St. Louis, MO) in 0.15 M MES buffer, 0.05 M NaCl, pH 5.8–6.0 at 4 °C.

² The term "phosphylated" denotes phosphorylation and phosphonylation reactions without distinction.

³ The OP inhibitors are extremely toxic; sarin and soman were handled according to established regulations governing chemical warfare materials.

Table 1: Kinetic Constants for Reaction of ATCh, BTCh, or DFP with TcAChE, HuAChE, or HuBChE^a

	substrate hydrolysis ($k_{cat}/K_m \times 10^{-8} \text{ (M}^{-1} \text{ min}^{-1})$)		DFP inhibition		
	ATCh	BTCh	$k_i \times 10^{-4} \text{ (M}^{-1} \text{ min}^{-1})$	$k_2 \text{ (min}^{-1})$	$K_d \text{ (}\mu\text{M)}$
TcAChE	46 ± 5	0.10 ± 0.01	2.0 ± 0.1	1.5 ± 0.5	70 ± 20
HuAChE ^b	30 ± 4	0.30 ± 0.05	5.0 ± 0.1	0.6 ± 0.1	13 ± 2
HuAChE F295L/F297V ^c	2.2 ± 0.3	14 ± 3	800 ± 60	0.8 ± 0.1	0.10 ± 0.02
HuBChE ^d	3.4 ± 0.5	7 ± 1	1660 ± 50	1.0 ± 0.2	0.06 ± 0.01

^a Each value is the mean ± standard error of at least four repetitions. ^b Recombinant, wild-type HuAChE expressed in 293 embryonic kidney cells (17, 18). ^c HuAChE mutant in which the acyl pocket residues corresponding to F288 and F290 in TcAChE have been replaced with those found in the sequence of HuBChE (17, 18). ^d Recombinant wild-type HuBChE expressed in 293 cells.

Although suitable crystals appeared spontaneously after 5–10 days, their quality was improved by seeding with microscopic crystalline fragments.

X-ray Diffraction and Data Processing. The exterior mother liquor that surrounds the crystals during their growth was exchanged with high-viscosity motor oil (Exxon, Houston, TX), and the crystals subsequently were flash-cooled in liquid nitrogen (21). X-ray diffraction data were collected at 100 K. Data for the DFP and soman conjugates were collected at the Weizmann Institute of Science using a Rigaku rotating anode FR300 (50 mA, 50 kV) source ($\lambda = 1.54 \text{ \AA}$) with a Rigaku Raxis-II detector. For the sarin conjugate, data were collected using the U.S. National Synchrotron Light Source at Brookhaven National Laboratory on beamline X12C ($\lambda = 1.1 \text{ \AA}$), with a 2×2 Brandeis charge-coupled device detector. Data collection parameters were optimized using the computer program STRATEGY (22), and intensity data were processed with DENZO and SCALEPACK (23).

Model Refinement. The 2.5 Å structure of native TcAChE (2ace in the Brookhaven Protein Data Bank, PDB) (24) was used to obtain the initial models by rigid-body refinement and simulated annealing (25). The solvent, carbohydrate, and OP atoms subsequently were built into ($F_o - F_c$) electron density difference maps. All three structures were refined by a combination of simulated annealing and torsion angle molecular dynamics with a maximum likelihood target function, using the programs of Crystallography & NMR System, CNS v.0.5 (26, 27). The quality of the refined structures was assessed using PROCHECK (28) and WHAT-IF (29). The C α atom positions of the OP-TcAChE structures were compared with those of native TcAChE using PROFIT (SciTech Software, University College, London). The program INSIGHTII v.97.0 (Biosym Technologies, San Diego, CA) was used to calculate the positions of hydrogen atoms, to generate theoretical solvent-accessible surfaces, and to produce the final figures.

RESULTS

Reaction Kinetics. The reaction rate constants of TcAChE with ATCh, BTCh, or DFP were similar to those of HuAChE, but considerably different from those of HuBChE (Table 1). For example, the K_d for the reversible complex of TcAChE and DFP was 6-fold less than that measured for HuAChE using identical methodology (18), but it was over 1200-fold less than that measured for HuBChE (Table 1).

X-ray Crystallography. Data were collected from trigonal crystals of space group $P3_121$ (10) and refined to 2.3 (DFP), 2.6 (sarin), or 2.2 Å (soman) resolution (Table 2). The highest positive difference density peak ($>15\sigma$) in the initial ($F_o -$

Table 2: Crystallographic Data Collection and Refinement Statistics

	MiPrP-AChE (DFP)	MeP-AChE (sarin)	MeP-AChE (soman)
Data Collection			
resolution (Å)	20–2.3	30–2.6	30–2.2
total number of reflections	278 106	200 755	286 328
unique reflections	42 410	30 011	49 048
% completeness: overall (highest refinement shell)	94.2 (66.3)	97.4 (99.3)	96.7 (94.1)
R_{sym}^a : overall (highest refinement shell)	0.07 (0.41)	0.09 (0.17)	0.05 (0.30)
average I /average σ : overall (highest refinement shell)	15.9 (1.7)	10.3 (2.2)	15.6 (2.6)
Refinement			
R factor ^b (no σ cutoff) (%)	18.6	18.6	21.0
number of reflections in working set	40 334	27 034	46 332
R free ^c (no σ cutoff) (%)	22.7	24.7	25.1
number of reflections in test set (% total)	1874 (4.2)	1497 (4.9)	2460 (4.9)
rmsd bond lengths (Å)	0.02	0.02	0.02
rmsd bond angles (deg)	1.9	2.0	1.9
total number of nonhydrogen atoms	4729	4497	4390
protein	4263	4245	4174
carbohydrate	70	28	28
inhibitor	7	4	4
water (MES ^d)	377 (12)	220	184

^a $R_{\text{sym}} = \sum |I - \langle I \rangle| / \sum I$, where I is an individual reflection measurement and $\langle I \rangle$ is the mean intensity for symmetry-related reflections.

^b R -factor = $\sum ||F_o| - |F_c|| / \sum |F_o|$, where F_o and F_c are observed and calculated structure factors, respectively. ^c R free is calculated for randomly selected reflections excluded from refinement. ^d A single molecule of MES (crystallization buffer) was refined on the surface of the MiPrP-AChE structure, adjacent to the TcAChE carboxyl-terminal α -helix. The MES molecule was apparently stabilized by the side-chain nitrogen atoms of Q500 and N409, as well as by a water molecule within possible hydrogen-bond distance to the imidazole ring of H406 (not shown).

F_c) maps corresponded to the phosphorus of the OP and was observed to be within covalent bonding distance of the S200 O γ in all three structures (Figure 2). Only one peak of this magnitude was found in each structure; this result confirmed that OP nerve agents form a covalent bond exclusively with the active-site serine of AChE (30).

The overall orientation of the bound OP, relative to the active-site gorge, was comparable in all three structures (Figures 3 and 4). There were no detectable alterations in the geometry of the active-site triad (S200-H440-E327) of the aged OP-TcAChE structures, compared with that of native TcAChE. A water molecule that is normally present within hydrogen-bond distance of the oxyanion hole in the active site of native TcAChE (water no. 682 in 2ace) was displaced by the OP in each structure.

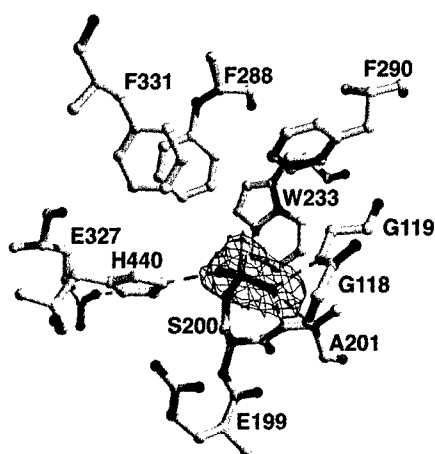


FIGURE 2: Initial difference electron density map for MeP-AChE. The final, refined active site of aged MeP-AChE, obtained by reaction with soman, is superimposed on the initial ($F_o - F_c$) electron density map (30–2.2 Å all data; map contour level 3σ) after rigid-body refinement of the protein, but before including the OP moiety in the refinement. Only density that is within 2.0 Å of the soman atoms is contoured. Note that the tetrahedral geometry of the soman phosphorus atom was clearly apparent in the initial, unbiased difference maps.

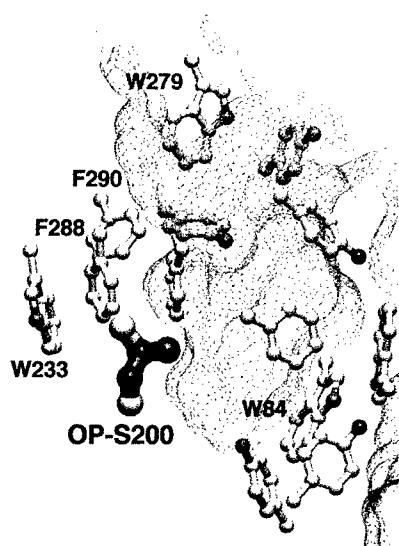


FIGURE 3: Orientation of the bound OP relative to the active-site gorge. The structure depicted is that of aged MeP-*TcAChE* (soman) viewed down the P=O bond with the oxanion hole oxygen atom (not visible) directly behind the phosphorus atom (colored purple). The position of the phosphonylated serine (OP-S200) is shown relative to those of the thirteen aromatic side chains that line the active-site gorge of AChE (10). The solvent-accessible surface (spherical probe of 1.4 Å radius) was calculated for 16 Å around the OP (grey mesh). Note that the OP methyl group is buried in a hydrophobic patch formed by W233, F288, and F290, but the oxygen that undergoes dealkylation (O' Scheme 2) points toward a solvent-accessible pocket in front of W84.

The strong stereoselectivity of AChE ensured that, under our experimental conditions, the primary OP reactants were the P_S stereoisomers of sarin and soman (31). The MeP-AChE structures establish the stereochemistry of the final reaction products and, thereby, demonstrate an overall inversion of the absolute configuration at the OP phosphorus (Figure 4). Inversion is consistent with a simple in-line nucleophilic attack by the S200 O γ during phosphorylation (Scheme 2), but the structures do not exclude more complicated reaction mechanisms.

At completion of the post-inhibitory aging process, the final reaction product was an anionic methylphosphonylated (MeP)-AChE in the case of sarin and soman, or an anionic monoisopropylphosphorylated (MiPrP)-AChE with DFP (Figure 4). Direct observation of the dealkylated OPs after aging proves that the original interpretations of low-molecular-mass product analysis (8, 9) and recent mass spectrometric data (32) were fundamentally correct.

In all three aged OP-*TcAChE* structures, the oxygen atom of the OP that underwent dealkylation (designated O' in Scheme 2) was oriented toward a polar pocket in the active site that contained several water molecules (corresponding to waters no. 633, 678, 679, and 742 in 2ace). At least one of these waters (no. 742 in 2ace) must move to accommodate the alkyl group that departs during aging. The geometry between O' and H440 N ϵ 2 was consistent with the presence of an imidazolium at H440 that could act as a hydrogen-bond donor (Table 3).

The overall root-mean-square deviation (rmsd) for C α atoms, relative to native *TcAChE*, was only 0.3 Å for each MeP-AChE structure and 0.4 Å for MiPrP-AChE. There was an unexpected conformational change, however, in the active-site acyl pocket of the MiPrP-AChE structure. The side chains of F288 and F290 moved significantly, and the main chain underwent "peptide flips" (33) between I287 and S291 to accommodate one of the *isopropyl* groups of DFP (Figures 4C and 5). The ψ -dihedral angle for I287 changed by 184°, moving from $\psi = 140^\circ$ in native *TcAChE* to $\psi = -44^\circ$ in MiPrP-AChE. This flip in the I287 ψ -dihedral angle was offset by successive changes in the ψ -dihedral angles for R289, F290, and S291. The calculated deviation for the C α atoms in residues 287–291 in the MiPrP-AChE structure, compared with native *TcAChE*, was 0.6, 2.9, 4.8, 2.2, and 0.8 Å, respectively.

A more subtle repositioning of F331 by rotation around its χ_1 and χ_2 angles also occurred in the MiPrP-AChE acyl pocket (not shown). The phenyl ring of F331 moved and partially filled the space created by displacement of the phenyl ring of F288.

The conformational change in MiPrP-AChE did not appear to be a consequence of the dealkylation reaction (aging), because no evidence was found for a significant conformational change in the other two aged structures. Moreover, the residues in the acyl pocket of the sarin conjugate showed no detectable movement, despite the fact that both DFP and sarin lose an identical *isopropyl* group during the dealkylation reaction (Scheme 2).

DISCUSSION

Serine hydrolases may catalyze the phosphorylation and aging reactions with OP inhibitors containing branched alkyl groups, and thus greatly accelerate their own irreversible inhibition (7, 34). The remarkably large rate enhancement of the aging reaction by cholinesterase has been ascribed to the precise juxtaposition of the departing alkyl group with specific amino acid residues in the enzyme active site (35–37).

The aged OP-*TcAChE* structures do not permit direct observation of the alkyl group that departs during dealkylation, but its general topography on the enzyme surface can be deduced from the steric constraints of the phosphylated active site (38). On the basis of the position of the residual

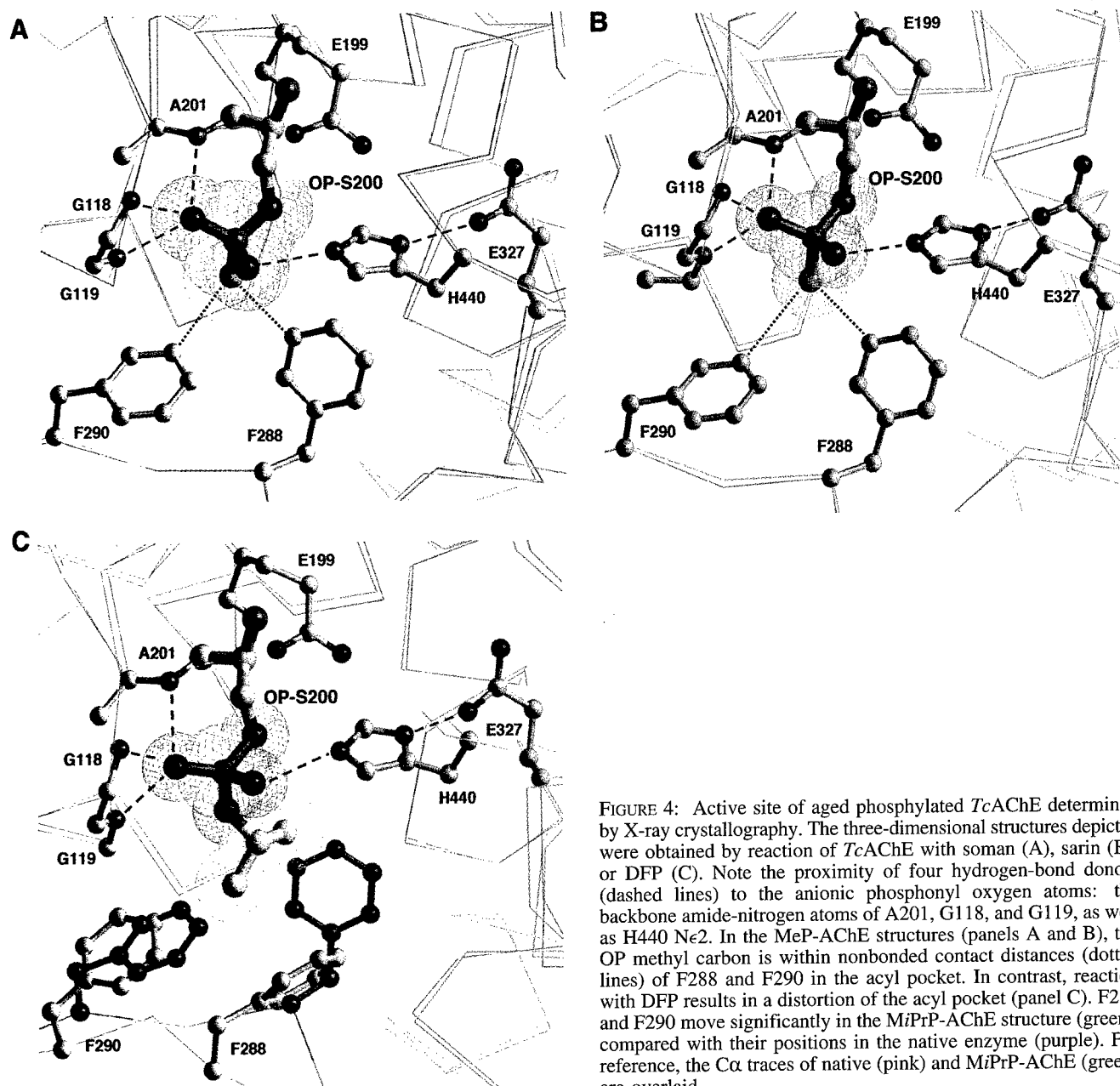


FIGURE 4: Active site of aged phosphorylated *TcAChE* determined by X-ray crystallography. The three-dimensional structures depicted were obtained by reaction of *TcAChE* with soman (A), sarin (B), or DFP (C). Note the proximity of four hydrogen-bond donors (dashed lines) to the anionic phosphonyl oxygen atoms: the backbone amide-nitrogen atoms of A201, G118, and G119, as well as H440 Nε2. In the MeP-AChE structures (panels A and B), the OP methyl carbon is within nonbonded contact distances (dotted lines) of F288 and F290 in the acyl pocket. In contrast, reaction with DFP results in a distortion of the acyl pocket (panel C). F288 and F290 move significantly in the MiPrP-AChE structure (green), compared with their positions in the native enzyme (purple). For reference, the Cα traces of native (pink) and MiPrP-AChE (green) are overlaid.

oxygen atom (O' Scheme 2), the bond that breaks during aging is close to the imidazole ring of H440 (Table 3). Furthermore, the departed alkyl group would have filled the solvent-accessible pocket in front of the indole ring of W84 (Figure 3). Dealkylation occurs selectively in this site because the crystal structure shows that DFP lost exclusively the *isopropyl* group in front of W84, while the residual *isopropyl* group in the acyl pocket is present at full occupancy.

The deduced position of the departed alkyl group in the crystal structures explains several biochemical features of the aging reaction in solution: (1) the catalytic histidine participates in aging (34, 39); (2) dealkylation occurs preferentially in the choline binding subsite (8, 40, 41), which is now widely accepted to be W84 (10, 42); and (3) aging rate constants for OPs with branched alkyl groups are reduced 60–1100-fold by the site-specific replacement of W86(84)⁴ in HuAChE (36, 43).

The negative charge introduced by the departure of an alkyl group during aging imposes an important barrier to

dephosphorylation because anionic phosphoesters are inherently resistant to nucleophilic attack (44). Electrostatic repulsion alone, however, does not adequately explain the truly irreversible character of aged enzyme. The presence of a negative charge retards nucleophilic attack of simple phosphorus diesters by only approximately 50–100-fold (45), and reactivation of anionic OP-chymotrypsin conjugates by an intramolecular nucleophile is possible (46). Furthermore, protein denaturation of aged MiPrP-AChE permits significant base-catalyzed dephosphorylation (47), suggesting that the resistance of aged OP-AChE to reactivation must be partly caused by specific structural interactions between the folded enzyme and the OP.

Structural Barriers to Enzyme Reactivation. The aged OP-*TcAChE* structures reveal a remarkable array of possible

⁴ The italicized number in parentheses immediately following an amino acid residue is the corresponding residue in the reference structure, *TcAChE*.

Table 3: Distances between TcAChE Active-site Residues and the OP Moiety

donor...acceptor	Possible Hydrogen Bonds (Å/deg) ^a		
	MeP-AChE sarin	MeP-AChE soman	MiPrP-AChE DFP
H440 Nε2...O ^b -P	2.9/154	2.6/173	2.7/168
G118 N...O ^c -P	2.8/165	2.8/160	2.7/161
G119 N...O ^c -P	2.6/152	2.6/161	2.6/158
A201 N...O ^c -P	3.1/163	3.0/169	3.0/169

	Acyl Pocket Distances (Å) ^d		
	sarin	soman	TMTFA complex
F288	4.8	4.8	5.1
F290	4.7	4.8	5.6
G119 ^e	4.0	3.9	4.3
W233	4.2	4.3	4.8
F331	5.5	5.5	5.6

^a Hydrogen bonds were considered possible if the straight-line distance between an appropriate donor and acceptor atom was ≤ 3.5 Å and the angle from donor-hydrogen-acceptor atom was $\geq 120^\circ$. For calculation of the angles, the positions of the putative hydrogen atoms were determined from the geometry of the heavy atom positions using INSIGHTII. ^b The residual oxygen atom after dealkylation (depicted as O' in Scheme 2). ^c The oxygen atom in the oxyanion hole (depicted as O in Scheme 2). ^d Straight-line distance from the methyl carbon atom of the phosphonate, or from the CF₃-carbon atom of TMTFA (42), to the geometric center of the phenyl or benzopyrrole ring of the indicated side chain. ^e Straight-line distance to G119 Cα.

noncovalent forces that contribute to the irreversible inhibition which is characteristic of OP nerve agents. Three possible hydrogen bonds from the oxyanion hole (main-chain nitrogen atoms of G118, G119, and A201) to one phosphonyl oxygen atom stabilize the bound OP adduct before and after aging (Table 3). Indeed, this interaction may be strengthened by dealkylation (aging) because electronic rearrangement could place the formal negative charge of the aged OP adduct partly or entirely in the dipolar oxyanion hole. It was shown by site-specific mutagenesis that replacement of the oxyanion hole residues equivalent to either G118 or G119 in HuAChE and HuBChE markedly slows the reaction rate constants for OP inhibitors (48–50).

The acyl pocket provides another barrier to reactivation. A "dry" hydrophobic patch formed by F288, F290, W233, and G119 Cα completely surrounds one OP alkyl (or alkoxy) group (Table 3; Figure 2). This could limit dephosphorylation by blocking access of attacking water molecules to the correct face of the phosphorus, as well as by providing stabilizing nonbonded contacts to the OP in the case of the sarin or soman (Figure 4). The G119 Cα is only 4.3 Å away from the phosphorus and is almost in-line with the phosphorus-S200 Oγ bond. Placing an imidazole side chain specifically at this position in HuBChE (G117(I19)H) confers OP hydrolase activity by increasing spontaneous dephosphorylation (49, 51).

A key structural feature of aged OP-serine hydrolases appears to be a favorable electrostatic interaction between Nε2 of the active-site imidazolium and one oxygen atom of the anionic OP moiety. A hydrogen bond is possible between H440 Nε2 (donor) and one oxygen of the OP (acceptor) in each of the three aged OP-TcAChE crystal structures (Table 3). Similar geometry is present in the aged structures of MiPrP-trypsin (PDB code 1ntp) (52), MiPrP-chymotrypsin

(1gmh) (53), and an MeP-esterase (from *Streptomyces scabies*; 1esd) (54). The presence of a hydrogen bond is consistent with the conclusion that the catalytic histidine Nε2 is immobilized in a protonated form in the aged enzyme, thereby locking the phosphorylated active site in an electrostatic and structural analogue of the natural substrate TI (55).

Structural Models for the Deacylation Tetrahedral Intermediate. The active sites of aged MeP-AChE (sarin and soman) provide the best available structural analogues for the negatively charged, deacylation TI formed during reaction with the natural substrate, ACh (55, 56). One phosphonyl oxygen in the oxyanion hole mimics the carbonyl oxygen in the substrate TI (14), while the other oxygen atom interacts with the H440 imidazolium. Thus, the anionic OP adduct strongly complements the preformed electrostatic environment of the AChE active site (reviewed in ref 57). Additionally, the position of the methyl group of sarin and soman should closely approximate that of the ACh methyl group (Scheme 1). Both F288 and F290 provide close nonbonded contacts to the sarin or soman methyl group (Figure 4), supporting the hypothesis that these aromatic side chains also bind the ACh methyl group in the substrate TI (42).

The side chain of W233 is proximal to the methyl group in the MeP-AChE structure (deacylation TI analog), as well as to the CF₃ group in the structure of TcAChE inhibited with m-(N,N,N-trimethylammonio)-2,2,2-trifluoroacetophenone (TMTFA; 42) (acylation TI analog) (Table 3). Furthermore, W233 is absolutely conserved in AChE and BChE, as is the adjacent P232 that constrains the position of the indole ring. The proximity and invariant position of W233 suggest to us a more general and primary role for this acyl pocket residue in catalysis; replacement of W233 in HuBChE was shown recently to result in a 32-fold decrease in the k_{cat} for substrate hydrolysis (58).

Movement of the Acyl Pocket in MiPrP-AChE. Structure-activity studies first suggested the presence of specific binding pockets in the active site of cholinesterase that interact with the acyl and alkoxy groups of carboxyl ester substrates and OP inhibitors (reviewed in refs 6, 59). This approach showed convincingly that the acyl pocket of AChE was more restrictive than that of BChE. After the crystal structure of TcAChE became available, two aromatic residues, F288 and F290, were implicated as the source of AChE selectivity on the basis of sequence alignments and site-specific mutagenesis data (reviewed in ref 15).

Movement of F288 and F290 during the reaction with DFP, but not with sarin or soman (Figure 4), supports the idea that the aromatic side chains of these residues are the primary source of acyl pocket selectivity in TcAChE. Previous molecular dynamics studies of TcAChE suggested either that the degrees of freedom available to substrates and inhibitors were restricted by F288 and F290 or that the side chains underwent compensatory movements to accommodate bulky ligands; the models did not predict that the polypeptide backbone atoms in the acyl pocket could move almost 5 Å (Figure 5). Concurrent movement of the phenyl rings of F331, F288, and F290 suggests that a network of cooperative π - π interactions may stabilize the acyl-binding pocket in native TcAChE.

The free-energy penalty associated with the observed conformational change in the acyl pocket offers a concrete explanation for the substrate specificity of TcAChE. The

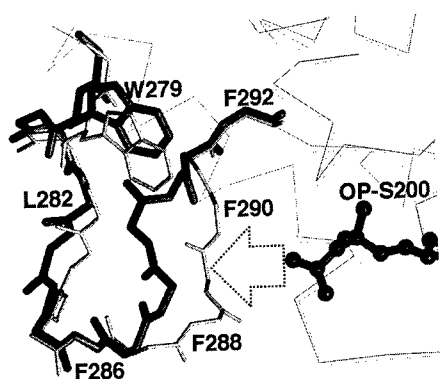


FIGURE 5: Conformational change in the acyl pocket. The main chain of MiPrP-AChE (thicker dark sticks) is compared with that of native TcAChE (thinner gray sticks) from position 278 to 292. The main chain displacement in the MiPrP-AChE stems from steric clashes between the bulky isopropyl group of DFP and the side chains of F288 and F290 (indicated by the arrow and also depicted in Figure 4C). The movement occurs on a loop that includes W279 (side chain shown) of the peripheral site. For reference, the Ca traces (thin lines) of the superimposed proteins are shown.

reversible dissociation constant with DFP, for example, is 2–3 orders of magnitude higher for either TcAChE or HuAChE than it is for HuBChE (Table 1). Replacement of the acyl pocket residues F295(288) and F297(290) in HuAChE with the smaller aliphatic side chains found in HuBChE abolishes this difference (17, 18). Likewise, the specificity constants for reaction of HuAChE or TcAChE with a substrate containing a butyryl group are 100–450-fold lower than those for reaction with an optimal substrate containing a methyl group (Table 1).

If TcAChE is phosphorylated with DFP and then rapidly dephosphorylated with an oxime nucleophile before aging can occur, the regenerated enzyme is essentially identical with native enzyme in its substrate specificity and affinity for a range of fluorescent bisquaternary ammonium ligands (38). Therefore, the conformational change we observe is probably reversible upon reactivation. The aging reaction stops dephosphorylation, however, and traps the acyl pocket of aged MiPrP-TcAChE in a conformation that may occur transiently during reaction with some substrates and inhibitors. Because the acyl pocket loop that moves also includes W279, which forms an important part of the AChE peripheral site (reviewed in ref 15), it is reasonable to speculate that this loop conjoins the active site with the peripheral site during catalysis (Figure 5). Such a link was first proposed by Changeux (60) to explain the allosteric binding of certain inhibitors to *Torpedo* AChE, but it continues to elude firm experimental proof.

Despite evidence in the literature for conformational changes associated with aging of some OP-AChE, -BChE, and -chymotrypsin conjugates in solution (61–63), we detected no major structural rearrangements in TcAChE as a result of the aging reaction itself. It remains possible, however, that reversible conformational changes occurred on the pathway to the final aged OP-TcAChE structures. We are testing this possibility by ongoing X-ray crystallographic studies of nonaged OP-TcAChE complexes.

ACKNOWLEDGMENT

We thank Ms Lilly Toker for valuable technical assistance. Dr. Clarence A. Broomfield provided advice on the role of

the oxyanion hole in aging and reactivation. The opinions or assertions contained herein belong to the authors and are not necessarily the official views of the U.S. Army or the U.S. Department of Defense.

REFERENCES

- Rosenberry, T. L. (1975) *Adv. Enzymol. Relat. Areas Mol. Biol.* 43, 103–218.
- Froede, H. C., and Wilson, I. B. (1984) *J. Biol. Chem.* 259, 11010–11013.
- Bernhard, S. A., and Orgel, L. E. (1959) *Science* 130, 625–626.
- Aldridge, W. N., and Reiner, E. (1972) *Enzyme inhibitors as substrates: Interactions of esterases with esters of organophosphorus and carbamic acids*, North-Holland Publishing, Amsterdam, The Netherlands.
- Steitz, T. A., Henderson, R., and Blow, D. M. (1969) *J. Mol. Biol.* 46, 337–348.
- Jarv, J. (1984) *Bioorg. Chem.* 12, 259–278.
- Kovach, I. (1988) *J. Enzyme Inhib.* 2, 199–208.
- Berends, F., Posthumus, C. H., Sluys, I. V. D., and Deierkauf, F. A. (1959) *Biochim. Biophys. Acta* 34, 576–578.
- Michel, H. O., Hackley, J., B. E., Berkowitz, L., List, G., Hackley, E. B., Gillilan, W., and Pankau, M. (1967) *Arch. Biochem. Biophys.* 121, 29–34.
- Sussman, J. L., Harel, M., Frolow, F., Oefner, C., Goldman, A., Toker, L., and Silman, I. (1991) *Science* 253, 872–879.
- Barak, D., Ariel, N., Velan, B., and Shafferman, A. (1992) in *Multidisciplinary Approaches to Cholinesterase Functions* (Shafferman, A., and Velan, B., Eds.) pp 195–199, Plenum Press, New York.
- Harel, M., Sussman, J. L., Krejci, E., Bon, S., Chanal, P., Massoulié, J., and Silman, I. (1992) *Proc. Natl. Acad. Sci. U.S.A.* 89, 10827–10831.
- Millard, C. B., and Broomfield, C. A. (1992) *Biochem. Biophys. Res. Commun.* 189, 1280–1286.
- Robertus, J. D., Kraut, J., Alden, R. A., and Birktoft, J. J. (1972) *Biochemistry* 11, 4293–4303.
- Taylor, P., and Radic, Z. (1994) *Annu. Rev. Pharmacol. Toxicol.* 34, 281–320.
- Futerman, A. H., Low, M. G., Ackerman, K. E., Sherman, W. R., and Silman, I. (1985) *Biochem. Biophys. Res. Commun.* 129, 312–317.
- Ordentlich, A., Barak, D., Kronman, C., Flashner, Y., Leitner, M., Segall, Y., Ariel, N., Cohen, S., Velan, B., and Shafferman, A. (1993) *J. Biol. Chem.* 268, 17083–17095.
- Ordentlich, A., Barak, D., Kronman, C., Ariel, N., Segall, Y., Velan, B., and Shafferman, A. (1996) *J. Biol. Chem.* 271, 11953–11962.
- Ellman, G. L., Courtney, K. D., Andres, V., Jr., and Featherstone, R. M. (1961) *Biochem. Pharmacol.* 7, 88–95.
- Main, A. R., and Dauterman, W. C. (1963) *Nature* 198, 551–553.
- Hope, H. (1988) *Acta Crystallogr., Sect. B* 44, 22–26.
- Ravelli, R. B. G., Sweet, R. M., Skinner, J. M., Duisenberg, A. J. M., and Kroon, J. (1997) *J. Appl. Crystallogr.* 30, 551–554.
- Otwinski, Z. (1993) in *Data Collection and Processing, Proceedings of the CCP4 Study Weekend 29–30 January 1993* (Sawyer, L., Isaacs, N., and Bailey, S., Eds.) pp 56–62, SERC, Daresbury, U.K.
- Raves, M. L., Harel, M., Pang, Y. P., Silman, I., Kozikowski, A. P., and Sussman, J. L. (1997) *Nat. Struct. Biol.* 4, 57–63.
- Brünger, A. T., and Krukowski, A. (1990) *Acta Crystallogr., Sect. A* 46, 585–593.
- Adams, P. D., Pannu, N. S., Read, R. J., and Brünger, A. T. (1997) *Proc. Natl. Acad. Sci. U.S.A.* 94, 5018–5023.
- Brünger, A. T., Adams, P. D., Clore, G. M., DeLano, W. L., Gros, P., Grosse-Kunstleve, R. W., Jian, J. S., Kuszewski, J., Nilges, M., Pannu, N. S., Read, R. J., Rice, L. M., Simonson, T., and Warren, G. L. (1998) *Acta Crystallogr., Sect. D* 54, 905–921.
- Laskowski, R. A., MacArthur, M. W., Moss, D., and Thornton, J. M. (1993) *J. Appl. Crystallogr.* 26, 283–291.

29. Vriend, G. (1990) *J. Mol. Graphics* 8, 52–56.
30. Schaffer, N. K., May, S. C., Jr., and Summerson, W. H. (1954) *J. Biol. Chem.* 206, 201–207.
31. Benschop, H. P., and de Jong, L. P. A. (1988) *Acc. Chem. Res.* 21, 368–374.
32. Barak, R., Ordentlich, A., Barak, D., Fischer, M., Benschop, H. P., de Jong, L. P. A., Segall, Y., Velan, B., and Shafferman, A. (1997) *FEBS Lett.* 407, 347–352.
33. Jones, T. A., Zou, J.-Y., Cowan, S. W., and Kjeldgaard, M. (1991) *Acta Crystallogr., Sect. A* 47, 110–119.
34. Bender, M. L., and Wedler, F. C. (1972) *J. Am. Chem. Soc.* 94, 2101–2109.
35. Kovach, I. M., Huber, J. H. A., and Schowen, R. L. (1988) *J. Am. Chem. Soc.* 110, 590–593.
36. Shafferman, A., Ordentlich, A., Barak, D., Stein, D., Ariel, N., and Velan, B. (1996) *Biochem. J.* 318, 833–840.
37. Viragh, C., Akhmetshin, R., Kovach, I. M., and Broomfield, C. A. (1997) *Biochemistry* 36, 8243–8252.
38. Taylor, P., and Jacobs, N. M. (1974) *Mol. Pharmacol.* 10, 93–107.
39. Beauregard, G., Lum, J., and Roufogalis, B. D. (1981) *Biochem. Pharmacol.* 30, 2915–2920.
40. Berry, W. K., and Davies, D. R. (1966) *Biochem. J.* 100, 572–576.
41. Boskovic, B., Maksimovic, M., and Minic, D. (1968) *Biochem. Pharmacol.* 17, 1738–1741.
42. Harel, M., Quinn, D. M., Nair, H. K., Silman, I., and Sussman, J. L. (1996) *J. Am. Chem. Soc.* 118, 2340–2346.
43. Barak, D., Ordentlich, A., Segall, Y., Velan, B., Benschop, H. P., de Jong, L. P. A., and Shafferman, A. (1997) *J. Am. Chem. Soc.* 119, 3157–3158.
44. Westheimer, F. H. (1987) *Science* 235, 1173–1178.
45. Kirby, A. J., and Younas, M. (1970) *J. Chem. Soc. B*, 1165–1172.
46. Kaiser, E. T., and Lee, T. W. S. (1971) *J. Am. Chem. Soc.* 93, 2351–2353.
47. Segall, Y., Waysbort, D., Barak, D., Ariel, N., Doctor, B. P., Grunwald, J., and Ashani, Y. (1993) *Biochemistry* 32, 13441–13450.
48. Broomfield, C. A., Millard, C. B., Lockridge, O., and Caviston, T. L. (1995) in *Enzymes of the Cholinesterase Family* (Quinn, D. M., Balasubramanian, A. S., Doctor, B. P., and Taylor, P., Eds.) pp 169–175, Plenum Press, New York.
49. Millard, C. B., Lockridge, O., and Broomfield, C. A. (1995) *Biochemistry* 34, 15925–15933.
50. Ordentlich, A., Barak, D., Kronman, D., Ariel, N., Segall, Y., Velan, B., and Shafferman, A. (1998) *J. Biol. Chem.* 273, 19509–19517.
51. Millard, C. B., Lockridge, O., and Broomfield, C. A. (1998) *Biochemistry* 37, 237–247.
52. Kossiakoff, A. A., and Spencer, S. A. (1981) *Biochemistry* 20, 6462–6474.
53. Harel, M., Su, C. T., Frolow, F., Ashani, Y., Silman, I., and Sussman, J. L. (1991) *J. Mol. Biol.* 221, 909–918.
54. Wei, Y., Schottel, J. L., Derewenda, U., Swenson, L., Patkar, S., and Derewenda, Z. S. (1995) *Nat. Struct. Biol.* 2, 218–223.
55. Kossiakoff, A. A., and Spencer, S. A. (1980) *Nature* 288, 414–416.
56. Ashani, Y., and Green, B. S. (1981) in *Chemical Approaches to Understanding Enzyme Catalysis: Biomimetic Chemistry and Transition State Analogues* (Green, B. S., Ashani, Y., and Chipman, D., Eds.) pp 169–188, Elsevier, Amsterdam, The Netherlands.
57. Warshel, A., Naray-Szabo, G., Sussman, F., and Hwang, J. K. (1989) *Biochemistry* 28, 3629–3637.
58. Masson, P., Legrand, P., Bartels, C. F., Froment, M.-T., Schopfer, L. M., and Lockridge, O. (1997) *Biochemistry* 36, 2266–2277.
59. Kabachnik, M. I., Brestkin, A. P., Godovikov, N. N., Michelson, M. J., Rozengart, E. V., and Rozengart, V. I. (1970) *Pharmacol. Rev.* 22, 355–388.
60. Changeux, J.-P. (1966) *Mol. Pharmacol.* 2, 369–392.
61. Amitai, G., Ashani, Y., Gafni, A., and Silman, I. (1982) *Biochemistry* 21, 2060–2069.
62. Aslanian, D., Grof, P., Renault, F., and Masson, P. (1995) *Biochim. Biophys. Acta* 1249, 37–44.
63. Steinberg, N., van der Drift, A. C. M., Grunwald, J., Segall, Y., Shirin, E., Haas, E., Ashani, Y., and Silman, I. (1989) *Biochemistry* 28, 1248–1253.

BI982678L

Effect of Mutations within the Peripheral Anionic Site on the Stability of Acetylcholinesterase

NATHALIE MOREL, SUZANNE BON, HARRY M. GREENBLATT, DANIEL VAN BELLE, SHOSHANA J. WODAK, JOEL L. SUSSMAN, JEAN MASSOULIÉ, AND ISRAEL SILMAN

Laboratoire de Neurobiologie Cellulaire et Moléculaire, Centre National de la Recherche Scientifique, Unité de Recherche Mixte 8544, Ecole Normale Supérieure, Paris, France (N.M., S.B., J.M., I.S.); Departments of Structural Biology (H.M.G., J.L.S.) and Neurobiology (I.S.), Weizmann Institute of Science, Rehovoth, Israel; and Unité de Conformation de Macromolécules Biologiques, Université Libre de Bruxelles, Bruxelles, Belgium (D.V.B., S.J.W.)

Received October 1, 1998; accepted February 12, 1999

This paper is available online at <http://www.molpharm.org>

ABSTRACT

Torpedo acetylcholinesterase is irreversibly inactivated by modifying a buried free cysteine, Cys231, with sulfhydryl reagents. The stability of the enzyme, as monitored by measuring the rate of inactivation, was reduced by mutating a leucine, Leu282, to a smaller amino acid residue. Leu282 is located within the "peripheral" anionic site, at the entrance to the active-site gorge. Thus, loss of activity was due to the increased reactivity of Cys231. This was paralleled by an increased susceptibility to thermal denaturation, which was shown to be due to a large decrease in the activation enthalpy. Similar results were obtained when either of two other residues in contact with Leu282 in *Torpedo* acetylcholinesterase, Trp279 and Ser291, was replaced by an amino acid with a smaller side chain. We studied the effects of various ligands specific for either the active or peripheral sites on both thermal inactivation and on

inactivation by 4,4'-dithiodipyridine. The wild-type and mutated enzymes could be either protected or sensitized. In some cases, opposite effects of the same ligand were observed for chemical modification and thermal denaturation. The mutated residues are within a conserved loop, W279-S291, at the top of the active-site gorge, that contributes to the peripheral anionic site. Theoretical analysis showed that *Torpedo* acetylcholinesterase consists of two structural domains, each comprising one contiguous polypeptide segment. The W279-S291 loop, located in the first domain, makes multiple contacts with the second domain across the active-site gorge. We postulate that the mutations to residues with smaller side chains destabilize the conserved loop, thus disrupting cross-gorge interactions and, ultimately, the entire structure.

Torpedo acetylcholinesterase (AChE) contains a nonconserved cysteine residue, Cys231, buried within the protein, ca. 8 Å from the active-site serine, Ser200 (Sussman et al., 1991). Chemical modification of the free thiol group of this amino acid residue by a repertoire of sulfhydryl reagents causes irreversible inactivation of the enzyme, even when modification is reversible (Kreimer et al., 1994). Inactivation is due to an irreversible conformational transition of the native enzyme to a molten globule (MG) species (Kreimer et al., 1994). Modification, as well as concomitant inactivation, obeys pseudofirst order kinetics (Steinberg et al., 1990; Kreimer et al., 1994). The rate of modification by a given thiol reagent is much slower than for a reaction with a low-molecular-weight thiol, as reflected by the high activation energy of the reaction (Kreimer et al., 1994).

The Ellman reaction for assay of AChE (Ellman et al.,

1961) involves the use of a thiol reagent, namely 5,5'-dithiobis(2-nitrobenzoic acid) (DTNB), also known as Ellman's reagent, which is reduced by the thiocholine generated by enzymic hydrolysis of acetylthiocholine (ATCh) to yield the chromophore 2-nitro-5-thiobenzoic acid. Nevertheless, *Torpedo* AChE can routinely be assayed by the Ellman method because the $T_{1/2}$ for its inactivation by DTNB at neutral pH and room temperature is approximately 9 h (Steinberg et al., 1990). Therefore, it was not anticipated that a mutant *Torpedo* AChE, L282S, generated by mutating Leu282, a leucine residue located close to the surface of the enzyme and near the mouth of the active-site gorge (Fig. 1; Sussman et al., 1991; Harel et al., 1995), to either serine or alanine, would be unstable under the conditions of the Ellman assay. This mutant had been generated to promote glycosylation of the adjacent residue, Asn280, by creating the glycosylation signal AsnXSer. However, instability was not due to glycosylation because the analogous mutant, L282A, displayed similar instability. With the following results, we demonstrate that

¹ For rat mutants, the residue number for the equivalent amino acid in *Torpedo* AChE is given in brackets, according to the accepted nomenclature (Massoulié et al., 1992).

such mutants, generated by replacement of Leu282 with a smaller residue, are, indeed, destabilized, and we present evidence that the instability observed under assay conditions derives from enhanced reactivity of Cys231 relative to its reactivity in the wild-type (WT) enzyme. This, in turn, is related to a decrease in the overall thermal stability of the mutant enzyme. Both the enhanced susceptibility to chemical modification and the decreased thermal stability can be modulated by reversible inhibitors specific for either the active site or the "peripheral" anionic site. Leu282 is within a loop stretching from Trp279 to Ser291. This loop is an important constituent of the peripheral anionic site (Harel et al., 1993, 1995; Bourne et al., 1995). It also contributes the principal hydrophobic stretch to a 5-kDa polypeptide, Gly268-Lys315, which serves to anchor a MG species of *Torpedo californica* AChE (*TcAChE*) to liposomes (Shin et al., 1996). The peripheral anionic site of AChE has been shown to enhance the rate of amyloid fibril assembly from A β peptide (Inestrosa et al., 1996), and, more recently, the isolated polypeptide sequence has been shown to be endowed with this capacity (De Ferrari and Inestrosa, 1998). Thus, elucidation of the physicochemical forces governing the stability of the Trp279-Ser291 loop warrants further investigation.

Experimental Procedures

Materials. ATCh, DTNB, propidium iodide, gallamine triethiodide, *d*-tubocurarine, decamethonium bromide, 4,4'-dithiodipyridine (DTP), and BSA were all purchased from Sigma Chemical Co. (St. Louis, MO). Edrophonium chloride was obtained from Hoffman-La Roche (Basel, Switzerland). All salts and buffers were of analytical grade.

Site-Directed Mutagenesis and Transfection. The coding sequences of the H catalytic subunits of *Torpedo marmorata* AChE (*TmAChE*; Duval et al., 1992) and of rat AChE (Legay et al., 1993)

were inserted into the pEF-BOS vector and were mutagenized with oligonucleotide primers, as described previously (Duval et al., 1992). COS-7 cells were transfected as described previously (Duval et al., 1992). After transfection, the COS cells were incubated for 2 days at 37°C and then for 4 days at 27°C in the case of the *Torpedo* enzyme, and incubated for 4 days at 37°C in the case of rat AChE.

AChE Activity Assays. AChE activity was determined by the colorimetric method of Ellman et al. (1961) at room temperature, with 0.75 mM ATCh as the substrate, in 50 mM sodium phosphate (pH 7.4) containing 0.5 mM DTNB and 0.1 mg/ml BSA. Assays were performed in microplates with a Labsystems (Helsinki, Finland) Multiskan RC automatic plate reader and recording at 414 nm every 20 s. K_m values were determined under the same experimental conditions in a concentration range of 0.02 to 10 mM ATCh, and IC_{50} values were determined with 0.5 mM ATCh. AChE samples were preincubated with the inhibitors in the reaction mixture for 20 min before the initiation of the enzymic reaction by addition of the substrate.

Inactivation by DTP. Chemical inactivation was performed in buffer 1 (0.01% BSA/40 mM NaCl/10 mM Tris hydrochloride; pH 7.4) containing 1 mM DTP in the case of *TmAChE* and 0.05 mM DTP for the rat enzyme. Ten-microliter aliquots of the appropriate AChE sample were added to 100 μ l of the DTP-containing buffer, which was then incubated at 26.5°C. At appropriate time intervals, 10- μ l aliquots were withdrawn and stored on ice for up to 1 h before assay of residual activity.

Thermal Inactivation. Thermal inactivation experiments were performed by the addition of 10- μ l aliquots of the appropriate AChE sample to 100 μ l of buffer 1, which was then brought to the appropriate temperature. Arrhenius plots were determined from the initial rates of loss of enzymic activity at four appropriate temperatures for each AChE sample, assuming that thermal denaturation obeys first order kinetics, yielding values of ΔH^\ddagger .

Software. Domain limits were computed from the atomic coordinates of the free *TcAChE* molecule (Protein Data Bank entry 2ace) by a recently developed procedure (Wernisch et al., 1999) that uses a graph heuristic to partition the protein into sets of residues that



Fig. 1. Ribbon diagram of *TcAChE*. Residues 4 to 305 are colored green, and residues 306 to 535 are colored cyan, highlighting the division of the molecule into two putative domains. The loop containing Leu282, viz. Trp279-Ser291, is colored yellow, with the side chains of Trp279 and Leu282 represented in stick form. The three regions of the second domain of the molecule that interact with this loop are colored purple, and two side chains, Phe 331 and Asn399, are shown in stick form. The active-site residues, Trp84 and Ser200, at the bottom of the active-site gorge, are also shown in stick form to provide orientation (picture was made in Insight II).

display minimum interactions between them. The interactions are evaluated from the contact areas between atoms, which are computed from the weighted Voronoi diagram (Richards, 1974). The accessible surface areas of residues in the protein and the area buried in the interface between the two domains were evaluated with the program SurVol (Alard, 1992). All of the procedures use a probe size of 1.4 Å for the water molecule and the set of radii implemented in the BRUGEL package (Delhaise et al., 1984).

The programs Insight II (MSI Corp. San Diego, CA) and XtalView (McRee, 1992) were used for display and analysis, and Raster3D (Merritt and Bacon, 1997) was used to render some of the images used in this study. The Collaborative Computational Project, Number 4 program (1994), CONTACT, was used to assess interdomain contacts.

Results

Figure 2 displays the enzymic activity of aliquots of WT *Tm*AChE and of the corresponding L282S mutant as a function of time, at 30°C, under standard Ellman assay conditions (see *Experimental Procedures*). Whereas the activity of

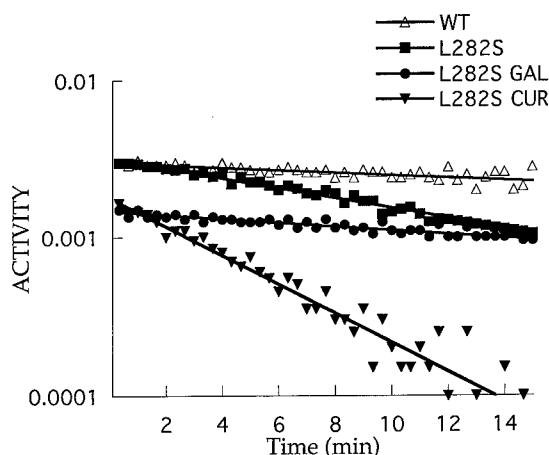


Fig. 2. Catalytic activity of WT and of L282S *Tm*AChE as a function of time under standard assay conditions. Catalytic activity was measured under standard assay conditions (see *Experimental Procedures*). The activity at a given time was calculated from the change in optical density of the reaction mixture over a time interval of 20 s. The change with time in the catalytic activity of the L282 mutant was also monitored in the presence of *d*-tubocurarine (50 μ M) and of gallamine (0.4 mM).

the WT enzyme, as expected, decreases only slightly over 15 min, that of the L282S mutant decays significantly. In addition, the effects of the two peripheral site ligands, *d*-tubocurarine and gallamine (Changeux, 1966), should be noted. Whereas the addition of 0.4 mM gallamine stabilizes L282S over the period monitored, *d*-tubocurarine (50 μ M) substantially enhances the rate at which its enzymic activity decays. Propidium, like gallamine, stabilizes the L282S mutant (not shown). Neither *d*-tubocurarine nor gallamine had a significant effect on the slow loss of activity of WT *Tm*AChE.

Our earlier studies of chemical modification and concomitant deactivation of *Tc*AChE by thiol reagents (Steinberg et al., 1990; Kreimer et al., 1994) suggested that the instability of L282S under the conditions of the Ellman assay might have its origin in the enhanced reactivity of Cys231 in the mutant enzyme relative to the WT enzyme. Therefore, this possibility was examined directly. Figure 3 shows the results of experiments in which samples of WT *Tm*AChE and of various mutant enzymes were preincubated in the presence of the disulfide DTP (Kreimer et al., 1994) before assay by the Ellman procedure. Both L282S (not shown) and the analogous mutant, L282A, are stable in the absence of DTP at

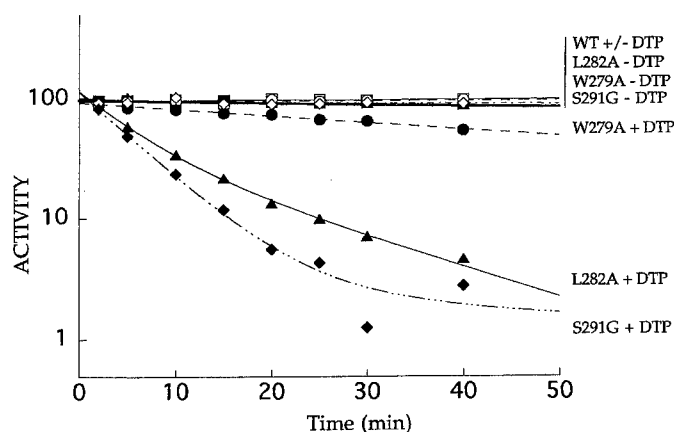


Fig. 3. Kinetics of inactivation of WT and of mutant *Tm*AChE by DTP. Inactivation was performed at 26.5°C. Ten-microliter aliquots of the *Tm*AChE sample were added to 100 μ l of 1 mM DTP in buffer 1. At appropriate time intervals, 10- μ l aliquots were withdrawn and stored on ice for up to 1 h before assay of residual enzymic activity.

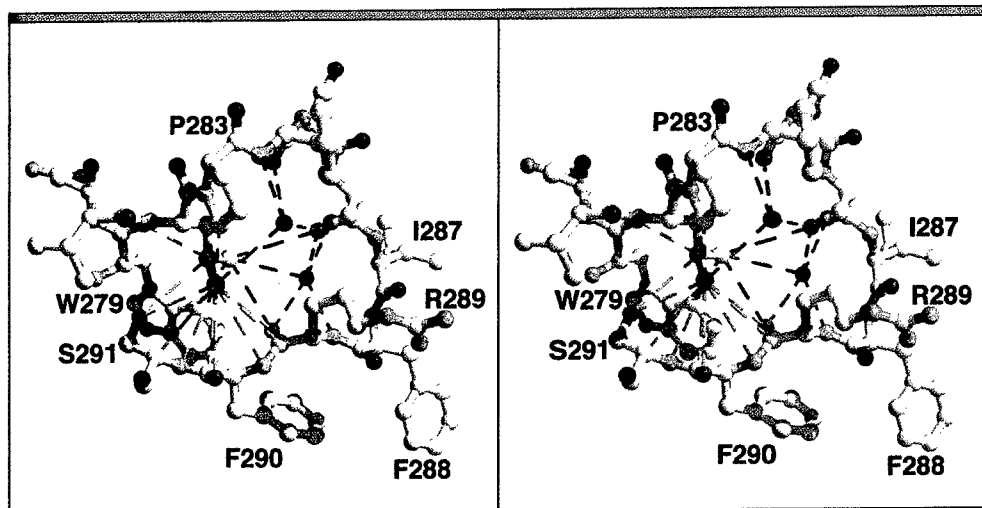


Fig. 4. Stereo view of the Trp279-Ser291 loop. Contacts made by the side chain atoms of Leu282 are shown by dashed lines: mauve for C γ , green for C δ ¹, and purple for C δ ². Red dashed lines represent possible hydrogen bonds between the two water molecules shown (red spheres) and protein atoms. Wat580 is the uppermost of the two and Wat584 is below. The orientation in this figure is similar to that in Fig. 1 (picture was made in XtalView/Raster3D).

26.3°C, but unstable in its presence, with $T_{1/2}$ values of ca. 7 min under the experimental conditions used. WT *TmAChE* is stable under the same conditions, as is the double-mutant C231S/L282A, which lacks the free thiol of Cys231 (not shown). The fact that the L282A mutant is destabilized to a similar extent as the L282S mutant shows that destabilization is not due to glycosylation. This was confirmed by the fact that the N280Q/L282S double mutant was also unstable in the presence of DTP (not shown).

Inspection of the three-dimensional structure of *Torpedo* AChE (see Discussion) revealed that the side chain of Leu282 makes contact principally with the side chains of two other residues, the indole ring of Trp279 and the hydroxyl group of Ser291 (Fig. 4). Thus, it was of interest to see whether substitution of either of these two residues by amino acids with smaller side chains would reduce the stability of *TmAChE* in a similar manner. Accordingly, two appropriate mutants, W279A and S291G, were generated, and Fig. 3 shows that these mutations also increase susceptibility to DTP. The degree of susceptibility produced by the S291G mutation is similar to or greater than that produced by the L282S/A mutation, whereas that produced by the W279A mutation is much smaller.

The instability of all three mutants relative to WT *TmAChE*, as monitored by susceptibility to chemical modification, was paralleled by reduced thermal stability. Thus, WT *TmAChE* was fairly stable at 38°C and pH 7.75, losing ca. 10% of its activity in 3 h. Under the same conditions, the L282A, S291G, and W279A mutants displayed $T_{1/2}$ values of ca. 25 min, 6 min, and 256 min, respectively. Arrhenius plots showed that the decreased thermal stability was due to large decreases in the activation energy, from 170 kcal/mol for WT enzyme to 100 kcal/mol and 90 kcal/mol, respectively, for the L282A and S291G mutants (Fig. 5). A smaller decrease, to 135 kcal/mol, was observed for the W279A mutant, paralleling its more limited sensitivity to DTP. Figure 5 also shows

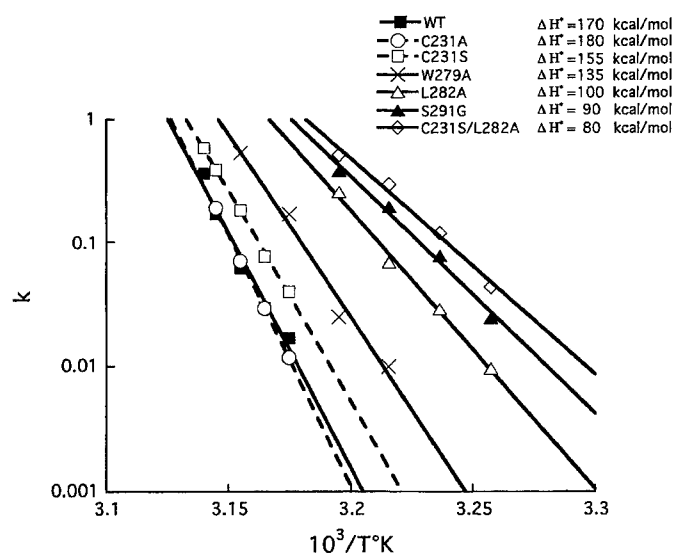


Fig. 5. Activation energies for thermal denaturation of WT and mutant *TmAChEs*. Arrhenius plots were derived from the experimental data for the kinetics of thermal inactivation at four temperatures for each AChE sample. A 10- μ l aliquot of the *TmAChE* sample was added to 100 μ l of buffer 1 before incubation at the desired temperature. At suitable time intervals, 10- μ l aliquots were withdrawn and stored on ice for up to 1 h before assay of residual enzymic activity.

that the C231S mutant is slightly less stable than the WT and that the C231S/L282S double mutant is slightly less stable than L282S, which is in agreement with the observations of Wilson et al. (1996).

Vertebrate AChE displays a high degree of conservation, with *Torpedo* AChE possessing ca. 50% sequence identity and ca. 70% sequence similarity to various mammalian AChEs (Cousin et al., 1998). Crystallographic studies on complexes of mouse recombinant, human recombinant, and *Torpedo* AChE with the mamba venom polypeptide neurotoxin fasciculin show that these three enzymes also possess very similar three-dimensional structures (Bourne et al., 1995; Harel et al., 1995; Kryger et al., 1998). Therefore, we investigated the effect of mutation to a smaller residue of the leucine residue in rat AChE equivalent to Leu282 in *Torpedo* AChE, which is either conserved or replaced by valine or methionine, in all of the vertebrate cholinesterases cloned and/or sequenced to date (Table 1; Cousin et al., 1998). We also investigated whether the inherent capacity of *Torpedo* AChE to be deactivated by chemical modification of Cys231 could be conferred on rat AChE by introducing a cysteine moiety in place of the homologous residue, Gly234.

Mutation to alanine of the leucine residue in rat AChE equivalent to Leu282 in *TmAChE*, viz. Leu289, produced a mutant enzyme, L289(282)A¹, that was much more susceptible to thermal denaturation than was the WT enzyme. Arrhenius plots (not shown) revealed that this is associated with a reduction in the energy of activation, from 125 kcal/mol to 90 kcal/mol, a reduction much smaller than that produced by the homologous mutation in *TmAChE*.

WT rat AChE, as might be expected, is not susceptible to DTP at 26.3°C. However, the G234(231)C mutant, in which a cysteine residue has been inserted at a position homologous to that of Cys231 in WT *TmAChE*, was deactivated, with a $T_{1/2}$ of 30 min, in the presence of 1 mM DTP (data not shown). As might be predicted from the thermal denaturation data for the L289A mutant, the double mutant G234(231)C/L289(282)A is much more susceptible to DTP under the same experimental conditions and loses activity with a $T_{1/2}$ of ca. 20 min, even in the presence of 0.05 mM DTP (data not shown).

Our initial observation (see above) was a modulation of the stability of the L282S mutant under conditions of the Ellman assay by the prototypic peripheral site ligand *d*-tubocurarine. Therefore, it seemed desirable to conduct a systematic survey of the effects of AChE-specific ligands on the stability of the various mutants discussed above, relative to WT *TmAChE*. In addition to *d*-tubocurarine and gallamine, which are spe-

TABLE 1

Conservation of residues in the Trp279-Ser291 loop and of residues in domain 2 that interact with this loop

	279	282	286	288	289	291	331	398	399
<i>Torpedo</i>	W	L	S	F	R	S	F	H	N
Rat, mouse	W	L	S	F	R	S	F	H	N
Rabbit	W	L	S	F	R	S	F	H	N
Human	W	L	S	F	R	S	F	H	N
Bovine	W	L	H	F	R	S	F	H	N
Chicken	G	M	S	F	R	A	F	H	N
Quail	G	L	S	F	R	A	F	H	N
<i>Bungarus</i>	W	L	S	F	R	P	F	H	N
Hagfish	G	V	S	F	R	P	F	Y	N
<i>Amphioxus</i> 1	W	V	D	A	D	P	W	P	F
<i>Amphioxus</i> 2	W	W				P	F	Y	N

cific for the peripheral site, edrophonium and tacrine, ligands specific for the "anionic" subsite of the active site (Harel et al., 1993), and decamethonium, a bisquaternary ligand that spans the two sites (Harel et al. 1993), were included for purposes of comparison. IC_{50} values for inhibition of the various *TcAChE* and rat *AChE* mutants by these ligands are summarized in Table 2. Not surprisingly, K_m was not greatly influenced by the mutations made in residues near the entrance of the gorge, nor did the C231S mutation influence this parameter. Similarly, only small effects were observed on the IC_{50} values for tacrine and edrophonium, which bind to the anionic subsite of the active site at the bottom of the aromatic gorge. However, the L282S/A and S291G mutations appeared to increase the affinity of *d*-tubocurarine for *TmAChE* by 2- to 3-fold, whereas they decreased the affinity of gallamine by 4- to 10-fold and of decamethonium by 2- to 3-fold. Whereas the W279A mutation had little effect on the affinity of *d*-tubocurarine and gallamine for *TmAChE*, it decreased the affinity of decamethonium by about 7-fold. The fact that mutations in the peripheral site region may increase affinity for some peripheral site ligands and decrease that for others is not unusual and may be due to interaction of different peripheral site ligands with diverse sets of amino acid residues (Cousin et al., 1996).

We investigated the effects of the ligands on both thermal denaturation and deactivation produced by chemical modification with DTP for both WT and peripheral site mutants of *TmAChE* and rat *AChE*.

For the L282A mutant, the thermal denaturation studies presented a fairly straightforward picture. Edrophonium, tacrine, decamethonium, and gallamine all provided substantial protection against thermal denaturation, whereas *d*-tubocurarine slightly destabilized the enzyme (Fig. 6). The observed protection was reflected in the activation energies calculated from Arrhenius plots obtained in the presence of the various ligands. For the first four ligands, these were substantially higher than the value obtained for L282A in the absence of any ligand. For tacrine (155 kcal/mol), the activation energy approached the value obtained for WT enzyme (170 kcal/mol), and for *d*-tubocurarine, the activation energy was slightly decreased. *d*-Tubocurarine had a similar effect on the W279A mutant (not shown).

Inactivation by DTP presented a more complex picture. At the temperature used, 26.3°C, the WT enzyme was fairly stable, but a slightly increased rate of inactivation was observed in the presence of either *d*-tubocurarine or tacrine (Fig. 7A). For the L282A mutant, gallamine and decamethonium exerted strong protection and edrophonium provided slight protection, whereas *d*-tubocurarine slightly increased the rate of inactivation, and tacrine substantially accelerated inactivation, producing 50% inhibition of enzymic activity within 2 min, as compared with ca. 6 min in its absence (Fig. 7B). Similar results were obtained for S291G, although edrophonium provided greater protection (Fig. 7C). However, for this latter mutant, *d*-tubocurarine enhanced the rate of inactivation (5-fold) much more than did tacrine (2-fold). In the case of W279A, the trend was similar, but the effects were less striking (Fig. 7D). Both gallamine and edrophonium afforded protection, whereas both *d*-tubocurarine and tacrine accelerated deactivation. Similar experiments performed on

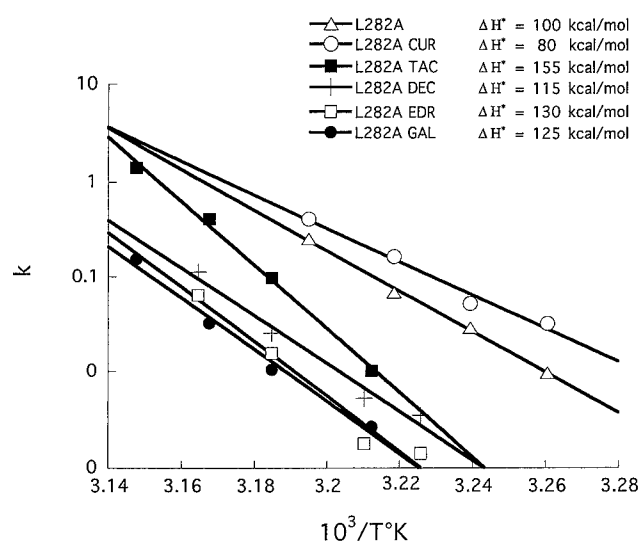


Fig. 6. Activation energies for thermal denaturation of the L282A mutant of *TmAChE* in the presence and absence of active-site and peripheral-site ligands. Assays were performed and Arrhenius plots were derived as described in the legend to Fig. 5. Ligand concentrations used were: *d*-tubocurarine, 0.5 mM; decamethonium, 20 μ M; edrophonium, 10 μ M; gallamine, 0.6 mM; tacrine, 100 nM.

TABLE 2

IC_{50} values for inhibition of wild-type and mutant *T. marmorata* and rat *AChEs* by active and peripheral site ligands

Assay conditions were as described in *Experimental Procedures*.

Enzymes	K_m	IC_{50} Curare	IC_{50} Decamethonium	IC_{50} Edrophonium	IC_{50} Gallamine	IC_{50} Tacrine
	mM			μ M		
<i>TmAChE</i>						
WT	0.108	170	1.4	0.92	64.2	0.014
L282A	0.152	65	3.6	2.22	398	0.013
W279A	0.199	220	10.7	0.87	118	0.010
S291G	0.172	40	4.7	3.2	375	0.022
C231S	0.074	250	1.3	0.92	98.3	0.013
CS/L282A	0.106	110	3.4	2.1	245	0.014
L282S	0.156	80	4.2	2.0	312	0.017
N280Q	0.098	230	1.7	0.83	118	0.013
NQ/L282S	0.148	64	5.7	2.22	573	0.020
CS/L282S	0.110	90	4.4	2.22	477	0.016
CS/NQ/L282S	0.114	64	5.7	2.74	933	0.020
<i>Rat AChE</i>						
WT	0.085	240	15.4	1.9	1190	0.106
L289A	0.107	120	18	2.6	1430	0.086
G234C		120	30.4	3.2	690	0.112
GC/L289A		60	33.7	4.6	690	0.086

the rat AChE double-mutant G234(231)C/L289(282)A yielded a rather different pattern of efficacy of ligands. Overall, the effects observed were not striking, but gallamine had a protective effect, decamethonium, *d*-tubocurarine, and

edrophonium had little or no effect, and only tacrine enhanced the rate of inactivation substantially, although not as markedly as for the peripheral site mutants of *Tm*AChE (data not shown).

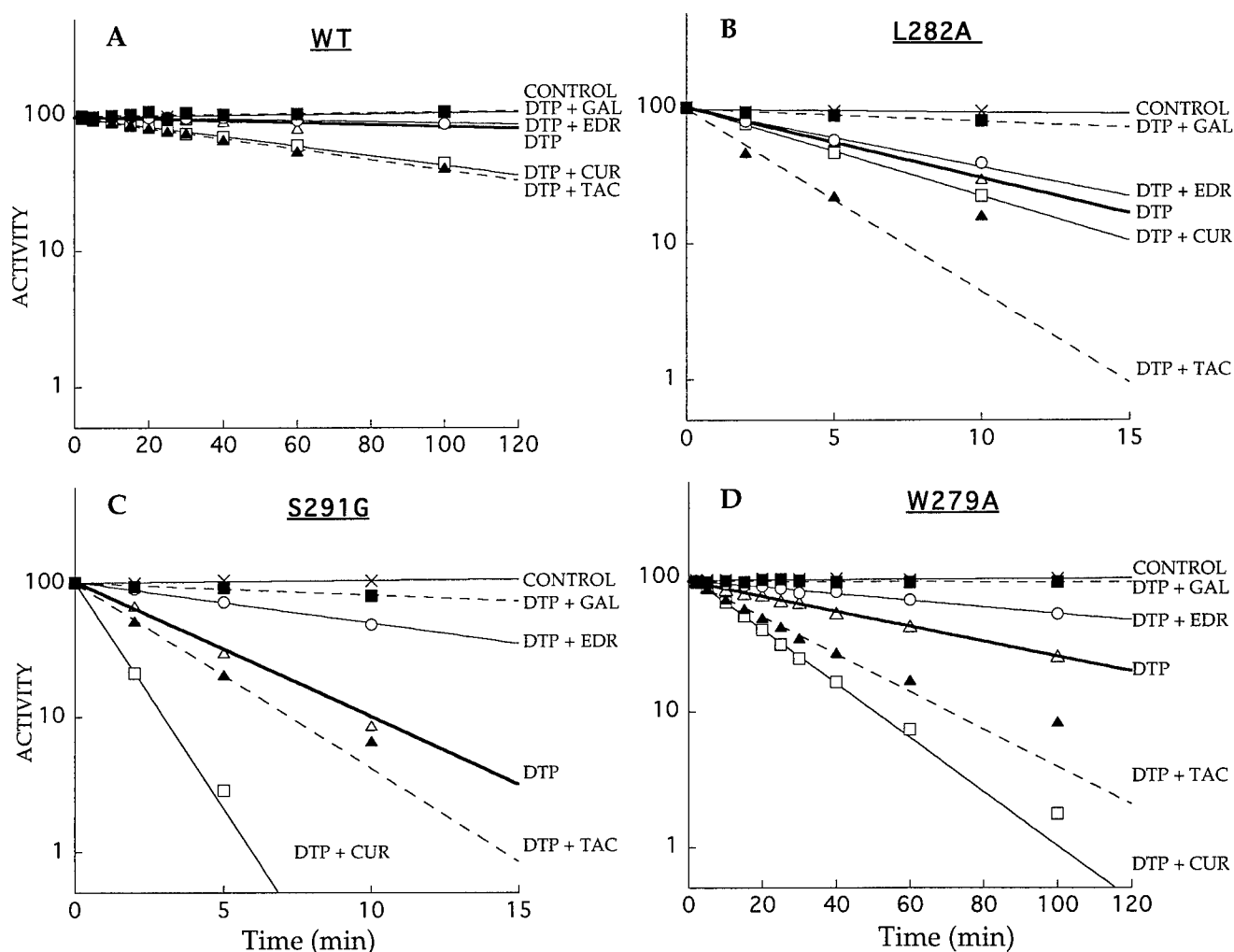


Fig. 7. Effects of active-site and peripheral-site ligands on the kinetics of inactivation of WT *Tm*AChE and the L282A, S291G, and W279A mutants by DTP. The experimental procedure was as described in the legend to Fig. 3. Ligand concentrations used were as described in the legend to Fig. 6. A, WT; B, L282A; C, S291G; and D, W279A.

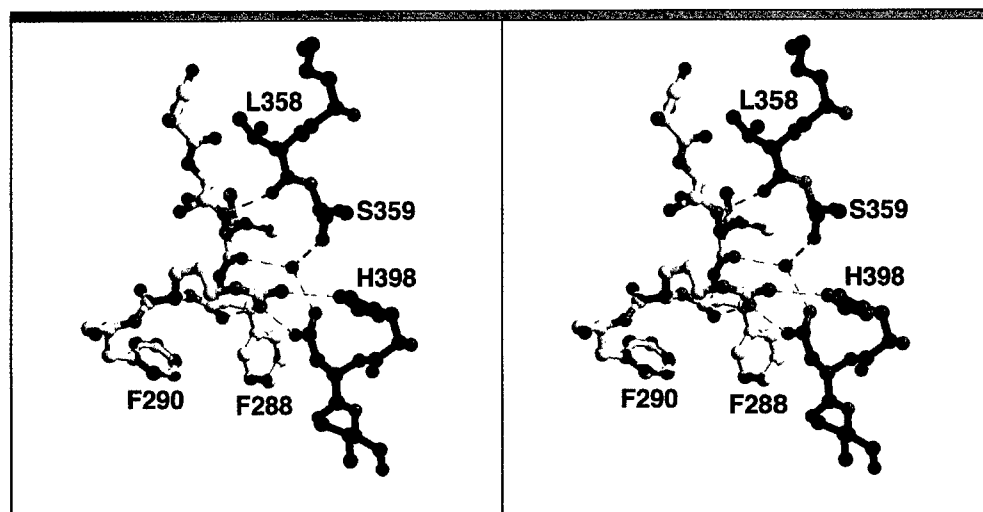


Fig. 8. Stereo figure showing possible hydrogen bonds (dashed lines) between atoms in the Trp279-Ser291 loop (carbon atoms are colored yellow) and domain 2 (carbon atoms are colored purple). Wat555 is the red sphere. Orientation is similar to that shown in Fig. 4 (picture was made in XtalView/Raster3D).

Discussion

Our data are in line with earlier experiments performed on *TcAChE*, which showed that chemical modification of the nonconserved Cys231 caused a loss of enzymic activity (Steinberg et al., 1990), with concomitant transformation to a partially unfolded state displaying the physicochemical features of a MG state (Kreimer et al., 1994). However, the data concerning mutation of Leu282 add another dimension. Although hydrophobic, this residue is located near the surface of the protein, close to the mouth of the active-site gorge (Fig. 1; Harel et al., 1995). We did not expect that mutation of Leu282, located at the periphery of the protein, would affect so drastically the stability of the entire catalytic subunit containing 537 amino acid residues. There is substantial documentation of studies in which large hydrophobic side chains have been mutated to smaller ones (see, e.g., Yutani et al., 1987; Matsumura et al., 1988; Eriksson et al., 1992b). In general, such mutations destabilize the protein under consideration. In cases where these mutations create empty cavities, the magnitude of the destabilization is greater than in those where the three-dimensional structure adjusts to fill the void created by reducing the size of the side chain (Eriksson et al., 1992b). The proteins so studied have been much smaller than the catalytic subunit of *TcAChE*, containing up to 268 amino acid residues in the case of the α subunit of tryptophan synthase (Yutani et al., 1987). It was reported that cavity-containing mutants of T4 lysozyme could be stabilized by the uptake of benzene or indole into the cavity (Eriksson et al., 1992a). We were not able to obtain similar stabilization of the L282A mutant by benzene (N. Morel, unpublished observations), probably because in this mutant, the conformation of the loop, and possibly elsewhere, was altered so that no cavity was left after the mutation.

The experimental data presented, whether monitoring loss of enzymic activity due to chemical modification or measuring rates of thermal inactivation and generating Arrhenius plots, are all kinetic. Therefore, at this stage, we cannot differentiate between thermodynamic and kinetic destabilization. Thus, an increase in the rate of thermal inactivation might result from a lowering of the free energy of the intermediate activation state rather than from destabilization of the native state. In any event, the Arrhenius plots reveal that mutations that accelerate the rate of thermal inactivation lower the transition enthalpy (Fig. 5). The effect of ligands on the inactivation of the L282A mutant was not directly correlated with the values of the transition enthalpies observed in their presence (Fig. 8). This suggests that for certain ligands, viz. gallamine, decamethonium, and edrophonium, entropic effects may play a role in stabilization.

To provide a structural basis for the observed destabilization by mutation of Leu282, we have examined the area surrounding the side chain of this residue. Figure 1 shows an overall ribbon view of the enzyme, with the loop containing Leu282 shown in yellow. This figure also shows that the *TcAChE* can be divided approximately into two halves. By using an older automatic procedure for identifying structural domains in proteins (Wodak and Janin, 1981) and a more recent algorithm (Wernisch et al., 1999), *TcAChE* is found to consist of two "structural domains," each comprising one contiguous segment of the polypeptide: domain 1 (residues 4–315) and domain 2 (residues 316–357). These domains

TABLE 3

Cross-gorge interactions of residues in the Trp279-Ser291 loop

Source Atom	Target Atoms	Distance Loop-Second Domain
PHE284 CB	PRO361 CB	3.69
PHE284 CG	PRO361 CB	3.97
PHE284 CD2	PRO361 CB	3.90
ASP285 C	LEU358 CD1	3.97
ASP285 O	PRO361 CB	3.97
	LEU358 CD1	3.71
	LEU358 CA	4.03
ASP285 CG	LEU358 CD1	3.54
ASP285 OD1	LEU358 CD1	3.51
ASP285 OD2	LEU358 CD1	3.70
SER286 CA	LEU358 O	3.49
SER286 C	LEU358 O	3.80
SER286 CB	PRO361 CG	3.68
	PRO361 CB	3.70
	LEU358 O	3.84
ILE287 N	LEU358 C	4.07
	LEU358 O	3.16***
ILE287 CA	LEU358 O	4.07
ILE287 C	WAT555 OW	3.74
ILE287 O	WAT555 OW	2.79***
	LEU358 O	3.90
ILE287 CB	LEU358 O	3.89
ILE287 CG1	PHE331 O	3.54
ILE287 CG2	WAT555 OW	4.04
	LEU358 O	4.08
	SER359 OG	3.89
ILE287 CD1	LEU358 CG	3.84
	GLY335 O	3.02
	LEU358 CD2	4.10
	GLY335 CA	3.69
	GLY335 C	3.53
PHE288 CA	PHE331 CD2	4.04
PHE288 O	ASN399 OD1	4.00
PHE288 CB	PHE331 CD2	4.06
	ASN399 CG	3.89
	ASN399 OD1	3.90
	ASN399 ND2	3.71
	WAT555 OW	3.61
PHE288 CG	PHE331 CG	3.95
	PHE331 CD2	3.69
	PHE331 CE2	3.96
	ASN399 CB	3.92
	ASN399 CG	3.57
	ASN399 OD1	3.77
	ASN399 ND2	3.70
PHE288 CD1	PHE331 CE2	4.09
	ASN399 CB	4.08
	ASN399 CG	4.00
	ASN399 OD1	3.92
PHE288 CD2	PHE331 CB	4.01
	PHE331 CG	3.37
	PHE331 CD1	3.55
	PHE331 CD2	3.57
	PHE331 CE1	3.85
	PHE331 CE2	3.90
	PHE331 CZ	4.00
	ASN399 CB	3.63
	ASN399 CG	3.61
	ASN399 ND2	3.53
PHE288 CE1	VAL395 CG1	3.71
PHE288 CE2	ASN399 CB	4.00
	PHE331 CG	3.79
	PHE331 CD1	3.49
	PHE331 CD2	4.02
	PHE331 CE1	3.35
	PHE331 CE2	3.94
	PHE331 CZ	3.58
	ASN399 CB	3.55
	ASN399 CG	4.08
PHE288 CZ	PHE331 CE1	3.81
	PHE331 CE2	4.08
	PHE331 CZ	3.63
	ASN399 CB	3.76
	VAL400 CG2	3.73
ARG289 NE	PRO361 CG	4.02
ARG289 CZ	HIS398 NE2	4.07
	ASN399 OD1	3.92
ARG289 NH1	ASN399 CG	3.91
	ASN399 OD1	2.83***
	WAT555 OW	3.61
ARG289 NH2	PRO361 CD	4.06
	HIS362 ND1	3.97
	HIS362 CE1	3.87
	HIS398 CE1	3.90
	HIS398 NE2	2.96***
	HIS398 CD2	3.85

Asterisks indicate possible hydrogen bonds.

have been defined so as to maximize the interactions between residues within each domain while minimizing the interactions between domains. This definition has been used in many algorithms, with the aim of identifying structural units most likely to fold independently and to be stable on their own (Wetlaufer, 1973). However, this is unlikely to be applicable to the two domains identified in *TcAChE*, given that they interact strongly with each other and possess a buried surface area of 5070 Å², a value nearly three times larger than that in the average protein-protein complex (Janin and Chothia, 1990). Furthermore, the domains represent portions of the α/β hydrolase architecture of AChE that do not seem to represent independent folding motifs found elsewhere. Interestingly, however, our programs detect surprisingly similar domain partitions in other proteins of the α/β hydrolase fold family (Ollis et al., 1992), such as the fungal and pancreatic lipases, that display weak sequence homology

with AChE. It is also noteworthy that the members of the catalytic triad of *TcAChE*, viz. Ser200, Glu327, and His440, come from both domains, and, thus, span the interdomain interface. This is quite common in multidomain enzymes where domain movement plays a role in catalysis (Gerstein

TABLE 4

Possible hydrogen bonds between atoms in the Trp279-Ser291 loop and atoms in domain 2, including Wat555

First Domain		Second Domain	Distance Å
Ile287 N		Leu358 O	3.2
Ile287 O	Wat555		2.8
	Wat555	Ser359 O	2.6
	Wat555	Asn399 N ⁸²	2.9
Arg289 N ⁷¹		Asn399 O ⁸¹	2.8
Arg289 N ⁷²		His398 N ⁸²	3.0

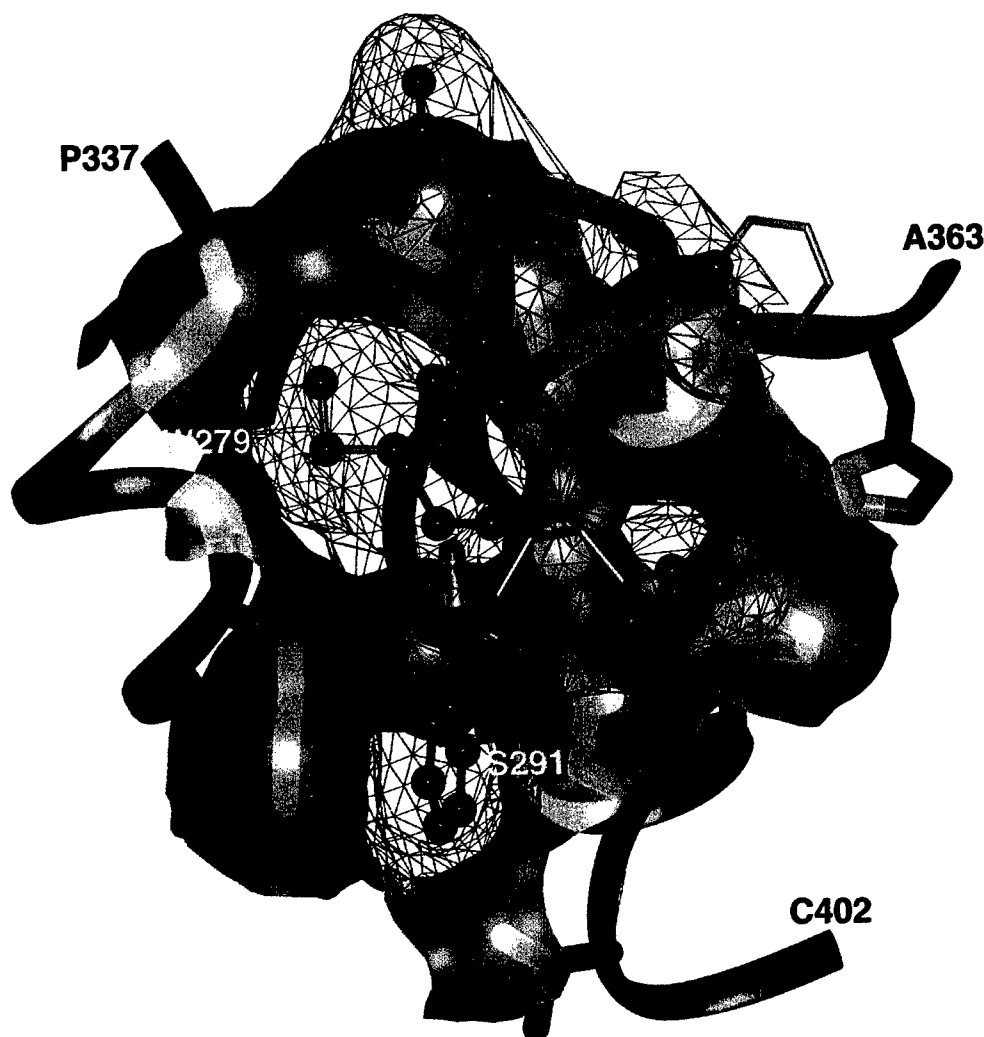


Fig. 9. Interaction of surfaces between the Trp279-Ser291 loop and domain 2. The loop is depicted as an orange ribbon, and only those side chain and main chain atoms that interact with atoms of the second domain (within 4.1 Å) are shown. The atoms of those interacting residues that actually make contact are shown as red balls, and the side chain atoms of the same residues that do not make contact are shown in orange stick representations (to provide context and connectivity). The solvent-accessible surface of only the contacting atoms is shown in dark red mesh. The surface is calculated in the context of the entire loop. Relevant residues from domain 2 are shown as three segments of ribbon. Each segment is labeled at its COOH-terminus. Medium blue indicates residues that have no contact with the 279-291 loop. Purple residues have some atoms that contact the loop atoms. Those main chains and side chains of domain 2 that actually contact the loop are colored cyan, and the solvent-accessible surface of these atoms (in the context of the whole second pseudodomain) is shown in light cyan, made transparent to show the atoms of which it is composed. The one cyan sphere is the water molecule, arbitrarily assigned to be part of domain 2 (picture was made in Insight II).

et al., 1994). This suggests that the AChE domains, or, more particularly, their interface, and their counterparts in other α/β hydrolases, might also play a role in enzyme function.

In *TcAChE*, the interdomain surface involves 548 atoms from a total of 78 residues in domain 1 and 74 residues in domain 2. The interface atoms are defined as those for which the accessible surface area (Lee and Richards, 1971) computed in the entire protein is different from that computed when the domains are considered independently. A sizable portion of the interface residues belongs to loops (52%), with the remainder belonging to helices and strands. It should also be mentioned that 73% of the buried interface area is provided by nonpolar atoms, whereas only 5.5% is contributed by charged atoms. Hence, the interdomain and, thus, also the intergorge interactions are primarily hydrophobic in nature.

TABLE 5

Interactions of side chain atoms of Leu282 with other atoms in the Trp279-Ser291 loop

Atom 1	Atom 2	Distance Å
Leu282 C γ	Trp279 O	4.0
	Ser291 O γ	3.9
Leu282 C δ^1	Trp279 C ϵ^3	4.1
	Ser286 O γ	4.1
	Arg289 O	3.7
	Wat584	3.8
Leu282C δ^2	Pro283 C δ	4.2
	Arg289 C	4.1
	Arg289 O	4.2
	Phe290 N	4.1
	Phe290 C	3.8
	Phe290 O	3.9
	Ser291 N	3.8
	Ser291 C α	3.9
	Ser291 O γ	3.8
	Wat580	4.1

Given the above analysis, visual inspection of Fig. 1 suggests that the loop comprising residues 279 to 291 plays several roles: 1) it makes an important contribution to the peripheral site at the top of the gorge; 2) it participates, via the side chains of residues Phe288 and Phe290, in the acyl binding pocket of the active-site (Harel et al., 1992); and 3) it makes significant cross-gorge interactions with residues in the second domain. To quantify this latter role of the loop, Table 3 lists all of the interactions between residues in the loop and residues in the second domain within a cutoff of 4.1 Å. The possible hydrogen bonds formed are displayed in Fig. 8 and listed in Table 4. Table 1 shows that the side chains of the residues involved in these polar cross-domain interactions are well conserved in vertebrate AChE sequences. Consequently, it may be postulated that these residues play a key role in preserving the active conformation of the enzyme and/or in its folding to the native conformation. This prediction could be examined by site-directed mutagenesis studies. Indeed, in preliminary experiments, mutation of Arg289 to glutamate produced an active enzyme that was, however, substantially less stable than WT *TmAChE* (N. Morel, unpublished observations).

To examine the nonpolar interactions listed in Table 3, Fig. 9 shows the complementarity between the solvent-accessible surfaces of the loop and neighboring atoms in the second domain. Of particular interest is the sandwiching of the loop residue Phe288 between the side chains of Phe331 and Asn399, both of domain 2. Also noteworthy is the fact that Ile287 buries 140 Å² in the interface, the second largest value after Phe448 (not interacting with the loop), which buries 164 Å². In all, the loop buries approximately 446 Å² of surface area in the interaction between the two domains.

The participation of residues in the Trp279-Ser291 loop in cross-gorge interactions implies that destabilization of the loop itself would perturb important interdomain interactions, thereby impairing the activity and, possibly, also the stabil-

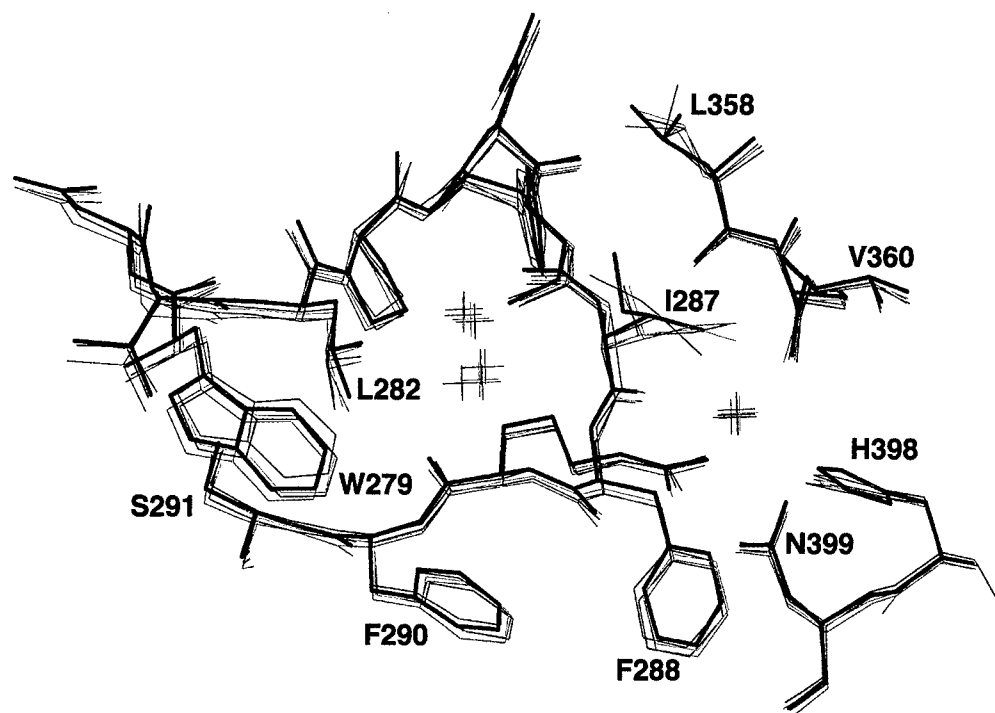


Fig. 10. Overlay of five AChE crystal structures in the region of the Trp279-Ser291 loop. The structures used are as follows: soman-inactivated (Millard et al., 1998; green); complex with huperzine A (Raves et al., 1997; PDB entry 1vot; dark blue); complex with edrophonium (Harel et al., 1993; PDB entry 1ack; cyan), sarin-inactivated (Millard et al., 1998; dark pink); and native AChE (Raves et al., 1997; PDB entry 2ace; brown). Overlap of structures is based on the assumption that all five of the crystals are isomorphous. The overlay shows that there are no large qualitative differences in the conformation of the loop, despite the presence or absence of inhibitors at the bottom of the active-site gorge. The largest differences are exhibited by the side chains of Ile287 and Leu358, which appear to adopt a number of different conformations. Furthermore, 2ace lacks one water molecule, uppermost in the representation (picture was made in Insight II).

ity of the entire subunit. The side chain of Leu282 is almost completely buried, with only 10 Å² of surface area exposed to solvent. Figure 4 shows that it fills the central cavity of this loop, making van der Waals interactions with other atoms in the vicinity (Table 5 and Fig. 10). Furthermore, we see that Phe288 adopts a left-handed helical backbone conformation, usually associated with glycine and asparagine residues. Thus, decreasing the size of the side chain of Leu282, as in the L282A mutant, would most probably change the conformation of the loop or increase its conformational flexibility. Consequently, this would compromise the cross-gorge interactions shown in Figs. 8 and 9, resulting in the observed loss of activity and the surmised loss of stability. Similar considerations would apply to the destabilization achieved by analogous substitution of Trp279 and Ser291 by amino acids with smaller side chains. However, although the destabilization produced by the S291G mutation is rather similar to that produced by the L282S or L282A mutation, that produced by the W279A mutation is much smaller. This difference may tentatively be ascribed to the fact that the principal interaction of Leu282 is with Ser291, and vice versa, both side chains being almost completely buried. As can be seen from Table 5, Ser291O^γ makes van der Waals contacts with both Leu282C^γ and L282C^{δ2}. In the case of Trp279, the indole ring, although hydrophobic, is largely oriented outwards, toward the active-site gorge, where it is available for interaction with peripheral site ligands (Harel et al., 1992, 1993, 1995; Bourne et al., 1995) and it makes a single, weaker interaction via its C^{ε3} atom with Leu282C^{δ1}. It is of interest that within the loop, two buried waters, Wat580 and Wat584, appear to contribute to stabilization via van der Waals interactions and hydrogen bonds.

The effects of the various reversible inhibitors on the stability of the mutant enzyme(s) are also of interest, although for the peripheral site ligands, no crystallographic data are available to reveal details of their interaction with the AChE, and it would be difficult to obtain meaningful assignments from docking studies. This was evident from comparison of the X-ray structures of complexes, e.g., of fasciculin/AChE (Harel et al., 1995) and of huperzine A/AChE (Raves et al., 1997), with the structures predicted by docking. The data for thermal denaturation of the L282A reveal that all of the ligands examined, whether peripheral, active-site directed, or spanning the two sites, stabilize the protein, with the exception of *d*-tubocurarine, the destabilizing effect of which was the starting point for the current study. In general, the binding energy conferred by a ligand might be expected to stabilize the structure of a protein unless it binds better to the transition state for unfolding than to the native ground state. The data obtained on the effect of the various ligands on chemical deactivation by DTP are rather unexpected. Again, it was found that edrophonium and gallamine retard deactivation, in agreement with our earlier observation that edrophonium retarded inactivation of TcAChE by *N*-ethylmaleimide and *p*-chloromercurisulfonic acid (Steinberg et al., 1990). Our finding that both the peripheral site ligand, *d*-tubocurarine, and the active-site ligand, tacrine, enhance the rate of inactivation, and that the latter has a strong effect on the rates of inactivation of L282A, S291G, and W279A, was quite unexpected. We earlier showed that *N*-methylacridinium, the structure of which is rather similar to that of tacrine and which, presumably, interacts with the anionic

site at the bottom of the active-site gorge in a similar way (Harel et al., 1993), does not affect chemical modification of TcAChE by *N*-ethylmaleimide (Steinberg et al., 1990). Furthermore, Abramson et al. (1989) found no effect of this ligand on the irreversible modification of TcAChE by the molluscan toxin onchidal. Indeed, in our present study, we found that tacrine has little effect on chemical modification of WT TmAChE. Because tacrine protects L282A against thermal denaturation, it must be speculated that its binding to the mutant enzyme produces a conformational change that renders the sulfhydryl group of Cys231 more accessible to chemical modification.

As presented in *Results*, comparison of the effect of the same set of ligands on susceptibility of the rat G234(231)C and G234(231)C/L289(282)A mutants to chemical modification revealed broad overall similarity to what was observed with the corresponding *Torpedo* mutants. However, it is of interest that *Bungarus fasciatus* AChE is much less susceptible to propidium and gallamine than the *Torpedo* enzyme, but slightly more susceptible to *d*-tubocurarine (Cousin et al., 1996), as is also the case for the L282A/S and S291G TmAChE mutants relative to the WT (see Table 2). In the absence of crystallographic data, it is premature to attempt to rationalize these different patterns of susceptibility.

The experimental data presented, taken together with the theoretical analysis, show how mutation of a single residue at the periphery of a relatively large native protein structure can affect its overall stability.

Acknowledgments

This study was supported by Centre National de la Recherche Scientifique; Direction des Systèmes de Force et de la Prospective; Association Française contre les Myopathies; Fourth Framework Program in Biotechnology of the European Union; U.S. Army Research and Materiel Command under Contract 17-97-2-7022; Kimmelman Center for Biomolecular Structure and Assembly; and Concerted Research Action Program of the French Community of Belgium (Contract 97/02-211). The expert technical assistance of Anne Le Goff is gratefully acknowledged, as is the participation of Philippe Chanal and Charles J. Waechter in the early stages of the project. I. S. is the Bernstein-Mason Professor of Neurochemistry.

References

- Abramson SN, Radic Z, Manker D, Faulkner DJ and Taylor P (1989) Onchidal: A naturally occurring irreversible inhibitor of acetylcholinesterase with a novel mechanism of action. *Mol Pharmacol* 36:349–354.
- Alard P (1992) Calculs de surface et d'énergie dans le domaine de macromolécules (Ph.D. Thesis). Brussels, Belgium: Free University of Brussels, 120 p.
- Bourne Y, Taylor P and Marchot P (1995) Acetylcholinesterase inhibition by fasciculin: Crystal structure of the complex. *Cell* 83:503–512.
- Changeux, J-P (1966) Responses of acetylcholinesterase from *Torpedo marmorata* to salts and curarizing drugs. *Mol Pharmacol* 2:369–392.
- Collaborative Computational Project, Number 4 (1994) The CCP4 Suite: Programs for Protein Crystallography. *Acta Crystallogr Sect D Biol Crystallogr* 50:760–763.
- Cousin X, Bon S, Duval N, Massoulié J and Bon C (1996) Cloning and expression of acetylcholinesterase from *Bungarus fasciatus* venom. *J Biol Chem* 271:15099–15108.
- Cousin, X., Hotelier T, Giles K, Toutant J-P and Chatonnet A (1998) aChEdb: The database system for ESTHER, the α/β fold family of proteins and the Cholinesterase gene server. *Nucleic Acids Res* 26:226–228.
- De Ferrari GV and Inestrosa NC (1998) Identification of an acetylcholinesterase fragment that promotes Alzheimer β-amyloid fibril formation, in *Structure and Function of Cholinesterases and Related Enzymes* (Doctor BP, Quinn DM, Rotundo RL and Taylor P eds) pp 185–186. Plenum Press, New York.
- Delhaise P, Bardiaux M and Wodak SJ (1984) Interactive computer animation of macromolecules. *J Mol Graphics* 2:103–106.
- Duval N, Massoulié J and Bon S (1992) H and T subunits of acetylcholinesterase from *Torpedo*, expressed in COS cells, generate all types of globular forms. *J Cell Biol* 118:641–653.
- Ellman GL, Courtney KD, Andres V Jr and Featherstone RM (1961) A new and rapid determination of acetylcholinesterase activity. *Biochem Pharmacol* 7:88–95.
- Eriksson AE, Baase WA, Wozniak JA and Matthews BW (1992a) A cavity-containing

- mutant of T4 lysozyme is stabilized by a buried benzene. *Nature (London)* **355**: 371–373.
- Eriksson AE, Baase WA, Zhang X-J, Heinz DW, Blaber M, Baldwin EP and Matthews BW (1992b) Response of a protein structure to cavity-creating mutations and its relation to the hydrophobic effect. *Science (Wash DC)* **255**:178–183.
- Gerstein M, Lesk A and Chothia C (1994) Structural mechanisms for domain movement in proteins. *Biochemistry* **33**:6739–6749.
- Harel M, Kleywegt GJ, Ravelli RBG, Silman I and Sussman JL (1995) Crystal structure of an acetylcholinesterase-fasciculin complex: Interaction of a three-fingered toxin from snake venom with its target. *Structure* **3**:1355–1366.
- Harel M, Schalk I, Ehret-Sabatier L, Bouet F, Goeldner M, Hirth C, Axelsen PH, Silman I and Sussman JL (1993) Quaternary ligand binding to aromatic residues in the active-site gorge of acetylcholinesterase. *Proc Natl Acad Sci USA* **90**:9031–9035.
- Harel M, Sussman, JL, Krejci E, Bon S, Chanal, P, Massoulié, J and Silman, I (1992) Conversion of acetylcholinesterase to butyrylcholinesterase: Modeling and mutagenesis. *Proc Natl Acad Sci USA* **89**:10827–10831.
- Inestrosa NC, Alvarez A, Pérez CA, Moreno RD, Vicente M, Linker C, Casanueva OI, Soto C and Garrido J (1996) Acetylcholinesterase accelerates assembly of amyloid- β -peptides into Alzheimer's fibrils: Possible role of the peripheral site of the enzyme. *Neuron* **16**:881–891.
- Janin J and Chothia C (1990) The structure of protein-protein recognition sites. *J Biol Chem* **265**:16027–16030.
- Kreimer DI, Dolginova EA, Raves M, Sussman JL, Silman I and Weiner L (1994) A metastable state of *Torpedo californica* acetylcholinesterase generated by modification with organomercurials. *Biochemistry* **31**:12248–12254.
- Kryger G, Giles K, Harel M, Tokar L, Velan B, Lazar A, Kronman C, Barak D, Ariel N, Shafferman A, Silman I and Sussman JL (1998) 3D structure studies of a complex of human recombinant acetylcholinesterase with fasciculin-II at 2.7 Å resolution, in *Structure and Function of Cholinesterases and Related Enzymes* (Doctor BP, Quinn DM, Rotundo RL and Taylor P eds) pp 323–326, Plenum Press, New York.
- Lee BK and Richards FM (1971) The interpretation of protein structures: Estimations of static accessibility. *J Mol Biol* **55**:379–400.
- Legay C, Bon S and Massoulié J (1993) Expression of a cDNA encoding the glycolipid-anchored form of rat acetylcholinesterase. *FEBS Lett* **315**:163–166.
- Massoulié J, Sussman JL, Doctor BP, Soreq H, Velan B, Cygler M, Rotundo R, Shafferman A, Silman I and Taylor P (1992) Recommendations for nomenclature in cholinesterases, in *Multidisciplinary Approaches to Cholinesterase Functions* (Shafferman A and Velan B eds) pp 285–288, Plenum Press, New York.
- Matsumara M, Becktel WJ and Matthews BW (1988) Hydrophobic stabilization in T4 lysozyme determined directly by multiple substitutions of Ile 3. *Nature (London)* **334**:406–410.
- McRee DE (1992) A visual protein crystallographic software system for X11/XView. *J Mol Graphics* **10**:44–46.
- Merritt EA and Bacon, DJ (1997) Raster3D: Photorealistic molecular graphics. *Methods Enzymol* **277**:505–524.
- Millard CB, Kryger G, Ordentlich A, Harel M, Raves ML, Greenblatt H, Segall Y, Barak D, Shafferman A, Silman I and Sussman JL (1998) Crystal structures of "aged" phosphorylated and phosphonylated acetylcholinesterase, in *Structure and Function of Cholinesterases and Related Enzymes* (Doctor BP, Quinn DM, Rotundo RL and Taylor P eds) pp. 425–432. Plenum Press, New York.
- Ollis DL, Cheah E, Cygler M, Dijkstra B, Frolow F, Franken SM, Harel M, Remington SJ, Silman I, Schrag J, Sussman JL, Verschuuren KHG and Goldman A (1992) The α/β hydrolase fold. *Protein Eng* **5**:197–211.
- Raves ML, Harel M, Pang Y-P, Silman I, Kozikowski AP and Sussman JL (1997) Structure of acetylcholinesterase complexed with the nootropic alkaloid, (–)-huperzine A. *Nat Struct Biol* **4**:57–63.
- Richards FM (1974) The interpretation of protein structures: Total volumes, group volumes distribution, and packing density. *J Mol Biol* **82**:1–14.
- Shin I, Silman I and Weiner LM (1996) Interaction of partially unfolded forms of *Torpedo* acetylcholinesterase with liposomes. *Protein Sci* **5**:42–51.
- Steinberg N, Roth E and Silman I (1990) *Torpedo* acetylcholinesterase is inactivated by thiol reagents. *Biochem Int* **21**:1043–1050.
- Sussman JL, Harel M, Frolow F, Oefner C, Goldman A, Tokar L and Silman I (1991) Atomic structure of acetylcholinesterase from *Torpedo californica*: A prototypic acetylcholine-binding protein. *Science (Wash DC)* **253**:872–879.
- Wernisch L, Hunting M and Wodak SJ (1999) Identifying structural domains in proteins by a graph heuristic. *Proteins* **35**:338–352.
- Wetlaufer DB (1973) Nucleation, rapid folding, and globular intrachain regions in proteins. *Proc Natl Acad Sci USA* **70**:679–701.
- Wilson EJ, Massoulié J, Bon S and Rosenberry TL (1996) The rate of thermal inactivation of *Torpedo* acetylcholinesterase is not reduced in the C231S mutant. *FEBS Lett* **379**:161–164.
- Wodak SJ and Janin, J (1981) Location of structural domains in proteins. *Biochemistry* **20**:6544–6552.
- Yutani K, Ogasahara K, Tsujita T and Sugino, Y (1987) Dependence of conformational stability on hydrophobicity of the amino acid residue in a series of variant proteins substituted at a unique position of tryptophan synthase α subunit. *Proc Natl Acad Sci USA* **84**:4441–4444.

Send reprint requests to: Dr. Israel Silman, Department of Neurobiology, Weizmann Institute of Science, Rehovoth 76100, Israel. E-mail: bnsilm@weizmann.weizmann.ac.il

Structure of acetylcholinesterase complexed with E2020 (Aricept®): implications for the design of new anti-Alzheimer drugs

Gitay Kryger^{1*}, Israel Silman² and Joel L Sussman^{1,3}

Background: Several cholinesterase inhibitors are either being utilized for symptomatic treatment of Alzheimer's disease or are in advanced clinical trials. E2020, marketed as Aricept®, is a member of a large family of *N*-benzylpiperidine-based acetylcholinesterase (AChE) inhibitors developed, synthesized and evaluated by the Eisai Company in Japan. These inhibitors were designed on the basis of QSAR studies, prior to elucidation of the three-dimensional structure of *Torpedo californica* AChE (TcAChE). E2020 significantly enhances performance in animal models of cholinergic hypofunction and has a high affinity for AChE, binding to both electric eel and mouse AChE in the nanomolar range.

Results: Our experimental structure of the E2020–TcAChE complex pinpoints specific interactions responsible for the high affinity and selectivity demonstrated previously. It shows that E2020 has a unique orientation along the active-site gorge, extending from the anionic subsite of the active site, at the bottom, to the peripheral anionic site, at the top, via aromatic stacking interactions with conserved aromatic amino acid residues. E2020 does not, however, interact directly with either the catalytic triad or the 'oxanion hole', but only indirectly via solvent molecules.

Conclusions: Our study shows, *a posteriori*, that the design of E2020 took advantage of several important features of the active-site gorge of AChE to produce a drug with both high affinity for AChE and a high degree of selectivity for AChE versus butyrylcholinesterase (BChE). It also delineates voids within the gorge that are not occupied by E2020 and could provide sites for potential modification of E2020 to produce drugs with improved pharmacological profiles.

Introduction

Observations documenting adverse effects of anticholinergic drugs on memory [1], taken together with postmortem data that revealed low cholinergic activities in Alzheimer's disease (AD) patients [2], led to the hypothesis, known as the 'cholinergic hypothesis', that AD is associated with an impairment in cholinergic transmission [3–5]. This led to the suggestion that cholinesterase (ChE) inhibitors would reverse a putative deficit in acetylcholine (ACh) levels associated with AD, and thus might reverse the memory impairments characteristic of the disease [5,6]. Consequently, a number of ChE inhibitors have been considered as candidates for the symptomatic treatment of AD and have been utilized in clinical trials. They include natural substances, such as physostigmine [6] and huperzine A [7], both of which are alkaloids, and synthetic compounds such as SDZ ENA-713, also known as Exelon® [8], and metrifonate [9]. Recently, evidence was presented that acetylcholinesterase (AChE) accelerates assembly of amyloid- β -peptides into the amyloid fibrils that form the senile plaques characteristic of AD [10]. It was suggested that a hydrophobic environment close to the peripheral binding site of the enzyme, at or near the entrance to the active-site gorge, might be involved in this process [11].

Addresses: ¹Department of Structural Biology, Weizmann Institute of Science, Rehovot 76100, Israel, ²Department of Neurobiology, Weizmann Institute of Science, Rehovot 76100, Israel and ³Department of Biology, Brookhaven National Laboratory, Upton, NY 11972, USA.

*Corresponding author.

E-mail: Gitay.Kryger@Weizmann.ac.il

Key words: acetylcholinesterase, Alzheimer's disease, crystal structure, drug–protein complex

Received: 18 November 1998

Revisions requested: 15 December 1998

Revisions received: 23 December 1998

Accepted: 11 January 1999

Published: 1 March 1999

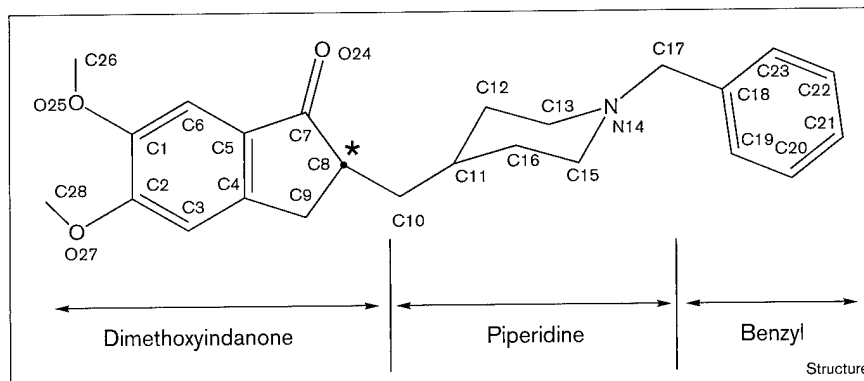
Structure March 1999, 7:297–307

<http://biomednet.com/elecref/0969212600700297>

© Elsevier Science Ltd ISSN 0969-2126

The first, and thus far the only, two drugs approved by the United States Food and Drug Administration (FDA) for treatment of AD are both reversible inhibitors of AChE. They are tacrine (THA), approved in 1993 and marketed as Cognex® [12], and the more potent ChE inhibitor, E2020 ((*R,S*)-1-benzyl-4-[(5,6-dimethoxy-1-indanon)-2-yl]methylpiperidine; Figure 1), also known by its trivial name donepezil hydrochloride and marketed as Aricept®, which was approved in 1996 [13]. E2020 is a member of a large family of *N*-benzylpiperidine-based AChE inhibitors that were developed, synthesized and evaluated by the Eisai Company in Japan [14], on the basis of QSAR studies [15,16], prior to elucidation of the three-dimensional (3D) structure of *Torpedo californica* AChE (TcAChE) [17]. It was shown to significantly enhance performance in animal models of cholinergic hypofunction [18], and to have high affinity for AChE, binding to both electric eel and mouse AChE in the nanomolar range [19]. THA and E2020 share the same target, but whereas THA must be administered up to four times a day, and is associated with hepatotoxicity, slow pharmacokinetics and a high incidence of side effects, E2020 offers the patient significant improvements by being administered only once a day and having fewer side effects. Furthermore, E2020 displays high selectivity for AChE in

Figure 1



Schematic drawing of E2020, (*R,S*)-1-benzyl-4-[(5,6-dimethoxy-1-indanon)-2-yl]methylpiperidine. *C8 is the chiral carbon.

comparison to butyrylcholinesterase (BChE); this may be important, as it has been suggested that inhibition of BChE, which is abundant in human plasma, may cause potentiating side effects [20,21]. The affinity of E2020 for human AChE is ~1000-fold greater than for human BChE, whereas THA has a similar affinity for the two enzymes [22,23].

Attempts to explain the specificity of E2020, and of other Eisai inhibitors, were made originally using QSAR and by theoretical conformational analysis. Subsequent to determination of the 3D structure of *TcAChE*, automated computational techniques based on the known coordinates were employed [24,25]. Although the earlier modeling studies attributed the differential specificity for AChE and BChE to differences in the geometry within the active site [26], the more recent studies suggested that E2020 and the other Eisai compounds are oriented along the axis of the active-site gorge and that the differential specificity can be attributed to structural differences in AChE and BChE at the top of the gorge, at the 'peripheral' anionic site [14,24,25]. Our experimental structure of the E2020-*TcAChE* complex broadly confirms these latter assignments and pinpoints the specific interactions that are responsible for the high affinity and selectivity demonstrated previously.

Results and discussion

Overall structure

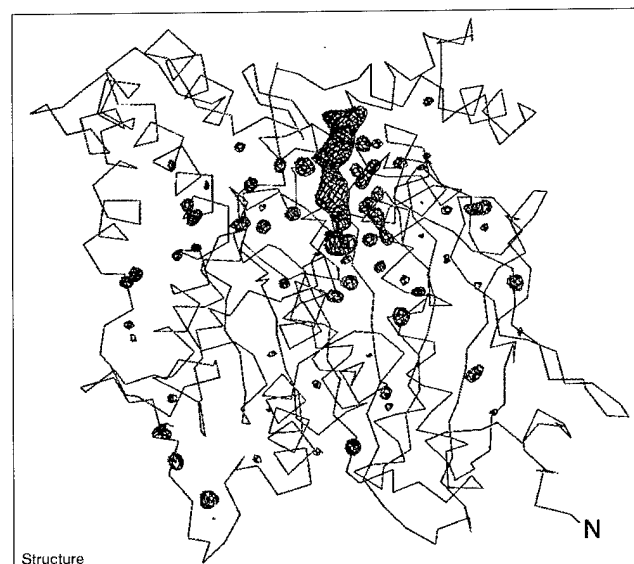
The overall structure of the E2020-*TcAChE* complex at 2.5 Å resolution is shown in Figure 2. The protein is displayed as a coil with the initial difference electron-density map of E2020 superimposed as a 'chicken-wire' net. It can be clearly seen that E2020 has a unique orientation along the active-site gorge, extending from the anionic subsite of the active site, at the bottom near Trp84, to the peripheral anionic site, at the top near Trp279 (see Figures 3 and 4). The 3D structure of the complex shows more detail of the AChE structure than the starting native model (Protein Data Bank [PDB] code 2ACE). Specifically, residues 2 and 3, at the N terminus, and the 484-490 loop, which were not seen in the original model, can be discerned. In

addition, it was possible to model the proximal *N*-acetylglucosamine (NAG) moiety at four out of five putative glycosylation sites [27], namely at residues Asn59, Asn416 (where two moieties could be fitted), Asn457 and Asn533. An analysis of the quality of the refined model is summarized in Table 1.

All three segments of E2020 interact with AChE

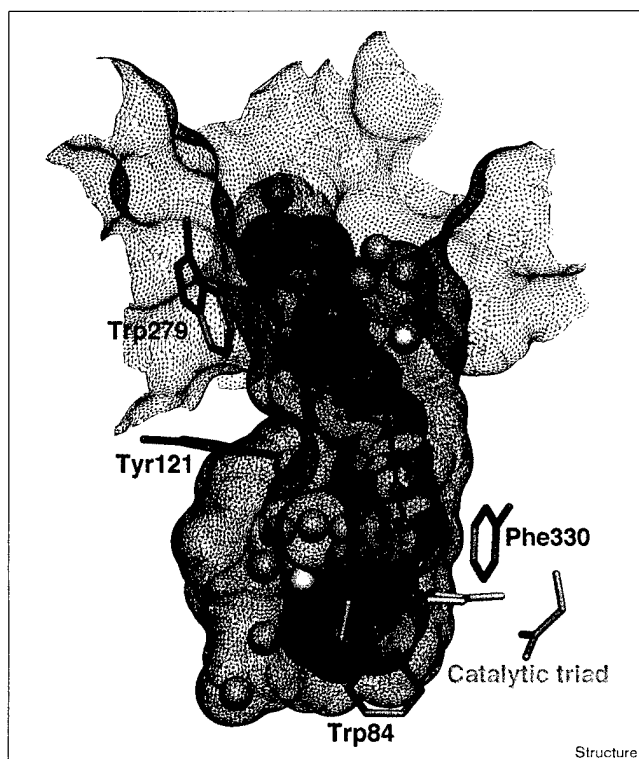
As seen in Figure 5, E2020 makes principal interactions along the active-site gorge of the enzyme through its three major functional groups: the benzyl moiety, the piperidine nitrogen, and the dimethoxyindanone moiety. These interactions involve discrete water-mediated contacts that seem to be crucial for binding and specificity.

Figure 2



Initial difference electron-density map, contoured at 4.5σ, based on the native *TcAChE* structure (PDB code 2ACE) and the diffraction data for the E2020-*TcAChE* complex.

Figure 3



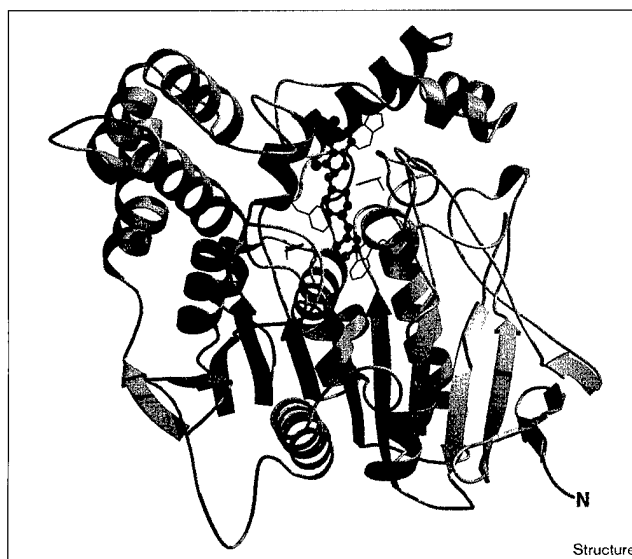
E2020 binds along the active site and interacts with the 'peripheral anionic' subsite at the top and with the 'anionic' subsite at the bottom. E2020 is displayed in green semi-transparent CPK and ball-and-stick representation, solvent molecules are shown as lilac balls, catalytic triad residues are in orange, binding residues are shown as purple sticks, and the solvent-accessible surface of the gorge is shown as a brown net.

Interactions at the bottom of the gorge

Near the bottom of the gorge, one face of the benzyl ring displays classic parallel π - π stacking with the six-membered ring of the Trp84 indole, similar to the interaction with THA [28]. It thus occupies the binding site for quaternary ligands [28,29], which was also modeled for the quaternary group of the natural substrate, ACh [17,26]. The ring-to-ring distances range from 3.7 Å between Trp84 C δ 2 and E2020 C19 to 4.4 Å between Trp84 C ϵ 2 and E2020 C22.

On the opposite face, the benzyl group makes a classic aromatic hydrogen bond (H bond) [30,31] with a water molecule (WAT 1160), with distances to the ring carbons of 3.5 Å–3.7 Å. This solvent molecule is held firmly, as assessed by a below-average temperature factor, by an H bond to another solvent molecule (WAT 1161) in the 'oxanion hole' and to WAT 1159 (see below). WAT 1161 is another example of a tightly bound water molecule with a relatively low temperature factor; it makes an H bond with the residues of the oxanion hole, namely with Gly118 N, Gly119 N and Gly201 N, as well as with

Figure 4



The E2020-*TcAChE* complex. Ribbon diagram showing the complex of the drug bound to the enzyme.

Ser200 O γ . Finally, the kinetic evidence showing that E2020 binds to the free and the acylated forms of AChE [32] is corroborated by our observation that E2020 does not interact with the catalytic triad. Other interactions are shown schematically in Figure 5.

Interactions in the middle of the gorge

In the constricted region, halfway up the gorge (Figures 3 and 4), the charged nitrogen of the piperidine ring makes a cation- π interaction [33,34] with the phenyl ring of Phe330, with distances of 3.9 Å–4.5 Å between the nitrogen and the ring carbons. The orientation of the phenyl ring is similar to that seen in the complex of decamethonium (DECA) with *TcAChE* (DECA-*TcAChE*; PDB code 1ACL) [28]. The ring nitrogen also makes an in-line 2.9 Å H bond with WAT 1159, which, in turn, makes H bonds with Tyr121 OH, with WAT 1158 and with WAT 1160 (see above). As already mentioned, the binding site for the quaternary nitrogen of ACh, and for homologous ligands, is the indole ring of Trp84 [17,26,28]. These data suggest that Phe330 may serve as an additional quaternary binding site, midway down the gorge, between the peripheral site and the anionic subsite of the active site.

Interactions at the entrance to the gorge

At the top of the gorge the indanone ring stacks against the indole ring of Trp279, in the peripheral binding site, by a classical π - π interaction. Specifically, E2020 C1, C2, C6, O25, C26, O27 and C28 stack against the six-membered ring of Trp279, with distances of 3.7 Å–4.2 Å. WAT 1249 lies in the plane of the indanone moiety, and H bonds to

Table 1

Data collection and refinement statistics.

Data collection

Detector	Raxis-II								
Source/wavelength (Å)	Rigaku FR300 (50 mA, 50 kV), 1.54184 (Cu K _α)								
Resolution range (Å)	30.0–2.5								
Number of reflections	34,264								
Completeness (%)	98.1								
Redundancy									
value	0	1	2	3	4	>5			
accumulated (%)	1.9	15.7	44.3	33.4	4.5	0.2			
I/σ									
value	0	1	2	3	5	10	20	>20	
accumulated (%)	5.5	14.2	23.4	30.7	41.2	57.6	78.1	20.0	
R _{sym} (%)	5								

Refinement

Number of protein non-H atoms	4255 = 2137 mainchain + 2118 sidechain							
Number of hetero non-H atoms								
Water molecules	396							
Carbohydrate	70 = 5 × 14 in five NAG groups							
Inhibitor	28 in one E2020 group							
Resolution (Å)	2.5							
R _{work} (%)	18.8 (no σ cutoff)							
R _{free} (%)	22.9 (no σ cutoff)							
B factor (Å ²); Average / σ / Minimum / Maximum								
Protein	28.0 / 12.5 / 2.0 / 90.2							
Inhibitor	20.4 / 4.8 / 13.2 / 31.6							
Carbohydrate	47.6 / 15.0 / 14.5 / 74.5							
Water molecules	37.2 / 14.7 / 2.2 / 86.7							
Rmsd bond length (Å)	0.005							
Rmsd bond angle (°)	1.2							
Rmsd dihedral angle (°)	22.9							
Rmsd improper angle (°)	0.98							

$R_{\text{sym}} = \sum |I_i - \langle I \rangle| / \sum I_i$; $R_{\text{work}} = \sum ||F_o| - |F_c|| / \sum F_o$. R_{free} is calculated using 2000 random reflections.

the methoxy group of E2020 O25; it is also H-bonded to Glu185 Oε1 of the symmetry-related crystal-lattice copy of the enzyme. The carbonyl on the five-membered ring of the indanone only interacts with AChE via edge-on van der Waals contacts with the aromatic rings of Phe331 and Phe290. It also makes indirect contact, via WAT 1254, with Phe288 N. This finding might initially appear puzzling in view of the fact that a homolog of E2020, which lacks this carbonyl, was reported to be inactive [15]. Our structure-based suggestion is that the van der Waals contacts made by the carbonyl function help orient the indanone moiety to make a favorable interaction with the indole ring of Trp279. In the homolog which lacks this carbonyl function, the indanone moiety would be less constrained and would consequently make a poorer interaction with Trp279.

AChE selects the *R* form of E2020

The reported pharmacological studies on (*R,S*)-E2020 emphasize that both enantiomers are active; they have similar pharmacological profiles [22,32], but show ~fivefold difference in binding affinity for AChE: $K_i = 3.35$ nM (*R*), 17.5 nM (*S*) [32]. Although we used the racemate in our crystallographic study, we were not, therefore, surprised to see only the *R* form in the experimental electron-density

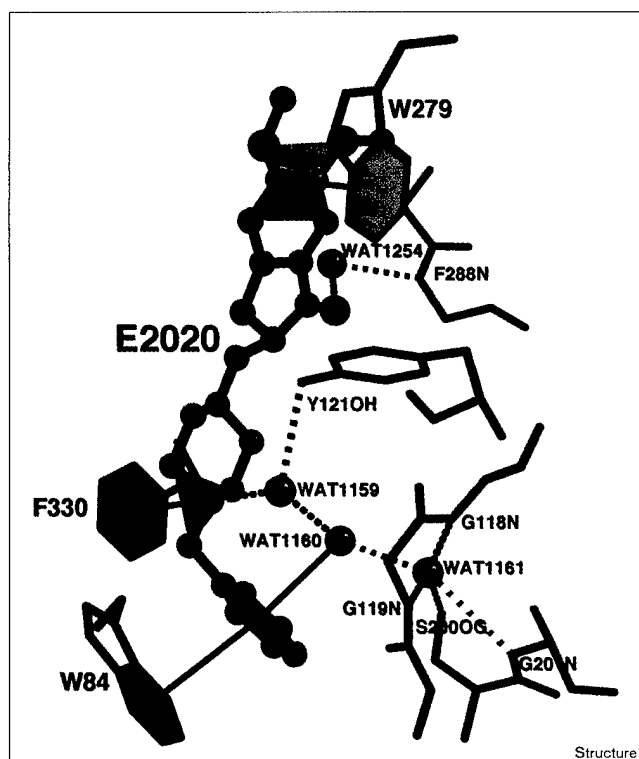
maps (see Figure 6). The observed conformation is very similar, if one allows for permitted adjustments of dihedral angles, to the energetically minimized E2020 conformation calculated with the InsightII package [35], and it is also similar to the 'small molecule' crystal structure of the pure *R* enantiomer (T Steiner, R Boer and J Kroon, personal communication).

E2020 analogs

Variation of the inhibitor backbone

Kawakami *et al.* [14] showed that at least two rotatable bonds on each side of the piperidine are needed to yield the high affinity displayed by E2020 and some of its analogs. We can now corroborate this observation by showing that the two aromatic moieties of E2020 interact closely with Trp84 and Trp279, while still maintaining the Phe330–piperidine–nitrogen interaction. This array of interactions calls for flexibility along the backbone of the inhibitor. The number of rotatable links is also important for optimal positioning of the aromatic systems of the inhibitor against their enzyme counterparts. Indeed, when two to three additional rotatable bonds are added between the indanone and the piperidine, affinity further increases (Table 2, lines 20–22), whereas adding rotatable bonds

Figure 5



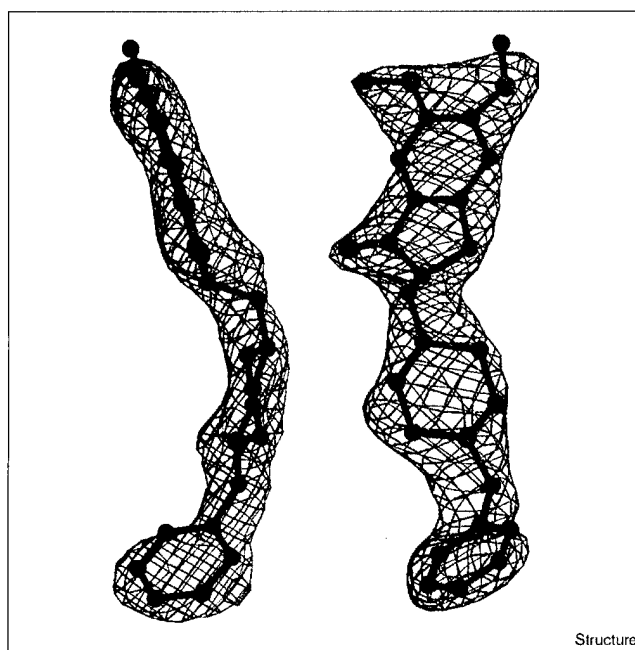
Major interactions between E2020 and TcAChE. Classical H bonds are shown as dashed lines, aromatic stacking and aromatic H bonds are shown as black lines connecting matching colored planes.

between the piperidine and the benzyl ring lowers it (Table 2, line 19). This distinction between adding rotatable bonds 'above' and 'below' the piperidine is likely to be based on the distances between Phe330 and either Trp84 or Trp279. Any change in the length of the spacer between Phe330 and Trp84 would weaken the interactions of the inhibitor with those sidechains. However, limited elongation of the indanone-piperidine link might allow more overlap of the indanone's aromatic system with that of Trp279.

Variation of the benzyl moiety

E2020 is highly sensitive to substitutions on the benzyl moiety, as found by Kawakami and coworkers [14], who noticed a general preference for substitution at the *meta* (E2020 C20, C22) positions in comparison to the *ortho* (E2020 C19, C23) and *para* (E2020 C21) positions (see Table 2). Although these solution studies could not differentiate between the two possible *ortho/meta* substitutions, it can be seen from the crystal structure how each position would experience different environments with respect to the lining of the gorge and the structural solvent molecules within it. In general there is little space left between the benzyl ring and the gorge surface (Figures 3 and 4), which

Figure 6



Two views of E2020 modeled in the initial difference Fourier map. Only one enantiomer is observed in the crystal structure. The shape of the electron density around the chiral carbon and the carbonyl clearly resolve the *R/S* ambiguity. 'Side' and 'front' views of E2020 are shown modeled in the initial difference electron-density map contoured at 4.5σ .

may explain the sensitivity to substitutions of this moiety. The ring carbon at the *para* position is 3.2 Å from Glu199 Oe1; thus a substituent must be both small and able to make an H bond. Indeed, according to Kawakami *et al.* [14], an analogue with a hydroxyl at this position binds with higher affinity than the corresponding fluorine derivative (Table 2, lines 9–12). A substituent at the *meta* position, E2020 C22, will point to a very small space left between Glu199, His440 and Ser200 (the last two of which are members of the catalytic triad). The other *meta* position, at E2020 C20, points to a wider space partially bordered by Gly117 and the 'oxanion hole'. In our structure, this space is mostly occupied by solvent molecules and can accommodate a small, preferably negatively charged, substituent (Table 2, lines 5–7). A cyclohexane in place of a benzyl ring cannot make a π - π stacking interaction with Trp84, resulting in reduced affinity (Table 2, line 18).

Variation of the piperidine moiety

A piperazine in place of piperidine lowers the affinity of the resulting analog by ~19-fold (Table 2, line 3), whereas a piperidine with a nitrogen at the opposite position (in place of E2020 C10) lowers the affinity by ~90-fold (Table 2, line 2). A piperazine, although containing a nitrogen at a position suitable for binding with Phe330, possesses a different

Table 2

E2020 analogs.

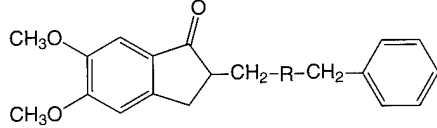
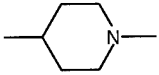
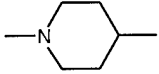
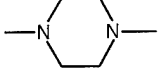
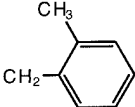
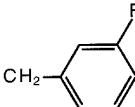
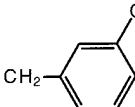
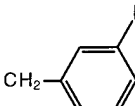
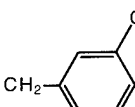
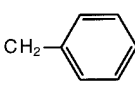
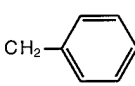
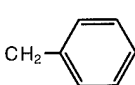
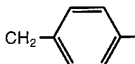
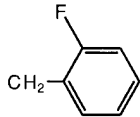
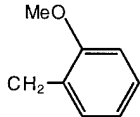
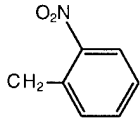
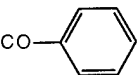
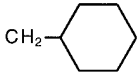
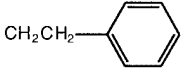
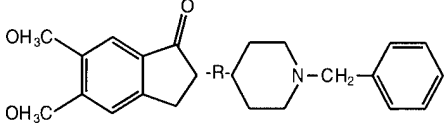
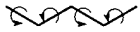
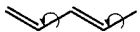
Analog number	Constant	Variable R	Inhibition of AChE IC ₅₀ (nM) [14]
1.		 (E2020)	5.7
2.			480
3.			94
4.			10
5.			1
6.			2
7.			4
8.			220
9.			1.8
10.			9.5
11.			40
12.			100

Table 2 continued

13.		9.5
14.		80
15.		160
16.		>10,000
17.	H	5400
18.		8.9
19.		180
20.		0.9
21.		1.5
22.		3.0

charge distribution, whereas a piperidine with a nitrogen at the opposite position does not allow a quaternary- π interaction with Phe330 to occur.

Variation of the indanone moiety

In general, substitutions on the indanone moiety have a smaller effect than substitutions on the benzyl group [15]. This is consistent with our crystal structure, as the indanone moiety is located in the wide section of the funnel-like

entrance to the gorge. Thus, some sites of substitution would point outwards towards the solvent, whereas others would point into the central region of the gorge. However, substitution on the same edge as the carbonyl group (C7 O24), which is juxtaposed to the wall of the gorge, would disrupt the parallel stacking to Trp279. This is consistent with the observation of Cardozo *et al.* [15] that a cyano substitution on E2020 C6 produces a relatively poor inhibitor. Suitable substitutions on the other edge of the

ring (namely E2020 C1, C2, C3 and C9) would be expected to have little effect or, possibly, result in improved affinity.

Comparison of the E2020-TcAChE complex with other complexes

The structures of native TcAChE and of six different complexes were overlaid according to their C α positions, namely native AChE (PDB code 2ACE) [36], and the complexes with tacrine (THA; PDB code 1ACJ) [28], DECA (PDB code 1ACL) [28], *m*-(*N,N,N*-trimethylammonio)trifluoroacetophenone (TMTFA; PDB code 1AMN) [29], huperzine (HUP; PDB code 1VOT) [36], edrophonium (EDR; PDB code 2ACK) and E2020 (PDB code 1EVE). Two issues arise from comparison of these structures: the role of Phe330, and the possible significance of structurally conserved solvent molecules within the gorge.

Phe330 as a 'swinging gate'

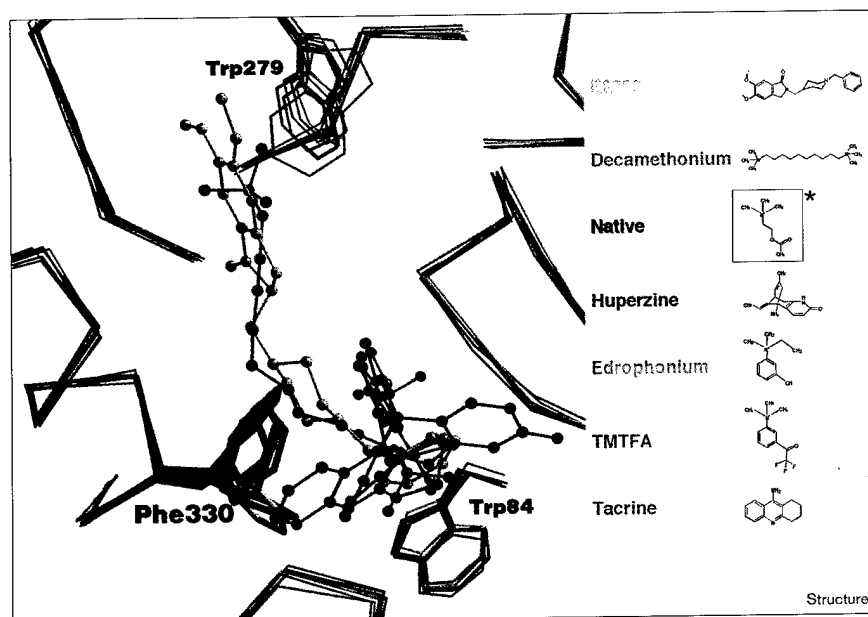
As seen in Figure 7, Phe330 adopts a wide range of conformations in the complex structures analyzed. These conformations can be assigned, primarily based on their χ_1 values, to three different groups. First, native, TMTFA, HUP and EDR ($\chi_1 = -162^\circ$, -174° , -171° and -177° , respectively). Second, THA ($\chi_1 = 157^\circ$). Third, E2020 and DECA ($\chi_1 = -130^\circ$ and -117° , respectively). In group 1, Phe330 adopts a similar conformation in the native enzyme and in the complexes with ligands that bind near the bottom of the gorge, with the exception of THA. This ligand defines Group 2, in which χ_1 and χ_2 of Phe330 change so as to permit its phenyl group to stack on top of the ligand, thus forming a 'sandwich' with the indole of Trp84. The common feature of Group 3 is the gorge-spanning ligand

that forces the aromatic ring of Phe 330 to swing out of the way towards the gorge wall. It is also of interest that the THA-TcAChE complex displays a different conformation for the indole group of Trp279 relative to native AChE and the other complexes (χ_2 value of 30° versus about 90° for the others). This provides some support for structural coupling along the gorge between the anion subsite of the active site and the peripheral anionic site, as suggested by Shafferman and coworkers [37]. The conformational flexibility displayed by the sidechain of Phe330, contrasted with the relative rigidity of the other sidechains lining the gorge, supports the notion that it contributes to the significantly higher catalytic activity of AChE relative to BChE, which lacks this residue. Site-directed mutagenesis studies [38,39] showed that elimination of this aromatic sidechain does not affect the K_m for both charged and uncharged ligands. It does, however, have a significant effect on k_{cat} , which decreases ~fourfold for cationic substrates, although it increases ~twofold for uncharged substrates. Thus, via the quaternary- π electron interaction clearly seen in the E2020 complex, it may serve to guide ACh towards the active site, while simultaneously isolating the reaction center from the rest of the gorge. In fact, substrate traffic down the gorge may actually occur concomitantly with a swinging movement of Phe330. Similar ideas have been proposed on the basis of molecular dynamics studies [40,41].

The solvent

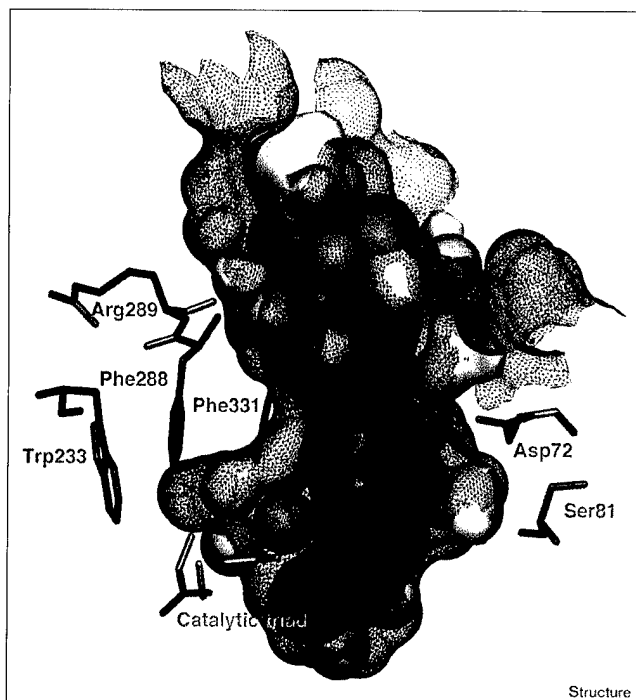
In the E2020-TcAChE complex, 25 ordered waters can be seen within the gorge. If one overlays this structure with that of the native enzyme and of five other complexes, as

Figure 7



Overlay of native TcAChE and six complexes. The flexibility of Phe330 in comparison with the rigidity of the rest of the gorge can be seen. Backbone trace and key residues are represented by thin lines, Phe330 by thick lines and inhibitors are shown in ball-and-stick representation. *A ChemDraw® representation of ACh is shown for purposes of comparison.

Figure 8



'Empty' spaces, where no ordered solvent molecule is observed, can accommodate a substituent branching from the inhibitor. Voids within the gorge are displayed in yellow, the solvent-accessible surface of E2020 is in purple, the solvent-accessible surface of the gorge is shown as a brown net, the CPK model of the solvent molecules is in lilac, residues near voids are in light blue, and the catalytic triad is represented by orange sticks.

shown in Figure 7, one can see that most of these waters are conserved (G Koellner, GK, IS, JLS and T Steiner, unpublished results). In the E2020 structure, in fact, only three of the conserved waters seen in the native enzyme are displaced. From this one can conclude that a large ligand, such as E2020, fits into the gorge by displacing primarily the unbound solvent molecules. Many of the conserved waters appear to adhere to the gorge wall and may, perhaps, be considered as an integral part of the structure of the gorge rather than as voids. This may be especially important in relation to drug design (see below), as well as in molecular dynamics studies. It should also be noted that water molecules not observed in the native structure are seen in the E2020 complex, where they bridge between the inhibitor and the enzyme. Specifically WAT 1159, WAT 1160 and WAT 1254 (see Figure 5) are 'novel' structured waters not previously seen in the native structure, while five ordered waters in the native structure are displaced.

Structure-based modification of E2020

Chemical modification of an already effective drug can often improve its pharmacological profile in terms of affinity and specificity. The calculated 'empty' spaces within

the gorge (see Figures 4 and 8), which are revealed in the 3D structure of the E2020-AChE complex, point to candidate sites on the inhibitor where added functions might indeed enhance its pharmacological profile. Separation of enantiomers, which are chemically indistinguishable by non-chiral environments, is difficult, inefficient and costly. In the case of E2020, we suggest that introduction of a second chiral center, with concomitant generation of a diastereomer system, would facilitate isolation of an active component from the mixture so generated [42,43]. Inspection of the empty spaces left within the aromatic gorge by the ordered solvent and by E2020 reveals a finger-shaped void at the acyl-binding pocket. This pocket, defined by Phe288, Phe290, Phe331 and Trp233, could envelop a non-polar substituent branching from the piperidine ring at position E2020 C12. Such a substitution, which would fit into the 'acyl pocket', combined with the existing chiral center, would produce a separable diastereomeric inhibitor.

The recent observations concerning the effect of peripheral-site ligands on AChE-enhanced amyloid deposition [10], mentioned above, raise the possibility that E2020, which our data clearly show as stacking against Trp279, might also moderate the rate of fibril formation. Many of the compounds synthesized and tested by the Eisai company involved modification of this segment of the molecule [15,16]. Nevertheless, it should be borne in mind that the screening that they carried out involved assessment of affinity for AChE, together with selectivity for AChE relative to BChE, but not a possible effect on amyloid fibril assembly or deposition.

Biological implications

Acetylcholinesterase (AChE), the enzyme that hydrolyzes the neurotransmitter acetylcholine (ACh) at cholinergic synapses [44], is the target of the first generation of drugs for the treatment of Alzheimer's disease. E2020 is the second drug targeted at AChE approved for use by the FDA for treatment of this condition. As design and development of the drug preceded the determination of the 3D structure of AChE, it was of interest to use X-ray crystallography to clearly delineate the structural factors governing its selectivity and specificity. This was particularly important because E2020 bears no structural resemblance to other anticholinesterase drugs either approved or under advanced clinical trial, such as tacrine, huperzine A and ENA-713 [45]. Our study shows, *a posteriori*, that the design of E2020 took advantage of several important features of the active-site gorge of AChE to produce a drug with both high affinity and a high degree of selectivity for the enzyme, but not for butyrylcholinesterase (BChE). The high affinity results from interaction of E2020 with the aromatic residue involved in recognition of ACh at the bottom of the gorge, Trp84, with a second aromatic residue at the midpoint of the gorge, Phe330, and with a third residue, Trp279, which is part of the peripheral

anionic site at the top of the gorge. The fact that these two latter residues are conserved in AChE, but absent in BChE, leads to the selectivity that may be an important clinical consideration, as inhibition of BChE may cause potentiating site effects. Our study also delineates voids within the gorge of AChE that are not occupied by E2020, which could serve as sites for modification of E2020 to produce drugs with greater affinity and/or selectivity for AChE. It is worth noting that the 3D structure of *Torpedo californica* AChE (TcAChE) is very similar to those of both mouse [46] and human AChE [47]. Thus, the conclusions drawn from the structure of the E2020-TcAChE complex should be valid for the mammalian enzyme.

Finally, analogs of E2020 are under consideration as a possible new class of insecticides [48]. The structure of *Drosophila* AChE has recently been solved to 2.7 Å resolution in our laboratory [49] (M Harel, GK, H Greenblatt, L Toker, W Mallender, TL Rosenberry, T Lewis, IS and JLS, unpublished results). Although *Drosophila* AChE shares overall structural features with the *Torpedo* and human enzymes, it also displays marked differences. Our combined knowledge of the vertebrate and invertebrate enzymes should be valuable in developing effective insecticides that combine high specificity for the insect enzyme with low toxicity in humans.

Materials and methods

Protein preparation and crystallization

TcAChE was purified and crystallized as described previously [36]. E2020, as the hydrochloride salt of the pure racemate, was a generous gift from Dr BP Doctor (Division of Biochemistry, Walter Reed Army Institute of Research, Washington, DC). TcAChE crystals of trigonal morphology were soaked for five days at 4°C in mother liquor (36% PEG 200, 10 mM NaCl, 50 mM MES, pH 5.8) containing ~10 mM (R,S) E2020.

X-ray data collection and processing

The X-ray data were collected from a single crystal that was flash cooled in a 100K nitrogen stream after exchanging the exterior solvent drop with a coating of Exxon high viscosity motor oil [50]. Data were collected in-house, at the Weizmann Institute, utilizing a Rigaku RAXIS-II image-plate system, and a Rigaku FR300 X-ray generator employing a copper target set at 50 mA and 50 kV. The data-collection scheme was optimized by use of the software STRATEGY [51], and consisted of 81 frames of 0.5° rotation and 30 min exposure time each. The diffraction data were extracted from the frames using the software package HKL [52], resulting in a 98.1% complete dataset of 34,264 reflections, overall R_{sym} of 5% and overall I/σ ratio 13.8 (see Table 1).

Model refinement and analysis

The structure was refined using the starting model of native TcAChE (PDB code 2ACE) with the program X-PLOR version 3.851 [53]. Refinement employed all 30–2.5 Å data. Following overall anisotropic B-factor and bulk-solvent corrections, the structure was first refined as a single rigid body. Subsequently, refinement was carried out on individual atoms, with restraints, using simulated annealing alternating with positional and temperature-factor refinement. The model was fitted to the observed electron density using the software O [54] on a Silicon Graphics workstation. This program was also used to overlay analogous models by least-squares minimization of C α positions. The intermediate and final models were analyzed using the software OOPS [55], PROCHECK [56] and WHATCHECK [57], and corrections to the model based on these

analyses were implemented (see Table 1). Voids of minimal continuous volume of one spherical cubic angstrom were calculated using the software SurfNet [58], between the inhibitor molecule as one entity and the protein and solvent molecules, taken together, as a second entity.

Accession numbers

The PDB code of the E2020-TcAChE complex is IEVE.

Acknowledgements

We thank BP Doctor (Walter Reed Army Institute of Research, Washington DC) for generously providing us with E2020, and Terry Lewis (Jealott's Hill Research Station, Zeneca Agrochemicals, Bracknell, UK) and Yoshiyuki Kawakami (Tsukuba Research Laboratories, Eisai Ltd, Tsukuba, Japan) for valuable discussions. This work was supported by the US Army Medical Research Acquisition Activity under Contract No. DAMD17-97-2-7022, the European Union IVth Framework in Biotechnology, the Kimmelman Center for Biomolecular Structure and Assembly, Israel, the Nella and Leon Benoziyo Center for Neurosciences, and the generous support of Tania Friedman. IS is Bernstein-Mason Professor of Neurochemistry.

References

- Drachman, D.A. & Leavitt, J. (1974). Human memory and the cholinergic system. *Arch. Neurol.* **30**, 113-121.
- Bowen, D.M., et al., & Davison, A.N. (1983). Biochemical assessment of serotonergic and cholinergic dysfunction and cerebral atrophy in Alzheimer's disease. *J. Neurochem.* **41**, 266-272.
- Bartus, R.T., Dean, R.L., Beer, B. & Lippa, A.S. (1982). The cholinergic hypothesis of geriatric memory dysfunction. *Science* **217**, 408-414.
- Dunnett, S.B. & Fibiger, H.C. (1993). Role of forebrain cholinergic systems in learning and memory: relevance to the cognitive deficits of aging and Alzheimer's dementia. *Prog. Brain Res.* **98**, 413-420.
- Weinstock, M. (1997). Possible role of the cholinergic system and disease models. *J. Neural Transm. Suppl.* **49**, 93-102.
- Becker, R., Giacobini, E., Elble, R., McIlhenny, M. & Sherman, K. (1988). Potential pharmacotherapy of Alzheimer's disease. A comparison of various forms of physostigmine administration. *Acta Neurol. Scand. Suppl.* **116**, 19-32.
- Zhang, R.W., et al., & Yang, R.M. (1991). Drug evaluation of huperzine A in the treatment of senile memory disorders. *Acta Pharm. Sinica* **12**, 250-252.
- Weinstock, M., Razin, M., Chorev, M. & Enz, A. (1994). Pharmacological evaluation of phenyl-carbamates as CNS-selective acetylcholinesterase inhibitors. *J. Neural Transm. Suppl.* **43**, 219-225.
- Knopman, D.S. (1998). Metrifonate for Alzheimer's disease: Is the next cholinesterase inhibitor better? *Neurology* **50**, 1203-1206.
- Inestrosa, N.C., et al., & Garrido, J. (1996). Acetylcholinesterase accelerates assembly of amyloid-beta-peptides into Alzheimer's fibrils: possible role of the peripheral site of the enzyme. *Neuron* **16**, 881-891.
- Reyes, A.E., et al., & Inestrosa, N.C. (1997). A monoclonal antibody against acetylcholinesterase inhibits the formation of amyloid fibrils induced by the enzyme. *Biochem. Biophys. Res. Commun.* **232**, 652-655.
- Davis, K.L. & Powchik, P. (1995). Tacrine. *Lancet* **345**, 625-630.
- Nightingale, S.L. (1997). Donepezil approved for treatment of Alzheimer's disease. *JAMA* **277**, 10.
- Kawakami, Y., Inoue, A., Kawai, T., Wakita, M., Sugimoto, H. & Hopfinger, A.J. (1996). The rationale for E2020 as a potent acetylcholinesterase inhibitor. *Bioorg. Med. Chem.* **4**, 1429-1446.
- Cardozo, M.G., Imura, Y., Sugimoto, H., Yamanishi, Y. & Hopfinger, A.J. (1992). QSAR analyses of the substituted indanone and benzylpiperidine rings of a series of indanone-benzylpiperidine inhibitors of acetylcholinesterase. *J. Med. Chem.* **35**, 584-589.
- Cardozo, M.G., Kawai, T., Imura, Y., Sugimoto, H., Yamanishi, Y. & Hopfinger, A.J. (1992). Conformational analyses and molecular-shape comparisons of a series of indanone-benzylpiperidine inhibitors of acetylcholinesterase. *J. Med. Chem.* **35**, 590-601.
- Sussman, J.L., et al., & Silman, I. (1991). Atomic structure of acetylcholinesterase from *Torpedo californica*: a prototypic acetylcholine-binding protein. *Science* **253**, 872-879.
- Rupniak, N.M., Tye, S.J. & Field, M.J. (1997). Enhanced performance of spatial and visual recognition memory tasks by the selective acetylcholinesterase inhibitor E2020 in rhesus monkeys. *Psychopharmacology Berlin* **131**, 406-410.
- Galli, A., Mori, F., Benini, L. & Cacciarelli, N. (1994). Acetylcholinesterase protection and the anti-diisopropylfluorophosphate efficacy of E2020. *Eur. J. Pharmacol.* **270**, 189-193.

20. Thomsen, T. & Kewitz, H. (1990). Selective inhibition of human acetylcholinesterase by galanthamine *in vitro* and *in vivo*. *Life Sci.* **46**, 1553-1558.
21. Loewenstein, Y., Gnatt, A., Neville, L.F. & Soreq, H. (1993). Chimeric human cholinesterase. Identification of interaction sites responsible for recognition of acetyl- or butyrylcholinesterase-specific ligands. *J. Mol. Biol.* **234**, 289-296.
22. Sugimoto, H., Imura, Y., Yamanishi, Y. & Yamatsu, K. (1995). Synthesis and structure-activity-relationships of acetylcholinesterase inhibitors - 1-Benzyl-4-[(5,6-dimethoxy-1-oxoindan-2-yl)methyl]piperidine hydrochloride and related compounds. *J. Med. Chem.* **38**, 4821-4829.
23. Cheng, D.H., Ren, H. & Tang, X.C. (1996). Huperzine A, a novel promising acetylcholinesterase inhibitor. *Neuroreport* **8**, 97-101.
24. Villalobos, A., et al., & Frost White, W. (1995). 5,7-dihydro-3-[2-[1-(phenylmethyl)-4-piperidinyl]ethyl]-6H-pyrrolo[3,2-f]-1,2-benzisoxazol-6-one: a potent and centrally-selective inhibitor of acetylcholinesterase with an improved margin of safety. *J. Med. Chem.* **38**, 2802-2808.
25. Pang, Y.P. & Kozikowski, A.P. (1994). Prediction of the binding site of 1-benzyl-4-[(5,6-dimethoxy-1-indanon-2-yl)methyl]piperidine in acetylcholinesterase by docking studies with the SYSDOC program. *J. Comput. Aided Mol. Des.* **8**, 683-693.
26. Harel, M., et al., & Silman, I. (1992). Conversion of acetylcholinesterase to butyrylcholinesterase: modeling and mutagenesis. *Proc. Natl Acad. Sci. USA* **89**, 10827-10831.
27. Schumacher, M., et al., & Taylor, P. (1986). Primary structure of *Torpedo californica* acetylcholinesterase deduced from its cDNA sequence. *Nature* **319**, 407-409.
28. Harel, M., et al., & Sussman, J.L. (1993). Quaternary ligand binding to aromatic residues in the active-site gorge of acetylcholinesterase. *Proc. Natl Acad. Sci. USA* **90**, 9031-9035.
29. Harel, M., Quinn, D.M., Nair, H.K., Silman, I. & Sussman, J.L. (1996). The X-ray structure of a transition state analog complex reveals the molecular origins of the catalytic power and substrate specificity of acetylcholinesterase. *J. Am. Chem. Soc.* **118**, 2340-2346.
30. Levitt, M. & Perutz, M.F. (1988). Aromatic rings act as hydrogen bond acceptors. *J. Mol. Biol.* **201**, 751-754.
31. Burley, S.K. & Petsko, G.A. (1986). Amino-aromatic interactions in proteins. *FEBS Lett.* **203**, 139-143.
32. Inoue, A., Kawai, T., Wakita, M., Imura, Y., Sugimoto, H. & Kawakami, Y. (1996). The simulated binding of (+/-)-2,3-dihydro-5,6-dimethoxy-2-[(1-(phenylmethyl)-4-piperidinyl)methyl]-1H-inden-1-one hydrochloride (E2020) and related inhibitors to free and acylated acetylcholinesterases and corresponding structure-activity analyses. *J. Med. Chem.* **39**, 4460-4470.
33. Verdonk, M.L., Boks, G.J., Kooijman, H., Kanters, J.A. & Kroon, J. (1993). Stereochemistry of charged nitrogen-aromatic interactions and its involvement in ligand-receptor binding. *J. Comput. Aided Mol. Des.* **7**, 173-182.
34. Dougherty, D. (1996). Cation- π interactions in chemistry and biology: A new view of benzene, Phe, Tyr, and Trp. *Science* **271**, 163-168.
35. Biosym (1993). *InsightII*. Biosym Technologies San Diego.
36. Raves, M.L., Harel, M., Pang, Y.P., Silman, I., Kozikowski, A.P. & Sussman, J.L. (1997). Structure of acetylcholinesterase complexed with the nootropic alkaloid, (-)-huperzine A. *Nat. Struct. Biol.* **4**, 57-63.
37. Shafferman, A., et al., & Ariel, N. (1992). Substrate inhibition of acetylcholinesterase: residues affecting signal transduction from the surface to the catalytic center. *EMBO J.* **11**, 3561-3568.
38. Ordentlich, A., et al., & Shafferman, A. (1993). Dissection of the human acetylcholinesterase active center determinants of substrate specificity. Identification of residues constituting the anionic site, the hydrophobic site, and the acyl pocket. *J. Biol. Chem.* **268**, 17083-17095.
39. Radic, Z., Pickering, N.A., Vellom, D.C., Camp, S. & Taylor, P. (1993). Three distinct domains in the cholinesterase molecule confer selectivity for acetyl- and butyrylcholinesterase inhibitors. *Biochemistry* **32**, 12074-12084.
40. Antosiewicz, J., Wlodek, S.T. & McCammon, J.A. (1996). Acetylcholinesterase: role of the enzyme's charge distribution in steering charged ligands toward the active site. *Biopolymers* **39**, 85-94.
41. Zhou, H.X., Wlodek, S.T. & McCammon, J.A. (1998). Conformation gating as a mechanism for enzyme specificity. *Proc. Natl Acad. Sci. USA* **95**, 9280-9283.
42. Shah, R.R. (1993). Clinical pharmacokinetics: current requirements and future perspectives from a regulatory point of view. *Xenobiotica* **23**, 1159-1193.
43. Nation, R.L. (1989). Enantioselective drug analysis: problems and resolutions. *Clin. Exp. Pharmacol. Physiol.* **16**, 471-477.
44. Barnard, E.A. (1974). Neuromuscular transmission - enzymatic destruction of acetylcholine. In *The Peripheral Nervous System*. (Hubbard, J.I., ed.), pp. 201-224, Plenum, NY.
45. Baron, P., Harel, M., Millard, C., Enz, A., Sussman, J.L. & Silman, I. (1998). Kinetic and X-ray crystallographic studies of the binding of ENA-713 to *Torpedo californica* acetylcholinesterase (TcAChE). In *Structure and Function of Cholinesterases and Related Proteins*. (Doctor, B.P., Quinn, D.M., Rotundo, R.L. & Taylor, P., eds), pp. 373-374, Plenum, NY.
46. Bourne, Y., Taylor, P., Kanter, J.R., Bougis, P.E. & Marchot, P. (1998). Crystal structure of mouse acetylcholinesterase. In *Structure and Function of Cholinesterases and Related Proteins*. (Doctor, B.P., Quinn, D.M., Rotundo, R.L. & Taylor, P., eds), pp. 315-322, Plenum, NY.
47. Kryger, G., et al., & Sussman, J.L. (1998). 3D structure of a complex of human recombinant acetylcholinesterase with fasciculin-II at 2.7 Å resolution. In *Structure and Function of Cholinesterases and Related Proteins*. (Doctor, B.P., Quinn, D.M., Rotundo, R.L. & Taylor, P., eds), pp. 323-326, Plenum, NY.
48. Greenblatt, H., et al., & Sussman, J.L. (1998). Crystal structures of complexes of E2020 related compounds with *Torpedo* acetylcholinesterase. In *Structure and Function of Cholinesterases and Related Proteins*. (Doctor, B.P., Quinn, D.M., Rotundo, R.L. & Taylor, P., eds), p. 371, Plenum, NY.
49. Kryger, G., et al., & Harel, M. (1998). Structural studies on human and insect acetylcholinesterase. *Abstract from the Sixth International Meeting on Cholinesterases*, La Jolla, CA, p. 14.
50. Hope, H. (1988). Cryocrystallography of biological macromolecules: a generally applicable method. *Acta Crystallogr. B* **44**, 22-26.
51. Ravelli, R.B.G., Sweet, R.M., Skinner, J.M., Duisenberg, A.J.M. & Kroon, J. (1997). STRATEGY: a program to optimize the starting spindle angle and scan range for X-ray data collection. *J. Appl. Crystallogr.* **30**, 551-554.
52. Otwinowski, Z. (1993). Oscillation data reduction program. In *Proceedings of the CCP4 Study Weekend: Data Collection and Processing*. (Sawyer, L., Isaacs, N. & Bailey, S., eds), pp. 56-62, SERC, Daresbury.
53. Brünger, A.T., Kuriyan, J. & Karplus, M. (1987). Crystallographic R factor refinement by molecular dynamics. *Science* **235**, 458-460.
54. Jones, T.A., Zou, J.Y., Cowan, S.W. & Kjeldgaard, M. (1991). Improved methods for the building of protein models in electron density maps and the location of errors in these models. In *Crystallographic Computing*. (Moras, D., Podany, A.D. & Thierry, J.C., eds), pp. 413-432, Oxford Univ. Press, Oxford.
55. Kleywegt, G.J. & Jones, T.A. (1996). Efficient rebuilding of protein structures. *Acta Crystallogr. D* **52**, 829-832.
56. Laskowski, R.A., MacArthur, M.W., Moss, D. & Thornton, J.M. (1993). PROCHECK: a program to check the stereochemical quality of protein structures. *J. Appl. Crystallogr.* **26**, 283-291.
57. Vriend, G. (1990). WHAT IF: a molecular modelling and drug design program. *J. Mol. Graph.* **8**, 52-56.
58. Laskowski, R.A. (1995). SURFNET: a program for visualizing molecular surfaces, cavities and intermolecular interactions. *J. Mol. Graph.* **13**, 323-330.



ELSEVIER

Chemico-Biological Interactions 119–120 (1999) 43–52

Chemico-Biological
Interactions

A preliminary comparison of structural models for catalytic intermediates of acetylcholinesterase

Israel Silman ^{a,*}, Charles B. Millard ^{a,b}, Arie Ordentlich ^c,
Harry M. Greenblatt ^d, Michal Harel ^d, Dov Barak ^c,
Avigdor Shafferman ^c, Joel L. Sussman ^{d,e}

^a Department of Neurobiology, Weizmann Institute of Science, Rehovot 76100, Israel

^b US Army Medical Research Institute of Chemical Defense, Aberdeen Proving Ground,
MD 21010, USA

^c Israel Institute for Biological Research, Ness Ziona 70450, Israel

^d Department of Structural Biology, Weizmann Institute of Science, Rehovot 76100, Israel

^e Biology Department, Brookhaven National Laboratory, Upton, NY 11973, USA

Abstract

Determination of the three dimensional structure of *Torpedo Californica* acetylcholinesterase (TcAChE) provided an experimental tool for directly visualizing interaction of AChE with cholinesterase inhibitors of fundamental, pharmacological and toxicological interest. The structure revealed that the active site is located near the bottom of a deep and narrow gorge lined with 14 conserved aromatic amino acids. The structure of a complex of TcAChE with the powerful 'transition state analog' inhibitor, TMTFA, suggested that its orientation in the experimentally determined structure was very similar to that proposed for the natural substrate, acetylcholine, by manual docking. The array of enzyme-ligand interactions visualized in the TMTFA complex also are expected to envelope the unstable TI that forms with acetylcholine during acylation, and to sequester it from solvent. In our most recent studies, the crystal structures of several 'aged' conjugates

Abbreviations: ACh, acetylcholine; AChE, acetylcholinesterase (EC 3.1.1.7); BChE, butyrylcholinesterase (EC 3.1.1.8); DFP, diisopropylphosphorofluoridate; MeP-AChE, methylphosphonylated AChE; MES, (2-[N-morpholino]ethanesulfonic acid); MiPrP-, monoisopropylphosphoryl; OP, organophosphorus; PEG, polyethylene glycol; Tc, *Torpedo californica*; TI, tetrahedral intermediate; TMTFA, *m*-(N,N,N-trimethylammonio)-2,2,2-trifluoroacetophenone.

* Corresponding author. Tel.: + 972-8-934-2128/3649; fax: + 972-8-947-1849.

E-mail address: bnsilm@weizmann.ac.il (I. Silman)

of *TcAChE* obtained with OP nerve agents have been solved and compared with that of the native enzyme. The methylphosphonylated-enzyme obtained by reaction with soman provides a useful structural analog for the TI that forms during deacylation after the reaction of *TcAChE* with acetylcholine. By comparing these structures, we conclude that the same 'oxanion hole' residues, as well as the aromatic side chains constituting the 'acyl pocket', participate in acylation (TMTFA-AChE) and deacylation (OP-AChE), and that AChE can accommodate both TIs at the bottom of the gorge without major conformational movements. © 1999 Elsevier Science Ireland Ltd. All rights reserved.

Keywords: Soman; Trifluoroketones; Tetrahedral intermediate; X-ray crystallography

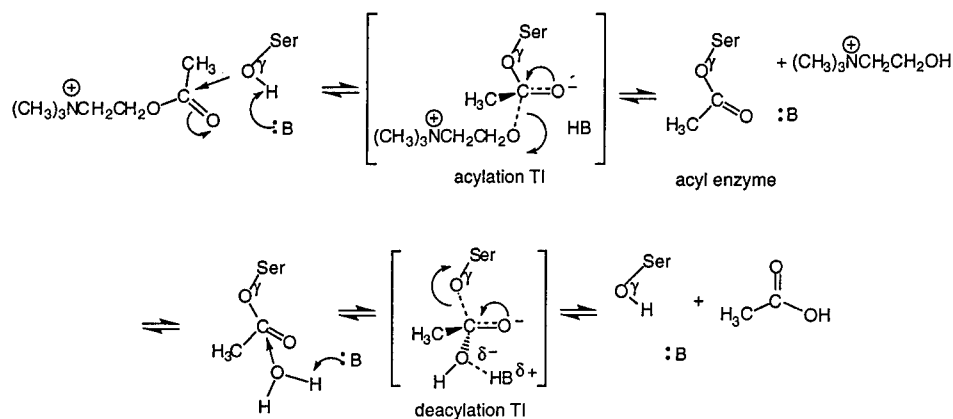
1. Introduction

The three-dimensional structure of acetylcholinesterase (EC 3.1.1.7) from *Torpedo californica* (*TcAChE*) [1], together with kinetic, spectroscopic and site-directed mutagenesis studies, has permitted tentative identification of the amino acid residues that interact with the natural substrate, ACh, during catalysis (reviewed in [2]). The AChE active site presently is believed to possess an oxanion hole, an acyl binding pocket, and a choline binding site (formerly called the 'anionic site'). Direct demonstration of these subsites with natural substrates has not yet been achieved because of the inherent instability of the Michaelis complex and the acyl-enzyme. To circumvent this limitation, we are studying the three-dimensional structures of stable enzyme-inhibitor complexes as structural models for intermediates in carboxyl ester hydrolysis.

The reaction of ACh and other carboxyl esters with AChE is believed to proceed through an unstable TI, or through a transition state resembling such a structure, before collapsing to a short-lived ($t_{1/2} \sim 50 \mu\text{s}$) acyl-enzyme [3] (Scheme 1). In the reverse reaction, the acyl-enzyme undergoes nucleophilic attack and proceeds through a second TI or transition state structure, and the regenerated enzyme is expelled as the leaving group (Scheme 1, lower panel).

The trifluoroketone compound, TMTFA (Fig. 1), is a potent inhibitor of AChE (apparent $K_i = 15 \text{ fM}$) which forms a covalent complex with the enzyme, that structurally mimics the theoretical acylation TI [4–6]. The TMTFA-AChE complex, with a trimethylammonium group in the choline binding subsite of the enzyme, is a good analog for the acylation TI of ACh (Scheme 1, upper panel). However, this structure does not address alterations that may occur in the acyl-enzyme, or in the formation of the deacylation TI.

O-pinacolylmethylphosphonofluoridate (soman; Fig. 1) is an OP nerve agent that reacts as a facile 'hemisubstrate' of AChE, mobilizing as much as 70% of the enzyme's natural catalytic power during inhibition [7]. OPs react with AChE to produce a covalent intermediate but, unlike the fleeting acyl-enzyme formed during carboxyl ester hydrolysis, the phosphoenzyme persists for many hours or days (reviewed in [8]). After phosphorylation, soman undergoes a rapid dealkylation reaction, called 'aging', to form a monoester anion adduct with the enzyme that is



Scheme 1. Reaction of AChE with ACh. The scheme begins with the reversible enzyme–substrate complex and ends with free enzyme. The top panel shows acylation and the lower panel shows deacylation. The enzyme's catalytic general base, probably Ne2 of His440, is depicted as :B, and the first product is choline. Hypothetical tetrahedral intermediates are indicated by brackets. Note that the TMTFA complex is expected to resemble the acylation TI (top panel), and the aged OP–AChE conjugate is expected to resemble the deacylation TI (bottom panel).

indefinitely stable [9]. The aged methyl phosphonylated (MeP)-*TcAChE* complex formed after reaction with soman is expected to share multiple structural features with the unstable ACh deacylation TI [10,11].

In this report, we compare the structure of the TMTFA–*TcAChE* complex [6] with that of MeP–*TcAChE*, obtained by reaction with soman [12], with the goal of identifying common topographical features of the theoretical acylation and deacylation TIs formed between ACh and AChE.

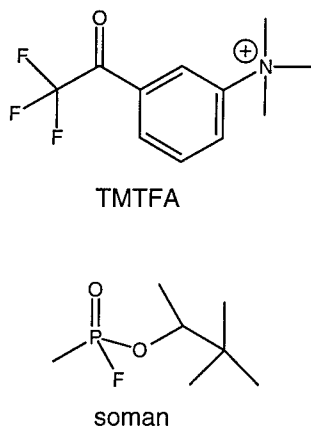


Fig. 1. Chemical structures of soman and TMTFA.

2. Materials and methods

2.1. Determination of MeP-AChE structure

TcAChE was purified from electric organ, essentially as described [13], and the pure enzyme was inhibited with a 2100-fold molar excess of soman. The OP-AChE conjugate was allowed to undergo complete aging in solution. Aging was judged to be greater than 95% complete because no reactivation was observed after incubation in 10 mM pyridine-2-aldoxime methiodide (2-PAM) or 1,1'-trimethylene-bis(4-formylpyridinium bromide) dioxime (TMB-4) for 20 h. Unbound OP was separated from the enzyme by gel filtration, and aged OP-AChE was crystallized using the hanging drop method, with PEG-200 as precipitant in 0.15 M MES buffer, pH 5.8–6.0, 4°C.

The exterior mother liquor which surrounds the crystals during their growth was exchanged with oil to remove water, and the crystals subsequently were flash cooled in liquid nitrogen [14]. Diffraction data were collected at 100 K using a Rigaku Raxis-II camera on a Rigaku rotating anode FR300 generator 'in-house' at the Weizmann Institute (Rehovot, Israel). X-ray diffraction data collection parameters were optimized using the computer program STRATEGY [15], and intensity data were processed with DENZO and SCALEPACK [16]. The OP structure was refined using difference Fourier methods.

2.2. Structure comparison

The coordinates of the TMTFA-TcAChE complex (1ACH) were obtained from the Brookhaven Protein Data Bank. Final refined structures were evaluated and compared using the programs PROCHECK [17] and WHAT-IF [18]. Comparisons of the main chain atom positions for each residue with those of native AChE were performed to identify significant movements using the software PROFIT (SciTech Software, University College, London, UK). Hydrogen positions were calculated and figures generated using the program InsightII v.97.0 (Biosym Technologies, San Diego, CA).

3. Results and discussion

Reaction with soman resulted in an MeP-AChE structure that was refined at 2.2 Å resolution (Fig. 2). The highest positive difference density peak, corresponding to the OP, was observed to be within covalent bonding distance of the O γ of Ser200. As expected, the large molar excess of OP resulted in almost exclusive reaction of AChE with the more toxic, P(S) stereoisomers [19]. No significant change was observed in the positions of the active site triad residues of the MeP-AChE structure compared with those of native AChE or of the TMTFA-AChE complex (Table 1).

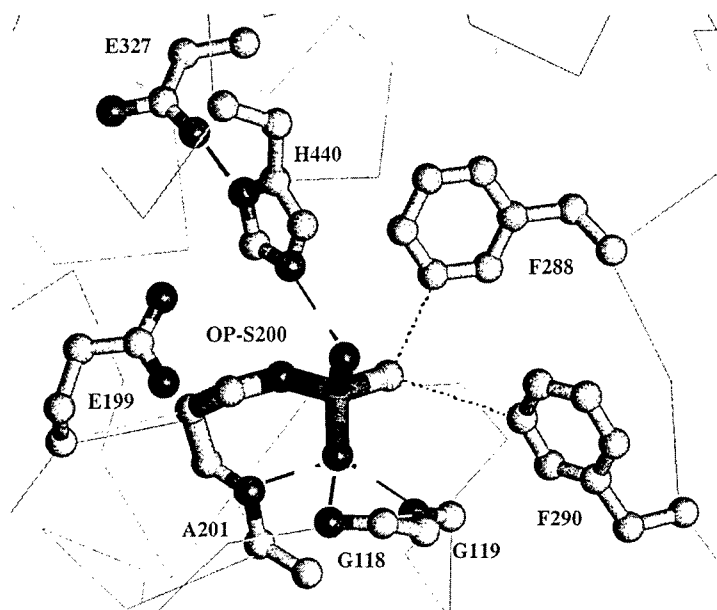


Fig. 2. Three-dimensional structure of the active site of MeP-AChE determined by X-ray crystallography. The conjugate was obtained by reaction of *Tc*AChE with soman. Note the proximity of four possible hydrogen bond donors (dashed lines) to the anionic phosphonyl oxygen atoms: backbone amide nitrogens of A201, G118, and G119, as well as N ϵ 2 of H440. The OP methyl carbon is within non-bonded contact distances (dotted lines) of F288 and F290 in the acyl pocket. For reference, the C α -traces of native- and OP-enzyme are overlaid.

A favorable electrostatic interaction between N ϵ 2 of the active-site imidazolium and one of the oxygen atoms of the anionic OP conjugate was postulated to be a key force in stabilizing aged mono*isopropyl*phosphoryl (MiPrP)-trypsin [11,20], as well as MiPrP-chymotrypsin [21]. The distance from the N ϵ 2 of His440 to the anionic oxygen in the MeP-AChE structure also is consistent with a favorable interaction [12]. The geometry is consistent with either a coulombic salt bridge or a strong hydrogen bond (Fig. 2).

Table 1
Active site distances in *Tc*AChE structures (Å)

Atom 1	Atom 2	Native AChE	TMTFA complex	MeP-AChE (soman)
S200 O γ	H440 N ϵ 2	2.7	2.7	3.2
H440 N δ 1	E327 O ϵ 1	2.5	2.7	2.4
H440 N δ 1	E327 O ϵ 2	4.4	4.4	4.4
Oxyanion ^a	G119 N	—	2.9	2.4
Oxyanion ^a	G118 N	—	2.9	2.8
Oxyanion ^a	A201 N	—	3.2	3.0

^a Refers to the carbonyl oxygen of TMTFA [6], or the phosphonyl oxygen of soman.

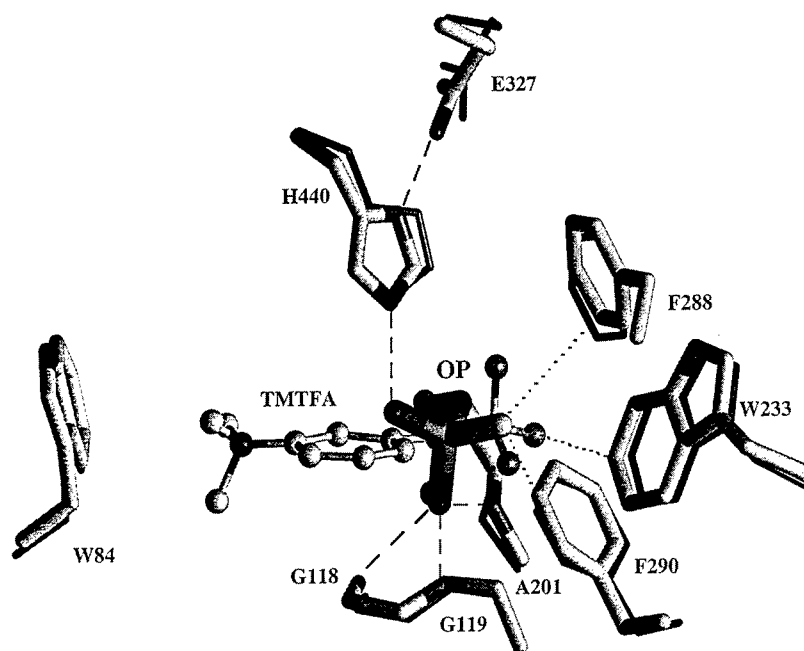


Fig. 3. Comparison of the active sites of MeP-*TcAChE* (soman) and TMTFA-*TcAChE*. The MeP-AChE residues are shown as thick lines, TMTFA-AChE residues are shown as thin dark lines, and TMTFA is shown as a ball-and-stick model. Note that the tetrahedral geometries allow for close superpositioning of the oxyanion hole oxygen atoms (dashed lines indicate potential H-bonds), as well as of the methyl and CF_3 groups in the acyl pocket (dotted lines indicate potential non-bonded contacts).

The phosphonyl oxygen atoms carry significantly greater fractional negative charges than do the oxygens of the ACh deacylation TI [11,22]. Despite this limitation, the active site of MeP-AChE is expected to provide a useful structural analog for modeling steric interactions of the ACh deacylation TI [11,23].

The position of the phosphonyl oxygen should mimic that of the TI carbonyl oxygen. The AChE oxyanion hole has been described as 'three-pronged' [6,24,25] because it has three potential hydrogen bond donors. The MeP-AChE structure corroborates that the oxyanion is stabilized in the deacylation TI by potential hydrogen bonds from the amide nitrogens of G118, G119 and A201 (Fig. 2 and Table 1). This is consistent with preliminary modeling of ACh bound to native *TcAChE* [1], as well as with the structure of TMTFA-*TcAChE* [6]. The carbonyl and phosphonyl oxygen atoms in the oxyanion hole are almost superposable for the TMTFA- and MeP-AChE structures (Fig. 3), as expected from the common tetrahedral geometry in both the acylation and deacylation TI structures. We note that the amide nitrogen atom (donor) of A201 is consistently farther away from the oxygen atom (acceptor) than are those of G118 or G119 (Table 1).

3.1. Acyl pocket

A hydrophobic pocket which surrounds the phosphonate methyl group in the MeP-AChE structure is formed by W233, F288 and F290. The phenyl rings of F288 and F290 provide close non-bonded contacts to the methyl group of soman (Fig. 2 and Table 2). Contacts from the acyl pocket to the phosphonate methyl group are generally closer than are those observed for the CF₃ carbon atom of TMTFA (Table 2). Site-directed mutagenesis studies, along with the TMTFA structure, have emphasized the role of F288 and F290 in determining the specificity of the acyl pocket for different substrates [6,24,26].

Although F288 and F290 have an established role in determining acyl pocket specificity, that of W233 is less clear. Several lines of evidence point to a functional role for W233: (1) both W233 and the adjacent proline (P232) are conserved in all known AChE and BChE sequences; (2) distances from the geometric center of the indole ring to the carbon atom of the CF₃ moiety of TMTFA, as well as to the methyl group of the OP-AChE structure, suggest that W233 is positioned to provide close hydrophobic contacts in the substrate TI (Table 2); and (3) replacement of W233 in human BChE by alanine results in a 30-fold decrease in k_{cat} , with little effect on K_{m} [28]. We also note that the positions of F288 and F290 are flexible and change significantly upon binding of a bulky inhibitor, diisopropylphosphorofluoridate (DFP), whereas W233 does not move [12].

It has been proposed that F331 also participates directly in the acyl pocket [6]. The distance of F331 to the methyl group is, however, appreciably greater than are those of F288, F290 or W233 (Table 2). An alternative possibility is that F331 plays a cooperative role in the acyl pocket structure by providing stabilizing π - π -interactions with the key aromatic side chain at F288. This hypothesis could be tested by appropriate double mutant thermodynamic cycles [27,29,30].

Table 2
Acyl pocket distances in TcAChE structures (Å)

From carbon ^a to:	TMTFA complex	MeP-AChE (soman)
F288 ^b	5.1	4.8
F290 ^b	5.6	4.7
W233 ^b	4.8	4.4
F331 ^b	5.6	5.4
G119C α	4.3	3.8

^a Straight line distances from the carbon atom of the phosphonate methyl group, or the carbon atom of the CF₃ group of TMTFA [6].

^b Distances shown are to the geometric center of the phenyl or benzopyrrole rings of the indicated side chain.

3.2. No conformational movement upon binding TI analogs

In the OP–AChE structure, the overall fold of the protein is very similar to that of the native enzyme or the TMTFA–AChE complex, suggesting that *Tc*AChE accommodates the TI for both the acylation and the deacylation reactions at the bottom of the active site gorge without major conformational movements. In contrast, several related serine lipases with extensive secondary structure homology to AChE [31] undergo a major conformational movement of a ‘lid’ region in the protein structure upon reaction with OP transition state analogs [32,33].

Although there is evidence for conformational changes associated with aging of some OP–AChE, –BChE, and –chymotrypsin conjugates in solution [34–36], we found no major structural rearrangements in *Tc*AChE as a result of the aging reaction itself. The rms deviation found by comparing the C α atoms of the MeP–AChE structure with native AChE was less than 0.3 Å. Moreover, superposing the active site residues of MeP–AChE upon those of native *Tc*AChE (Table 1), as well as of 13 other previously solved *Tc*AChE structures, showed no significant movements that could be attributed to aging. It remains possible, however, that a transient conformational change occurred on the pathway to the final aged structure observed by X-ray crystallography. This possibility may be addressed by ongoing X-ray crystallographic studies of OP–AChE complexes that are not aged.

Acknowledgements

This work was supported by the US Army Medical Research & Materiel Command under Agreements No. DAMD17-97-2-7022 and DAMD17-96-C-6088 and the US Army Scientist/Engineer Exchange Program. The opinions or assertions contained herein belong to the authors and are not necessarily the official views of the US Army or the US Department of Defense.

References

- [1] J.L. Sussman, M. Harel, F. Frolow, C. Oefner, A. Goldman, L. Toker, I. Silman, Atomic structure of acetylcholinesterase from *Torpedo californica*: a prototypic acetylcholine-binding protein, *Science* 253 (1991) 872–879.
- [2] P. Taylor, Z. Radic, The cholinesterases: from genes to proteins, *Annu. Rev. Pharmacol. Toxicol.* 34 (1994) 281–320.
- [3] H.C. Froede, I.B. Wilson, Direct determination of acetyl-enzyme intermediate in the acetylcholinesterase-catalyzed hydrolysis of acetylcholine and acetylthiocholine, *J. Biol. Chem.* 259 (1984) 11010–11013.
- [4] U. Brodbeck, K. Schweikert, R. Gentinetta, M. Rottenberg, Fluorinated aldehydes and ketones acting as quasi-substrate inhibitors of acetylcholinesterase, *Biochim. Biophys. Acta* 567 (1979) 357–369.
- [5] H.K. Nair, J. Seravalli, T. Arbuckle, D.M. Quinn, Molecular recognition in acetylcholinesterase catalysis: free-energy correlations for substrate turnover and inhibition by trifluoroketone transition-state analogs, *Biochemistry* 33 (1994) 8566–8576.

- [6] M. Harel, D.M. Quinn, H.K. Nair, I. Silman, J.L. Sussman, The X-ray structure of a transition state analog complex reveals the molecular origins of the catalytic power and substrate specificity of acetylcholinesterase, *J. Am. Chem. Soc.* 118 (1996) 2340–2346.
- [7] I.M. Kovach, J.H.-A. Huber, R.L. Schowen, Catalytic recruitment in the inactivation of acetylcholinesterase by soman: temperature dependence of the solvent isotope effect, *J. Am. Chem. Soc.* 110 (1988) 590–593.
- [8] W.N. Aldridge, E. Reiner, *Enzyme Inhibitors as Substrates: Interactions of Esterases with Esters of Organophosphorus and Carbamic Acids*, vol. 26, North-Holland, Amsterdam, 1972.
- [9] F. Berends, C.H. Posthumus, I.V.D. Sluys, F.A. Deierkauf, The chemical basis of the “ageing process” of DFP-inhibited pseudocholinesterase, *Biochim. Biophys. Acta* 34 (1959) 576–578.
- [10] Y. Ashani, B.S. Green, Are the organophosphorous inhibitors of acetylcholinesterase transition-state analogs?, in: B.S. Green, Y. Ashani, D. Chipman (Eds.), *Chemical Approaches to Understanding Enzyme Catalysis: Biomimetic Chemistry and Transition*, Elsevier, Amsterdam, 1981, pp. 169–188.
- [11] A.A. Kossiakoff, S.A. Spencer, Direct determination of the protonation states of aspartic acid-102 and histidine-57 in the tetrahedral intermediate of the serine proteases: neutron structure of trypsin, *Biochemistry* 20 (1981) 6462–6474.
- [12] C.B. Millard, G. Kryger, A. Ordentlich, M. Harel, M.L. Raves, H.M. Greenblatt, Y. Segall, D. Barak, A. Shafferman, I. Silman, J.L. Sussman, Crystal structures of “aged” phosphorylated and phosphonylated *Torpedo californica* acetylcholinesterase, in: B.P. Doctor, D.M. Quinn, R.L. Rotundo, P. Taylor (Eds.), *Structure and Function of Cholinesterases and Related Proteins*, Plenum Press, New York, (1998) pp. 425–431.
- [13] A.H. Futerman, M.G. Low, I. Silman, A hydrophobic dimer of acetylcholinesterase from *Torpedo californica* is solubilized by phosphatidylinositol-specific phospholipase-C, *Neurosci. Lett.* 40 (1983) 85–89.
- [14] H. Hope, Cryocrystallography of biological macromolecules: a generally applicable method, *Acta Crystallogr. (Sect. B)* 44 (1988) 22–26.
- [15] R.B.G. Ravelli, R.M. Sweet, J.M. Skinner, A.J.M. Duisenberg, J. Kroon, STRATEGY: a program to optimize the starting spindle angle and scan range for X-ray data collection, *J. Appl. Cryst.* 30 (1997) 551–554.
- [16] Z. Otwinowski, Oscillation data reduction program, in: L. Sawyer, N. Isaacs, S. Bailey (Eds.), *Data Collection and Processing, Proceedings of the CCP4 Study Weekend of 29–30 January*, SERC, Daresbury, 1993.
- [17] R.A. Laskowski, M.W. MacArthur, D. Moss, J.M. Thornton, PROCHECK: a program to check the stereochemical quality of protein structures, *J. Appl. Cryst.* 26 (1993) 283–291.
- [18] G. Vriend, WHAT IF: a molecular modeling and drug design program, *J. Mol. Graphics* 8 (1990) 52–56.
- [19] H.P. Benschop, L.P.A. deJong, Nerve agent stereoisomers: analysis, isolation, and toxicology, *Acc. Chem. Res.* 21 (1988) 368–374.
- [20] R.M. Stroud, L.M. Kay, R.E. Dickerson, The structure of bovine trypsin: electron density maps of the inhibited enzyme at 5 Å and 2.7 Å resolution, *J. Mol. Biol.* 83 (1974) 185–208.
- [21] M. Harel, C.T. Su, F. Frolow, Y. Ashani, I. Silman, J.L. Sussman, The refined crystal structures of ‘aged’ and ‘non-aged’ organophosphoryl conjugates of γ -chymotrypsin, *J. Mol. Biol.* 221 (1991) 909–918.
- [22] A. Bencsura, I. Enyedy, I.M. Kovach, Origins and diversity of the aging reaction in phosphonate adducts of serine hydrolase enzymes: what characteristics of the active site do they probe?, *Biochemistry* 34 (1995) 8989–8999.
- [23] J. Kraut, Serine proteases: structure and mechanism of catalysis, *Ann. Rev. Biochem.* 46 (1977) 331–358.
- [24] A. Ordentlich, D. Barak, C. Kronman, Y. Flashner, M. Leitner, Y. Segall, N. Ariel, S. Cohen, B. Velan, A. Shafferman, Dissection of the human acetylcholinesterase active center determinants of substrate specificity. Identification of residues constituting the anionic site, the hydrophobic site, and the acyl pocket, *J. Biol. Chem.* 268 (1993) 17083–17095.

- [25] T. Selwood, S.R. Feaster, M.J. States, A.N. Pryor, D.M. Quinn, Parallel mechanisms in acetylcholinesterase-catalyzed hydrolysis of choline esters, *J. Am. Chem. Soc.* 115 (1993) 10477–10482.
- [26] Z. Radic, N.A. Pickering, D.C. Vellom, S. Camp, P. Taylor, Three distinct domains in the cholinesterase molecule confer selectivity for acetyl- and butyrylcholinesterase inhibitors, *Biochemistry* 32 (1993) 12074–12084.
- [27] C.B. Millard, L. Lockridge, C.A. Broomfield, Organophosphorus acid anhydride hydrolase activity in human butyrylcholinesterase: synergy results in a somanase, *Biochemistry* 37 (1998) 237–247.
- [28] P. Masson, P. Legrand, C.F. Bartels, M.-T. Froment, L.M. Schopfer, O. Lockridge, Role of aspartate 70 and tryptophan 82 in binding of succinylthiocholine to human butyrylcholinesterase, *Biochemistry* 36 (1997) 2266–2277.
- [29] G.K. Ackers, F.R. Smith, Effects of site-specific amino acid modification on protein interactions and biological function, *Ann. Rev. Biochem.* 54 (1985) 597–629.
- [30] A. Horovitz, Measures of cooperativity in the binding of ligands to proteins and their relation to non-additivity in protein–protein interactions, *Proc. Royal. Soc. Lond. B* 229 (1986) 315–329.
- [31] D.L. Ollis, E. Cheah, M. Cygler, B. Dijkstra, F. Frolow, S.M. Franken, M. Harel, S.J. Remington, I. Silman, J. Schrag, J.L. Sussman, K.V.G. Verschueren, A. Goldman, The α/β hydrolase fold, *Protein Eng.* 5 (1992) 197–211.
- [32] A.M. Brzozowski, U. Derewenda, Z.S. Derewenda, G.G. Dodson, D.M. Lawson, J.P. Turkenburg, F. Bjorkling, B. Huge-Jensen, S.A. Patkar, L. Thim, A model for interfacial activation in lipases from the structure of a fungal lipase-inhibitor complex, *Nature* 351 (1991) 491–494.
- [33] U. Derewenda, A.M. Brzozowski, D.M. Lawson, Z.S. Derewenda, Catalysis at the interface: the anatomy of a conformational change in a triglyceride lipase, *Biochemistry* 31 (1992) 1532–1541.
- [34] G. Amitai, Y. Ashani, A. Gafni, I. Silman, Novel pyrene containing organophosphates as fluorescent probes for studying aging-induced conformational changes in organophosphate-inhibited acetylcholinesterase, *Biochemistry* 21 (1982) 2060–2069.
- [35] D. Aslanian, P. Grof, F. Renault, P. Masson, Raman spectroscopic study of conjugates of butyrylcholinesterase with organophosphates, *Biochim. Biophys. Acta* 1249 (1995) 37–44.
- [36] N. Steinberg, A.C.M. van der Drift, J. Grunwald, Y. Segall, E. Shirin, E. Haas, Y. Ashani, I. Silman, Conformational differences between aged and non-aged pyrenbutyl-containing organophosphoryl conjugates of chymotrypsin as detected by optical spectroscopy, *Biochemistry* 28 (1989) 1248–1253.

Three-dimensional structure of a complex of E2020 with acetylcholinesterase from *Torpedo californica*

Gitay Kryger^a, Israel Silman^b, Joel L. Sussman^{a, c}

Departments of ^aStructural Biology and ^bNeurobiology, Weizmann Institute of Science, Rehovoth 76100, Israel
^cBiology Department, Brookhaven National Laboratory, Upton, NY 11973, USA

Abstract — The 3D structure of a complex of the anti-Alzheimer drug, E2020, also known as Aricept[®], with *Torpedo californica* acetylcholinesterase is reported. The X-ray structure, at 2.5 Å resolution, shows that the elongated E2020 molecule spans the entire length of the active-site gorge of the enzyme. It thus interacts with both the 'anionic' subsite, at the bottom of the gorge, and with the peripheral anionic site, near its entrance, via aromatic stacking interactions with conserved aromatic residues. It does not interact directly with either the catalytic triad or with the 'oxyanion hole'. Although E2020 is a chiral molecule, and both the S and R enantiomers have similar affinity for the enzyme, only the R enantiomer is bound within the active-site gorge when the racemate is soaked into the crystal. The selectivity of E2020 for acetylcholinesterase, relative to butyrylcholinesterase, can be ascribed primarily to its interactions with Trp279 and Phe330, which are absent in the latter. (©Elsevier, Paris)

Résumé — Structure d'un complexe de E2020 avec l'acétylcholinestérase de *Torpedo californica*. La structure 3D d'un complexe formé par une drogue anti-Alzheimer E2020 aussi connue sous le nom de Aricept[®] avec l'acétylcholinestérase de *Torpedo californica* est décrite. La structure aux rayons X, à la résolution de 2.5 Å, montre que la molécule allongée E2020 s'étire sur l'entière longueur de la gorge catalytique de l'enzyme. Elle interagit donc à la fois avec le sous-site anionique, au fond de la gorge et avec le site périphérique anionique, près de l'entrée par les interactions avec les résidus conservés aromatiques empilés. (©Elsevier, Paris)

Alzheimer's disease / drug design / peripheral site

1. Introduction

Acetylcholinesterase (AChE) terminates synaptic transmission at cholinergic synapses by rapid hydrolysis of acetylcholine (ACh) [15]. Anticholinesterase agents are used in the treatment of various disorders [21], and have been proposed as therapeutic agents for the management of Alzheimer's disease [7]. Two such anticholinesterase agents, both of which act as reversible inhibitors of AChE, have been licensed by the FDA: tacrine (1,2,3,4-tetrahydroacridine) [6], under the trade name Cognex[®], and, more recently, E2020 ((R,S)-1-benzyl-4-[5,6-dimethoxy-1-indanon-2-yl]methylpiperidine) [18], under the trade name Aricept[®]. Tacrine and E2020 share the same target, but, whereas tacrine must be administered up to four times a day, and displays hepatotoxic side effects, E2020 may be administered once daily, and has fewer side effects. Furthermore, E2020 displays very high selectivity, ~1000-fold, for AChE relative to butyrylcholinesterase (BChE), whereas THA has similar affinity for the two enzymes. This may be important, since it has been suggested that inhibition of human plasma BChE may cause potentiating side effects [23].

The active site of AChE contains a catalytic subsite, and a so-called 'anionic' subsite, which binds the quaternary group of ACh [15]. A second, 'pe-

ripheral', anionic site is so named since it is distant from the active site [22]. Bisquaternary inhibitors of AChE derive their enhanced potency, relative to homologous monoquaternary ligands [13], from their ability to span these two 'anionic' sites, which are ca. 14 Å apart.

The 3D structure of *Torpedo californica* (Tc) AChE [20] reveals that the active site is located at the bottom of a deep and narrow cavity; named the 'aromatic gorge', since > 50% of its lining is composed of the rings of 14 conserved amino acids [1, 20]. The peripheral site is located at the entrance to the gorge [8].

X-ray crystallographic studies of complexes of AChE with drugs of pharmacological interest can reveal which amino acid residues are important for binding the drug, and where space might exist for modifying the drug itself, information crucial for structure-based drug design. In the following, we describe the crystallographic structure, at 2.5 Å resolution, of a complex of E2020 with TcAChE.

2. Materials and methods

2.1. Protein preparation and crystallization

TcAChE was purified and crystallized as described previously [16]. E2020, as the hydrochloride salt of the pure racemate, was a generous gift from Dr. B.P. Doctor (Division of

Biochemistry, Walter Reed Army Institute of Research, Washington, DC, USA). *TcAChE* crystals were soaked in ~10 mM (R,S)E2020 for 5 days at 4 °C, and flash cooled to 100°K.

2.2. X-ray data collection and processing

Data were collected 'inhouse', at the Weizmann Institute of Science, on a Rigaku FR300 generator set at 50 mA, 50 kV and 1.54184 Å wavelength (Cu K radiation), equipped with a R-AXI-SII detector.

2.3. Model refinement and analysis

The structure was refined on the basis of the starting model of native *TcAChE* (PDB ID 2ACE), using only the polypeptide and none of the solvent atoms, employing XPLOR [2]. Voids were calculated between the inhibitor molecule as one entity, and the protein and solvent molecules as a second entity [12].

3. Results and discussion

The 3D structure of the complex shows more detail of the *AChE* structure than the starting native model (2ACE). Primarily, residues 2 and 3, at the N-terminus, and the 484–490 loop, which were not seen in the original model, can be discerned. In addition, it was possible to model the proximal Nacetyl glucosamine (NAG) moiety at four out of five putative glycosylation sites, viz. at residues Asn59, Asn416 (where two NAG moieties could be fitted), Asn457 and Asn533.

3.1. All three segments of E2020 interact with *AChE*

E2020 binds along the active site gorge. All three major segments of the elongated molecule make specific interactions with the enzyme, and each of these interactions involves discrete watermediated contacts which appear crucial for specificity (*figure 1*). E2020 makes principal interactions with the enzyme through: 1) the benzyl moiety; 2) the piperidine nitrogen; and 3) the dimethoxyindanone moiety. It utilizes the conserved aromatic residues which line the gorge for hydrophobic and stacking interactions, and does not make direct contact with the protein through H-bonds or salt-bridges other than via water molecules.

3.2. Interactions at the bottom of the gorge

Near the bottom of the gorge, one face of the benzyl ring stacks against the six-membered ring of the indole moiety of Trp84, similarly to THA [8]. On the opposite face, it makes a classic aromatic hydrogen bond with a water molecule (WAT1160). This water is held firmly by a hydrogen bond to another water molecule (WAT1161), in the 'oxyanion hole',

and to WAT1159. WAT1161 is another example of a tightly bound water molecule; it hydrogen bonds to residues in the 'oxyanion hole' and to S200O. E2020 does not interact directly either with the catalytic triad or with the 'oxyanion hole'.

3.3. Interactions in the middle of the gorge

In the constricted region, halfway up the gorge, the charged nitrogen of the piperidine ring makes a cation- π interaction [5] with the phenyl ring of Phe330. The ring nitrogen also makes an in-line H-bond with WAT1159. The principal binding site for the quaternary nitrogen of ACh within the active site, and for homologous ligands, is the indole ring of Trp84 [9]. These data suggest that Phe330 may serve as an additional quaternary binding site, of possible functional significance, midway down the gorge, between the peripheral binding site and the anionic subsite of the active site.

3.4. Interactions at the entrance to the gorge

At the top of the gorge, the indanone ring stacks against the 6-membered ring of the indole moiety of Trp279, in the peripheral binding site, in a classic parallel π - π interaction. The fact that the binding of E2020 is strongly dependent on interaction with Trp279 and Phe330, which are absent in BChE, may explain its high relative specificity for *AChE* versus BChE. The carbonyl function on the indanone is not in direct contact with the protein, but appears to make a water-bridged contact with F288N.

3.5. Only one enantiomer of E2020 is bound to *AChE*

The reported pharmacological studies on E2020 emphasize that both enantiomers are active, and exhibit similar, but not identical, binding affinities for *AChE* [11, 19]. Since we used the racemate in our crystallographic study, we expected either to find evidence, in the form of electron density, for the presence of both enantiomers in the crystal structure, or partial disorder which would support the presence of both. Yet, when we attempted to fit a number of plausible inhibitor conformations within the active-site gorge, a unique fit to the experimental electron density was found for one conformation of the R form, which is very similar to our energetically minimized E2020 conformation, with the indanone carbonyl group pointing towards F288N as mentioned above. Thus, *TcAChE* appears to have bound the R form selectively, despite the similarity in binding constants. Selective binding cannot be due to a limitation in the amount of the S form, since the racemate was soaked into the crystal at 10 mM, i.e.,

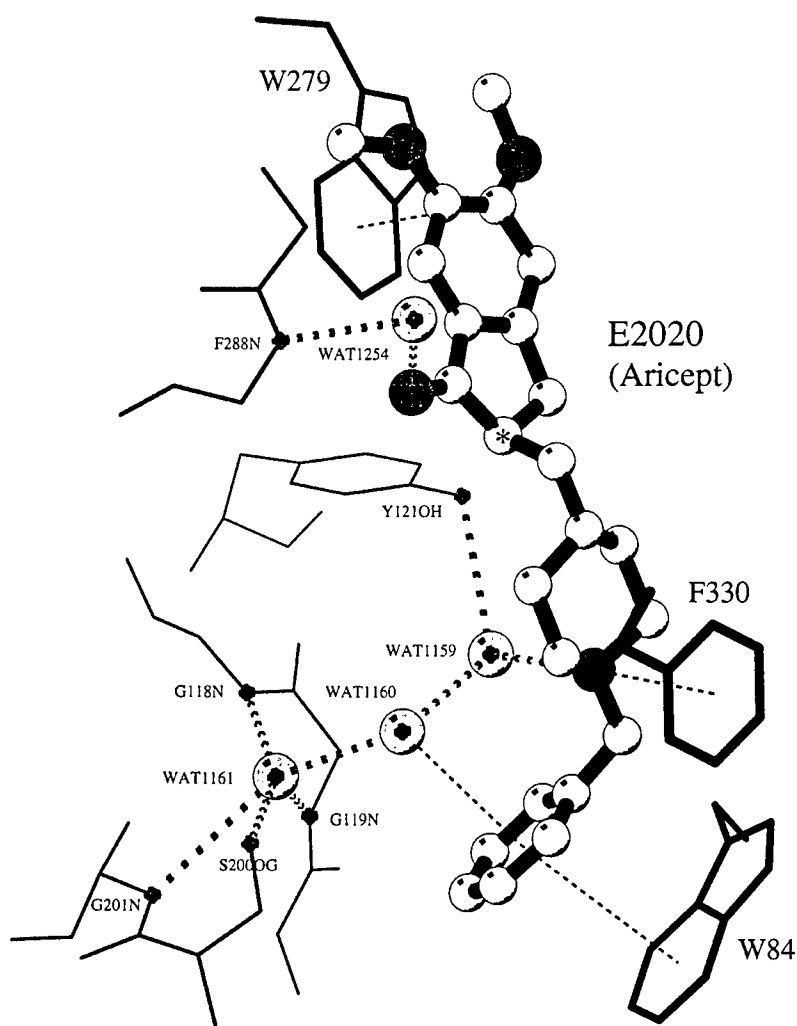


Figure 1. Binding modes of E2020 to TcAChE. E2020 are displayed as a ball-and-stick model (chiral center marked with black star); direct binding residues are represented as dark grey sticks; water-mediated binding residues as light grey sticks; water molecules as light grey balls; 'standard' H-bonds as heavy dashed lines; aromatic H-bonds, -cation and -stacking as light dashed lines.

at a great molar excess. Although the two of E2020 interconvert readily in aqueous solution, via a ketoenol intermediate [14], it is not immediately obvious what could cause such a preferential binding of one form, taking into account their similar affinities. It should, however, be borne in mind that not only are the ligand and active site chiral, but also the entire lattice of the crystalline enzyme. Such a chiral environment might cause the stereoisomers to tautomerize at different rates. Based on steric considerations, it appears that both the R and S enantiomers could bind in very similar conformations, with only the position of the carbonyl function on the 5-membered ring of the indanone moiety distinguishing between them. A model which we built displaying a carbonyl on the other side of the indanone,

representing the S form, does not make contact with any protein atom, and thus might be bound less tightly than the observed R form, even though this is inconsistent with the published inhibition data [11]. Furthermore, the 4.0 Å link between the indanone carbonyl and F288N, whether bridged by a water molecule or not, combined with the fact that the carbonyl 'nests' amongst three aromatic systems of residues Phe288, Phe290 and Phe331, might be sufficient to introduce a bias in favor of preferential binding of the R form. As already mentioned, R-S interconversion, via tautomerization, is known to occur, and might indeed take place under the experimental conditions employed. Thus, one explanation for the inhibitory potency of the S form would invoke AChE-induced S-to-R tautomerization.

3.6. Possible effect on amyloid deposition

Recently, evidence was presented that AChE may contribute to the generation of amyloid proteins and/or physically affect the process of fibril assembly which results in the formation of the senile plaques characteristic of AD [10]. The acceleration in fibril assembly produced by AChE could be retarded by the peripheral site inhibitor, propidium, and it was suggested that a hydrophobic environment close to the peripheral binding site might be involved in this process [17]. This raises the possibility that E2020, which our data clearly show as stacking against Trp279, might also moderate the rate of fibril formation. Many of the compounds synthesized and tested by the Eisai company involved modification of this segment of the molecule [3, 4]. It should be noted, however, that the screening which they performed involved assessment of affinity for AChE, together with selectivity for AChE relative to BChE, not a possible effect on amyloid fibril assembly or deposition.

Acknowledgments

This research was supported by the European Union, by the U.S. Army Medical Research and Materiel Command, under Contract No. DAMD17-97-2-7022, and by the Kimmelman Center for Biomolecular Structure and Assembly. The generous support of Tania Friedman is gratefully acknowledged. I.S. is Bernstein-Mason Professor of Neurochemistry.

References

- [1] Axelsen P.H., Harel M., Silman I., Sussman J.L., Structure and dynamics of the active site gorge of acetylcholinesterase: synergistic use of molecular dynamics simulation and X-ray crystallography, *Prot. Sci.* 3 (1994) 188–197.
- [2] Brünger A.T., Kuriyan J., Karplus M., Crystallographic R factor refinement by molecular dynamics, *Science* 235 (1987) 458–460.
- [3] Cardozo M.G., Iimura Y., Sugimoto H., Yamanishi Y., Hopfinger A.J., QSAR analyses of the substituted indanone and benzylpiperidine rings of a series of indanone benzylpiperidine inhibitors of acetylcholinesterase, *J. Med. Chem.* 35 (1992) 584–589.
- [4] Cardozo M.G., Kawai T., Imura Y., Sugimoto H., Yamanishi Y., Hopfinger A.J., Conformational-analyses and molecular-shape comparisons of a series of indanone benzylpiperidine inhibitors of acetylcholinesterase, *J. Med. Chem.* 35 (1992) 590–601.
- [5] Dougherty D., Cation- π interaction in chemistry and biology: a new view of benzene, Phe, Tyr, and Trp, *Science* 271 (1996) 163–1684.
- [6] Gauthier S., Gauthier L., in: Giacobini E., Becker R. (Eds.), *Cholinergic Basis for Alzheimer Therapy*, Birkhäuser, Boston, 1991, pp. 224–230.
- [7] Giacobini E., Becker R., *Alzheimer Disease: Therapeutic Strategies* Birkhäuser, Boston, 1994.
- [8] Harel M., Schalk I., Ehret-Sabatier L., Bouet F., Goeldner M., Hirth C., Axelsen P., Silman I., Sussman J.L., The X-ray structure of a transition state analog complex reveals the molecular origins of the catalytic power and substrate specificity of acetylcholinesterase, *Proc. Natl. Acad. Sci. USA* 90 (1993) 9031–9035.
- [9] Harel M., Quinn D.M., Nair H.K., Silman I., Sussman J.L., Quaternary ligand binding to aromatic residues in the active-site gorge of acetylcholinesterase, *J. Am. Chem. Soc.* 118 (1996) 2340–2346.
- [10] Inestrosa N.C., Alvarez A., Perez C.A., Moreno R.D., Vicente M., Linker C., Casanueva O.I., Soto C., Garrido J., Acetylcholinesterase accelerates assembly of amyloid-beta-peptides into Alzheimer's fibrils: possible role of the peripheral site of the enzyme, *Neuron* 16 (1996) 881–91.
- [11] Inoue A., Kawai T., Wakita M., Iimura Y., Sugimoto H., Kawakami Y., The simulated binding of (+/-)-2,3-dihydro-5,6-dimethoxy-2-((L-phenylmethyl)-4-piperidinyl)methyl)-1H-inden-1-one hydrochloride (E2020) and related inhibitors to free and acetylated acetylcholinesterase and corresponding structure-activity analyses, *J. Med. Chem.* 39 (1996) 4460–4470.
- [12] Laskowski R.A., SURFNET: a program for visualizing molecular surfaces, cavities and intermolecular interactions, *J. Mol. Graph.* 13 (1995) 323–330.
- [13] Main A.R., in: Goldberg A.M., Hanin I. (Eds.), *Biology of Cholinergic Function*, Raven, New York, 1976, pp. 269–353.
- [14] Matsui K., Oda Y., Ohe H., Tanaka S., Asakawa N., Direct determination of 2020 enantiomers in plasma by liquid chromatography-mass spectrometry and column-switching techniques, *J. Chromatogr. A* 694 (1995) 209–218.
- [15] Quinn D.M., *Chem. Rev.* 87 (1987) 955–975.
- [16] Raves M.L., Harel M., Pang Y.-P., Silman I., Kozikowski A.P., Sussman J.L., Structure of acetylcholinesterase complexed with the nootropic alkaloid, (-)-huperzine A, *Nature Struct. Biol.* 4 (1996) 57–63.
- [17] Reyes A.E., Perez D.R., Alvarez A., Garrido J., Gentry M.K., Doctor B.P., Inestrosa N.C., A monoclonal antibody against acetylcholinesterase inhibits the formation of amyloid fibrils induced by the enzyme, *Biochem. Biophys. Res. Commun.* 232 (1997) 652–655.
- [18] Sugimoto H., Tsuchiya Y., Sugumi H., Higurashi K., Karibe N., Imura Y., Sasaki A., Araki S., Yamanishi Y., Yamatsu K., Synthesis and antiacetylcholinesterase activity of 1-benzyl-4-((5,6-dimethoxy-1-indanon-2-yl)methyl)piperidine hydrochloride (E2020) and related-compounds, *J. Med. Chem.* 35 (1992) 4542–4548.
- [19] Sugimoto H., Iimura Y., Yamanishi Y., Yamatsu K., Synthesis and structure-activity-relationships of acetylcholinesterase inhibitors - 1-benzyl-4-(2-phthalimidoethyl)piperidine and related derivatives, *Bioorg. Med. Chem. Lett.* 2 (1992) 871–876.
- [20] Sussman J.L., Harel M., Frolow F., Oefner C., Goldman A., Tokar L., Silman I., Atomic structure of acetylcholinesterase from *Torpedo californica*: a prototypic acetylcholine-binding protein, *Science* 253 (1991) 872–879.
- [21] Taylor P., in: Gilman A.G., Nies A.S., Rall T.W., Taylor P. (Eds.), *The Pharmacological Basis of Therapeutics*, Macmillan, New York, 5th edn., 1990, pp. 131–150.
- [22] Taylor P., Lappi S., Interaction of fluorescence probes with acetylcholinesterase. The site and specificity of propidium binding, *Biochemistry* 14 (1975) 1989–1997.
- [23] Thomsen T., Kewitz H., Selective inhibition of human acetylcholinesterase by galanthamine in vitro and in vivo, *Life Sci.* 46 (1990) 1553–1558.

Electrotactins: a class of adhesion proteins with conserved electrostatic and structural motifs

Simone A. Botti^{1,2}, Clifford E. Felder², Joel L. Sussman^{2,3,4} and Israel Silman¹

Departments of ¹Neurobiology and of ²Structural Biology, Weizmann Institute of Science, 76100 Rehovot, Israel and ³Biology Department, Brookhaven National Laboratory, Upton NY 11973, USA

⁴To whom correspondence should be addressed

The concept of an electrostatic motif on the surface of biological macromolecules as a definite topographical pattern of electrostatic potentials in three-dimensional space, provides a powerful tool for identification of functionally important regions on the surface of structurally related macromolecules. Using this approach, we identify a functional region common to cholinesterases (ChEs) and to a set of neural cell-adhesion proteins that have been suggested to be structurally related to cholinesterases due to their high sequence similarity, but lacking the key catalytically active serine. Quantitative analysis of the electrostatic surface potential in the area surrounding the entrance to the active site of acetylcholinesterase, and in the analogous zone for the ChE-like domain of the adhesion proteins reveals very good correlation. These findings, examined in the context of previous evidence involving this same region in a possible cell-recognition function for ChEs, leads us to define a class of adhesion proteins which we have named 'electrotactins'.

Keywords: acetylcholinesterase/cell adhesion/electrostatics/nervous system/homology modelling

The concept of an electrostatic motif on the surface of biological macromolecules as a definite topographical pattern of electrostatic potentials in three-dimensional space (3D), provides a powerful tool for identification of functionally important regions on the surface of structurally related macromolecules (Honig and Nicholls, 1995). This pattern can only be defined in the context of molecules of similar 3D structure, for only in such a case is it possible to unambiguously orient the motif with respect to zones of the related macromolecules which might be functionally significant. We use this approach to localize a functional region common to cholinesterases (ChEs), a family of enzymes of the nervous system, and to a set of neural cell-adhesion proteins, which includes gliotactin (GLI), neurotactin (NRT) and neuroligin (NL), that have been suggested to be structurally related to ChEs due to their high sequence similarity (Krejci *et al.*, 1991), but lack the catalytically active serine. This enables us to identify structural properties involved in possible cell-adhesion functions of ChEs.

Cholinesterases are a family of enzymes which fall broadly into two types, acetylcholinesterase (AChE) and butyrylcholinesterase (BChE). They are distinguished primarily by their substrate specificity: AChE hydrolyzes acetylcholine (ACh) faster than other choline esters and is much less active on butyrylcholine, whereas BChE displays similar activity towards the two substrates (Mendel and Rudney, 1943;

Chatonnet and Lockridge, 1989). Although the main physiological function of AChE is believed to be termination of impulse transmission at cholinergic synapses by rapid hydrolysis of ACh, the function of BChE is still unknown. The 3D structure of AChE has been solved (Sussman *et al.*, 1991), and the high degree of identity among AChE and BChE sequences has permitted construction of homology models of the 3D structures of BChE (Harel *et al.*, 1992) and of AChE from different species. Inspection of these structures has shown that the active site of the ChEs is located at the bottom of a deep and narrow gorge. Examination of the 3D structure of *Torpedo californica* AChE (TcAChE) showed the enzyme to be characterized by a marked asymmetric spatial distribution of charged residues, that were shown to roughly segregate into a 'northern' negative hemisphere (taking the mouth of the gorge as the north pole) and a 'southern' positive one (Ripoll *et al.*, 1993). This electrostatic pattern was shown to give rise to a large dipole moment which was calculated to be ~1600 Debye and roughly oriented along the axis of the active-site gorge (Ripoll *et al.*, 1993; Tan *et al.*, 1993; Antosiewicz *et al.*, 1994). Electro-optical measures performed on AChE from *Bungarus fasciatus* gave a value of ~1000 Debye, thus confirming experimentally the order of magnitude of the macrodipole (Porschke *et al.*, 1996).

The asymmetric distribution of surface potentials was thought to be essential for the fast catalysis effected by ChEs. This assumption has been reevaluated in the light of site-directed mutagenesis experiments on human AChE (hAChE) in which up to seven charged residues in the vicinity of the entrance to the active-site gorge were neutralized. The ensuing drastic reduction of the asymmetric distribution of surface potentials did not have a major effect on catalysis (Shafferman *et al.*, 1994). Brownian dynamics simulations of bimolecular rate association constants for ACh and AChE also failed to show a meaningful correlation between the distribution of electrostatic surface potentials and catalysis (Antosiewicz *et al.*, 1996). A further analysis of the electrostatic properties of the 3D structures and homology models of ChEs, aimed at generating a detailed and quantitative topographical map of the electrostatic surface potentials, identified the presence of an 'annular' electrostatic motif of negative surface potential around the entrance of the active site gorge (Felder *et al.*, 1998). The role of surface potentials in catalysis is not clear-cut. It has been shown to play only a minor role in the case of isozymes of trypsin differing by as much as 12.5 charge units. The catalytic efficiency of these isozymes was shown to be influenced not by electrostatic surface potentials, but by a few charged amino acids localized close to the active site. (Soman *et al.*, 1989). These considerations drove us to investigate whether the role of surface potentials in ChE might be related to roles other than catalysis.

ChEs possess a 3D fold different from those of 'classical' serine-hydrolases, such as chymotrypsin or subtilisin. This fold is called the α/β hydrolase fold (Ollis *et al.*, 1992)

and has been shown to characterize a family of hydrolytic enzymes of widely different phylogenetic origin and substrate specificity. Some of these enzymes, like the fungal triacylglycerol lipases from *Geotrichum candidum* and *Candida rugosa* (Cygler et al., 1993), show substantial sequence similarity with ChEs. Other members of the family, like haloalkane halogenase from *Xenobacter autotrophicus* and diene lactone hydrolase from *Pseudomonas* sp., do not show significant sequence similarity to the ChEs; but inspection of their 3D structures shows that their polypeptide chain has the structural core typical of the α/β hydrolase fold (Ollis et al., 1992). A systematic search of sequence databases has retrieved a large number of proteins with a high degree of sequence similarity to α/β hydrolases (Krejci et al., 1991). Inspection of the sequences reveals that amongst an overwhelming majority of enzymes, there are also a few proteins involved in cell adhesion; these contain a ChE-like domain whose function is most probably independent of hydrolase activity since the active-site serine is mutated to a glycine. Amongst them are the three proteins which we chose to investigate, because of their presumed involvement in cell adhesion and signaling in the nervous system.

GLI is a transmembrane protein transiently expressed on peripheral glia of *Drosophila melanogaster* embryos and required for formation of the peripheral blood-nerve barrier (Auld et al., 1995). The C-terminal extracellular domain of this protein shows substantial sequence similarity with ChEs. Such similarity can also be found in the extracellular domain of NRT, a transmembrane glycoprotein which is expressed in neuronal and epithelial tissues during embryonic and larval stages (Barthalay et al., 1990; Hortsch et al., 1990). Sequence similarities suggest that neuroligins (NLs), a family of mammalian neuronal cell surface proteins that act as ligands for β -neurexins (Ichtchenko et al., 1995), also contain an extracellular ChE-like domain. NLs and neurexins mediate interactions between neurons and contribute to the specific organization of synapses. All these proteins are involved in heterophilic cell-cell interactions, suggesting that their ChE-like domains possess a recognition function that has been conserved from invertebrates to vertebrates. It is worth noticing that both GLI and NRT display substantially higher sequence similarity with *TcAChE* than with the *D.melanogaster* enzyme (*DmAChE*) (Table I) and that the targets of their adhesive functions have not yet been identified.

The sequence similarity between ChEs, NL, GLI and NRT prompted us to build homology models of their extracellular domains, both to confirm the presence of shared structural motifs and to investigate the possibility that they might display similar electrostatic characteristics. Our underlying assumption is that the ChE-like domains of these adhesion proteins are independently folded, and that neither their conformation nor their electrostatic properties will be greatly affected by the association with the non-ChE like regions of GLI, NL and NRT, which are mostly transmembrane and intracellular (Figure 1).

The homology models were built with the automated knowledge-based building tool Swiss-Model (Peitsch, 1995) and validated as described previously (Felder et al., 1998). The same modeling procedure was applied as a control to the neutral lipase from *G.candidum* (*GcLip*) (Schrage and Cygler, 1993) whose 3D structure is known, to check for the bias in modeling introduced by the templates. The modeling of *GcLip* gave a structure very close to the actual 3D structure solved by X-ray crystallography (α -carbon r.m.s. deviation ~ 1.1 Å

Table I. Percent sequence identity and similarity between electrotactins, lipases and ChEs as given by the BestFit algorithm from the GCG package (version 9, Genetics Computer Group, 575 Science Drive, Madison, WI 53711, USA)

Protein	Percent identity to <i>TcAChE</i> (<i>DmAChE</i>)	Percent similarity to <i>TcAChE</i> (<i>DmAChE</i>)
Cholinesterases		
<i>TcAChE</i>	100.0	100.0
hAChE	57.6	85.0
mAChE	59.0	85.3
<i>DmAChE</i>	36.3	65.8
7-hAChE	57.6	85.0
hBChE	52.4	83.1
Adhesion proteins		
NRT (<i>Dros.</i>)	31.1 (25.1)	57.7 (50.4)
GLI (<i>Dros.</i>)	30.6 (23.5)	61.0 (55.7)
NL (mouse)	32.3	60.1
Lipases		
<i>GcLip</i>	29.4	56.8
rBSSL	31.2	61.4
CrCE	31.9	56.8

The values are calculated with respect to the sequence of *TcAChE*.

from the 3D X-ray structure of *GcLip*). Since all the proteins involved in this study possess about the same degree of sequence identity as *GcLip* does with *TcAChE* (Table I), we can reasonably assume our models to be close approximations of the actual structures of these domains.

The electrostatic surface potentials of *TcAChE* (PDB entry 2ACE), GLI, NL and NRT were calculated solving the Poisson-Boltzmann equation by the finite difference method (FDPB) (Warwicker and Watson, 1982), using the DelPhi algorithm (Gilson and Honig, 1988) as implemented in the GRASP program (Nicholis et al., 1991). As a control, we checked the distribution of surface potentials for other members of the α/β hydrolase family to check whether the 'annular' electrostatic motif was a characteristic shared by most members of this family. We chose three enzymes with a sequence identity to ChEs similar to that of NL, NRT and GLI. The three enzymes selected were cholesterol esterase from *Candida rugosa* (Ghosh et al., 1995) (*CrCE*, PDB entry 1CLE), *GcLip* (PDB entry 1THG) and bile-salt-stimulated lipase from rat (rBSSL) (Kissel et al., 1989). In this last case the 3D structure is not yet available, and a homology model was built following the same procedure used for GLI, NRT and NL. We also calculated the surface potentials for wild-type human BChE (hBChE), for human AChE (hAChE) and for the mutant of hAChE in which seven negatively charged residues near the entrance of the gorge had been neutralized (7-hAChE). The structures of 7-hAChE, NL, NRT, GLI, *GcLip*, *CrCE* and rBSSL were superimposed on that of *TcAChE* by a least-squares fitting procedure implemented in the program LSQMAN (Kleywegt, 1996), and placed in a common orientation in which the axis of the active-site gorge of *TcAChE* (as defined by Antosiewicz et al., 1994) is aligned with the cartesian Z-axis.

Our most significant result is shown in Figure 2. It is immediately apparent that the electrostatic surface potential contours of *TcAChE*, GLI, NRT and NL are strikingly similar. All three proteins show a characteristic 'annular' electrostatic motif of negative potential around the zone homologous to the active-site gorge of the ChEs. In contrast, *GcLip*, rBSSL and

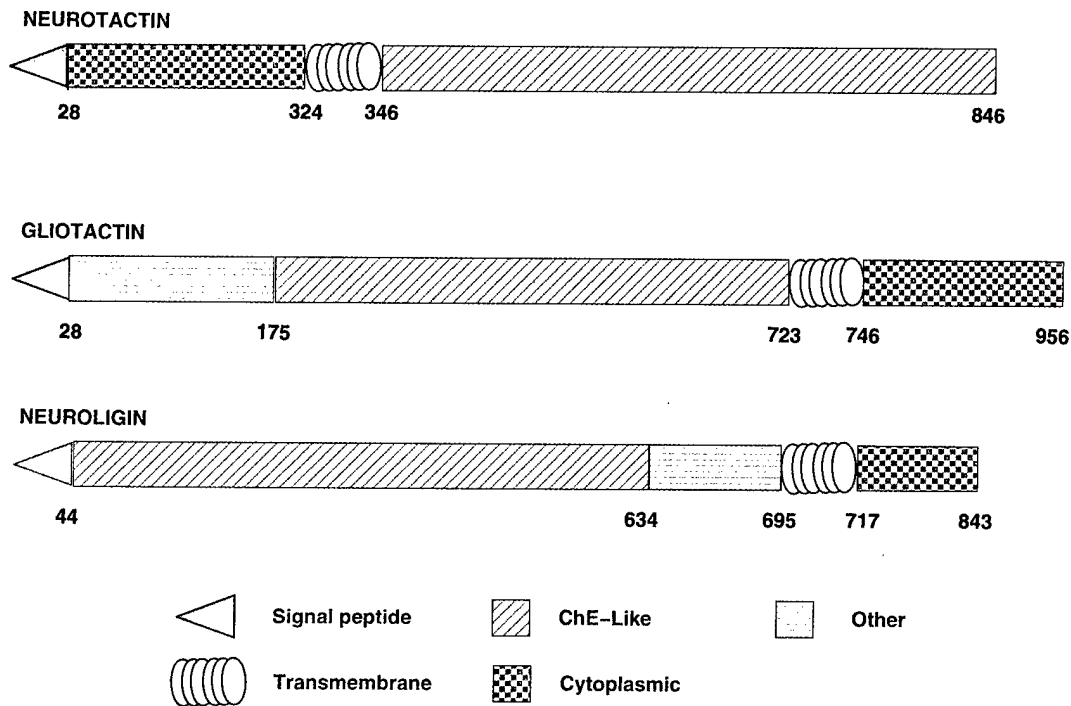


Fig. 1. Schematic representations of the domain organizations of GLI, NRT and NL.

CrCE appear to display a different topographical distribution of surface potentials (Figure 2a).

In the case of the 7-hAChE mutant, neutralization of seven negatively charged residues in the 'annular' region virtually erases the electrostatic motif, while not affecting the negative potential gradient within the active-site gorge. This distribution of electrostatic surface potentials is very similar to that of hBChE (Figure 2b). This finding correlates well with the contention that the potential gradient inside the active-site gorge makes a more important contribution to ChE catalysis than the surface potentials around the rim of the active-site gorge (Shafferman *et al.*, 1994; Zhou *et al.*, 1996).

In order to provide a quantitative measure of the electrostatic motif of the molecules studied, we calculated the average surface potential over a 20 Å wide region of accessible surface around the zone homologous to the entrance of the active site gorge of TcAChE (which constitutes the common Z axis). This region was divided into 1 Å wide concentric sections, and the average potentials in the sections were plotted and correlated by a linear regression fit with the results obtained for TcAChE (Table II and Figure 3). GLI, NRT and NL are all characterized by a high correlation coefficient and an average potential in the 'annular' region very similar to that of TcAChE; in addition, their potential gradient closely follows that of TcAChE. Of the three lipases, only CrCE shows a high correlation coefficient and an average potential similar to AChE, but its r.m.s. deviation from the ChE-like fold is the largest amongst all the proteins examined, and its potential gradient is substantially different from that of TcAChE. It is of interest that hBChE displays a lower average potential in the 'annular' region and a very poor correlation coefficient, in addition to a potential gradient similar to that of the lipases.

The biological significance of the electrostatic surface potential of ChEs has been the subject of speculations, and it has been proposed that it might have a non-catalytic function (Shafferman *et al.*, 1994). There is mounting evidence

that ChEs may be involved in functions distinct from their catalytic activity. During development of the nervous system of vertebrates, expression of ChEs is associated with periods of enhanced neurite outgrowth (Layer and Willbold, 1994; Layer *et al.*, 1993), suggesting that they might serve as neuronal growth factors or cell-adhesion molecules. It has been speculated that the site responsible for the non-catalytic interaction of ChEs is localized close to the entrance of the active-site gorge, perhaps overlapping with what has been termed the 'peripheral' anionic site (PAS) of AChE, a possible locus of regulation of enzymatic activity (Radic *et al.*, 1991; Eichler *et al.*, 1994; Barak *et al.*, 1995), which is located in the region of the 'annular' electrostatic motif. In a recent study, AChE was shown to promote neurite regeneration in cultured adult neurons of the mollusk *Aplysia* (Srivatsan and Peretz, 1997). The growth-promoting action of AChE was shown to be independent of its catalytic function. Inhibition of the active site did not influence the neurotrophic action of AChE, but occupancy of its PAS suppressed neurite regeneration (Srivatsan and Peretz, 1997). There is also evidence that the PAS of AChE can enhance the rate of formation of amyloid fibrils, a major component of the senile plaques found in the brains of Alzheimer patients (Inestrosa *et al.*, 1996). Strong evidence for a common recognition mechanism in cell-adhesion between ChEs, GLI and NLs comes from a recent study, in which chimeric constructs of the C-terminal transmembrane domain of NRT, fused to the extracellular cholinesterase-like domains of DmAChE or TcAChE, were shown to be endowed with the same heterophilic adhesion properties as wild type NRT (Darboux *et al.*, 1996).

Electrostatic complementarity between interacting proteins has been found to be one of the major driving forces for complex formation (McCoy *et al.*, 1997). Mutagenesis and electrostatic screening studies of the association rates between barnase, a ribonuclease, and barstar, its inhibitor, have shown the limiting step to be the formation of a binding transition

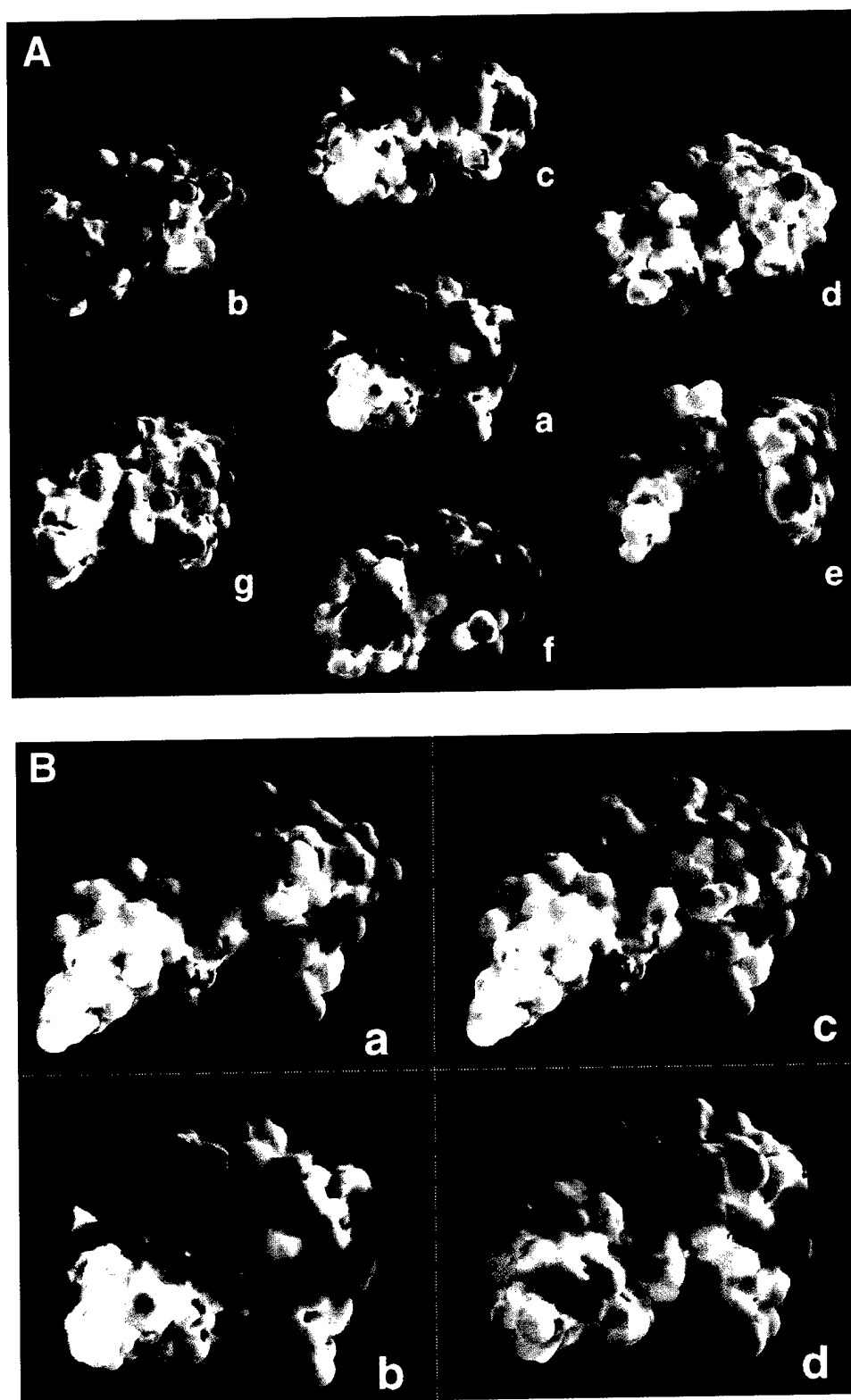


Fig. 2. (a) GRASP representations of the distribution of electrostatic surfaces potentials for (a) *TcAChE*; (b) *NRT*; (c) *NL*; (d) *GLI*; (e) *CrCE*; (f) *rBSSL*; (g) *GcLip*, showing the presence of the 'annular' electrostatic motif in the adhesion molecules and AChE. The values of surface potentials are expressed as a spectrum ranging from $+0.25kT/e$ (deep blue) through $0kT/e$ (white) to $-0.25kT/e$ (deep red). At a temperature of 298.15 K, $kT/e = 25.7$ mV. The surface potentials are calculated for a salt concentration of 0.145 M, with a cubic grid of linear dimensions of 65 Å, a protein dielectric constant of 4 and a solvent dielectric constant of 78. (b) GRASP representations of the distribution of electrostatic surface potentials for (a) *hAChE*; (b) *TcAChE*; (c) *7-hAChE* and (d) *hBChE*, showing the absence of the 'annular' motif in *hBChE* and its neutralization in the *7-hAChE* mutant. Calculation and color coding of surface potential values are the same as for Figure 2a.

Table II. R.m.s. structural deviation (\AA) of the C α atoms, average surface potentials (kt/e) and correlation coefficients for electrostatic surface potentials between electrotactins, lipases and ChEs

Protein	R.m.s. deviation (\AA) of C α atoms relative to TcAChE (percent of matched residues)	Average surface potentials (kt/e) in the 'annular' motif region	Correlation coefficients for surface potentials in concentric sections of the 'annular' motif region
Cholinesterases			
TcAChE	0.00 (100)	-2.272	1.00
hAChE	0.48 (97.9)	-1.139	0.89
mAChE	0.31 (97.1)	-1.409	0.80
DmAChE	0.77 (98.1)	-2.358	0.86
7-hAChE	0.48 (97.9)	-0.052	0.90
hBChE	0.42 (94.9)	-0.724	0.66
Adhesion proteins			
Nrt (<i>Dros.</i>)	1.19 (94.7)	-2.132	0.83
Gli (<i>Dros.</i>)	1.12 (86.5)	-1.194	0.94
NL-1 (mouse)	1.10 (84.6)	-1.332	0.89
Lipases			
GcLip	1.46 (64.4)	-0.551	-0.45
rBSSL	0.85 (93.0)	-0.020	0.59
CcLip	1.54 (71.5)	-1.571	0.89

The values are calculated with respect to the 3D structure and electrostatic properties of TcAChE.

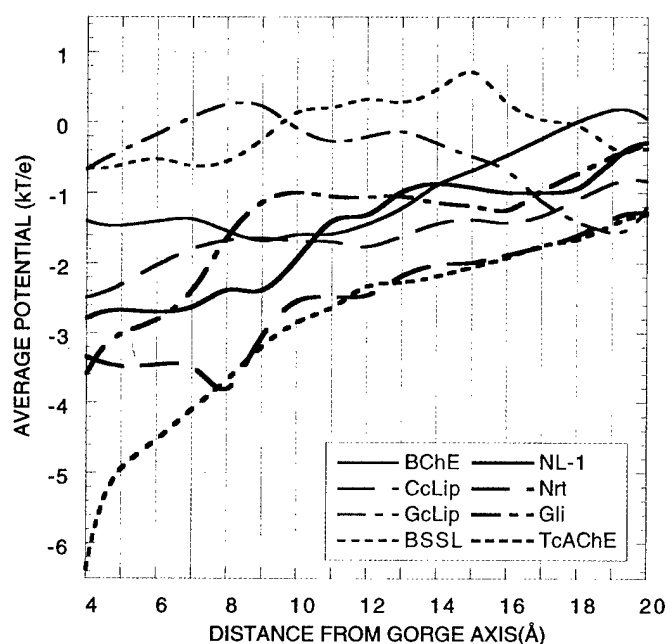


Fig. 3. Plots of average surface potentials measured in concentric sections of the 'annular' motif region for hBChE, CrCe, GcLip, BSSL, NL, NRT, GLI and TcAChE. The origin is placed on the axis of the active-site gorge of TcChE (Antosiewicz *et al.*, 1994) and the potential values are expressed in units of kt/e , where k is Boltzmann's constant, T the temperature in K and e the electronic charge. At a temperature of 298.15 K, $kt/e = 25.7$ mV.

state, in which the two proteins form a low-affinity non-specific complex held together by long-range electrostatic interactions (Schreiber and Fersht, 1996). We speculate that a possible mechanism effected by the 'annular' motif might be the facilitation of target recognition via low specificity associations mediated by long-range electrostatic interactions with a pool of ligands displaying a complementary motif, followed by a subsequent docking step with the unique functional ligand(s), to yield the final high affinity complex. Some support for our hypothesis comes from the mode of binding of AChE to one of its strongest inhibitors, fasciculin

II (FAS), a three-fingered polypeptide toxin from the venom of the green mamba (Karlsson *et al.*, 1984). These polypeptide snake venom toxins constitute a family of 6–8 kDa proteins, of which α -bungarotoxin, a potent antagonist for the nicotinic ACh receptor, is the best known member.

FAS has been shown to bind in a 'cork-and-bottle fashion' to the entrance of the active-site gorge of AChE which is situated in the negatively charged 'northern' hemisphere (Bourne *et al.*, 1995; Harel *et al.*, 1995). The surface complementarity between enzyme and inhibitor is very large; about 2000 \AA^2 of accessible surface are buried upon binding, including the region of the 'annular' motif. In addition to this large surface complementarity, the AChE–FAS complex displays significant electrostatic complementarity. Analysis of the topography of surface potentials of FAS shows that it also possesses a 'bipolar' motif, with a preponderance of positive surface which is absent in other three-fingered snake toxins. (Karlsson *et al.*, 1984). This positive surface characterizes the zone of interaction between FAS and AChE (Harel *et al.*, 1995).

Analysis of the sequence alignment of the proteins we investigated shows no sequence motif shared exclusively by AChE, GLI, NRT and NL. Thus the conjunction of the topographical distribution of surface potentials with the topological arrangement of the polypeptide chain seems the most important common structural factor conserved between these proteins. It is thus plausible that the shared electrostatic motif indicates a common recognition mechanism or even a common ligand. We hypothesize that a chimeric construct of the cytoplasmic domain of NRT with the mutant form of AChE, in which seven negative residues have been neutralized to abolish the electrostatic motif, will not display the same adhesive properties as a construct built with wild-type AChE. We further predict that constructs with hBChE and CrCE will not be able to promote heterogeneous cell adhesion, the former because it lacks the 'annular' motif, and the latter because of a large deviation from the common ChE-like fold.

The above considerations lead us to conclude that GLI, NRT, NLs and AChE are the first members of a class of adhesion proteins that, because of their common electrostatic and structural motif, we have named 'electrotactins'.

Acknowledgements

The authors wish to thank Gitay Kryger, Charles Millard and Mia Raves for valuable discussions, and Kurt Giles, Amnon Horowitz and Gideon Schreiber for their critical comments on the manuscript. This work was supported by the US Army Medical Research Acquisition activity under Contract no. 17-97-2-7022, the Kimmelman Center for Biomolecular Structure and Assembly, Rehovot, Israel, and the European Union. I.S. is Bernstein-Mason Professor of Neurochemistry. The generous support of Mrs Tania Friedman is gratefully acknowledged.

References

- Antosiewicz,J., Gilson,M.K. and McCammon,A. (1994) *Israel J. Chem.*, **34**, 151–158.
- Antosiewicz,J., Wlodek,S.T. and McCammon,J.A. (1996) *Biopolymers*, **39**, 85–94.
- Auld,V.J., Fetter,R.D., Broadie,K. and Goodman,C.S. (1995) *Cell*, **81**, 757–767.
- Barak,D. et al. (1995) *Biochemistry*, **34**, 15444–15452.
- Barthalay,Y., Hipeau-Jacquotte,R., de la Escalera,S., Jimenez,F. and Piovant,M. (1990) *EMBO J.*, **9**, 3603–3609.
- Bourne,Y., Taylor,P. and Marchot,P. (1995) *Cell*, **83**, 503–512.
- Chatonnet,A. and Lockridge,O. (1989) *Biochem. J.*, **260**, 625–634.
- Cygler,M., et al. (1993) *Protein Sci.*, **2**, 366–382.
- Darboux,I., Barthalay,Y., Piovant,M. and Hipeau-Jacquotte,R. (1996) *EMBO J.*, **15**, 4835–4843.
- Eichler,J., Anselment,A., Sussman,J.L., Massoulie,J. and Silman,I. (1994) *Mol. Pharmacol.*, **45**, 335–340.
- Felder,C.E., Botti,S.A., Lifson,S., Silman,I. and Sussman,J.L. (1997) *J. Mol. Graphics Mod.*, **15**, 318–327.
- Ghosh,D. et al. (1995) *Structure*, **3**, 279–288.
- Gilson,M.K. and Honig,B. (1988) *Proteins*, **4**, 7–18.
- Harel,M. et al. (1992) *Proc. Natl Acad. Sci. USA*, **89**, 10827–10831.
- Harel,M., Kleywegt,G.J., Ravelli,R.B.G., Silman,I. and Sussman,J.L. (1995) *Structure*, **3**, 1355–1366.
- Honig,B.H. and Nicholls,A. (1995) *Science*, **268**, 1144–1149.
- Hortsch,M., Patel,N.H., Bieber,A.J., Traquina,Z.R. and Goodman,C.S. (1990) *Development*, **110**, 1327–1340.
- Ichtchenko,K. et al. (1995) *Cell*, **81**, 435–443.
- Inestrosa,N.C. et al. (1996) *Neuron*, **16**, 881–891.
- Karlsson,E., Mbugua,P.M. and Rodriguez-Ithurralde,D. (1984) *J. Physiol. (Paris)*, **79**, 232–240.
- Kissel,J.A., Fontaine,R.N., Turck,C.W., Brockman,H.L. and Hui,D.Y. (1989) *Biochim. Biophys. Acta.*, **1006**, 227–236.
- Kleywegt,G.J. LSQMAN, version 960821/4.7.3. For the Department of Molecular Biology, University of Uppsala, Uppsala, Sweden, 1996.
- Krejci,E., Duval,N., Chatonnet,A., Vincens,P. and Massoulie,J. (1991) *Proc. Natl Acad. Sci. USA*, **88**, 6647–6651.
- Lager,P.G., Weikert,T. and Alber,R. (1993) *Cell Tissue Res.*, **273**, 219–226.
- Lager,P.G. and Willbold,E. (1994) *Int. Rev. Cytol.*, **151**, 139–181.
- McCoy,A.J., Epa,V.C. and Colman,P.M. (1997) *J. Mol. Biol.*, **268**, 570–584.
- Mendel,B. and Rudney,H. (1943) *Biochem. J.*, **37**, 59–63.
- Nicholls,A., Sharp,K. and Honig,B. (1991) *Proteins: Struct. Funct. Genet.*, **11**, 281–296.
- Ollis,D.L. et al. (1992) *Protein Engng*, **5**, 197–211.
- Pietsch,M.C. (1995) *BioTechnology*, **13**, 658–660.
- Porschke,D. et al. (1996) *Biophys. J.*, **70**, 1603–1608.
- Radic,Z., Reiner,E. and Taylor,P. (1991) *Mol. Pharmacol.*, **39**, 98–104.
- Ripoll,D.R., Faerman,C.H., Axelsen,P.H., Silman,I. and Sussman,J.L. (1993) *Proc. Natl Acad. Sci. USA*, **90**, 5128–5132.
- Schrag,J.D. and Cygler,M. (1993) *J. Mol. Biol.*, **230**, 575–591.
- Schreiber,G. and Fersht,A.R. (1996) *Nature Struct. Biol.*, **3**, 427–431.
- Shafferman,A. et al. (1994) *EMBO J.*, **13**, 3448–3455.
- Soman,K., Yang,A.S., Honig,B. and Fletterick,R. (1989) *Biochemistry*, **28**, 9918–9926.
- Srivatsan,M. and Peretz,B. (1997) *Neuroscience*, **77**, 921–931.
- Sussman,J.L. et al. (1991) *Science*, **253**, 872–879.
- Tan,R.C., Truong,T.N., McCammon,J.A. and Sussman,J.L. (1993) *Biochemistry*, **32**, 401–403.
- Warwick,J. and Watson,H.C. (1982) *J. Mol. Biol.*, **157**, 671–679.
- Zhou,H.X., Briggs,J.M. and McCammon,J.A. (1996) *J. Amer. Chem. Soc.*, **118**, 13069–13070.

External and internal electrostatic potentials of cholinesterase models

Clifford E. Felder,* Simone A. Botti,*† Shneior Lifson,‡
Israel Silman,† and Joel L. Sussman*§

Departments of *Structural Biology, †Neurobiology ‡Chemical Physics, Weizmann Institute
of Science, Rehovot 76100, Israel

§Department of Biology, Brookhaven National Laboratory, Upton, NY 11973 USA

The electrostatic potentials for the three-dimensional structures of cholinesterases from various species were calculated, using the Delphi algorithm, on the basis of the Poisson–Boltzmann equation. We used structures for Torpedo californica and mouse acetylcholinesterase, and built homology models of the human, Bungarus fasciatus, and Drosophila melanogaster acetylcholinesterases and human butyrylcholinesterase. All these structures reveal a negative external surface potential, in the area around the entrance to the active-site gorge, that becomes more negative as the rim of the gorge is approached. Moreover, in all cases, the potential becomes increasingly more negative along the central axis running down the gorge, and is largest at the base of the gorge, near the active site. Ten key acidic residues conserved in the sequence alignments of AChE from various species, both in the surface area near the entrance of the active-site gorge and at its base, appear to be primarily responsible for these potentials. The potentials are highly correlated among the structures examined, down to sequence identities as low as 35%. This indicates that they are a conserved property of the cholinesterase family, could serve to attract the positively charged substrate into and down the gorge to the active site, and may play other roles important for cholinesterase function. © 1998 by Elsevier Science Inc.

Keywords: cholinesterase, electrostatics, electric potential, electrostatic motif

INTRODUCTION

Inspection of the X-ray structure of acetylcholinesterase (AChE, or acetylcholine acetylhydrolase, EC 3.1.1.7) from

Color Plates for this article are on pages 335–337.

Address reprint requests to: J. L. Sussman, Department of Structural Biology, Weizmann Institute of Science, Rehovot 76100, Israel; e-mail: joel@sgjs3.weizmann.ac.il).

Received 15 January 1998; accepted 6 February 1998.

Torpedo californica (TcAChE)¹ revealed that the active site is buried within the enzyme, near the bottom of an approximately 20-Å-long gorge that in places is less than 4 Å wide. It is thought that the substrate acetylcholine (ACh) must travel down this gorge to reach the active site.^{1–3} More recently, it has been noticed that TcAChE has a large “dipole moment,” calculated to be 500⁴ to 1 500 debyes.⁵ This would suggest that there is an excess of negative charge in the vicinity of the gorge entrance that might aid in attracting the positively charged substrate toward the gorge. Well before the three-dimensional (3D) structure of AChE was determined, Nolte et al.⁶ had already suggested that a high density of negative charge in the vicinity of the active site might serve to attract the substrate toward it.

The concept of a dipole moment can be defined formally only for an electrically neutral entity. This is because, in a charged species, the dipole is no longer a fixed, intrinsic property, but depends on its position in the coordinate system. Nevertheless, there is value in calculating dipole moments even for charged molecules positioned in a consistent way in a common coordinate system, as a measure of the inhomogeneity of the distribution of their partial atomic charges. To distinguish such a dipole from a true dipole moment, we shall call it a position-dependent first moment of charge distribution, $\mu = \sum(\mathbf{r}_i q_i)$, where \mathbf{r}_i is the position vector and q_i is the partial charge located on each atom i in the molecule.

Here we examine whether such large first moments are common in cholinesterases (ChEs) in general, and study the relationship between the overall charge distributions and the actual electric potentials, both external and inside the catalytic gorge. The potentials were calculated by solving the Poisson–Boltzmann equation, as implemented in the DelPhi algorithm⁷. Two X-ray structures from the Protein Databank (PDB) were employed, **2ace**² for *T. californica* AChE (TcAChE) and **1mah**⁸, with the inhibitor fasciculin removed, for *Mus musculus* (mouse) AChE (mAChE). In addition, homology models were prepared for human AChE (hAChE), *Bungarus fasciatus* (snake) AChE (BfAChE), *Drosophila melanogaster* AChE (DmAChE), and human butyrylcholinesterase (hBChE, acylcholine acylhydrolase, EC 3.1.1.8). We also analyze the rela-

tion between these potentials and a set of conserved, negatively charged residues.

METHODS

Homology models

Homology models of hAChE, BfAChE, DmAChE, and hBChE were constructed using the Swiss-Model server on the World Wide Web^{9,10} (URL <http://www.expasy.ch/swissmod/SWISS-MODEL.html>). This procedure was chosen because it automatically runs the FASTA¹¹ and BLAST¹² sequence homology searches against its structural database, and constructs an initial sequence alignment from which it generates an initial model. These initial sequence alignments were later improved by comparison with a multisequence alignment obtained from the program Pileup¹³ to produce better models.

The models were constructed using an existing TcAChE structure that Swiss-Model retrieved automatically from its database (**1acj**, a complex of TcAChE with 1,2,3,4-tetrahydro-9-aminoacridine [tacrine] with the tacrine removed), and the appropriate sequences in the Swiss-Prot database, except for BfAChE, whose sequence came from Ref. 14. The final sequence alignments of the model structures with TcAChE are shown in Figures 1–4.

Missing atoms were added to the incomplete side chains of

each of these models, using the program WHAT-IF¹⁵, to ensure proper assignment of hydrogens and atomic charges. Each structure was then oriented so that the gorge axis was aligned along the +z-coordinate axis. The gorge axis was defined as extending from residue I444 atom CD (I444-CD) to the average of atoms E73-CA, N280-CB, D285-CG, and L333-O (TcAChE numbering)¹⁶. This orientation is illustrated in the ribbon diagram of Figure 5¹⁷. While it differs somewhat from that used in previous studies⁴, it has the advantage of simplifying the calculation and analysis of properties with respect to the gorge axis. The missing residues 486–489 (HSQE) were added to the TcAChE structure. Throughout this study, the numbering of residues is that of TcAChE¹⁸.

RMS comparisons of the backbone fold

We calculated the root mean square (RMS) deviation of each model from the PDB structure **1acj**, based on the α carbons, using application LSQMAN^{19,20}. As shown in Table 1, the average RMS deviations are generally within 1 Å, indicating that the peptide chains of the homology models faithfully follow the TcAChE fold. Table 1 also gives the percent sequence identity and similarity for each model against the **1acj** sequence¹⁸, on the basis of the sequence alignments in Figures 1–4. For evaluations of similarity, we used as sets of similar

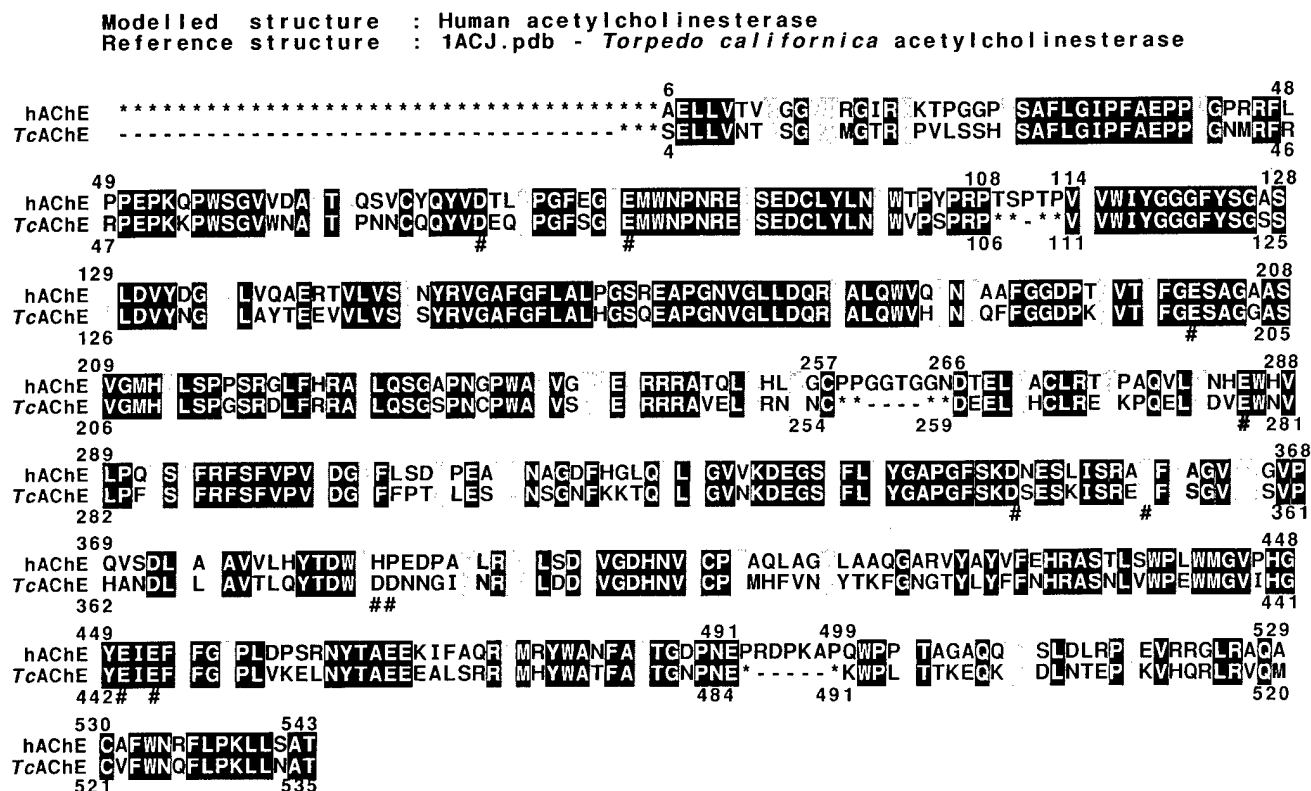


Figure 1. Sequence alignment, in Swiss-Model format, used to construct the homology model of hAChE relative to structure **1acj**. Identical residues are presented against a dark background, and similar residues (A and G; T and S; D and E; K and R; F and Y; N and Q; and I, V, L, and M) are presented against a gray background. Residue positions indicated by an asterisk (*) indicate **1acj** residues that were not used in the homology modeling, and dashes (–) mark the locations of missing residues (e.g., locations in the alignment where no residues of a given structure correspond with those given for the other). Hash marks (#) indicate the positions of conserved acidic residues.

Modelled structure : *Bungarus fasciatus* acetylcholinesterase
Reference structure: 1ACJ.pdb - *Torpedo californica* acetylcholinesterase

```

BfAChE *****1GELKVSTQ GSVRGLS PVL DGH SAFLGIPFAEPP GRMRFLRP 45
TcAChE -----4SELLVNTK GKVMGTR PVLSSH SAFLGIPFAEPP GNMRFRRP 48

125
BfAChE 46EPVKPWQHVLDA YKPACYQMVDTS PGFOG EMWNPNRMS SEDCLYLNIIWVSPRPKDAPV VWIYGGGFYSGAA LD
TcAChE EPKKPWSGVWNA YPNNCQQYVDEQ PGFSG EMWNPNRMS SEDCLYLNIIWVSPRPKSTTV VWIYGGGFYSGSS LD 128

129
BfAChE 126VYDG LITVTQNV LVLSYRVGAFGFL LPGSPEAPGN GLLDQR ALQW QNTHPFEGGNP AVT FGESAG ASVGM
TcAChE VYNG LAYTEEV LVLSYRVGAFGFL LFGSCEAPGN GLLDQR ALQW HDNIQFFGGDP TVT # FGESAG ASVGM 208

205
BfAChE 206H LSTQSRILFQRAILQSGGPNAPWA V PAESRGRAAL LG QLGHFNNDSEL SCLRSKNPQELID EWSVLP KSIF
TcAChE H LSPGSRDLFRRAILQSGSPNCPWA V VAEGRRRAVELG NLNCLNLSDEEL HCLREKKPQELID VEWNVLP DSIF 288

285
BfAChE 286RFPFVPVIDG FFPD PEAMLSSGNFKETQ LLGVVKDEGS FL YGLPGFSKD NESLISRADF EGV SVPHAND AT
TcAChE RFSFVPVIDG FFPT LESMLNSGNFKKTQ LLGVNKDEGS FL YGAPGFSKDS ESKISREDF SGV SVPHAND GL 368

365
BfAChE 366DAVV LQYTDWQDQDNREKNR LDDIVGDHNVICP QFANDYAKRNSKVYAYLFDHRASN L WPPWMGVPHGYEIEFVF 445
TcAChE DAVT LQYTDWMDDNNGIKNR LDDIVGDHNVICP HFVNKYTKFGNGTYLYFFNHRASN L WPEWMGVPHGYEIEFVF 448

445
BfAChE 446GLPLNDS LNYTPQEKLSRR MRYWANFA TGNPT PADKSGAWPT TASQPQ QLNTOP ATQPSLRAQ CAFWNHFL 525
TcAChE GLPLVKELNYTAE EALSRR MRYWATFA TGNPN PHSQSGSKWPL TTKEQK DLNTEP KVHQRRLRQ CVFWNQFL 528

525
BfAChE 526PKLLNA 531
TcAChE PKLLNA 534

```

Figure 2. Swiss-Model sequence alignment used to construct the homology model of BfAChE relative to 1acj.

Modelled structure : *D. melanogaster* acetylcholinesterase
Reference structure : 1ACJ.pdb - *Torpedo californica* acetylcholinesterase

```

DmAChE *****41DRL V TSSGPVGRSVTVQGRE HV TGIP AKPPVED 79
TcAChE -----4SEL V TKSGKVMGTRVPLSSH SA LGIP AEPPVGN 42

80
DmAChE 80RFR PVPAEPWHGVLD A GLSATCVQERYEYFPGFSGEE WNPNTN SEDCLY N WAPAKARLRHGRGANGGEHPNGK 159
TcAChE 80RFR PEPKKPWSGVWNA TYPNNCQQYVDEQFPGFSGSE WNPNRE SEDCLY N WV***** 101

160
DmAChE 160QADTDHLIHNGNPQNTTNGLPIL WIYGGGF M GSATLD YN DI AAVGNV ASFOYRVGAFGFLH LAPEMPSEFAEE 239
TcAChE 160*****PKS*** WIYGGGFY GSSTLD YN KY AYTEEV VLSYRVGAFGFLAL***** 163

240
DmAChE 240APGNVGLWQDA A RW KDNAHAFGGNPEW T FGESAGSSSVNAQ SPV RGLV R QSG MNAPWSH SEK VE 319
TcAChE 240APGNVGLLDQR A QW HDNIQFFGGDPKT T FGESAGASVGMH SPG RLDF R QSG PNCPWAS VAE RR 243

320
DmAChE 320I KALINDCNCNASMLKTNPAH SC RSVDAKT SVQQWN--S SGTLSFSPAPTIDGAFLPADPM K DLKOYDI 387
TcAChE 320R VELGRNLNC*****DEE HC REKKPQE IDVEW*** DSIFRFSFVPVIDGEFFPTSLE N NFKKTOI 319

388
DmAChE 388L GNVRDEG 404FLLYDFIDYFDKDDA A PR K EI NNIFGKATQAER A IFQYTSW- GNPQYQNNQQQ GRAVGDH 477
TcAChE 388L GVNKDEG 336FLLYGA***KDSE K SR D SG KLSVPHANDLGL A TLQYTD** DNNGIKNRDG DDI VGDH 398

478
DmAChE 478FFTPTNE AQALAERGASVHYYYFTHRTSTS WGEWMGV HGEIE FFGQPLNNSLQYRPVERELGKR SAVIEFAK 546
TcAChE 478NVICPLMH VNKYTKFNGTYLYFFNHRASN L WPEWMGV HGYEIE VFGLPLVKELNYTAE EALSRR HYWATFAK 478

547
DmAChE 547TGNPAQ--DGEW-WPNF KE PV IFST DKIEKLARGPLAARCSFWNDYLPK 588
TcAChE 547TGNPNE*****WPLF TK QK DLNT *****HQRLRVQM CVFWNQFLPK 531

```

Figure 3. Swiss-Model sequence alignment used to construct the homology model of DmAChE relative to 1acj.

Modelled structure : Human butyrylcholinesterase
Reference structure : 1ACJ.pdb - *Torpedo californica* acetylcholinesterase

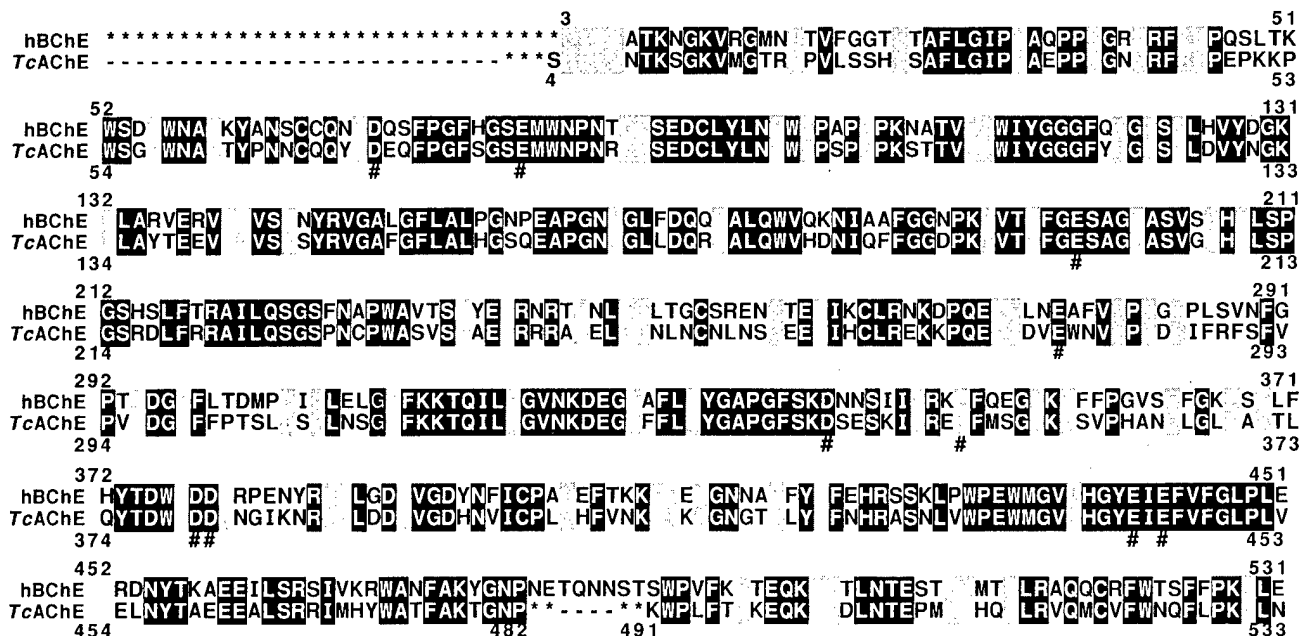


Figure 4. Swiss-Model sequence alignment used to construct the homology model of hBChE relative to 1acj.



Figure 5. Ribbon diagram of TcAChE. The diagram was prepared by MOLSCRIPT¹⁷, and shows the orientation employed in Color Plate 1. The gorge axis is denoted by a dark vertical bar, and residues W84, S200, W279, and F330 are drawn as stick figures.

residues A and G; T and S; D and E; K and R; F and Y; N and Q; and I, V, L, and M (Figure 4 of Ref. 1).

Calculations of position-dependent first moments

The first moments of charge distribution (equivalent to dipole moments; see above) were calculated using the Parse set of partial electric charges on the atoms (optimized specifically for DelPhi to fit data for small molecules; see Ref. 21). Two methods of positioning were used: geometric centering by use of the InsightII DelPhi module²², and by center of charge, as calculated by GRASP²³.

Calculations of electrostatic potentials by DelPhi

Calculation of electrostatic potentials was performed by solving the Poisson-Boltzmann equation, employing the finite difference method²⁴ as implemented in the DelPhi algorithm²⁵. We employed the Parse partial atomic charges and radii²¹, internal and external dielectric constant values of 2 and 80, solvent and ionic probe radii of 1.4 and 2 Å (i.e., closest approach to the molecular surface), respectively, and 0.145 M (physiological) ionic strength. For the electrostatic figures and surface potentials, the easy-to-use application GRASP²³ proved satisfactory. After the electrostatic potentials were calculated, an accessible molecular surface figure, colored according to potential, was prepared, and two files were written, one containing the Cartesian coordinates of the surface points in PDB format, and another containing the corresponding potentials at these points. On the basis of trial profiles of surface point potentials, we established the space containing the external surface points near the gorge entrance to be a cylindrical region starting 25 Å above the gorge base (e.g., atom I444-CD) and between 3.5 and 20.5 Å from the gorge axis. This region was

Table 1. Calculated properties of cholinesterase models, relative to those of *Torpedo californica* acetylcholinesterase

Structure	Percent sequence		Average C α RMS		Correlation coefficients for:	
	Identity ^a	Similarity ^a	Deviation (Å) ^b	No. of residues ^c	Surface potentials ^d	Gorge potentials ^d
<i>TcAChE</i> ^e	100	100	0.35	528	1.00	1.00
<i>BfAChE</i> ^f	66	75	0.31	524	0.80	0.96
<i>mAChE</i> ^g	58	70	0.89	520	0.89	0.99
<i>hAChE</i> ^h	57	70	0.48	524	0.89	0.99
<i>hBChE</i> ⁱ	53	69	0.42	525	0.66	0.94
<i>DmAChE</i> ^j	35	48	0.78	508	0.86	0.94

^a Sequence identity or similarity versus structure **1acj**, according to the sequence alignments given in Figures 1–4, and using as sets of similar residues A and G; T and S; D and E; K and R; F and Y; N and Q; and I, V, L, and M.

^b Compared with structure **1acj**, as calculated using the program LSQMAN^{19,20}.

^c That is, the number of residue pairs LSQMAN used to calculate the RMS deviation.

^d Compared with the corresponding potentials for the *TcAChE* structure **2ace**, as determined using the program Linfit²⁶.

^e X-Ray structure **2ace** (*TcAChE*).

^f Homology model of *BfAChE*.

^g X-Ray structure **1mah** (*mAChE*).

^h Homology model of *hAChE*.

ⁱ Homology model of *hBChE*.

^j Homology model of *DmAChE*.

divided into 1-Å-thick concentric annular sections, e.g., from 3.5 to 4.5 Å from the gorge axis, with mean distance 4 Å, from 4.5 to 5.5 Å, with mean distance 5 Å, etc., as shown in Figure 6, and the average potentials of the surface points in each annulus and in the entire region were calculated.

GRASP is not accurate enough for calculations inside the gorge, which in places is only about 4 Å wide, smaller than the

grid spacing in the GRASP potential grid. A commercial version of the program DelPhi²² was, therefore, employed. This allows a finer grid and greater control over the calculations, e.g., of the nonlinear Poisson–Boltzmann equation, which is not available in GRASP. An initial potential grid with a 35-Å border space, and a grid spacing of about 2.3 Å, was later focused onto a second grid with 10-Å border space and grid spacing of about 1.45 Å (atomic resolution). Finally, we calculated the potential at 1-Å intervals along the gorge axis (as defined above), starting 4 Å above atom I444-CD (*TcAChE* numbering), using the InsightII DelPhi module. Correlation analyses of the surface and gorge potentials for the specified model were done by a linear regression fit against the corresponding values for the *TcAChE* structure, using the Linfit algorithm.²⁶

RESULTS AND DISCUSSION

Sequence similarities and structural RMS deviations

Table 1 presents the sequence identities and similarities versus PDB entry **1acj** for the sequence alignments used to generate the different models. Also presented are the structural RMS deviations of the α carbons relative to those of **1acj**. Most of the sequences have about 55–60% identity, and their corresponding structures have average RMS deviations within 1 Å of that of **1acj**. Our calculated RMS value for *mAChE*, 0.89 Å, compares well with the value of 0.84 Å calculated in Ref. 8.

Calculated position-dependent first moments of charge distribution

Table 2 shows the calculated net molecular charges, the first moments of charge distribution, and the angles the first-moment vectors make with the gorge axis, for the ChE structures analyzed. All the structures have a rather large moment of

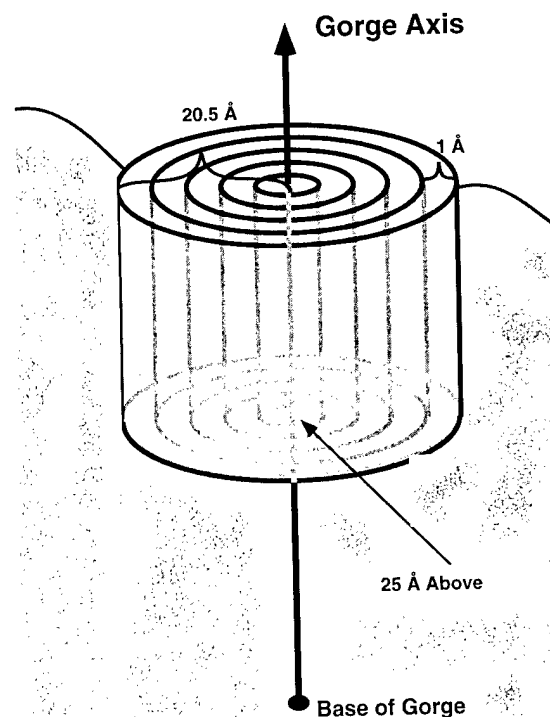


Figure 6. Definition of the annular sections of the accessible molecular surface about the gorge axis.

Table 2. Calculated position-dependent first moments of charge distribution (debyes) for cholinesterases and other proteins

Structure	Net charge	Centered geometrically		Center-of-charge centered	
		First moment	Angle with gorge axis (degrees)	First moment	Angle with gorge axis (degrees)
<i>TcAChE</i>	-11	1 666	32	1 676	35
<i>BfAChE</i>	-9	1 688	31	1 639	32
<i>mAChE</i>	-8	1 070	13	1 016	18
<i>hAChE</i>	-10	883	16	948	19
<i>hBChE</i>	-1	1 527	30	1 523	31
<i>DmAChE</i>	-18	1 135	31	1 232	31

800–1 800 debyes, aligned roughly along the gorge axis, and both centering methods agree to within 20%. The calculated value for *BfAChE* is in fair agreement with the experimentally measured value of 1 000²⁷. It can thus be concluded that all the ChEs that we have studied have an asymmetric charge distribution, such that there is an excess of negative charge in the region near the gorge entrance, relative to the far side of the enzyme.

External potentials and those near the gorge entrance

The external potentials of the different ChEs are displayed in Color Plate 1, which shows red (+0.25 kT/e) and blue (-0.25 kT/e) isopotential surfaces (1 kT/e = 25.6 mV). The green arrows represent the directions of the first-moment vectors. The ribbon diagram of *TcAChE* in Figure 5 defines the view

used. In all the structures, the pattern of external potentials reflects strongly the calculated nonhomogeneous charge distributions. In particular, the face of the enzyme leading into the gorge (yellow bar) has a mostly negative potential (red surface), while positively charged regions (blue surface) are mostly on the opposite side.

The surface potentials in the region around the gorge for most of the ChEs are depicted in Color Plate 2, which displays accessible surfaces colored by potential and viewed down the gorge axis. In all the structures, the region around the gorge entrance is red, indicating a negative potential in this area. A close-up view of this region for *TcAChE*, including a series of isopotential rings (Color Plate 3, top), illustrates clearly the gradually increasing negative potential in this region that could play a significant role in accelerating diffusion of the cationic substrate toward the active site.

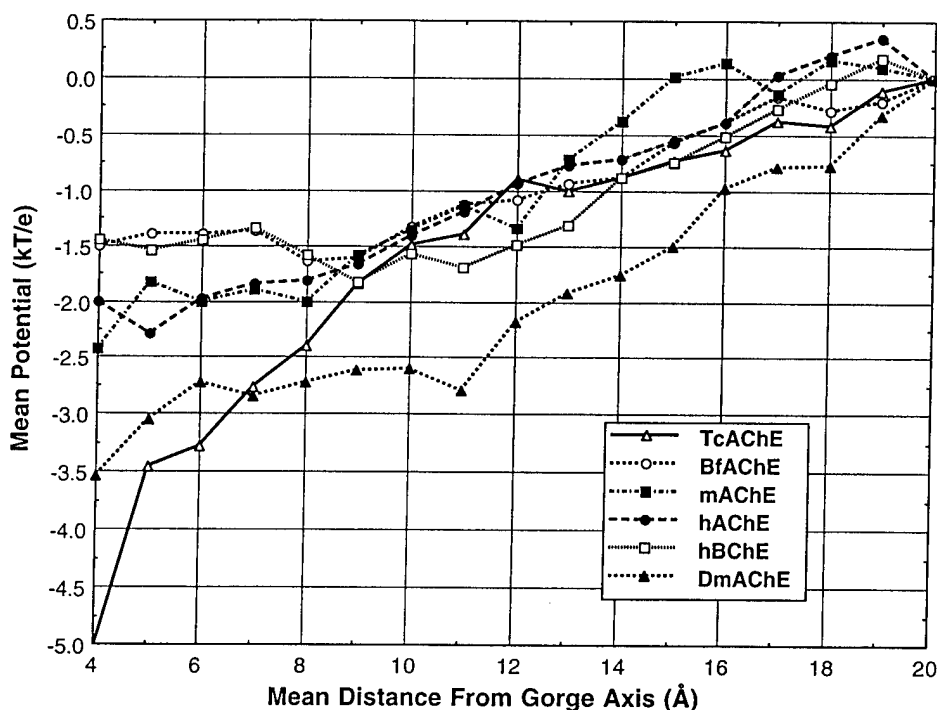


Figure 7. Scaled mean surface potentials in annular sections about the gorge axis in ChE models. These annular regions are defined in Figure 6.

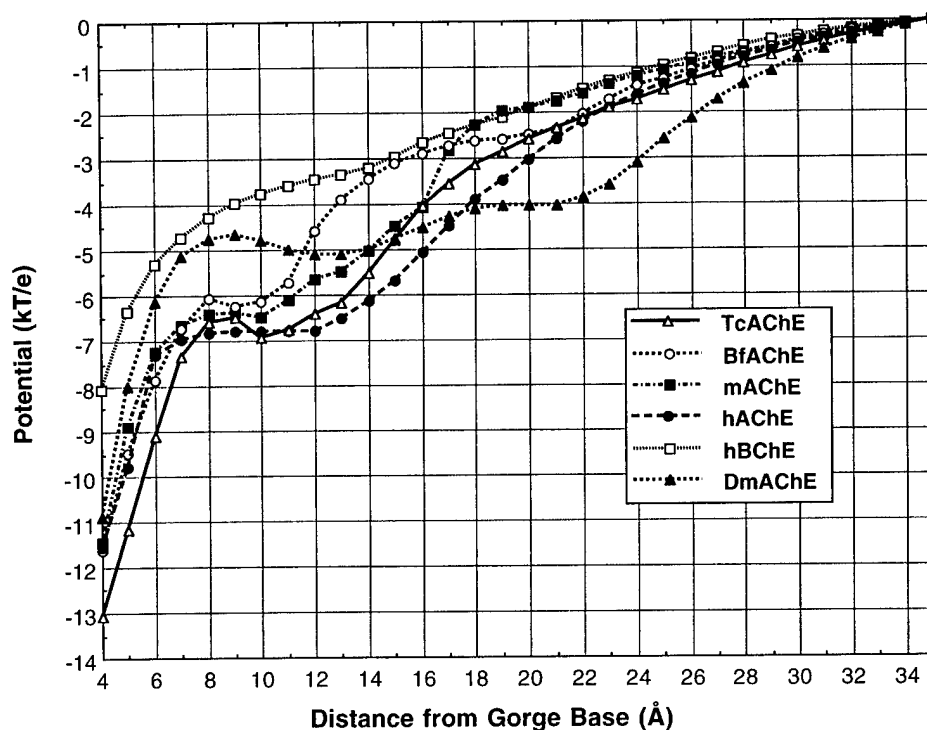


Figure 8. Scaled potentials along the gorge axis in ChE models.

Figure 7 shows the calculated mean potential in a series of 1-Å-thick annular sections out to 20 Å from the gorge axis, for the various ChE structures. They all display a gradually increasing negative potential as the gorge entrance is approached. The correlation coefficients for these curves relative to those

for TcAChE are given in Table 1. The average potentials (in kT/e units, equal to 25.6 mV or $0.593 \text{ kcal mol}^{-1} \text{ e}^{-1}$) for the different models over the entire 20-Å cylindrical region are as follows: TcAChE, -2.27; BfAChE, -1.14; mAChE, -1.41; hAChE, -1.14; hBChE, -0.05; and DmAChE, -2.36. All the

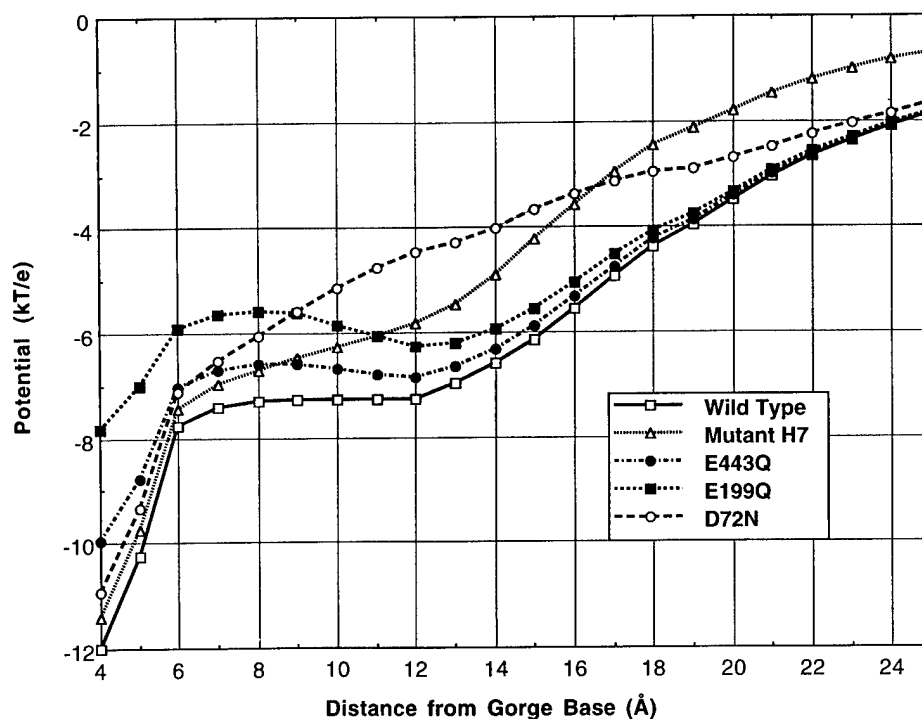


Figure 9. Potentials along the gorge axis in hAChE mutants.

Table 3. Conservation of critical acidic residues in the cholinesterase sequence alignments,^a relative to the TcAChE sequence

Model	D72	E82	E199	E278	D342	D351	D380	D381	E443	E445
BfAChE	*	*	*	*	*	*	*	—	*	*
mAChE	*	*	*	*	*	—	— ^b	— ^b	*	*
hAChE	*	*	*	*	*	(*)	— ^b	— ^b	*	*
hBChE	*	*	*	*	*	(*)	*	*	*	*
DmAChE	—	*	*	—	*	—	(*)	—	*	*

^a According to the sequence alignments given in Figures 1–4, and a similar alignment for mAChE. The presence of the given residue aligned to that of TcAChE is indicated by an asterisk. An asterisk in parentheses means that glutamate and aspartate have been interchanged, which should not affect the electrostatics. A dash (—) indicates that the residue is not conserved.

^b In the sequence alignment, these two residues are offset by two positions.

structures show a fairly good correlation to TcAChE, except for hBChE, whose average potential and correlation coefficient are significantly lower. Hence, all the AChEs studied have a common electrostatic pattern or motif²⁸ around the gorge entrance, while BChE displays a somewhat different pattern. The biological significance of this region of conserved negative potential is under investigation.²⁹

Electrostatic potentials along the axis of the catalytic gorge

A slice view through the catalytic gorge of TcAChE (Color Plate 3, bottom, a and b) illustrates clearly that the potential increases gradually as one goes down the gorge, and reaches a maximum near its base. Figure 8 shows a plot of these calculated potentials at 1-Å intervals along the gorge axis, starting 4 Å from the gorge base, for all the models examined. The potentials were scaled such that the potentials 35 Å from the gorge base were set to zero, so as to permit meaningful comparison of the values for the different models. All the AChE models display a similar, gradually increasing negative potential, beginning several angstroms outside the gorge entrance, and continuing down the gorge toward the active site. In an area ~14–8 Å from the base of the gorge, depending on the particular species, the potentials are relatively level, and then drop sharply toward the bottom of the gorge. A similar pattern of potentials for TcAChE was calculated by Wlodek et al.³⁰ In the case of hBChE the plateau region is essentially absent. Table 1 shows that the gorge potentials, including that for hBChE, have correlations approaching unity versus TcAChE, which is a much smaller degree of variation than that calculated for the external potentials, for the fold or for the sequence similarity. Hence, these potentials are strongly conserved among all the ChEs, and thus may play an important role in drawing the positively charged substrate down the gorge to the active site^{4,31,32}.

Relation to conserved acidic residues in the sequence alignments

The origin of these conserved potentials can be understood by examining the conservation of key acidic residues in the sequence alignments. Shafferman et al.³³ identified seven surface acidic residues near the gorge (E82, E278, E285, E342, D351, D380, and D381) thought to be primarily responsible for the

negative surface potential near the gorge entrance (see also Antosiewicz et al.¹⁶) Also important is an additional negatively charged residue, D72, located midway down the gorge.¹ Finally, E199 and E443, near the gorge base, together with nearby E445, appear to be primarily responsible for the large negative potential in this region.^{30,34} Table 3 shows that 10 of these residues are highly conserved in the sequence alignments of our homology models. In particular, E82, D342, E443 and E445 are conserved among all the models, as is D72 in all but the DmAChE model. E285 is conserved only in hAChE and mAChE, and is not included in Table 3. Hence, the calculated electrostatic properties are a function of certain key acidic residues conserved in the sequence alignment on the backdrop of a common backbone fold. Figure 10 shows the position of these conserved residues within the three-dimensional structure of TcAChE.

As a check, we prepared a second hAChE homology model using version 4 of the program Modeller^{35,36}, in which four different TcAChE structures and one mAChE structure from the PDB were used together to build the hAChE model. Its



Figure 10. Ribbon diagram showing the position in the 3D structure of TcAChE of the ten conserved residues listed in Table 3. The black bar denotes the gorge axis.

calculated surface and gorge potentials are practically identical to those of the original model, with correlation coefficients of 0.97 and 0.99, respectively, against the original hAChE model, and 0.88 and 0.98 against TcAChE, even though the RMS deviation between the two hAChE models was 0.50 Å. Hence our conclusions are valid even if the homology models are only approximate. As a second check, we prepared (by residue replacement) from the first hAChE model a series of mutant models, including E199Q, E443Q, D72N, and the Shafferman et al. H7 mutant³³, in which all seven acidic residues near the gorge entrance listed above were neutralized. Their effects on the gorge potentials are shown in Figure 9, where the H7 mutations affect mainly the potentials in the top half of the gorge, D72N influences the potentials mainly in the middle, at ~12 Å from the base of the gorge, and E199Q and E443Q affect primarily the potential near the base of the gorge. Furthermore, the average surface potential for the H7 mutant was reduced from -1.14 to -0.05 kT/e units relative to the wild type (and the patterns of surface and gorge potentials correlated as 0.96 and 0.99 against hAChE WT and as 0.93 and 0.99 against TcAChE). The relatively larger effect of the E199Q and E443Q mutations probably results from these residues being buried within the molecule below the gorge.

We can conclude that the consistent pattern of electric potentials around the entrance to the active-site gorge and within it has its origin in a small number of critical acidic residues that are conserved within highly homologous regions of the sequence alignments, such that they occupy the same key locations in the ChE fold. This explains how structures with sequence identities as low as 35% can have such highly correlated potentials, and suggests that they are important for the functional roles of the ChEs.

ACKNOWLEDGMENTS

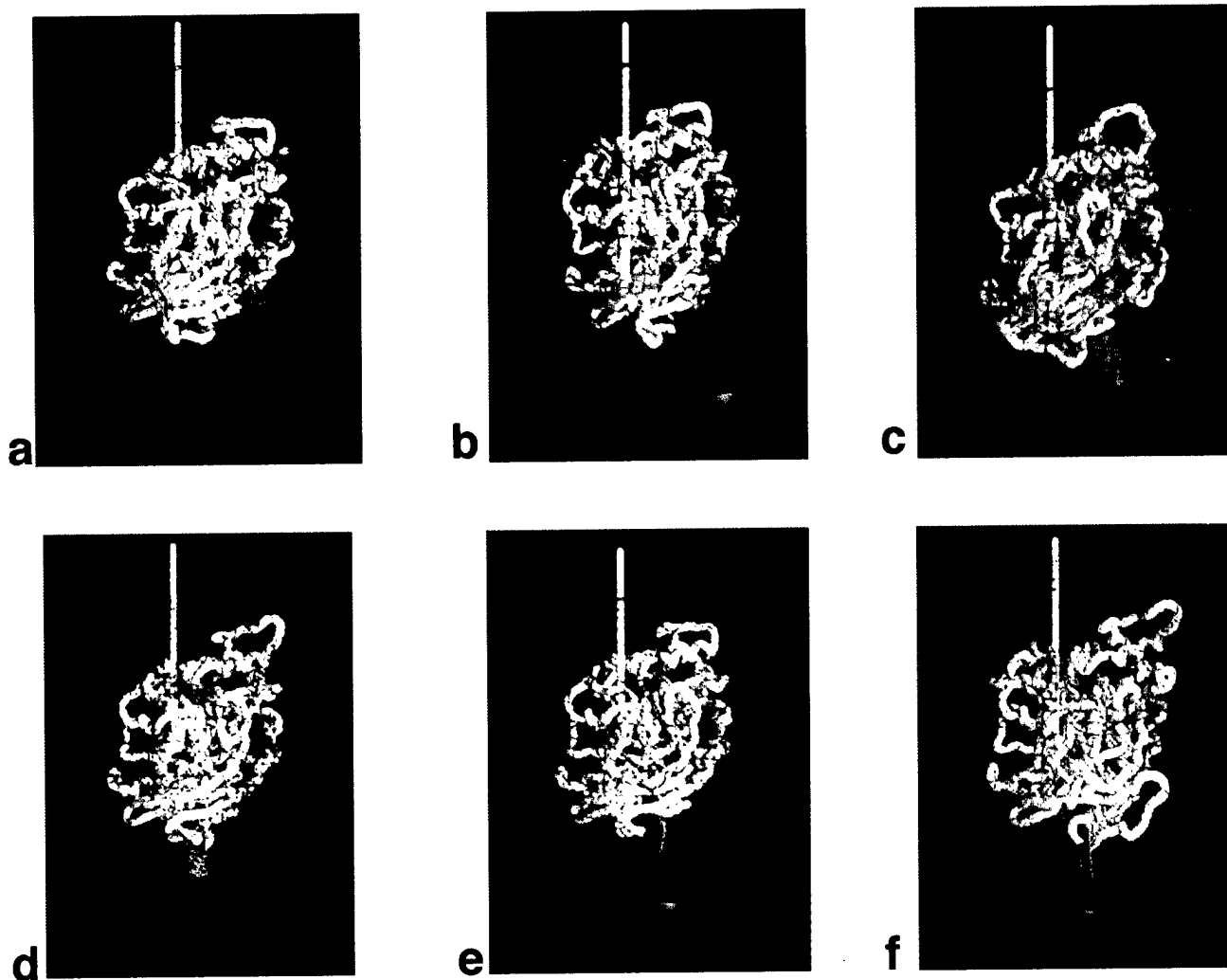
The authors thank Charles Millard for valuable comments on the manuscript. This work was supported by the U.S. Army Medical Research Acquisition Activity under Contract No. 17-97-2-7022, the Kimmelman Center for Biomolecular Structure and Assembly (Rehovot, Israel), and the European Union. The generous support of Mrs. Tania Friedman is gratefully acknowledged. I.S. is Bernstein-Mason Professor of Neurochemistry.

REFERENCES

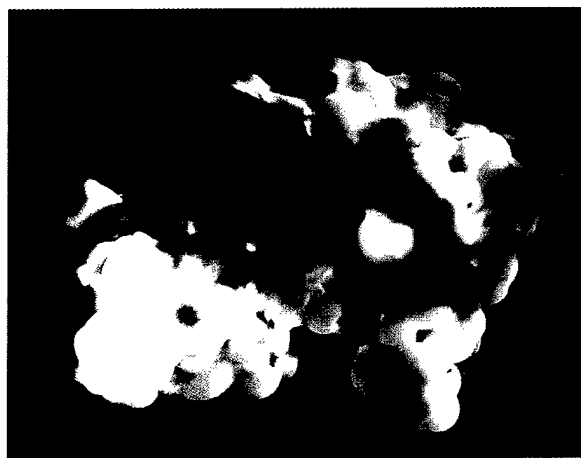
- 1 Sussman, J.L., Harel, M., Frolow, F., Oefner, C., Goldman, A., Toker, L., and Silman, I. Atomic structure of acetylcholinesterase from *Torpedo californica*: A prototypic acetylcholine-binding protein. *Science* 1991, **253**, 872-879
- 2 Raves, M.L., Harel, M., Pang, Y.-P., Silman, I., Kozikowski, A.P., and Sussman, J.L. Structure of acetylcholinesterase complexed with the nootropic alkaloid, (-)-huperzine A. *Nature Struct. Biol.* 1997, **4**, 57-63
- 3 Axelsen, P.H., Harel, M., Silman, I., and Sussman, J.L. Structure and dynamics of the active site gorge of acetylcholinesterase: Synergistic use of molecular dynamics simulation and X-ray crystallography. *Protein Sci.* 1994, **3**, 188-197
- 4 Ripoll, D.R., Faerman, C.H., Axelsen, P.H., Silman, I., and Sussman, J.L. An electrostatic mechanism of substrate guidance down the aromatic gorge of acetylcholinesterase. *Proc. Natl. Acad. Sci. U.S.A.* 1993, **90**, 5128-5132
- 5 Antosiewicz, J., Gilson, M.K., and McCammon, J.A. Acetylcholinesterase: Effects of ionic strength and dimerization on the rate constants. *Israel J. Chem.* 1994, **34**, 151-158
- 6 Nolte, H.-J., Rosenberry, T.L., and Neumann, E. Effective charge on acetylcholinesterase active sites determined from the ionic strength dependence of association rate constants with cationic ligands. *Biochemistry* 1980, **19**, 3705-3711
- 7 Honig, B., Sharp, K.A., and Yang, A.-S. Macroscopic models of aqueous solutions: Biological and chemical applications. *J. Phys. Chem.* 1993, **97**, 1101-1109
- 8 Bourne, Y., Taylor, P., and Marchot, P. Acetylcholinesterase inhibition by fasciculin: crystal structure of the complex. *Cell* 1995, **83**, 503-512
- 9 Peitsch, M.C. Protein modelling by e-mail. *Bio/Technology* 1995, **13**, 658-660
- 10 Peitsch, M.C. ProMod and SwissModel: Internet-based tools for automated comparative protein modelling. *Biochem. Soc. Trans.* 1996, **24**, 274-279
- 11 Pearson, W.R., and Lipman, D.J. Improved tools for biological sequence comparison. *Proc. Natl. Acad. Sci. U.S.A.*, 1988, **85**, 2444-2448
- 12 Altschul, S.F., Gish, W., Miller, W., Myers, E.W., and Lipman, D.J. Basic local alignment search tool. *J. Mol. Biol.* 1990, **215**, 403-410
- 13 Feng, D.F., and Doolittle, R.F. Progressive sequence alignment as a prerequisite to correct phylogenetic trees. *J. Mol. Evol.* 1987, **25**, 351-360
- 14 Cousin, X., Bon, S., Duval, N., Massoulié, J., and Bon, C. Cloning and expression of acetylcholinesterase from *Bungarus fasciatus* venom—a new type of COOH-terminal domain; involvement of a positively charged residue in the peripheral site. *J. Biol. Chem.* 1996, **271**, 15099-15108
- 15 Vriend, G.A. WHAT-IF, version 3.0, for Silicon Graphics Indigo, EMBL, Heidelberg, Germany, 1995
- 16 Antosiewicz, J., McCammon, J.A., Wlodek, S.T. and Gilson, M.K. Simulation of charge-mutant acetylcholinesterases. *Biochemistry* 1995, **34**, 4211-4219
- 17 Kraulis, P.J. MOLSCRIPT: A program to produce both detailed and schematic plots of protein structures. *J. Appl. Crystallogr.* 1991, **24**, 946-950
- 18 Schumacher, M., Camp, S., Maulet, Y., Newton, M., MacPhee-Quigley, K., Taylor, S.S., Friedmann, T., and Taylor, P. Primary structure of *Torpedo californica* acetylcholinesterase deduced from its cDNA sequence. *Nature (London)* 1986, **319**, 407-409
- 19 Kleywegt, G.J. LSQMAN, version 960821/4.7.3, for the Department of Molecular Biology, University of Uppsala, Uppsala, Sweden, 1996
- 20 Kleywegt, G.J., and Jones, T.A. A super position. *ESF/CCP4 Newsllett.* 1994, **31**, 9-14
- 21 Sitkoff, D., Sharp, K.A., and Honig, B. Accurate calculation of hydration free energies using macroscopic solvent models. *J. Phys. Chem.* 1994, **98**, 1978-1988
- 22 Biosym. DelPhi, version 2.5. Biosym/MSI, San Diego, California 1994
- 23 Nicholls, A., Sharp, K., and Honig, B. Protein folding and association: Insights from the interfacial and ther-

- modynamic properties of hydrocarbons. *Protein Struct. Funct. Genet.* 1991, **11**, 281–296
- 24 Warwicker, J., and Watson, H.C. Calculation of the electric potential in the active site cleft due to alpha-helix dipoles. *J. Mol. Biol.* 1982, **157**, 671–679
 - 25 Gilson, M.K., Sharp, K.A., and Honig, B.H. Calculating electrostatic interactions in bio-molecules: Method and error assessment. *J. Comput. Chem.* 1988, **9**, 327–335
 - 26 Bevington, P.R. *Data Reduction for the Physical Sciences*. McGraw-Hill, New York, 1969, p. 104
 - 27 Porschke, D., Créminon, C., Cousin, X., Bon, C., Sussman, J.L., and Silman, I. Electrooptical measurements demonstrate a large permanent dipole moment associated with acetylcholinesterase. *Biophys. J.* 1996, **70**, 1603–1608
 - 28 Honig, B., and Nicholls, A. Classical electrostatics in biology and chemistry. *Science* 1995, **268**, 1144–1149
 - 29 Botti, S.A., Felder, C., Sussman, J.L., and Silman, I. *Protein Engineering*, in press
 - 30 Wlodek, S.T., Antosiewicz, J., and Briggs, J.M. On the mechanism of acetylcholinesterase action: The electrostatically induced acceleration of the catalytic acylation step. *J. Am. Chem. Soc.* 1997, **119**, 8159–8165
 - 31 Tan, R.C., Truong, T.N., McCammon, J.A., and Sussman, J.L. Acetylcholinesterase: Electrostatic steering increases the rate of ligand binding. *Biochemistry* 1993, **32**, 401–403
 - 32 Antosiewicz, J., Gilson, M.K., Lee, I.H., and McCammon, J.A. Acetylcholinesterase: Diffusional encounter rate constants for dumbbell models of ligand. *Biophys. J.* 1995, **68**, 62–68
 - 33 Shafferman, A., Ordentlich, A., Barak, D., Kronman, C., Ber, R., Bino, T., Ariel, N., Osman, R., and Velan, B. Electrostatic attraction by surface charge does not contribute to the catalytic efficiency of acetylcholinesterase. *EMBO J.* 1994, **13**, 3448–3455
 - 34 Ordentlich, A., Kronman, C., Barak, D., Stein, D., Ariel, N., Marcus, D., Velan, B., and Shafferman, A. Engineering resistance to “aging” of phosphonylated human acetylcholinesterase: Role of the hydrogen bond network in the active center. *FEBS Lett.* 1993, **334**, 215–220
 - 35 Sali, A., and Blundell, T.L. Comparative protein modelling by satisfaction of spatial restraints. *J. Mol. Biol.* 1993, **234**, 779–815
 - 36 Sanchez, R., and Sali, A. Advances in comparative protein-structure modelling. *Curr. Opin. Struct. Biol.* 1997, **7**, 206–214

External and internal electrostatic potentials of cholinesterase models



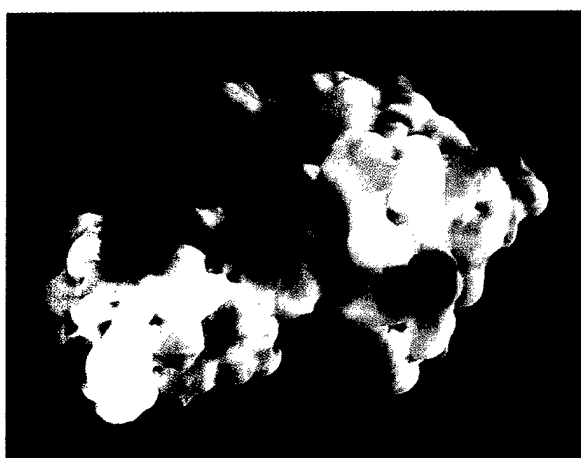
Color Plate 1. Schematic view of the ± 0.25 -kT/e isopotential surfaces for *TcAChE*, *mAChE*, and the various homology models. These representations were prepared using GRASP²³, and the orientation is the same as in the ribbon diagram shown in Figure 5. The red and blue isopotential surfaces are, respectively, negative and positive. The unscaled green arrows represent the directions of the first-moment vectors, the peptide backbones are presented in white, and the yellow bars indicate the gorge axes. (1 kT/e unit = 25.6 mV.) (a) *TcAChE*; (b) *BfAChE*; (c) *mAChE*; (d) *hAChE*; (e) *hBChE*; (f) *DmAChE*.



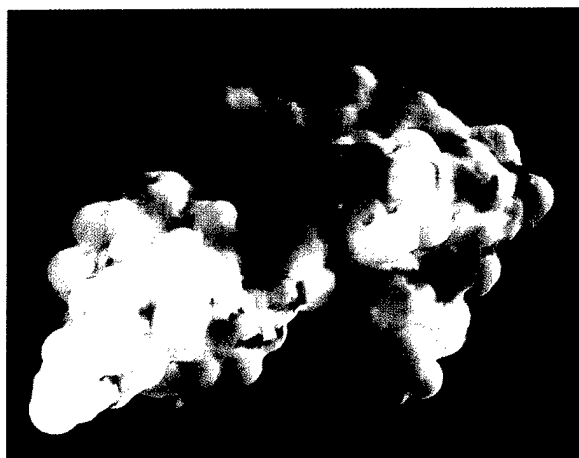
a



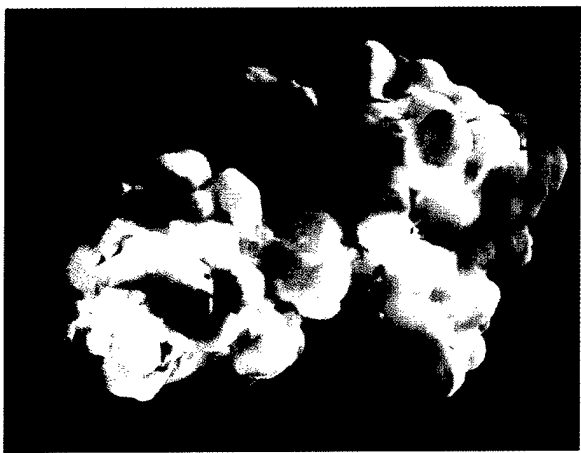
b



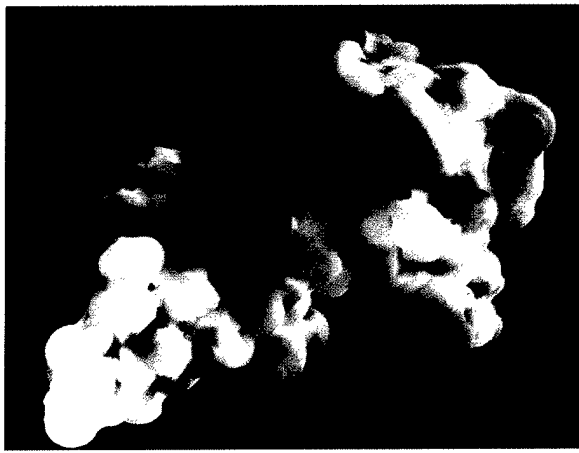
c



d

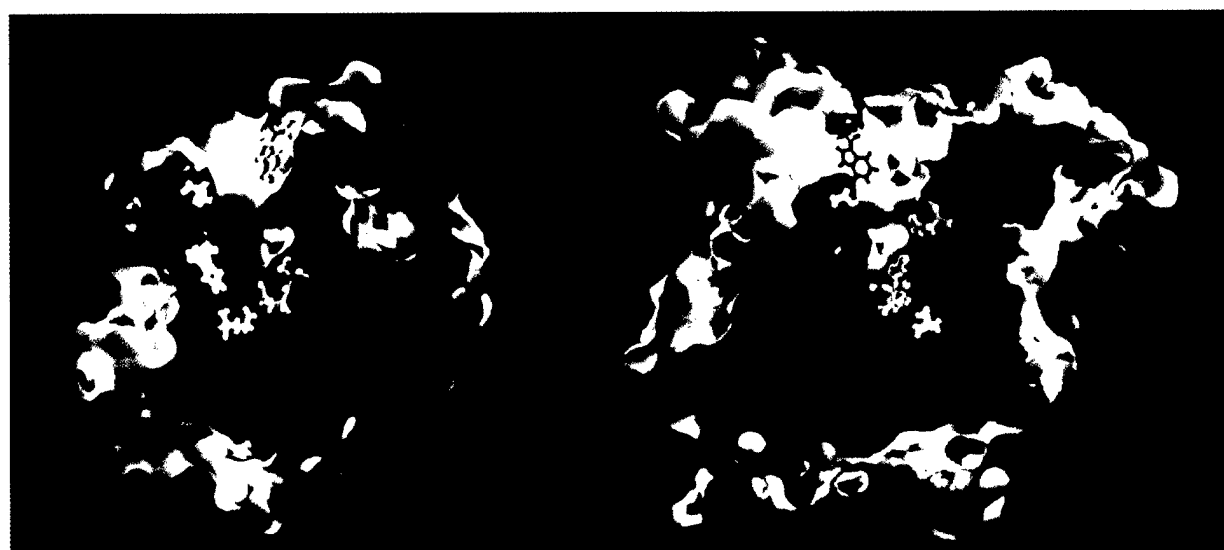


e



f

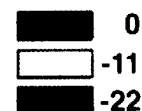
Color Plate 2. GRASP drawing of the solvent-accessible molecular surface, looking down the catalytic gorge, color coded by electrostatic potential. All regions of the surface with potentials of 2.5 kT/e and above are colored blue, those near 0 kT/e are white, and those that are -2.5 kT/e and below are red. Note that the gorge entrance in the center, and the entire region around it, are colored red. (a) *TcAChE*; (b) *BfAChE*; (c) *mAChE*; (d) *hAChE*; (e) *hBChE*; (f) *DmAChE*.



a

b

Potential (kT/e)



Color Plate 3. (top) Close-up view of the accessible surface of *TcAChE* around the gorge entrance. The orientation is as in Color Plate 2a, and a series of isopotential rings is shown at values of -3.0 (blue), -4.2 (green), -5.7 (amber), -7.8 (gray), -9.5 (red), and -11.5 (purple) kT/e units. (bottom) GRASP drawings of slices through the molecular surface of *TcAChE*. The slices are colored by electrostatic potential, and display the catalytic gorge and residues D72 (yellow), W84 (white), D199 (red), S200 (green), W279 (magenta), F330 (blue), and E443 (tan). Regions of the surface with potential $\geq 0 \text{ kT/e}$ are blue, those near -11 kT/e are white, and those $\leq -22 \text{ kT/e}$ and below are red. (a) View in the same orientation as in Color Plate 1; (b) view rotated 90° about the vertical axis relative to (a).

STRUCTURAL AND FUNCTIONAL STUDIES ON ACETYLCHOLINESTERASE

A Perspective

Israel Silman¹ and Joel L. Sussman²

¹Department of Neurobiology

²Department of Structural Biology

Weizmann Institute of Science

Rehovot 76100, Israel

INTRODUCTION

Many of the salient features of the active site of acetylcholinesterase (AChE), both in terms of catalytic mechanism and of recognition of substrates and inhibitors, were delineated almost 50 years ago by Irwin Wilson, in collaboration with Felix Bergmann and the late David Nachmansohn. These seminal observations were made several decades prior to cloning, sequencing and, eventually, determination of the 3D structure of AChE. Furthermore, they were made without the benefit of fluorescence (or even absorption) spectroscopy, not to mention NMR, EPR and circular dichroism.

In the following, we will first discuss the studies of Wilson and his colleagues, which set the stage for much of the subsequent work on AChE. We will then go on to show how both chemical modification and spectroscopic techniques were utilized to supplement the data acquired by kinetic studies, and to discuss the contributions of sequencing and cloning studies. The open questions raised by the 3D structure will then be analyzed, and finally, recent developments arising out of the structural work will be discussed which may shed new light on the noncholinergic functions of AChE.

THE ACYL-ENZYME CONCEPT

In a remarkable series of papers, published in the years 1950-2 (1-8), Wilson and his colleagues put forward the pioneering concept that the mechanism of action of AChE involved an acyl-enzyme intermediate. They provided experimental evidence in support

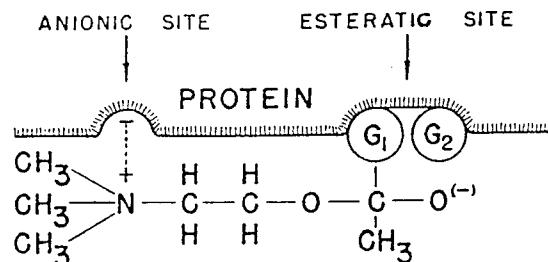


Figure 1. Schematic representation of the active site of acetylcholinesterase (adapted from Irwin B. Wilson & Felix Bergmann [1950] *J. Biol. Chem.* 186, 683–692)

of this notion by demonstrating formation of butyrylcholine from monobutyrin and choline (4), and by means of an ingenious experiment in which AChE was shown to catalyze the hydrolysis of thiolacetic acid with concomitant release of hydrogen sulfide (8). They also proposed a model for the active-site (Fig. 1), defining an esteratic subsite, containing the catalytic machinery for hydrolysis of the ester bond, and the so-called 'anionic' subsite, which would provide the recognition site for binding the quaternary choline moiety (2). Within the esteratic subsite they proposed an entity, G_2 , corresponding to what we would now call the 'oxyanion hole', and another entity, G_1 , with which the putative covalent bond would be formed, which they believed to be the same histidine residue involved in catalysis, but which we now know to be a serine residue. The rapid turnover of AChE made isolation of the corresponding acetyl enzyme extremely difficult. It was only in 1984 that Wilson himself, together with his long-standing associate, Harry Froede, finally provided the direct experimental evidence for what he had predicted almost 35 years earlier (9).

THE ANIONIC SITE

Wilson, together with his colleagues, made an equally thorough and perceptive study of the 'anionic' site. In particular, he compared the interaction with AChE of ACh and of a series of analogs, including the uncharged isoster, and analogs of ACh in which 1-3 methyl groups were added successively to the nitrogen atom of the choline moiety. He was thus able to assess the contribution of both the methyl groups and the positive charge to the affinity of the substrate for the enzyme (10). He also studied a series of inhibitors generated by successive methylation of the ammonium ion or of ethanolamine (10). These studies enabled him to conclude that 'most of the binding of ACh is accounted for by Coulombic and hydrophobic interactions at the anionic site' (11). However, Wilson was aware that the structure-function relationships that he had delineated could not be explained by a simple fitting of substrate to enzyme. His data showed that all four methyl groups of ACh contributed to its binding to the enzyme. This, in turn, implied that all four must be in contact with the protein, and Wilson postulated that the interaction must involve some sort of 'reshaping' of the protein molecule (10), what we would now call a conformational change. In fact, he was presenting evidence favoring a buried active site, which, from the 3D structure (12), we now know to be the case. Indeed, we have argued that a buried active site, permitting maximal interaction of the enzyme with its substrate, drastically lowers the energy of the transition state, thus contributing to the unusual catalytic power of AChE (13).

ANALOGIES BETWEEN AChE AND THE ACETYLCHOLINE RECEPTOR

Although no high-resolution structure of the nicotinic acetylcholine receptor (nAChR) is yet available, it has been argued that, as in the case of AChE, its ACh-binding site is at the bottom of a deep cleft (14). Stauffer and Karlin (15) have defined its electrostatic characteristics, and the late Christian Hirth, in collaboration with Maurice Goeldner and the group of Jean-Pierre Changeux, used photoaffinity labeling to provide evidence for the presence of a number of aromatic residues in the immediate vicinity of the ACh-binding site (16, 17). Thus, even though the evidence points to this binding site being at the interface between two subunits (17, 18), it does seem to share many structural features with AChE. Wilson and Nachmansohn addressed this issue at a time when consideration of receptors in molecular terms was to make a daring leap into the future, and actually proposed that a conformational change induced in the nAChR upon binding of ACh might be responsible for the change in ion permeability induced (10, 19).

THE PERIPHERAL ANIONIC SITE

Not only did the pioneering studies of Wilson and his coworkers provide the first description of the esteratic and 'anionic' subsites; they also postulated the existence of a 'peripheral' anionic site, due to their observation that diquaternary salts displayed much greater inhibition constants than homologous monoquaternary salts (6). They rationalized this as being due to these elongated compounds bridging the two 'anionic' sites, as the structural data now confirm completely (20).

PYRIDINE-2-ALDOXIME METHIODIDE-AN ACTIVE-SITE-DIRECTED REACTIVATOR

A direct outcome of Wilson's studies on the structure-function relationships of AChE with substrates and inhibitors was the development, together with Sara Ginzburg, of the active-site directed reactivator, pyridine-2-aldoxime methiodide (2-PAM), as a treatment for intoxication by nerve agents and insecticides (21). Even today, over 40 years later, despite the emergence of structure-related drug design, making use of data obtained by X-ray crystallography, and utilizing sophisticated docking programs, run on super computers equipped with state-of-the-art graphics, this still remains one of the most impressive and effective examples of drug design. Even though various improved versions of the original compound have been developed, including bisquaternary oximes, 2-PAM itself is still in use in the protective kits which are issued to soldiers in the field by the US Army (22), and is employed to treat insecticide poisoning in casualty wards (23). As was pointed out at the time, "the quaternary oxime is a million times better than the non-methylated compound... in reactivating TEPP-inhibited enzyme" (21), or, in another publication: "With this new compound we have for the first time obtained large and indeed complete reactivation of diisopropyl fluorophosphate inhibition. The practical significance of this theory and of the new compound are self-evident" (24).

CHEMICAL MODIFICATION AND SPECTROSCOPIC STUDIES

During the years which elapsed after these pioneering achievements, which took place, for the most part in the early fifties, a massive body of structure-function work on AChE continued, due to its crucial role at cholinergic synapses, and consequently serving as a target for insecticides, nerve agents and certain drugs (25). But at the basic level, work on its mechanism of action was overshadowed by work on simpler and more accessible serine hydrolases (26). Thus the amino-acid sequence of chymotrypsin was known by mid-sixties, and its 3D structure had been solved by the end of the same decade (27). Much of the work on AChE focused on its quaternary structure and modes of anchoring (28, 29), and often went along with developmental studies (29). However, alongside this large body of structural and developmental work, there was a continuing effort to identify subsites and residues participating in enzymic activity, primarily by chemical modification, but also by use of absorption and fluorescence spectroscopy. Thus, the group of Palmer Taylor showed that propidium could serve as a probe for the 'peripheral' anionic site (30). The late Christian Hirth, who died an untimely death just after the Fourth Cholinesterase Meeting in Eilat, in 1992 (31), together with Maurice Goeldner, pioneered the elegant use of photoaffinity labels for characterization of AChE (32), as well as for the nAChR, as mentioned above (16, 17), and also of some ingenious suicide substrates (33), tools which could be eventually used, in combination with sequencing, to complement structural studies (20, 34).

EVIDENCE FOR AROMATIC RESIDUES IN THE ACTIVE SITE

Our own laboratory also adopted the chemical modification approach, together with absorption and fluorescence spectroscopy, to probe the active site of AChE. Like the results obtained by other groups, our data also indicated an important role for aromatic amino acid residues in or adjacent to the active site of AChE, and I present a number of examples.

Mooser et al. (35) had shown that the fluorescent ligand, *N*-methyl-acridinium (MAC) was a competitive inhibitor, whose fluorescence was quenched completely upon binding at the 'anionic' subsite of the active site. We extended his observations by showing that the spectrum of a complex of MAC with *Electrophorus* AChE displayed a new absorption band in the red, very similar to that observed for a complex of MAC with a low molecular weight tryptophan derivative (36). This spectral band was ascribed to formation of a charge-transfer complex by stacking of MAC against a tryptophan within the active site. This assignment was fully borne out by the X-ray structure of the complex in which tacrine was shown to be stacked against W84 of TcAChE (20).

Together with Shmaryahu Blumberg, we utilized a novel series of reagents, *N*-hydroxy-succinimide (NHS) esters of amino acid derivatives, which he had developed in the laboratory of Bert Vallee, at Harvard Medical School, for chemical modification of neutral proteases (37). Although modification by these reagents actually enhanced the activity of the neutral protease, they served as inhibitors of AChE, and their efficiency increased with the size of the side-chain, the best one tested being the NHS ester of *N*-acetyl-*p*-(2,4-dinitroanilino)-L-phenylalanine (38). It might be expected that inhibition would be by interaction with the active-site serine, as is the case for organophosphates and carbamates. However, we noticed that some residual activity always remained. Furthermore, if the enzyme was sequentially blocked by diethyl phosphorofluoridate and the NHS ester, yielding completely inactive enzyme, reactivation by 2-PAM produced the same residual

activity produced by inhibition with the NHS ester alone. These data proved that the NHS ester was inhibiting enzymic activity by modification of a residue distinct from the active-site serine, and the fact that rapid reactivation could be achieved by exposure to hydroxylamine suggested that a tyrosine phenolic group had been modified. Spectral examination of the conjugate further revealed a red shift in the absorption spectrum of the chromophore which could be ascribed to a charge transfer complex with the indole ring of a Trp residue. So it is plausible that the NHS ester is modifying a Tyr residue within the active-site gorge, e.g. Y121 or Y70, with its chromophore stacking against the indole of W279.

Irwin Wilson spent two sabbatical leaves at the Weizmann Institute, during one of which he studied the inhibition of AChE by arsenite. This reagent had earlier been shown to inhibit AChE by Mounter & Whittaker (39), but Irnie extended their studies and showed that inhibition was occurring via bimolecular kinetics, strongly suggesting that a covalent reaction was occurring (40). Arsenite is known to inhibit enzymes containing vicinal thiol groups, but the *Electrophorus* AChE was known to be devoid of free thiols (41). At the time, we proposed that arsenite might be acting by simultaneously modifying 2-3 suitably juxtaposed hydroxyl groups. Several years later, Irnie's student, Jimmy Page, showed that arsenite reduced by two the number of tyrosines available for modification by tetranitromethane in *Electrophorus* AChE (42). Now that we know that the gorge contains several conserved Tyr residues (12), it would be of interest to carry out docking studies in order to see which of them might be involved, or to try to locate them crystallographically in an arsenite-AChE crystalline complex.

CLONING AND SEQUENCING

AChE, together with butyrylcholinesterase (BChE), entered the modern (or maybe postmodern) era in the mid-eighties when, in a very short period of time, cloning of *TcAChE* by the Taylor laboratory (43), was followed by both sequencing and cloning of human BChE, by Lockridge, La Du and coworkers (44, 45), by cloning of human BChE by Soreq and coworkers (46), by cloning of *Torpedo marmorata* AChE by the Massoulié laboratory (47), and by cloning of *Drosophila* AChE by Hall & Spierer (48) in Geneva. The information so gained was of immense value to molecular geneticists and developmental biologists working on the cholinesterases, but produced very little progress in terms of structure-function relationships. Perhaps the only clear-cut advance was the identification of two of the three members of the catalytic triad, S200, by radioactive labeling (49), and H440 on the basis of consensus sequences (50) and site-directed mutagenesis (51). The third member of the triad, E327, had to await the 3D structure (12). In retrospect, one may ascribe this lack of progress both to the size of the catalytic subunit and to the fact that, as it turned out, the cholinesterases belong to a family with a novel fold, no member of which had yet been described, the α/β hydrolase fold family (52). Thus, except at the level of the catalytic triad, no useful comparisons could be made. Even for the triad, the fact that all the serine hydrolases then known contained an Asp residue as the acidic member of the triad turned out to be misleading, since both AChE and the homologous *G. candidum* lipase (53) turned out to have a Glu residue instead.

THE 3D STRUCTURE

So the 3D structure of AChE, when finally solved, came as a complete surprise to all of us! However, when one considers both the scope and accuracy of the predictions made by

Wilson and his coworkers, with the modest tools and data available to them, one has to ask if, by careful consideration of all the data available to us, we might not have been able to predict that the active site would be buried. These would include the extensive kinetic and spectroscopic data on the 'peripheral' and bisquaternary inhibitors, as well as the data of Wilson, referred to above, demonstrating the interaction of all four methyl groups of ACh with the enzyme, which he interpreted as indicating that, in the complex, the enzyme would envelope the substrate (10). But I think that all of us were overwhelmed by the high catalytic activity. Similarly, the ionic strength dependence, indicating several negatively charged groups in the active site (54), masked the large body of chemical modification data which might, if they had been viewed dispassionately, have suggested the possibility of quaternary ion- π electron interactions. Physical organic chemists and scientists studying host-guest interactions were aware of such interactions (55, 56) well before demonstration of W84 within the 'anionic' site by affinity labeling (57), and solution of the 3D structure of *Tc*AChE (12).

OPEN QUESTIONS

Although the 3D structure has now been at our disposal for over seven years, it has provided us with a whole set of new problems which await solution. Some of the principal questions, which are not mutually exclusive, are as follows: 1. Why is the active site deeply buried within the enzyme? 2. What is the functional significance of the array of aromatic residues which line the active-site gorge? 3. What is the role of the highly asymmetric distribution of charge? 4. What are the structural features which account for the unusually high catalytic activity, relative to other serine hydrolases? 5. Is there a 'back' or 'side' door, or does traffic of substrate and products proceed exclusively along the gorge axis?

Unlike Wilson and his colleagues, almost 50 years ago, we are fortunate in having at our disposal, at the end of the millennium, an extensive repertoire of experimental techniques, e.g. site-directed mutagenesis, steady-state and time-resolved x-ray crystallography, and a variety of spectroscopic methods, together with an arsenal of computational tools, combined with sophisticated computer graphics, such as molecular docking programs and molecular dynamics protocols.

The various techniques have allowed us to provide interim answers to some of the questions raised. Thus, as already mentioned, it is plausible that the deeply buried active-site permits a large reduction in the energy level of the transition state (13). The large dipole moment generated by the asymmetric charge distribution is aligned along the axis of the active-site gorge (58-60), suggesting that it plays a role in attraction of the positively charged substrate towards and down the gorge. Site-directed mutagenesis, resulting in elimination of seven of the negative charges responsible for the charge asymmetry, does not produce a dramatic change in kinetic constants (61). Nevertheless, it can be calculated that electrostatic steering is responsible for an increase in rate constants by about one order of magnitude (62), and that both long-range and short-range electrostatic forces contribute (63). Molecular dynamics simulations provide evidence in support of one or another 'side' or 'back' door hypothesis (64, 65). Furthermore, the residual catalytic activity observed in the presence of the snake venom toxin, fasciculin (66-68), which, on the basis of crystallographic evidence, appears to block the entrance to the active-site gorge completely (69, 70), also argues in favor of alternative routes to the active site. Again, site-directed mutagenesis experiments argue against such a possibility (71-73). It is hoped that time-resolved crystallography will provide a direct approach to this issue, and we are developing appropriate experimental tools (74, 75).

NONCHOLINERGIC FUNCTIONS

Finally, the pioneering observations suggesting noncatalytic and/or noncholinergic functions for AChE (76, 77) are being vindicated, and coming to fruition, in the context of the 3D structure of the enzyme. The fact that various adhesion proteins, such as glutactin (78) and neurotactin (79, 80), display significant sequence homology with AChE, but lack one or more of the key catalytic residues, was recognized even prior to elucidation of the 3D structure, in the wake of the cloning studies (81). But definition of the α/β hydrolase fold family (52, 82) led to the modeling of the extracellular domain of neurotactin on the basis of the 3D structure of TcAChE (83). On this basis, a chimeric construct was produced in which the extracellular domain of neurotactin was replaced by TcAChE or *Drosophila* AChE. The chimeric proteins were shown to be endowed with the same heterophilic adhesion properties as wild-type neurotactin (83). A comparison was made of the electrostatic characteristics of three such adhesion proteins, the *Drosophila* proteins, neurotactin (79) and gliotactin (84), and the mammalian protein, neuroligin (85), with those of various AChEs. This comparison permitted identification of a shared electrostatic motif (86) in the area corresponding to an annulus surrounding the entrance to the active-site gorge of the enzyme (87). These findings, examined in the context of previous evidence involving this same region in a possible cell-recognition functions for AChE (88, 89), suggest that the ChE-like domain of the adhesion proteins and of AChE may share a common recognition mechanism and/or ligand. This has led us to define a class of adhesion proteins which we have named the 'electrotactins' (87).

CONCLUDING REMARKS

It may be hoped that by the time of the 7th International Cholinesterase Meeting, early in the next millennium, just 50 years after the pioneering observations of Wilson, Bergmann and Nachmansohn, many of the controversies, relating to both catalytic and noncatalytic functions of the cholinesterases, will have been resolved. They will, however, surely have been replaced by a fresh set of interesting and challenging questions!

ACKNOWLEDGMENTS

The supported of the European Union, the U.S. Army Medical Research and Materiel Command, under Contract No. DAMD17-97-2-7022, and the Kimmelman Center for Biomolecular Structure and Assembly is gratefully acknowledged. I.S. is Bernstein-Mason Professor of Neurochemistry.

REFERENCES

1. Wilson, I.B.; Bergmann, F.; J. Biol. Chem. 1950, 185, 479-489
2. Wilson, I.B.; Bergmann, F.; J. Biol. Chem. 1950, 186, 683-692
3. Bergmann, F.; Wilson, I.B.; Nachmansohn, D.; J. Biol. Chem. 1950, 186, 693-703
4. Wilson, I.B.; Bergmann, F.; Nachmansohn, D.; J. Biol. Chem. 1950, 186, 781-790
5. Wilson, I.B.; J. Biol. Chem. 1950, 190, 111-117
6. Bergmann, F.; Wilson, I.B.; Nachmansohn, D.; Biochim. Biophys. Acta 1950, 6, 217-224
7. Wilson, I.B.; Biochim. Biophys. Acta 1951, 7, 466-470

8. Wilson, I.B.; *Biochim. Biophys. Acta* 1951, 7, 520-525
9. Froede, H.C.; Wilson, I.B.; *J. Biol. Chem.* 1984, 259, 11010-11013
10. Wilson, I.B.; *J. Biol. Chem.* 1952, 197, 215-225
11. Froede, H.C.; Wilson, I.B.; in *The Enzymes* (Ed. Boyer, P.D.), 3rd Ed. 1971, 5, 87-114
12. Sussman, J.L.; Harel, M.; Frolow, F.; Oefner, C.; Goldman, A.; Toker, L.; Silman, I.; *Science* 1991, 253, 872-879
13. Harel, M.; Quinn, D.M.; Nair, H.K.; Silman, I.; Sussman, J.L.; *J. Am. Chem. Soc.* 1996, 118, 2340-2346
14. Unwin, N.; *J. Mol. Biol.* 1996, 257, 586-596
15. Stauffer, D.A.; Karlin, A.; *Biochemistry* 1994, 33, 6840-6849
16. Dennis, M.; Giraudat, J.; Kotzyba-Hibert, F.; Goeldner, M.; Hirth, C.; Chang, J.Y.; Lazure, C.; Chrétien, M.; Changeux, J.P.; *Biochemistry* 1988, 27, 2346-2357
17. Galzi, J.-L.; Revah, F.; Bouet, F.; Ménez, A.; Goeldner, M.; Hirth, C.; Changeux, J.-P.; *Proc. Natl. Acad. Sci. USA* 1991, 88, 5051-5055
18. Karlin, A.; Akabas, M.H.; *Neuron* 1995, 15, 1231-1244
19. Nachmansohn, D.; *Harvey Lectures* 1955, Series XLIX, 57-99
20. Harel, M.; Schalk, I.; Ehret-Sabatier, L.; Bouet, F.; Goeldner, M.; Hirth, C.; Axelsen, P.; Silman, I.; Sussman, J.L.; *Proc. Natl. Acad. Sci. USA* 1993, 90, 9031-9035
21. Wilson, I.B.; Ginsburg, S.; *Biochim. Biophys. Acta* 1955, 18, 168-170
22. Dunn, M.A.; Sidell, F.R.; *J. Am. Med. Assoc.* 1989, 262, 649-652
23. Willems, J.L.; De Bisschop, H.C.; Verstraete, A.G.; Declerck, C.; Christiaens, Y.; Vanscheeuwyck, P.; Buy-laert, W.A.; Vogelaers, D.; Colardyn, F.; *Arch. Toxicol.* 1993, 67, 79-84
24. Wilson, I.B.; Meislich, E.; *J. Am. Chem. Soc.* 1953, 75, 4628-4629
25. Taylor, P.; in *The Pharmacological Basis of Therapeutics* (Eds. Gilman, G.A.; Rall, T.W.; Nies, A.; Taylor, P.), 8th Ed., 1990, 131-149, Pergamon, New York
26. Steitz, T.A.; Shulman, R.G.; *Ann. Rev. Biophys. Bioeng.* 1982, 11, 419-444
27. Blow, D.M.; in *The Enzymes* (Ed. Boyer, P.D.), 3rd Ed. 1971, 3, 185-212
28. Silman, I.; Futerman, A.H.; *Eur. J. Biochem.* 1987, 170, 11-22
29. Massoulié, J.; Pezzementi, L.; Bon, S.; Krejci, E.; Vallette, F.-M.; *Prog. Neurobiol.* 1993, 41, 31-91
30. Taylor, P.; Lwbuga-Mukasa, J.; Lappi, S.; Rademacher, J.; *Mol. Pharmacol.* 1974, 10, 703-708
31. Shafferman, A.; Velan, B.; *Multidisciplinary Approaches to Cholinesterase Functions* 1992, Plenum Press, New York
32. Goeldner, M.; Hirth, C.G.; *Proc. Natl. Acad. Sci. USA* 1980, 77, 6439-6442
33. Goeldner, M.; Hirth, C.G.; Kieffer, B.; Ourisson, G.; *Trends Biochem. Sci.* 1982, 7, 310-312
34. Ehret-Sabatier, L.; Schalk, I.; Goeldner, M.; Hirth, C.; *Eur. J. Biochem.* 1992, 203, 475-481
35. Mooser, G.; Schulman, H.; Sigman, D.S.; *Biochemistry* 1972, 11, 1595-1602
36. Shinitzky, M.; Dudai, Y.; Silman, I.; *FEBS Lett.* 1973, 30, 125-128
37. Blumberg, S.; Vallee, B.L.; *Biochemistry* 1975, 14, 2410-2419
38. Blumberg, S.; Silman, I.; *Biochemistry* 1978, 17, 1125-1130
39. Mounter, L.A.; Whittaker, V.P.; *Biochem. J.* 1953, 53, 167-173
40. Wilson, I.B.; Silman, I.; *Biochemistry* 1977, 16, 2701-2708
41. Rosenberry, T.L.; *Adv. Enzymol.* 1975, 43, 103-218
42. Page, J.D.; Wilson, I.B.; *J. Biol. Chem.* 1985, 260, 1475-1478
43. Schumacher, M.; Camp, S.; Maulet, Y.; Newton, M.; MacPhee-Quigley, K.; Taylor, S.S.; Taylor, P.; *Nature* 1986, 319, 407-409
44. Lockridge, O.; Barbells, C.F.; Vaughan, T.A.; Wong, C.K.; Norton, S.E.; Johnson, L.L.; *J. Biol. Chem.* 1987, 262, 549-557
45. McTiernan, C.; Adkins, S.; Chatonnet, A.; Vaughan, T.A.; Bartels, C.; Kott, M.; Rosenberry, T.L.; La Du, B.N.; Lockridge, O.; *Proc. Natl. Acad. Sci. USA* 1987, 84, 6682-6686
46. Prody, C.A.; Zevin-Sonkin, D.; Gnatt, A.; Goldberg, O.; Soreq, H.; *Proc. Natl. Acad. Sci. USA* 1987, 84, 3555-3559
47. Sikorav, J.L.; Krejci, E.; Massoulié, J.; *EMBO J.* 1987, 6, 1865-1873
48. Hall, L.M.C.; Spierer, P.; *EMBO J.* 1986, 5, 2949-2954
49. MacPhee-Quigley, K.; Taylor, P.; Taylor, S.; *J. Biol. Chem.* 1985, 260, 12185-12189
50. Doctor, B.P.; Gentry, M.K.; Wu, S.-J.; Ashani, Y.; De La Hoz, D.M.; in *Cholinesterases: Structure, Function, Mechanism, Genetics and Cell Biology* (Eds. Massoulié, J.; Bacou, F.; Barnard, E.; Chatonnet, A.; Doctor, B.P.; Quinn, D.M.), 1991, pp. 37-41, American Chemical Society, Washington, DC
51. Gibney, G.; Camp, S.; Dionne, M.; MacPhee-Quigley, K.; Taylor, P.; *Proc. Natl. Acad. Sci. USA* 1990, 87, 7546-7550

52. Ollis, D.L.; Cheah, E.; Cygler, M.; Dijkstra, B.; Frolo, F.; Franken, S.M.; Harel, M.; Remington, S.J.; Silman, I.; Schrag, J.; Sussman, J.L.; Verschueren, K.H.G.; Goldman, A.; *Protein Eng.* 1992, 5, 197-211
53. Schrag, J.D.; Li, Y.; Wu, S.; Cygler, M.; *Nature* 1991, 351, 761-764
54. Nolte, H.J.; Rosenberry, T.L.; Neumann, E.; *Biochemistry* 1980, 19, 3705-3711
55. Dhaenens, M.; Lacombe, L.; Lehn, J.-M.; Vigneron, J.-P.; *J. Chem. Soc. Chem. Commun.* 1984, 1097-1099
56. Dougherty, D.A.; Stauffer, D.A.; *Science* 1990, 250, 1558-1560
57. Weise, C.; Kreienkamp, H.-J.; Raba, R.; Pedak, A.; Aaviksaar, A.; Hucho, F.; *EMBO J.* 1990, 9, 3885-3888
58. Ripoll, D.; Faerman, C.; Axelsen, P.; Silman, I.; Sussman, J.L.; *Proc. Natl. Acad. Sci. USA* 1993, 90, 5128-5132
59. Tan, R.C.; Truong, T.N.; McCammon, J.A.; Sussman, J.L.; *Biochemistry* 1993, 32, 401-403
60. Felder, C.E.; Botti, S.A.; Lifson, S.; Silman, I.; Sussman, J.L.; *J. Mol. Graphics & Modeling* 1997, 15, 318-327
61. Shafferman, A.; Ordentlich, A.; Barak, D.; Kronman, C.; Ber, R.; Bino, T.; Ariel, N.; Osman, R.; Velan, B.; *EMBO J.* 1994, 13, 3448-3455
62. Antosiewicz, J.; McCammon, A.J.; Wlodek, S.T.; Gilson, M.K.; *Biochemistry* 1995, 34, 4211-4219
63. Botti, S.A.; Felder, C.; Lifson, S.; Sussman, J.L.; Silman, I.; this volume
64. Gilson, M.K.; Straatsma, T.P.; McCammon, J.A.; Ripoll, D.R.; Faerman, C.H.; Axelsen, P.H.; Silman, I.; Sussman, J.L.; *Science* 1994, 263, 1276-1278
65. Wlodek, S.T.; Clark, T.W.; Scott, R.L.; McCammon, A.J.; *J. Am. Chem. Soc.* 1997, 119, 9513-9522
66. Radic, Z.; Quinn, D.M.; Vellom, D.C.; Camp, S.; Taylor, P.; *J. Biol. Chem.* 1995, 270, 20391-20399
67. Eastman, J.; Wilson, E.J.; Cerveñansky, C.; Rosenberry, T.L.; *J. Biol. Chem.* 1995, 270, 19694-19701
68. Rosenberry, T.L.; Rabl, C.R.; Neumann, E.; *Biochemistry* 1996, 35, 685-690
69. Harel, M.; Kleywegt, G.J.; Ravelli, R.B.G.; Silman, I.; Sussman, J.L.; *Structure* 1995, 3, 1355-1366
70. Bourne, Y.; Taylor, P.; Marchot, P.; *Cell* 1995, 83, 503-512
71. Kronman, C.; Ordentlich, A.; Barak, D.; Velan, B.; Shafferman, A.; *J. Biol. Chem.* 1994, 269, 10854-10861
72. Faerman, C.; Ripoll, D.; Bon, S.; Le Feuvre, Y.; Morel, N.; Massoulié, J.; Sussman, J.L.; Silman, I.; *FEBS Lett.* 1996, 386, 65-71
73. Velan, B.; Barak, D.; Ariel, N.; Leitner, M.; Bino, T.; Ordentlich, A.; Shafferman, A.; *FEBS Lett.* 1996, 395, 22-28
74. Peng, L.; Silman, I.; Sussman, J.L.; Goeldner, M.; *Biochemistry* 1996, 35, 10854-10861
75. Ravelli, R.B.G.; Raves, M.L.; Ren, Z.; Bourgeois, D.; Roth, M.; Kroon, J.; Silman, I.; Sussman, J.L.; *Acta Cryst. D* 1998, in press
76. Greenfield, S.; Cheramy, A.; Leviel, V.; Glowinski, J.; *Nature* 1980, 284, 355-357
77. Layer, P.G.; *Proc. Natl. Acad. Sci. USA* 1983, 80, 6413-6417
78. Olson, P.F.; Fessler, L.I.; Nelson, R.E.; Stern, R.E.; Campbell, A.G.; Fessler, J.H.; *EMBO J.* 1990, 9, 1219-1227
79. Barthalay, Y.; Hipeau-Jacquotte, R.; De la Escalera, S.; Jiménez, F.; Poivant, M.; *EMBO J.* 1990, 9, 3603-3609
80. Hortsch, M.; Patel, N.H.; Bieber, A.J.; Traquina, Z.R.; Goodman, C.S.; *Development* 1990, 110, 1327-1340
81. Krejci, E.; Duval, N.; Chatonnet, A.; Vincens, P.; Massoulié, J.; *Proc. Natl. Acad. Sci. USA* 1991, 88, 6647-6651
82. Cygler, M.; Schrag, J.D.; Sussman, J.L.; Harel, M.; Silman, I.; Gentry, M.K.; Doctor, B.P.; *Protein Sci.* 1993, 2, 366-382
83. Darboux, I.; Barthalay, Y.; Poivant, M.; Hipeau-Jacquotte, R.; *EMBO J.* 1996, 15, 4835-4843
84. Auld, V.J.; Fetter, R.D.; Broadie, K.; Goodman, C.S.; *Cell* 1995, 81, 757-767
85. Ichtchenko, K.; Hata, Y.; Nguyen, T.; Ullrich, B.; Missler, B.; Moomaw, C.; Sudhof, T.C.; *Cell* 1995, 81, 435-443
86. Honig, B.H.; Nicholls, A.; *Science* 1995, 268, 1144-1149
87. Botti, S.A.; Felder, C.E.; Sussman, J.L.; Silman, I.; *Protein Eng.* 1998, 11, in press
88. Inestrosa, N.C.; Alvarez, A.; Pérez, C.A.; Moreno, R.D.; Vicente, M.; Linker, C.; Casanueva, O.I.; Soto, C.; Garrido, J.; *Neuron* 1996, 16, 881-891
89. Srivatsan, M.; Peretz, B.; *Neuroscience* 1997, 77, 921-931

QUATERNARY STRUCTURE OF TETRAMERIC ACETYLCHOLINESTERASE

Mia L. Raves,¹ Kurt Giles,^{1,2} Joseph D. Schrag,³ Michael F. Schmid,⁴
George N. Phillips, Jr.,⁵ Wah Chiu,⁴ Andrew J. Howard,⁶ Israel Silman,² and
Joel L. Sussman,^{1,7}

¹Department of Structural Biology

²Department of Neurobiology, Weizmann Institute of Science
Rehovot 76100, Israel

³Biotechnology Research Institute
Montreal, Quebec, H4P 2R2, Canada

⁴Department of Biochemistry, Baylor College of Medicine
Houston, Texas 77030

⁵Department of Biochemistry and Cell Biology, Rice University
Houston, Texas 77005

⁶Argonne National Laboratory
Argonne, Illinois 60439

⁷Biology Department, Brookhaven National Laboratory
Upton, New York 11973

INTRODUCTION

Most vertebrates contain a single gene encoding for AChE, and alternative splicing gives rise to two catalytic subunits, H and T. H subunits form GPI-anchored dimers, whereas T subunits can occur as monomers, dimers and tetramers, which are dimers of disulfide-linked dimers. T subunits also associate with structural subunits (P and Q) to form membrane-anchored tetramers and asymmetric forms, in which one to three tetramers are attached to a collagen-like tail (1).

The first known three-dimensional structure of AChE was that of *Torpedo californica* (TcAChE), which is a dimer of H subunits (2). Since then, the structure of AChE from other species has been determined, but all consist of H subunits (3,4). The only experimental evidence for the quaternary structure of tetrameric AChE was obtained from crystals of *Electrophorus electricus* AChE (EeAChE). The tetramers were obtained by tryptic cleavage of asymmetric forms of EeAChE.

Crystals of the eel enzyme were reported as early as 1968 (5), and the first diffraction experiments were described in 1975 (6). The crystals took a few years to grow to a

useable size, and diffracted to about 4 Å resolution. A few precession photographs were taken, giving space group $P6_22$ ($a=b=187$ Å, $c=292$ Å). In 1988 a new crystal form was reported, orthorhombic $F222$ ($a=141.0$ Å, $b=202.4$ Å, $c=237.4$ Å), with crystals that grew up to 0.8 mm long in a few days (7). A data set was collected with this crystal form, to 4.4 Å resolution, but no heavy-atom derivatives were found. When the structure of *TcAChE* to 2.8 Å resolution was published in 1991 (2), work on this structure was discontinued.

In higher vertebrates, the predominant molecular forms of AChE are all based on T subunits. With reports of new clinically important drugs having selectivity for certain molecular forms (8), it is important to understand the molecular basis for the association of catalytic subunits with one another and with structural subunits. Since the data on *EeAChE* represent the only published data on a tetrameric form of AChE, elucidation of the structure was attempted.

METHODS

The raw data consist of 360 frames with an oscillation step of 0.25° , which were collected on an in-house rotating anode at Argonne National Laboratory (7). The data were processed with XENGEN v1.2 (9) to 4.4 Å resolution, giving 10,192 unique reflections with a completeness of 92% (99% to 4.66 Å) and an R_{sym} of 14.1%.

The asymmetric unit of the crystal was expected to contain two monomers, related by non-crystallographic symmetry (see below). For molecular replacement, the coordinates of the native *TcAChE* structure (10) were used in the program AMORE (11). The search for a monomer yielded only one peak in the cross-rotation search, instead of the expected two. This solution gave an R-factor of 42.2% and a correlation coefficient of 61.7%, over a background of solutions with R-factors higher than 50%. A second solution could not be found, even when the first solution was fixed and a second one was searched for. The self-rotation search basically shows only 180° rotations in three orthogonal directions, which coincide with the crystallographic twofold symmetry.

RESULTS

In the crystal structure of *EeAChE*, a solution was found for the position and the orientation of the protein molecule in the unit cell of the experimental data, using molecular replacement. Starting with this solution for the monomer, one of the three crystallographic twofold axes generates a proper biological dimer, with a four-helix bundle at the interface, as is seen in crystal structures of other species of AChE (2-4). A second twofold axis, perpendicular to the first, reveals the relative arrangement of dimers in a tetramer, with a slight twist of $\sim 20^\circ$ from planarity (Fig. 1).

There is a large gap between the two dimers, about 30 Å wide, where the four C-termini point towards each other. This space is most likely to be partly occupied by the extra 4 times 40 residues at the C-termini (12). An electron-density difference map shows very little density in the gap, which may be due to the current resolution and R-factor.

DISCUSSION

Based on sequence analysis, biochemical analysis and mutagenesis studies, a model was recently constructed of the additional ~ 40 C-terminal residues in the T form of AChE. Using this model, combined with spatial information such as the proximity of the four C-terminal cysteines, an arrangement for the monomers in the AChE tetramer was proposed.

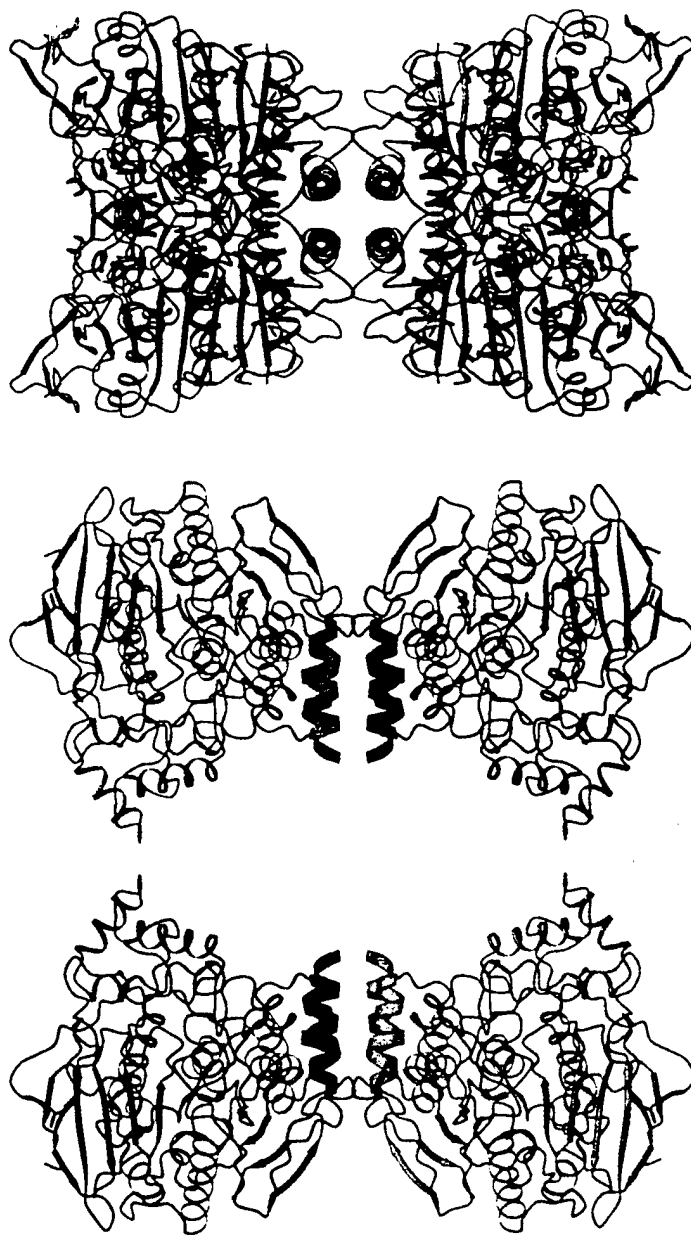


Figure 1. Tetramer of *EeAChE* in two orthogonal views looking down one of the twofold axes. The familiar dimers, their four-helix bundles highlighted with thick ribbons, are shown vertically. The second picture is rotated by 90° around the y axis, compared to the orientation of the first. A color version of this figure appears on the color insert facing page xxvi.

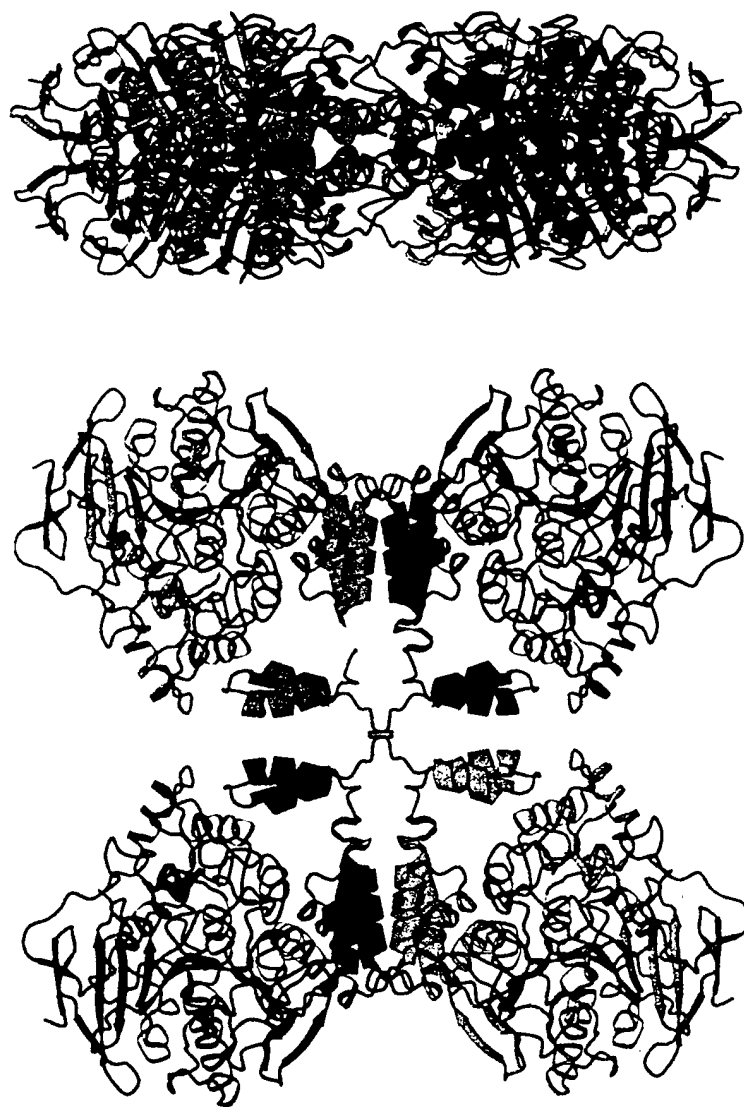


Figure 2. Square-planar arrangement of monomers in a model of tetrameric AChE. The familiar dimers are shown vertically; at the interface in the center, the extra C-terminal regions form additional four-helix bundles. All four-helix bundles are highlighted with thick ribbons. The second picture is rotated by 90° around the y axis, compared to the orientation of the first. A color version of this figure appears on the color insert facing page xxvi.

prior to the determination of the crystal structure. In this model, four subunits form a pseudo-square arrangement (Fig. 2). At the interface between the two dimers, the mostly helical fragments form two additional four-helix bundles (12).

Comparison of Figs. 1 and 2 immediately shows the excellent agreement between the model and the crystal structure, apart from the twist between the two dimers.

Schrag *et al.* (7) determined the protein content of the unit cell to be about 60%, on the basis of the measured density of the crystals (1.25 g/cm^3) and the specific volume of the *EeAChE* tetramer ($0.714 \text{ cm}^3/\text{g}$). Using the unit cell volume ($141.20 \times 202.20 \times 237.30 \text{ \AA}^3$) and the number of equivalent positions in space group F222 (*viz.* 16), the specific weight of the asymmetric unit was calculated to be $206,000 \text{ g/mol}$. If it is assumed that two monomers occupy the asymmetric unit, the density measurements can be reconciled with the calculated solvent content and the weight percentage of protein. This assumption also gives a reasonable number for Matthew's coefficient ($V_M=3.2$).

In analogy to dimeric trigonal *TcAChE*, the monomers in a tetramer of *EeAChE* were expected to be related by crystallographic two-fold symmetry, since the unit cell contains no less than three intersecting twofold axes. The two monomers in the asymmetric unit were, therefore, expected to be related by non-crystallographic symmetry. However, the search for a monomer yielded only one peak in the cross-rotation search, instead of two, resulting in a rather sparsely occupied asymmetric unit.

Despite the limited success with molecular replacement, the initial goal was achieved, since the crystallographic 222 symmetry applied to the monomer gave the structure of the *EeAChE* tetramer. The fact that a proper dimer with a four-helix bundle at the interface was obtained, strongly argues that the molecular replacement solution, and, therefore, the crystallographic model of the tetramer, is correct.

Nevertheless, using all 16 symmetry operations, generating four tetramers, to obtain the full packing of the unit cell shows that there are large voids that could easily and neatly be occupied by four more tetramers by simple translation of the obtained tetramers by half the *c* axis. The empty spaces have a volume of $70 \times 100 \times 120 \text{ \AA}^3$, large enough for an entire *AChE* tetramer. It was therefore suspected that the unit cell dimensions and/or the space group might not have been determined correctly. With this suspicion in mind, the data were reprocessed using X-GEN, the modern version of XENGEN (9). The resulting data set still had the same space group and similar unit cell dimensions, and yielded the same results in molecular replacement.

In the current structure, the calculated solvent content of the crystal is 81% ($V_M=6.5$). A second molecular replacement solution, which would have provided another four tetramers to pack into the unit cell, could not be found. This could mean that the additional tetramers are either disordered, or simply absent. Even though a solvent content higher than 80% is uncommon, there are other known cases.

CONCLUSIONS

The quaternary structure of the tetramer of *EeAChE* has been solved, using the structure of a *TcAChE* monomer as a model. In the resulting structure, the relative positioning of subunits is in excellent agreement with a recently proposed model (12) except that the dimers are slightly twisted with respect to one another, rather than coplanar. The fact that the crystallographic symmetry applied on the *EeAChE* monomer yields a dimer, with a four-helix bundle at the interface, as seen in the *TcAChE* structure, indicates that

the obtained structure of the tetramer is correct. This is the first crystallographic determination of the quaternary structure of a tetrameric form of AChE.

REFERENCES

1. Massoulié, J.; Pezzementi, L.; Bon, S.; Krejci, E.; Vallette, F.-M.; *Prog. Neurobiol.* 1993, 41, 31-91
2. Sussmán, J.L.; Harel, M.; Frolow, F.; Oefner, C.; Goldman, A.; Toker, L.; Silman, I.; *Science* 1991, 253, 872-879
3. Bourne, Y.; Taylor, P.; Marchot, P.; *Cell* 1995, 83, 503-512
4. Kryger, G.; Giles, K.; Harel, M.; Toker, L.; Velan, B.; Lazar, A.; Kronman, C.; Barak, D.; Ariel, N.; Shaffer, A.; Silman, I.; Sussman, J.L.; these proceedings
5. Leuzinger, W.; Baker, A.L.; Cauvin, E.; *P.N.A.S.* 1968, 59, 620-623
6. Chothia, C.; Leuzinger, W.; *J. Mol. Biol.* 1975, 97, 55-60
7. Schrag, J.D.; Schmid, M.F.; Morgan, D.G.; Phillips Jr., G.N.; Chiu, W.; Tang, L.; *J. Biol. Chem.* 1988, 263, 9795-9800
8. Enz, A.; Chappuis, A.; Probst, A.; In *Multidisciplinary Approaches to Cholinesterase Functions*: A. Shaffer, man and B. Velan, Eds.; Plenum Press, New York, 1992, 243-249
9. Howard, A.J.; Gilliland, G.L.; Finzel, B.C.; Poulos, T.L.; Ohlendorf, D.H.; Salemme, F.R.; *J. Appl. Cryst.* 1987, 20, 383-387
10. Raves, M.L.; Harel, M.; Pang, Y.-P.; Silman, I.; Kozikowski, A.P.; Sussman, J.L.; *Nature Structural Biology* 1997, 4, 57-63
11. Navaza, J.; *Acta Cryst.* 1994, A50, 157-163
12. Giles, K.; *Protein Engineering* 1997, 10, 677-685

3D STRUCTURE OF A COMPLEX OF THE ANTI-ALZHEIMER DRUG, E2020, WITH ACETYLCHOLINESTERASE AT 2.5Å RESOLUTION

Gitay Kryger,¹ Israel Silman,² and Joel L. Sussman^{1,3}

¹Department of Structural Biology, Weizmann Institute of Science
Rehovot 76100, Israel

²Department of Neurobiology, Weizmann Institute of Science
Rehovot 76100, Israel

³Biology Department, Brookhaven National Laboratory
Upton, New York 11973

INTRODUCTION

Observations documenting adverse effects of anticholinergic drugs on memory, taken together with postmortem data which revealed low cholinergic activities in Alzheimer's Disease (AD) patients, led to the hypothesis, known as the 'cholinergic hypothesis', that AD is associated with an impairment in cholinergic transmission (1). This led to the suggestion that cholinesterase (ChE) inhibitors would reverse deficits in acetylcholine (ACh) levels associated with AD, and thus might reverse the memory impairments characteristic of the disease. Consequently, a number of ChE inhibitors have been considered as candidates for the symptomatic treatment of AD, and have been utilized in clinical trials. They include natural substances, such as physostigmine (2) and huperzine A (3), both of which are alkaloids, and synthetic compounds, such as SDZ ENA-713, also known as Exelon® (4), and metrifonate (5). Recently, evidence was presented that AChE may contribute to the generation of amyloid proteins and/or physically affect the process of fibril assembly which results in the formation of the senile plaques characteristic of AD (6). It was suggested that a hydrophobic environment close to the peripheral binding site of the enzyme, at or near the entrance to the active-site gorge, may be involved in this process (7).

The first two drugs, and the only ones so far, approved by the FDA for the management of AD, are both reversible inhibitors of AChE, namely tacrine (THA), approved in

Structure and Function of Cholinesterases and Related Proteins,
edited by Doctor *et al.*, Plenum Press, New York, 1998.

1993, and marketed as Cognex[®] (8), and the more potent ChE inhibitor, E2020 ((R,S)-1-benzyl-4-[(5,6-dimethoxy-1-indanon)-2-yl]methylpiperidine), also known by its trivial name donepezil hydrochloride, and marketed as Aricept[®], which was approved in 1996 (9). E2020 is a member of a large family of N-benzylpiperidine-based AChE inhibitors which were developed, synthesized and evaluated by Eisai Company Ltd. in Japan (10) on the basis of QSAR studies (11,12) prior to elucidation of the 3D structure of *Torpedo californica* AChE (*TcAChE*) (13). It was shown to significantly enhance performance in animal models of cholinergic hypofunction (14), and to have high affinity for AChE, binding to both electric eel and mouse AChE in the nanomolar range (15). THA and E2020 share the same target, but while THA must be administered up to four times a day, and is associated with hepatotoxicity, slow pharmacokinetics and high incidence of side effects, E2020 offers the patient significant improvements by being administered only once daily, and by having fewer side effects. Furthermore, E2020 displays high selectivity for AChE relative to butyrylcholinesterase (BChE); this may be important, since it has been suggested that inhibition of BChE, abundant in human plasma, may cause potentiating side effects (16,17). Thus the affinity of E2020 for human AChE is ~1000 fold greater than for human BChE, whereas THA has a similar affinity for the two enzymes.

EXPERIMENTAL

Protein Preparation and Crystallization

TcAChE was purified and crystallized as described previously (18). E2020, as the hydrochloride salt of the pure racemate, was a generous gift from Dr. B.P. Doctor (Division of Biochemistry, Walter Reed Army Institute of Research, Washington, DC). *TcAChE* crystals were soaked in ~10mM (R,S)-E2020 for five days at 4°C, and flash cooled to 100°K.

X-Ray Data Collection and Processing

Data were collected 'in-house', at the Weizmann Institute of Science, on a Rigaku FR300 generator set at 50mA, 50kV and 1.54184Å wavelength (Cu K_α radiation), equipped with a Rigaku RAXIS-II detector.

Model Refinement and Analysis

The structure was refined on the basis of the starting model of native *TcAChE* (PDB ID 2ACE), using only the polypeptide and none of the solvent atoms, employing XPLOR (19). Voids were calculated between the inhibitor molecule as one entity, and the protein and solvent molecules as a second entity (20).

RESULTS AND DISCUSSION

The 3D structure of the complex shows more detail of the AChE structure than the starting native model (2ACE). Primarily, residues 2 and 3, at the N-terminus, and the 484-490 loop, which were not seen in the original model, can be discerned. In addition, it was possible to model the proximal N-acetyl glucosamine (NAG) moiety at four out of five putative glycosylation sites, viz. at residues Asn59, Asn416 (where two NAG moieties

Table 1. Data collection and refinement statistics

Data Collection	
Resolution range (Å)	30.0 - 2.5
No. of reflections	34264
No. of unique reflections	15670
Completeness (%)	98.1
R _{sym} (%)	5
Refinement	
No. of protein non-hydrogen atoms	4255 = 2137 m.c. + 2118 s.c.
No. of hetero non-hydrogen atoms:	
Water molecules	396
Carbohydrate	5 x 14 = 70 in five NAG groups
Inhibitor	28 in one E20 group
Resolution (Å)	2.5
R _{work} (%)	18.8 (no s cutoff)
R _{free} (%)	22.9 (no s cutoff)
Average B-factor (Å ²):	
Main chain	27.19
Side chain	28.75
Protein	27.97
Inhibitor	20.40
Carbohydrate	47.62
Water molecules	37.19
All atoms	28.98
RMSD bond length (Å)	0.005
RMSD bond angle (°)	1.2
RMSD dihedral angle (°)	22.9
RMSD improper angle (°)	0.98

$$R_{\text{merge}} = \frac{\sum |I_i - \langle I \rangle|}{\sum I_i}$$

$$R_{\text{work}} = \frac{\sum ||F_o| - |F_c||}{\sum |F_o|}$$

R_{free} is calculated using 2000 randomly selected reflections excluded from the refinement

could be fitted), Asn457 and Asn533. An analysis of the quality of the refined model is summarized in Table 1.

ALL THREE SEGMENTS OF E2020 INTERACT WITH AChE

E2020 binds along the active site gorge. All three major segments of the elongated molecule make specific interactions with the enzyme, and each of these interactions involves discrete water-mediated contacts which appear crucial for specificity (figure 1). E2020 makes principal interactions with the enzyme through: 1) the benzyl moiety; 2) the piperidine nitrogen, and 3) the dimethoxyindanone moiety. It is material to recognize how the ligand utilizes the aromatic residues, which line the gorge in abundance, for hydrophobic and π -stacking interactions, and does not make direct contact with the protein though such interactions as H-bonds or salt-bridges other than via water molecules.

Interactions at the Bottom of the Gorge

Near the bottom of the gorge, one face of the benzyl ring makes a classic parallel π - π stacking with the six-membered ring of the W84 indole, similarly to THA (21). It thus oc-

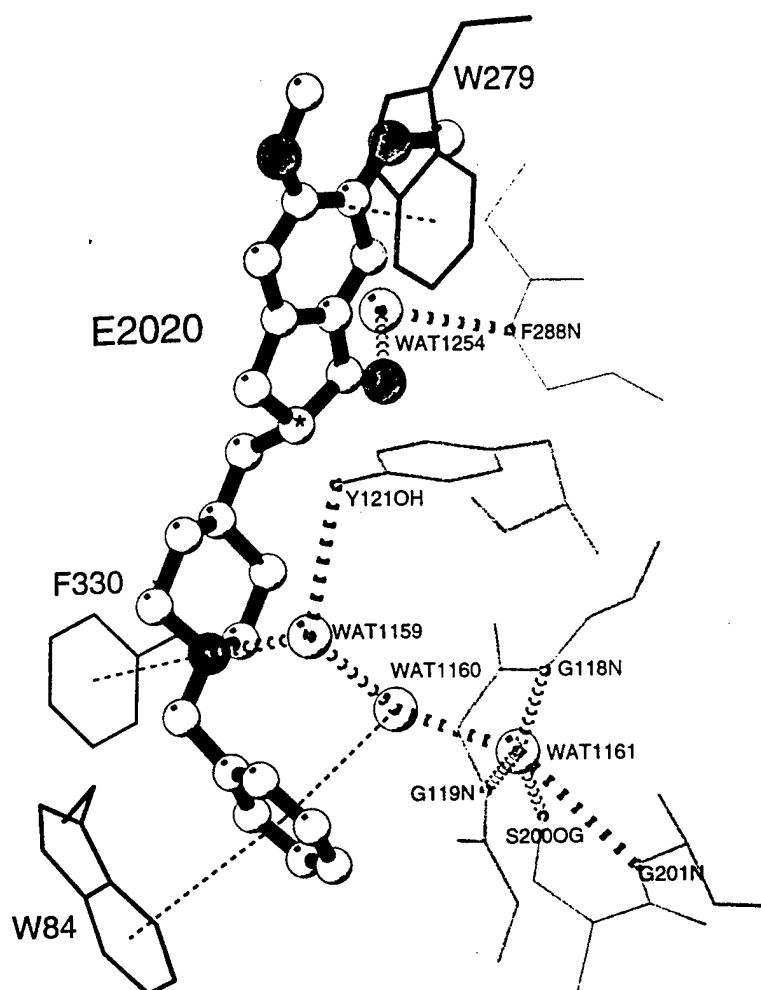


Figure 1. Binding modes of E2020 to AChE. E2020 is displayed as a ball-and-stick model (chiral center marked with black star); direct binding residues are represented as dark grey sticks, water-mediated binding residues as light grey sticks, water molecules as light grey balls, "standard" H-bonds as heavy dashed lines, aromatic H-bonds, π -cation and π - π stacking as light dashed lines

cupies the binding site occupied by quaternary ligands, such as edrophonium (21), and modeled for the quaternary group of the natural substrate, ACh (13,22). On the opposite face, the benzyl group makes a classic aromatic hydrogen bond with a water molecule (WAT1160). This water is held firmly by a hydrogen bond to another water molecule (WAT1161), in the "oxyanion hole", and to WAT1159. WAT1161 is another example of a tightly bound water molecule; it makes a hydrogen bond with the residues of the oxyanion hole and with S200OG. E2020 does not interact directly either with the catalytic triad or with the "oxyanion hole".

Interactions in the Middle of the Gorge

In the constricted region, halfway up the gorge, the charged nitrogen of the piperidine ring makes a cation- π interaction (23,24) with the phenyl ring of F330. The ring nitro-

gen also makes an in-line H-bond with WAT1159. As already mentioned, the binding site for the quaternary nitrogen of ACh within the active site, and for homologous ligands, is the indole ring of W84 (13). These data suggest that F330 may serve as an additional quaternary binding site, of possible functional significance, midway down the gorge, between the peripheral binding site and the anionic subsite of the active site.

Interactions at the Entrance to the Gorge

At the top of the gorge, the indanone ring stacks against the 6-membered ring of the indole moiety of W279, in the peripheral binding site, in a classic parallel π - π interaction. The fact that the binding of E2020 is strongly dependent on interaction with W279 and F330, which are absent in BChE, may explain its high relative specificity for AChE vs. BChE. The carbonyl function on the indanone is not in direct contact with the protein, but appears to make a water-bridged contact with F288N.

ONLY ONE ENANTIOMER OF E2020 IS BOUND TO AChE

The reported pharmacological studies on E2020 emphasize that both enantiomers are active, and even exhibit similar, but not identical, binding affinities for AChE (25,26). Based on these reports, and on the fact that we used the racemate in our crystallographic study, we expected either to find evidence, in the form of electron density, for the presence of both enantiomers in the crystal structure, or partial disorder which would support the presence of both. Yet, when an attempt was made to fit a number of plausible inhibitor conformations within the active-site gorge, a unique fit to the experimental electron density was found for one conformation of the R form, which is also very similar to our energetically minimized E2020 conformation, with the indanone carbonyl group pointing towards F288N as mentioned above. Thus, the enzyme appears to have bound the R form selectively, despite the similarity in binding constants. Selective binding cannot be due to a limitation in the amount of S form, since (R,S)-E2020 was soaked into the crystal at 10mM, i.e. at a great molar excess. It should also be noted that the two enantiomers of E2020 interconvert readily in aqueous solution, via a ketoenol intermediate (27). It is not immediately obvious what could cause such a preferential binding of one form, taking into account their similar affinities. It should, however, be born in mind that not only are the ligand and active site chiral, but also the entire lattice of the crystalline enzyme into which the E2020 is being soaked. A chiral environment, such as a protein, a crystal lattice, or any biological system, may cause the stereoisomers to tautomerize at different rates. Based on steric considerations, it appears that both the R and S enantiomers could bind in very similar conformations, with only the position of the carbonyl function on the 5-membered ring of the indanone moiety distinguishing between them. A model which we built displaying a carbonyl on the other side of the indanone, representing the S form, does not make contact with any protein atom, and thus might be bound less tightly than the observed R form, even though this is inconsistent with the published inhibition data (25). Furthermore, the 4.0Å link between the indanone carbonyl and F288N, whether bridged by a water molecule or not, combined with the fact that the carbonyl "nests" amongst three aromatic systems of residues F288, F290 and F331, might be sufficient to introduce a bias in favor of preferential binding of the R form. As already mentioned, R-S interconversion, via tautomerization, is known to occur, and might indeed take place under the experimental

conditions employed. Thus, one explanation for the inhibitory potency of the S form would invoke AChE-induced S-to-R tautomerization.

STRUCTURE-BASED MODIFICATION OF E2020

Chemical modification of an already effective drug can often improve its pharmacological profile in terms of affinity and specificity. The calculated "empty" spaces within the gorge which are revealed in the 3D structure of the E2020/AChE complex point to candidate sites on the ligand where added functions might indeed enhance its pharmacological profile. Separation of enantiomers, which are chemically indistinguishable by non-chiral environments, is difficult, inefficient and costly. In the case of E2020, we suggest that introduction of a second chiral center, with concomitant generation of a diastereomer system, would facilitate isolation of an active component from the mixture so generated. Inspection of the "empty" spaces left within the aromatic gorge by the ordered solvent and by E2020 reveals a finger-shaped void at the acyl-binding pocket. This pocket, defined by F288, F290, F331 and W233, could envelop a non-polar substituent branching from the piperidine ring at position E2020:C12. A substituent on the piperidine, which would interact with the "acyl pocket", combined with the existing chiral center, would produce a separable diastereomeric inhibitor.

The recent observations, mentioned above, concerning the effect of peripheral-site ligands on AChE-enhanced amyloid deposition (6), raise the possibility that E2020, which our data clearly show as stacking against W279, might also moderate the rate of fibril formation. Many of the compounds synthesized and tested by the Eisai company involved modification of this segment of the molecule (11,12). But it should be borne in mind that the screening which they carried out involved assessment of affinity for AChE, together with selectivity for AChE relative to BChE, not a possible effect on amyloid fibril assembly or deposition.

ACKNOWLEDGMENTS

This work was supported by the U.S. Army Medical Research Acquisition Activity under Contract No. DAMD17-97-2-7022, the Kimmelman Center for Biomolecular Structure and Assembly, Rehovot, Israel, the European Union, and the generous support of Tania Friedman. I.S. is Bernstein-Mason Professor of Neurochemistry.

REFERENCES

1. Dunnett, S. B.; Fibiger, H. C. *Prog. Brain Res.* **1993**, *98*, 413-420.
2. Davis, K. L.; Mohs, R. C.; Tinklenberg, J. R.; Pfefferbaum, A.; Hollister, L. E.; Kopell, B. S. *Science* **1978**, *201*, 272-4.
3. Cheng, D. H.; Ren, H.; Tang, X. C. *Neuroreport* **1996**, *8*, 97-101.
4. Enz, A.; Boddeke, H.; Gray, J.; Spiegel, R. *Ann. NY Acad. Sci.* **1991**, *640*, 272-5.
5. van der Staay, F. J.; Hinz, V. C.; Schmidt, B. H. *J. Pharmacol. Exp. Ther.* **1996**, *278*, 697-708.
6. Inestrosa, N. C.; Alvarez, A.; Perez, C. A.; Moreno, R. D.; Vicente, M.; Linker, C.; Casanueva, O. I.; Soto, C.; Garrido, J. *Neuron* **1996**, *16*, 881-91.
7. Reyes, A. E.; Perez, D. R.; Alvarez, A.; Garrido, J.; Gentry, M. K.; Doctor, B. P.; Inestrosa, N. C. *Biochem Biophys. Res. Commun.* **1997**, *232*, 652-5.

8. Davis, K. L.; Thai, L. J.; Gamzu, E. R.; Davis, C. S.; Woolson, R. F.; Gracon, S. I.; Drachman, D. A.; Schneider, L. S.; Whitehouse, P. J.; Hoover, T. M.; Morris, J. C.; Kawa, C. H.; Knopman, D. S.; Earl, N. L.; Kuman, V.; Doody, R. S.; Group, T. C. S. *N. Engl. J. Med.* **1992**, *327*, 1253-1259.
9. Nightingale, S. L. *J. Am. Med. Assn.* **1997**, *277*, 10.
10. Kawakami, Y.; Inoue, A.; Kawai, T.; Wakita, M.; Sugimoto, H.; Hopfinger, A. J. *Bioorg. Med. Chem. Letts.* **1996**, *4*, 1429-46.
11. Cardozo, M. G.; Imura, Y.; Sugimoto, H.; Yamanishi, Y.; Hopfinger, A. J. *J. Med. Chem.* **1992**, *35*, 584-589.
12. Cardozo, M. G.; Kawai, T.; Imura, Y.; Sugimoto, H.; Yamanishi, Y.; Hopfinger, A. J. *J. Med. Chem.* **1992**, *35*, 590-601.
13. Sussman, J. L.; Harel, M.; Frolov, F.; Oefner, C.; Goldman, A.; Toker, L.; Silman, I. *Science* **1991**, *253*, 872-9.
14. Rupniak, N. M.; Tye, S. J.; Field, M. J. *Psychopharmacol. Berl.* **1997**, *131*, 406-10.
15. Galli, A.; Mori, F.; Benini, L.; Cacciarelli, N. *Eur. J. Pharmacol.* **1994**, *270*, 189-193.
16. Loewenstein, Y.; Gnatt, A.; Neville, L. F.; Soreq, H. *J. Mol. Biol.* **1993**, *234*, 289-96.
17. Thomsen, T.; Kewitz, H. *Life Sci.* **1990**, *46*, 1553-8.
18. Raves, M. L.; Harel, M.; Pang, Y.-P.; Silman, I.; Kozikowski, A. P.; Sussman, J. L. *Nature Struct. Biol.* **1996**, *4*, 57-63.
19. Brünger, A. T.; Kuriyan, J.; Karplus, M. *Science* **1987**, *235*, 458-460.
20. Laskowski, R. A. *J. Mol. Graph.* **1995**, *323-330*.
21. Harel, M.; Schalk, I.; Ehret Sabatier, L.; Bouet, F.; Goeldner, M.; Hirth, C.; Axelsen, P. H.; Silman, I.; Sussman, J. L. *Proc. Natl. Acad. Sci. U S A* **1993**, *90*, 9031-5.
22. Harel, M.; Quinn, D. M.; Nair, H. K.; Silman, I.; Sussman, J. L. *J. Am. Chem. Soc.* **1996**, *118*, 2340-2346.
23. Dougherty, D. A.; Stauffer, D. A. *Science* **1990**, *250*, 1558-1560.
24. Dougherty, D. *Science* **1996**, *271*, 163-168.
25. Inoue, A.; Kawai, T.; Wakita, M.; Imura, Y.; Sugimoto, H.; Kawakami, Y. *J. Med. Chem.* **1996**, *39*, 4460-4470.
26. Sugimoto, H.; Imura, Y.; Yamanishi, Y.; Yamatsu, K. *Bioorg. Med. Chem. Letts.* **1992**, *2*, 871-876.
27. Matsui, K.; Oda, Y.; Ohe, H.; Tanaka, S.; Asakawa, N. *J. Chromatogr. A* **1995**, *694*, 209-18.

CRYSTAL STRUCTURES OF "AGED" PHOSPHORYLATED AND PHOSPHONYLATED *TORPEDO CALIFORNICA* ACETYLCHOLINESTERASE*

Charles B. Millard,^{1,2} Gitay Kryger,³ Arie Ordentlich,⁴ Michal Harel,³
Mia L. Raves,³ Harry M. Greenblatt,³ Yoffi Segall,⁴ Dov Barak,⁴
Avigdor Shafferman,⁴ Israel Silman,² and Joel L. Sussman^{3,5}

¹U.S. Army Medical Research Institute of Chemical Defense
APG, Maryland 21010

²Department of Neurobiology

³Department of Structural Biology
Weizmann Institute of Science
Rehovot 76100, Israel

⁴Israel Institute for Biological Research
Ness Ziona 70450, Israel

⁵Biology Department
Brookhaven National Laboratory
Upton, New York 11973

BACKGROUND

Acetylcholinesterase (AChE; EC 3.1.1.7) is an especially efficient serine hydrolase that catalyzes acetylcholine (ACh) hydrolysis at the neuromuscular junction (reviewed in 1). The catalytic pathway includes an acyl-enzyme intermediate that is hydrolyzed with a half-time of approximately 50 μ sec (2). The acylation-deacylation mechanism renders AChE susceptible to rapid, stoichiometric and essentially irreversible inhibition by a class of organophosphate (OP) inhibitors, typified by diisopropylphosphorofluoridate (DFP) and the phosphonate nerve agents, which react as "hemisubstrates" to yield stable analogs of the deacylation transition state.

* The opinions or assertions contained herein belong to the authors and are not necessarily the official views of the U.S. Army or the U.S. Department of Defense.

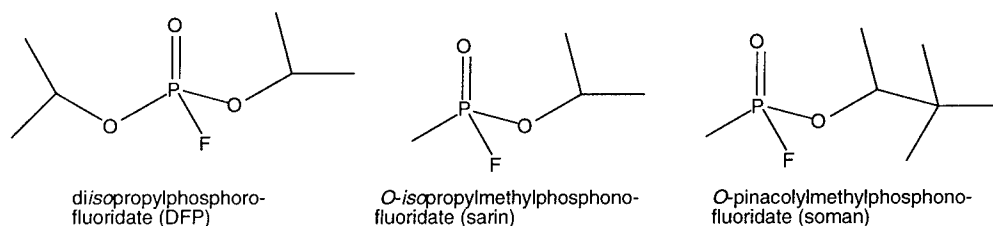


Figure 1. Structures of OP Inhibitors

Unlike the intermediates formed by carboxyl ester substrates, the OP-enzyme persists for many hours or days (reviewed in 3). The prolonged stability of phosphonylated AChE accounts for the high toxicity of nerve agents. Slow hydrolysis has been explained by steric exclusion; the active site histidine residue is not positioned to carry a water molecule to the correct face of the phosphorus required for nucleophilic attack (4,5). It also has been proposed that the catalytic His is immobilized by unproductive hydrogen bonding with an oxygen atom of the OP (6). Some OP-AChE conjugates undergo an internal dealkylation reaction, called "aging," which has been proposed to introduce a formal negative charge that further stabilizes the phosphoenzyme (7).

The three-dimensional structures of AChE (8) and computer-based homology models of related cholinesterases, combined with site-directed mutagenesis studies, have permitted tentative identification of specific amino acid residues which constitute several catalytic subsites, including an oxyanion hole, an acyl pocket, and a choline binding site (also called the "anionic site") (9-12). Direct testing of these hypothetical domains with natural substrates has not yet been achieved because of the inherent instability of the acyl-enzyme. Our goal was to solve structures of phosphylated* AChEs as a means of: (i) understanding the basis for stability of the aged, OP-enzyme complex, and (ii) providing structural models for intermediates of carboxyl ester hydrolysis that could validate hypothetical catalytic subsites.

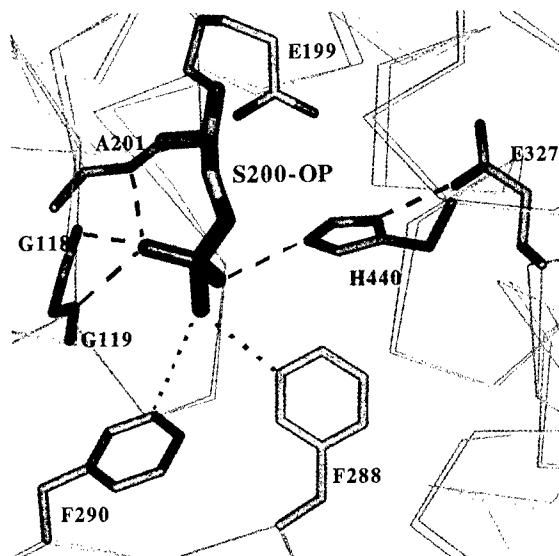
MATERIALS AND METHODS

AChE was purified from *Torpedo californica* (Tc) and inhibited with DFP, *O*-isopropylmethylphosphonofluoridate (sarin), or *O*-pinacolylmethylphosphonofluoridate (soman) (Figure 1). DFP and sarin were used at 300-fold molar excess to enzyme, and soman was used at a 2,100-fold molar excess. Enzyme was allowed to undergo complete aging in solution (>95% aged as judged by no reactivation after incubation in 10mM 2-PAM or TMB-4 for 20 hrs).

Excess OP was removed by gel filtration and aged OP-AChE was crystallized by the hanging drop method using PEG-200 as precipitant in 0.25M MES buffer, pH 5.8, 4°C. Protein crystals were flash cooled to cryogenic temperature after exchanging the mother liquor with oil, and subsequently were mounted on a Rigaku R-Axis-II camera on a Ri-

* The term "phosphylated" denotes phosphorylation and phosphonylation reactions without distinction.

Figure 2. Active site of MeP-*TcAChE*, obtained by reaction with sarin. Note the proximity of four H-bond donors (dashed lines) to the anionic phosphonyl oxygen atoms: backbone amide nitrogens of A201, G118, and G119, as well as Ne2 of H440. The OP methyl carbon is within non-bonded contact distances (dotted lines) of F288 (3.59 Å to Cε1) and F290 (3.59 Å to Cε1) in the acyl pocket. For reference, the α -traces of native- and OP-enzyme are overlaid. The active site shown is essentially identical to that obtained with soman (not shown), except for minor differences in inter-atomic distances (Table 1).



gaku rotating anode FR300 generator at the Weizmann Institute (Rehovot, Israel). Data collection parameters were optimized using the software STRATEGY (13).

The starting model of native *TcAChE* (2ACE coordinates in the Brookhaven Protein Data Bank) was used for initial rigid-body refinement (14). Each of the three OP structures was refined independently, using difference Fourier methods. Final structures were compared, root mean square (rms) calculations were performed, and figures were made using the Biosym Insight97 software.

RESULTS AND DISCUSSION

The aged OP-AChE structures were refined at 2.2 Å (DFP), 2.5 Å (sarin), and 2.2 Å (soman) resolution. In each structure, the highest positive difference density peak, corresponding to the OP, was observed to be within covalent bonding distance of Ser200. Reaction with sarin or soman resulted in a methylphosphonylated (MeP)-AChE (Figure 2), and

Table 1. Distances in *TcAChE*-OP conjugates (Å)

Atom 1	Atom 2	DFP	sarin	soman
H440 Nε2	O (-P)	2.91	2.83	2.67
G118 N	O (=P)	2.58	2.90	2.78
G119 N	O (=P)	2.50	2.69	2.44
A201 N	O (=P)	3.19	2.98	2.98
S200 Oγ	H440 Nε2	3.20	2.87	3.17
H440 Nδ1	E327 Oε1	2.49	2.78	2.41
H440 Nδ1	E327 Oε2	4.27	4.66	4.40

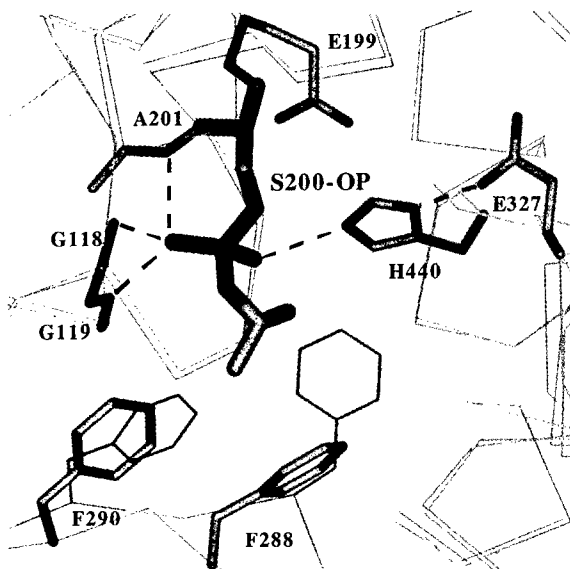


Figure 3. Active site of MiPrP-TcAChE obtained by reaction with DFP. As with aged, phosphonylated AChE, the stability of MiPrP-AChE apparently stems from four potential H-bond donors (dashed lines) to the anionic phosphoryl oxygen atoms. However, unlike for soman or sarin, the reaction with DFP results in a distortion of the main chain in the acyl pocket of AChE. F288 and F290 move significantly from their positions in the native enzyme (shown with thin dark lines for reference). The α -traces of native- and MiPrP-TcAChE are overlaid.

reaction with DFP resulted in a monoisopropylphosphorylated (MiPrP)-AChE structure (Figure 3).

The large molar excess of sarin or soman used should have resulted in almost exclusive reaction of AChE with the toxic, P(S) stereoisomers (15). Assuming no reorientation of the inhibitor in the active site during aging, the absolute configuration at the phosphorus (P) atom in the MeP-AChE structures is consistent with a simple in-line nucleophilic attack and inversion of stereochemistry at P during phosphonylation. The inversion mechanism has been proposed for AChE by analogy with other serine hydrolases (16). Comparison of the aged sarin and DFP conjugates, both of which have lost an isopropoxy group during aging, supports this conclusion.

Why Aged Enzyme Does Not Reactivate

The primary problem created by the dealkylation reaction of aging is the introduction of a formal negative charge, because anionic phosphoesters are inherently resistant to nucleophilic attack (17). Specific interactions between the enzyme's active site and the OP also may contribute to the stability of aged AChE, however, because denatured "aged" MiPrP-AChE does undergo base-catalyzed dephosphorylation (18).

A hydrogen bond from Ne2 of the active site imidazolium to one oxygen atom of the anionic OP conjugate has been postulated to be a key interaction that stabilizes aged, MiPrP-trypsin (19,20), as well as MiPrP-chymotrypsin (21). Active site distances of the three solved OP-AChE structures (Table 1) are consistent with the formation of this putative H-bond.

Our results reinforce the conclusion that there are multiple factors militating against reactivation of aged AChE: (i) the anionic character of the phosphoester; (ii) three potential H-bond donors from the oxyanion hole to one of the oxygen atoms bound to P; (iii) an additional H-bond from the His440 Ne2 to the other oxygen atom; and (iv) the wrong protonation state and poor geometry for His440 to act as a general base catalyst.

Structural Model for the Enzyme-Substrate Transition State

The phosphoryl oxygen atoms may carry significantly greater fractional negative charges than do the oxygens of the ACh transition state (TS) adduct (cf., 16 and 20). Despite this limitation, the active sites of MeP-AChE should provide useful structural analogs for modeling the deacylation TS formed by the natural substrate (ACh) (20, 22).

The position of the phosphoryl oxygen should mimic that of the TS carbonyl oxygen. All three OP structures corroborate that the oxyanion is stabilized in AChE by potential H-bonds from the amide nitrogens of G118, G119 and A201 (Figure 2, 3; Table 1). This is consistent with preliminary modeling of ACh binding to native AChE (8), as well as with the structure of a trifluoroketone TS inhibitor complex with AChE (TMTFA; 23).

A hydrophobic pocket which surrounds the phosphonate methyl group is formed in *Tc*AChE by W233, G119, F288, and F290. F331 may contribute to the acyl pocket by providing π - π -interactions with F288. Both F288 and F290 provide close non-bonded contacts to the sarin or soman methyl group (Figure 2), suggesting that these aromatic side chains also complement the methyl of ACh in the TS. Contacts from the acyl pocket to the phosphonate methyl group are generally closer than are those observed for the CF₃ group of TMTFA.

Movement in the Acyl Pocket

Structure-activity studies with carboxyl ester substrates and OP inhibitors first suggested the presence of specific binding pockets in the active site of AChE that complement the acyl and alkoxy groups (reviewed in 5, 24). Furthermore, this approach showed convincingly that the acyl pocket of AChE was more restricted than that of the closely related enzyme, butyrylcholinesterase (BChE; EC 3.1.1.8). When the crystal structure of AChE became available, homology models of BChE were built and, by inference from site-specific mutagenesis results, two aromatic residues, F288 and F290, were implicated as the source of greater AChE selectivity (9, 11, 12, 25). The pocket of BChE was viewed as more "open" because it contained Leu and Val (or Ile) residues at these positions, whereas the two Phe residues in the pocket of AChE were described as a "clamp" for the methyl group of ACh that would poorly accommodate bulkier acyl groups (25).

DFP is an approximately 300-fold poorer inhibitor of AChE than of BChE. Using mutagenesis and a series of OPs, it was shown that the relatively poor binding of DFP was almost completely accounted for by an increase in the K_d of the human AChE-DFP reversible complex that was mediated primarily by F295 and, to a lesser extent by F297, corresponding to residues F288 and F290, respectively, in *Tc*AChE (26).

We observed the first major conformational change in a *Tc*AChE complex for the MiPrP-AChE structure (obtained after reaction with DFP; Figure 3). Significant movement of the main chain atoms apparently allows the re-positioning of F288 and F290 to accommodate one *isopropyl* group of the OP (Figure 4). Superposing the MiPrP-AChE structure with native AChE showed that DFP causes the C α atoms at positions 288, 289, 290 and 291 to move 3.17, 1.59, 1.38 and 1.27 Å, respectively. The free energy penalty associated with this protein movement probably explains the reduced binding affinity of AChE, relative to BChE, for DFP, the P(R) phosphonates, and other substrates or inhibitors with bulky acyl groups. The conformational change in the acyl pocket observed by X-ray crystallography belies earlier molecular modeling studies, which generally predicted that the degrees of freedom available to the substrate or inhibitor were restricted by F288 and F290 and not that AChE itself undergoes a major conformational movement of the main chain to accommodate bulky ligands.

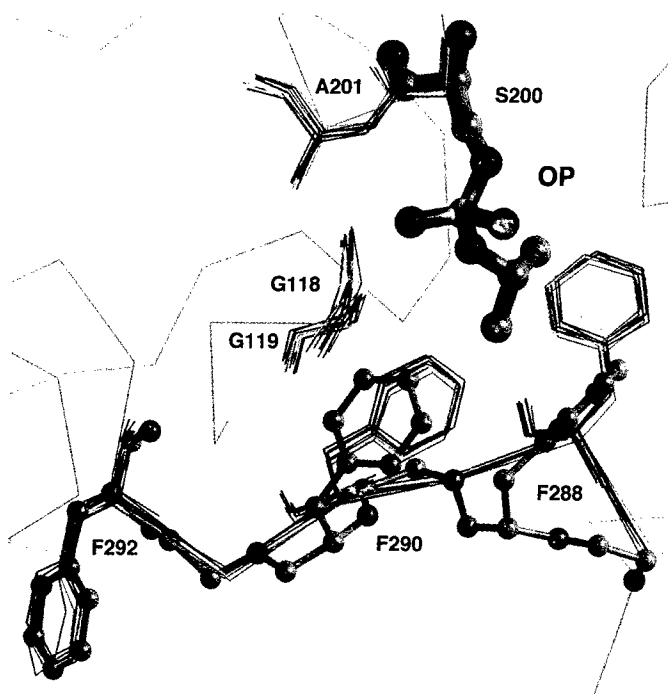


Figure 4. Reaction with DFP distorts the *TcAChE* acyl pocket. The bulky -OiPr group of DFP apparently causes movement of F288 and F290 in the crystal structure of MiPrP-AChE (green ball-and-stick model, including green α trace). The extent and unusual nature of this acyl pocket movement is shown by superimposing eight different *TcAChE* structures: native AChE (2ACE, orange); aged sarin-AChE (purple); aged soman-AChE (red); decamethonium complex (1ACL, yellow); edrophonium complex (2ACK, pink); tacrine complex (1ACJ, brick); TMTFK-AChE (1AMN, blue); huperzine complex (1VOT, green stick). Note that movement in the MiPrP-AChE structure is not limited to side chains, but also includes the acyl pocket main chain. A color version of this figure appears on the color insert facing page xxvii.

Although there is evidence for conformational changes associated with aging of some OP-AChE, -BChE, or -chymotrypsin conjugates in solution (27-29), we found no major structural rearrangements in *TcAChE* as a result of the aging reaction itself. The rms deviation found by comparing the α atoms of either MeP-AChE structure with native AChE was less than 0.3 Å. Moreover, superposing the active site residues of each MeP-AChE with those of native 2ACE, as well as thirteen other previously solved *TcAChE* structures, showed no significant movements that could be attributed to aging. It remains possible, however, that a transient conformational change occurred on the pathway to the final aged structure observed by X-ray crystallography. This possibility may be approached by solution studies, as well as by future X-ray crystallographic studies of OP-AChE complexes that are not aged.

REFERENCES

1. Rosenberry, TL. *Adv. Enzymol.* 1975, 43, 103-218.
2. Froede, H.C.; Wilson, I.B. *J. Biol. Chem.* 1984, 259, 11010-11013.
3. Aldridge, W.N.; Reiner, E. *Enzyme inhibitors as substrates: Interactions of esterases with esters of organophosphorus and carbamic acids*; North-Holland Publishing: Amsterdam, 1972.

4. Steitz, T.A.; Henderson, R.; Blow, D.M. *J. Mol. Biol.* 1969, 46, 337-348.
5. Jarv, J. *Bioorg. Chem.* 1984, 12, 259-278.
6. Kovach, I. *J. Enzyme Inhibit.* 1988, 2, 199-208.
7. Berends, F.; Posthumus, C.H.; Sluys, I.V.D.; Deierkauf, F.A. *Biochim. Biophys. Acta.* 1959, 34, 576-578.
8. Sussman, J.L.; Harel, M.; Frolow, F.; Oefner, C.; Goldman, A.; Toker, L.; Silman, I. *Science* 1991, 253, 872-9.
9. Harel, M.; Sussman, J.L.; Krejci, E.; Bon, S.; Chanal, P.; Massoulié, J.; Silman, I. *P.N.A.S. (USA)* 1992, 89, 10827-10831.
10. Millard, C.B.; Broomfield, C.A. *Biochem. Biophys. Res. Commun.* 1992, 189, 1280-6.
11. Barak, D.; Ariel, N.; Velan, B.; Shafferman, A. In *Multidisciplinary Approaches to Cholinesterase Functions*; Plenum Press: New York, 1992; pp. 195-199.
12. Ordentlich, A.; Barak, D.; Kronman, C.; Flashner, Y.; Leitner, M.; Segall, Y.; Ariel, N.; Cohen, S.; Velan, B.; Shafferman, A. *J. Biol. Chem.* 1993, 268, 17083-17095.
13. Ravelli, R.B.G.; Sweet, R.M.; Skinner, J.M.; Duisenberg, A.J.M.; Kroon, J. *J. Appl. Cryst.* 1997, 30, 551-554.
14. Raves, M.L.; Harel, M.; Pang, Y.-P.; Silman, I.; Kozikowski, A.P.; Sussman, J.L. *Nature Struct. Biol.* 1997, 4, 57-63.
15. Benschop, H.P.; DeJong, L.P.A. *Acc. Chem. Res.* 1988, 21, 368-374.
16. Bencsura, A.; Enyedy, I.; Kovach, I.M. *Biochemistry* 1995, 34, 8989-8999.
17. Westheimer, F.H. *Science* 1987, 235, 1173-1178.
18. Segall, Y.; Waysbort, D.; Barak, D.; Ariel, N.; Doctor, B.P.; Grunwald, J.; Ashani, Y. *Biochemistry* 1993, 32, 13441-13450.
19. Stroud, R.M.; Kay, L.M.; Dickerson, R.E. *J. Mol. Biol.* 1974, 83, 185-208.
20. Kossiakoff, A.A.; Spencer, S.A. *Biochemistry* 1981, 20, 6462-6474.
21. Harel, M.; Su, C.T.; Frolow, F.; Ashani, Y.; Silman, I.; Sussman, J.L. *J. Mol. Biol.* 1991, 221, 909-18.
22. Kraut, J. *Ann. Rev. Biochem.* 1977, 46, 331-358.
23. Harel, M.; Quinn, D.M.; Nair, H.K.; Silman, I.; Sussman, J.L. *J. Am. Chem. Soc.* 1995, 118, 2340-2346.
24. Kabachnik, M.I.; Brestkin, A.P.; Godovikov, N.N.; Michelson, M.J.; Rozengart, E.V.; Rozengart, V.I. *Pharmacol. Rev.* 1970, 22, 355-388.
25. Vellom, D.C.; Radic, Z.; Li, Y.; Pickering, N.A.; Camp, S.; Taylor, P. *Biochemistry* 1993, 32, 12-17.
26. Ordentlich, A.; Barak, D.; Kronman, C.; Ariel, N.; Segall, Y.; Velan, B.; Shafferman, A. *J. Biol. Chem.* 1996, 271, 11953-11962.
27. Amitai, G.; Ashani, Y.; Gafni, A.; Silman, I. *Biochemistry* 1982, 21, 2060-2069.
28. Aslanian, D.; Grof, P.; Renault, F.; Masson, P. *Biochim. Biophys. Acta* 1995, 1249, 37-44.
29. Steinberg, N.; van der Drift, A.C.M.; Grunwald, J.; Segall, Y.; Shirin, E.; Haas, E.; Ashani, Y.; Silman, I. *Biochemistry* 1989, 28, 1248-1253.

CRYSTALLOGRAPHIC STUDIES ON COMPLEXES OF ACETYLCHOLINESTERASE WITH THE NATURAL CHOLINESTERASE INHIBITORS FASCICULIN AND HUPERZINE A

Israel Silman, Michal Harel, Mia Raves, and Joel L. Sussman

Departments of Neurobiology and Structural Biology
Weizmann Institute of Science
Rehovoth 76100, Israel

INTRODUCTION

Acetylcholinesterase (AChE) terminates synaptic transmission at cholinergic synapses by rapid hydrolysis of acetylcholine (ACh) (Quinn, 1987). Anticholinesterase agents are used in the treatment of various disorders (Taylor, 1990), and have been proposed as therapeutic agents for the management of Alzheimer's disease (Giacobini & Becker, 1991, 1994). Two such anti-cholinesterase agents, both of which act as reversible inhibitors of AChE, have been licensed by the FDA: tacrine (Gauthier & Gauthier, 1991), under the trade name Cognex, and, more recently, E2020 (Sugimoto *et al.*, 1992), under the trade name Aricept. Several other anticholinesterase agents are at advanced stages of clinical evaluation. The active site of AChE contains a catalytic subsite, and a so-called 'anionic' subsite, which binds the quaternary group of ACh (Quinn, 1987). A second, 'peripheral' anionic site is so named since it is distant from the active site (Taylor & Lippi, 1975). Bisquaternary inhibitors of AChE derive their enhanced potency, relative to homologous monoquaternary ligands (Main, 1976), from their ability to span these two 'anionic' sites, which are *ca.* 14 Å apart.

The 3D structure of *Torpedo* AChE (Sussman *et al.*, 1991) reveals that, like other serine hydrolases, it contains a catalytic triad. Unexpectedly, however, for such a rapid enzyme, the active site is located at the bottom of a deep and narrow cavity; this cavity was named the 'aromatic gorge', since >50% of its lining is composed of the rings of 14 conserved amino acids (Sussman *et al.*, 1991; Axelsen *et al.*, 1994).

X-ray crystallographic studies of complexes of AChE with drugs of pharmacological interest can reveal which amino acid residues are important for binding the drug, and where space might exist for modifying the drug itself, information crucial for structure-

based drug design. Valuable information can also be achieved by site-directed mutagenesis (Harel *et al.*, 1992). In earlier studies (Harel *et al.*, 1993), we described the structures of complexes of *Torpedo* AChE (TcAChE) with three ligands of pharmacological interest: namely, edrophonium, a strong competitive AChE inhibitor (Wilson & Quan, 1958), whose pharmacological action is in the peripheral nervous system (Taylor, 1990); decamethonium, a bisquaternary ligand which is both a neuromuscular blocker and a cholinesterase inhibitor (Zaimis, 1976); and tacrine, already licensed as an anti-Alzheimer drug (see above), which is also a strong reversible inhibitor (Heilbronn, 1961). Modelling had predicted that the principal interaction of the quaternary group of ACh would be with Trp84, via electrostatic interaction with the π electrons of its indole ring (Sussman *et al.*, 1991), rather than with a cluster of acidic amino acids, as had been predicted previously (Nolte *et al.*, 1980); such an assignment was also supported by affinity labelling (Weise *et al.*, 1990). The crystallographic data fully confirmed this unexpected interaction (Harel *et al.*, 1993). Furthermore, they revealed a prominent role for others of the conserved aromatic residues within the gorge. Thus the phenyl ring of Phe330 contributed substantially to the 'anionic' subsite of the active site, while the 'peripheral' anionic site, located at the top of the gorge, contained three aromatic residues, Tyr70, Tyr121 and Trp279. The interaction of the two quaternary groups of decamethonium, located at the top and the bottom of the gorge, was primarily with these two sets of aromatic residues (Harel *et al.*, 1993).

In the following, we describe the structure of two additional TcAChE-ligand complexes recently solved in our laboratory: with fasciculin-II (FAS), a member of the three-finger polypeptide toxin family, which was isolated from mamba venom (Harel *et al.*, 1995); and with (-)-huperzine A (HupA), an alkaloid purified from a moss used in Chinese herbal medicine (Raves *et al.*, 1997).

RESULTS AND DISCUSSION

FAS-TcAChE Complex

The venoms of elapid snakes, including the Asian cobras and kraits, as well as the African mambas, contain a number of small proteins, containing 60–70 amino acids, which display a broad spectrum of toxic activities (Harvey, 1991). Among the best studied are the α -neurotoxins of the venoms of the kraits and cobras, such as α -bungarotoxin, from the Formosan krait, *Bungarus multicinctus*, which are potent and specific blockers of the nicotinic acetylcholine receptor (Changeux *et al.*, 1970). Other toxins of this family have been shown to act as blockers of ion channels (Albrand *et al.*, 1995), muscarinic agonists (Ségalas *et al.*, 1995) and anticholinesterases (Cerveñansky *et al.*, 1991). Despite their diverse biological activities, they display substantial sequence and structural homology. X-ray and NMR studies show that the toxins share a common structural motif: a core, containing four disulfide bridges, from which three loops protrude, roughly like the fingers of a hand (le Du *et al.*, 1992). Accordingly, they are known as the three-fingered toxin family (Wonnacott & Dajas, 1994). Superposition of their structures reveals that, whereas the structure of the central core is conserved, the orientation of the fingers can vary considerably (Albrand *et al.*, 1995), suggesting that they serve as determinants of biological specificity. No three-dimensional structure of a complex of a three-fingered toxin with its target was, however, available.

Whereas in previous cases, the AChE-ligand complex was obtained by soaking the ligand into crystals of the native enzyme, FAS is too large to permit such an approach. Accordingly, orthorhombic crystals of the complex were obtained from a solution containing

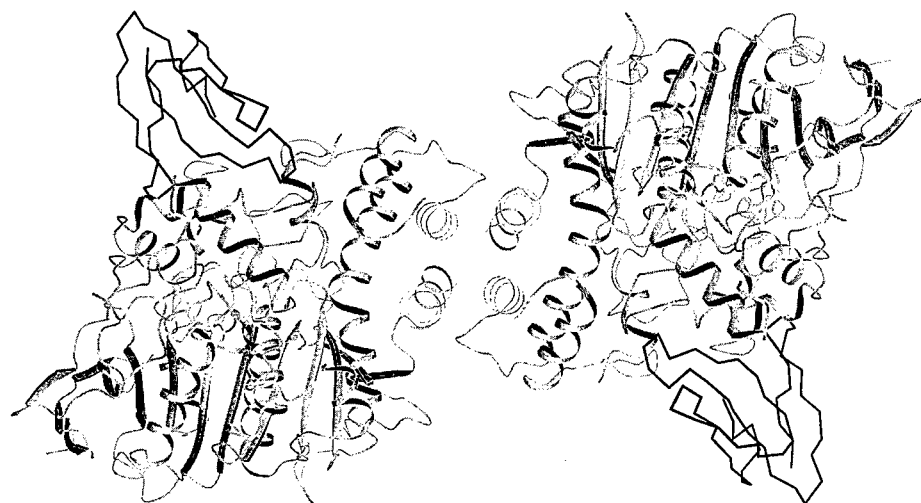


Figure 1. Stoichiometric complex of fasciculin-II (FAS) with TcAChE. Shown is a ribbon diagram of the biological dimer, in which the two subunits interact via a 4-helix bundle and a disulfide bridge (not shown). The two FAS molecules, displayed as a line trace, are positioned over the top of the gorge leading to the active site of each subunit.

stoichiometric (1:1) amounts of the purified TcAChE and of FAS purified from the venom of the green mamba (*Dendroaspis angusticeps*), and a data set was obtained which could be refined at 3.0 Å resolution. The structure indeed reveals a stoichiometric complex, with one FAS molecule bound to each subunit of the TcAChE dimer (Fig. 1). FAS is bound on the surface of the subunit, at the 'peripheral' anionic site, thus sealing the top of the narrow gorge leading to the active site. A similar structure was reported independently, by Bourne *et al.* (1995), for a complex of FAS with mouse recombinant AChE.

It has been noted previously that AChE has a large dipole moment (>1000 Debye), aligned approximately along the axis of the 'aromatic' gorge (Ripoll *et al.*, 1993; Porschke *et al.*, 1996). The field generated by this dipole might actually draw the positively charged substrate, ACh, down the gorge towards the active site. Similarly, FAS has its charges separated (dipole moment *ca.* 185 Debye), with most basic residues occurring in the first two fingers, which make intimate contact with TcAChE, and most acidic residues in the third finger. Visual inspection suggests that the two dipole moments are roughly aligned, and electrostatic calculations show that the angle between the dipole vectors is only 30°.

The high affinity of FAS for AChE can be attributed to many residues either unique to FAS or rare in other three-fingered toxins (Giles *et al.*, 1997), and to a remarkable surface complementarity, involving a large contact area (2000 Å²). This is substantially larger, for example, than the contact area between lysozyme and an antibody raised against it, 1700 Å², or between trypsin and bovine pancreatic trypsin inhibitor, 1400 Å² (Janin & Chothia, 1990). A most striking and rare interaction is a stacking of the side chains of Met33 in FAS and of Trp279 in *Torpedo* AChE. Mutation of this tryptophan residue to a nonaromatic residue decreases the affinity of FAS for AChE by over five orders of magnitude (Radic *et al.*, 1994), and its absence from the AChEs cloned so far from avian and invertebrate sources (e.g. Eichler *et al.*, 1994; Cousin *et al.*, 1996), as well as from butyrylcholinesterase BChE (Harel *et al.*, 1992), provides a clear structural explanation for their poor inhibition by FAS.

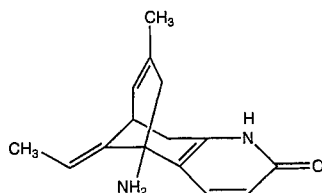


Figure 2. Molecular structure of (-)-huperzine A (HupA).

HupA-TcAChE Complex

(-)-Huperzine A (HupA, Fig. 2) is a nootropic alkaloid extracted from the club moss, *Huperzia serrata*, which has been used in China for centuries as a folk medicine (Liu *et al.*, 1986). HupA is a potent reversible inhibitor of AChE that lacks potentially complicating muscarinic effects (Kozikowski *et al.*, 1992). The existence of a natural AChE inhibitor, taken together with its unique pharmacological features and relative lack of toxicity (Laganière *et al.*, 1991), render HupA a particularly promising candidate for treatment of Alzheimer's disease. Indeed, studies on experimental animals reveal significant cognitive enhancement (Xiong *et al.*, 1995), and clinical trials in China have both established the safety of HupA, and provided preliminary evidence for significant effects on patients exhibiting dementia and memory disorders (Zhang *et al.*, 1991). The structure of HupA reveals no obvious similarity to that of ACh. In fact, a number of studies, utilising either computerised docking techniques and/or site-directed mutagenesis (Ashani *et al.*, 1994; Pang *et al.*, 1994; Saxena *et al.*, 1994), predicted various possible orientations of HupA within the active site of AChE. It seemed, therefore, desirable to solve the structure of a TcAChE-HupA complex by X-ray crystallography. It would thus be possible to establish that it indeed binds at the active-site and to determine its correct orientation, thus providing the basis for future structure-based drug design.

Soaking of HupA into native trigonal crystals of *Torpedo* AChE yielded a crystalline complex from which a data set was collected which could be refined to 2.5 Å resolution. Examination of a difference map for the complex, as compared to the native enzyme, clearly revealed a prominent electron density peak near the bottom of the 'aromatic gorge' with an outline resembling that of HupA. Indeed, excellent fitting of the molecule to the electron density was obtained.

The crystal structure of the HupA-TcAChE complex (Fig. 3) shows an unexpected orientation for the inhibitor, with surprisingly few strong direct interactions with protein residues to explain its high affinity. The principal interactions include: (a) a strong hydrogen bond (2.6 Å) of the carbonyl group of the ligand to Tyr130; (b) hydrogen bonds to water molecules within the active-site gorge which are, themselves, hydrogen-bonded to other waters or to side-chain and backbone atoms of the protein, notably to the carboxylic oxygens of Glu199 and to the hydroxyl oxygen of Tyr121; (c) interaction of the primary amino group of the ligand, which can be assumed to be charged at the pH of the mother liquor, with the aromatic rings of Trp84 and Phe330; (d) an unusually short (3.0 Å) C-H...O bond between the ethylidene methyl group of HupA and the main-chain oxygen of His440; and (e) several hydrophobic contacts notably with the side chains and main-chain atoms of Trp84 and with residues Gly118 through Ser122.

Modelling Phe330 in the crystal structure as tyrosine, which is the corresponding residue in mammalian AChE, permits formation of a 3.3 Å hydrogen bond between the

hydroxyl oxygen and the primary amino group of HupA. This extra hydrogen bond, in addition to π -cation interactions, may help to explain why HupA binds to mammalian AChE 5–10-fold more strongly than to TcAChE, and only weakly to BChE, which lacks an aromatic residue at this position (Ashani *et al.*, 1994).

It seems surprising that an inhibitor with a relatively high affinity for AChE— K_i ca. 6 nM for fetal bovine serum AChE, and 250 nM for TcAChE (Saxena *et al.*, 1994)—binds through so few direct contacts. Even though HupA has three potential hydrogen-bond donor and acceptor sites (Fig. 2), only one strong hydrogen bond is seen, between the pyridone oxygen and Tyr130. Analogous compounds with a methoxy replacing the oxygen show no inhibition at all (Kozikowski *et al.*, 1992). It is also of interest that the ring nitrogen is hydrogen-bonded to the protein via a water molecule, and hydrogen bonds between the NH_3^+ group and the protein are mediated through at least two waters. The aromatic rings of both Trp84 and Phe330 are near the primary amino group. However, the structure displays a large number of hydrophobic interactions: there are 11 contacts between a carbon atom of HupA and oxygen or nitrogen atoms of the protein, and 20 carbon-to-carbon contacts within 4.0 Å. Consequently, there does not appear to be much room for adding additional groups without causing clashes. Nevertheless, addition of a methyl group near the amide group of HupA leads to an 8-fold increase in affinity, probably due to extra hydrophobic contacts with Trp84 (Kozikowski *et al.*, 1996).

In summary, the crystal structure of the HupA-TcAChE complex reveals an unexpected orientation of the ligand within the active site, as well as unusual protein-ligand interactions. This information should be of value in the design and analysis of analogs of HupA with improved pharmacological characteristics.



Figure 3A. Ribbon diagram of the HupA-TcAChE complex, showing the HupA molecule at the bottom of the active-site gorge.



Figure 3B. Enlargement of the active site region, showing the catalytic triad to the right, and some of the aromatic residues surrounding the HupA molecule making contact.

ACKNOWLEDGMENTS

This research was supported by the U.S. Army Medical Research and Development Command, the Minerva Foundation, the Kimmelman Center for Biomolecular Structure and Assembly, and the Scientific Cooperation of the European Union with Third Mediterranean Countries through the Israeli Ministry of Science. I.S. is Bernstein-Mason Professor of Neurochemistry.

REFERENCES

- Albrand, J.-P., Blackledge, M.J., Pascaud, F., Hollecker, M., and Marion, D., 1995, *Biochemistry* 34:5923–5937.
- Ashani, Y., Grunwald, J., Kronman, C., Velan, B., and Shafferman, A., 1994, *Mol. Pharmacol.* 45:555–560.
- Axelsen, P.H., Harel, M., Silman, I., and Sussman, J.L., 1994, *Protein Sci* 3:188–197.
- Bourne, Y., Taylor, P., and Marchot, P., 1995, *Cell* 83:503–512.
- Cerveñansky, C., Dajas, F., Harvey, A.L., and Karlsson, E., 1991, In: *Snake Toxins*, Harvey, A.L., ed., pp. 131–164, Pergamon, New York.
- Changeux, J.-P., Kasai, M., and Lee, C.Y., 1970, *Proc. Natl. Acad. Sci. USA* 67:1241–1247.
- Cousin, X., Bon, S., Duval, N., Massoulié, J., and Bon, C., 1996, *J. Biol. Chem.* 271:15099–15108.
- Eichler, J., Anselmet, A., Sussman, J.L., Massoulié, J., and Silman, I., 1994, *Mol. Pharmacol.* 45:335–340.
- Sugimoto, H., Tsuchiya, Y., Sugumi, H., Higurashi, K., Karibe, N., Imura, Y., Sasaki, A., Araki, S., Yamanishi, Y., and Yamatsu, K., 1992, *J. Med. Chem.* 35:4542–4548.
- Gauthier, S., and Gauthier, L., 1991, In: *Cholinergic Basis for Alzheimer Therapy*, Giacobini, E., and Becker, R., eds., Birkhäuser, Boston, pp. 224–230.
- Giacobini, E., and Becker, R., 1991, *Cholinergic Basis for Alzheimer Therapy*, Birkhäuser, Boston.
- Giacobini, E., and Becker, R., 1994, *Alzheimer Disease: Therapeutic Strategies*, Birkhäuser, Boston.
- Giles, K., Raves, M.L., Silman, I., and Sussman, J.L., 1997, In: *Theoretical and Computational Methods in Genome Research*, Suhai, S., ed., Plenum Press, New York, in press.
- Harel, M., Sussman, J.L., Krejci, E., Bon, S., Chanal, P., Massoulié, J., and Silman, I., 1992, *Proc. Natl. Acad. Sci. USA* 89, 10827–10831.
- Harel, M., Schalk, I., Ehret-Sabatier, L., Bouet, F., Goeldner, M., Hirth, C., Axelsen, P., Silman, I., and Sussman, J.L., 1993, *Proc. Natl. Acad. Sci. USA* 90:9031–9035.
- Harel, M., Kleywegt, G.J., Ravelli, R.B.G., Silman, I., and Sussman, J.L., 1995, *Structure* 3:1355–1366.
- Harvey, A.L., 1991, *Snake Toxins*, Pergamon, New York.
- Heilbronn, E., 1961, *Acta Chem. Scand.* 15:1386–1390.
- Janin, J., and Chothia, C., 1990, *J. Biol. Chem.* 265:16027–16030.
- Kozikowski, A., Thiels, E., Tang, X.-C., and Hanin, I., 1992, *Adv. Med. Chem.* 1:175–205.
- Kozikowski, A.P., Campiani, G., Sun, L.-Q., Wang, S., Sega, A., Saxena, A., and Doctor, B.P., 1996, *J. Am. Chem. Soc.* 118:11357–11362.
- Laganière, S., Corey, J., Tang, X.-C., Wülfert, E., and Hanin, I., 1991, *Neuropharmacology* 30:763–768.
- le Du, M.H., Marchot, P., Bougis, P.E., and Fontecilla-Camps, J.C., 1992, *J. Biol. Chem.* 267:22122–22130.
- Liu, J.-S., Zhu, Y.-L., Yu, C.-M., Zhou, Y.-Z., Han, Y.-Y., Wu, F.-W., and Qi, B.-F., 1986, *Can. J. Chem.* 64, 837–839.
- Main, A.R., 1976, In: *Biology of Cholinergic Function*, Goldberg, A.M., and Hanin, I., eds., pp. 269–353, Raven, New York.
- Nolte, H.-J., Rosenberry, T.L., and Neumann, E., 1980, *Biochemistry* 19:3705–3711.
- Pang, Y.-P., and Kozikowski, A., 1994, *J. Computer-Aided Mol. Design* 8:669–681.
- Porschke, D., Crémion, C., Cousin, X., Bon, C., Sussman, J., and Silman, I., 1996, *Biophys. J.* 70:1603–1608.
- Quinn, D.M., 1987, *Chem. Revs.* 87:955–975.
- Radic, Z., Durán, R., Vellom, D.C., Li, Y., Cerveñansky, C., and Taylor, P., 1994, *J. Biol. Chem.* 269:11233–11239.
- Raves, M.L., Harel, M., Pang, Y.-P., Silman, I., Kozikowski, A.P., and Sussman, J.L., 1997, *Nature Struct. Biol.* 4:57–63.
- Ripoll, D., Faerman, C., Axelsen, P., Silman, I., and Sussman, J.L., 1993, *Proc. Natl. Acad. Sci. USA* 90:5128–5132.
- Saxena, A., Qian, N., Kovach, I.M., Kozikowski, A.P., Pang, Y.P., Vellom, D.C., Radic, Z., Quinn, D., Taylor, P., and Doctor, B.P., 1994, *Protein Sci.* 3:1770–1778.
- Ségalas, I., Roumest, and C., Zinn-Justin, C., Gilquin, B., Ménez, R., Ménez, A., and Toma, F., 1995, *Biochemistry* 34:1248–1260.
- Silman, I., Harel, M., Eichler, J., Sussman, J.L., Anselmet, A., and Massoulié, J., 1994, In: *Alzheimer Disease: Therapeutic Strategies*, Giacobini, E., and Becker, R., eds., pp. 88–92, Birkhäuser, Boston.
- Sussman, J.L., Harel, M., Frolov, F., Oefner, C., Goldman, A., Toker, L., and Silman, I., 1991, *Science* 253:872–879.
- Taylor, P., 1990, In: *The Pharmacological Basis of Therapeutics*, Gilman, A.G., Nies, A.S., Rall, T.W., and Taylor, P., eds., 5th Ed., Macmillan, New York, pp. 131–150.
- Taylor, P., and Lappi, S., 1975, *Biochemistry* 14:1989–1997.
- Weise, C., Kreienkamp, H.-J., Raba, R., Pedak, A., Aaviksaar, A., and Hucho, F., 1990, *EMBO J* 9:3885–3888.
- Wilson, I.B., and Quan, C., 1958, *Arch. Biochem. Biophys.* 73:131–143.

- Wonnacott, S.M., and Dajas, F., 1994, *Trends Pharmacol. Sci.* 15:1-3.
- Xiong, Z.Q. , and Tang, X.C., 1995, *Pharmacol. Biochem. Behav.* 51:415-419.
- Zaimis, E. , and Head, S., 1976, *Handb. Exp. Pharmacol.* 42:365-420.
- Zhang, R.W., Tang, X.C., Han, Y.Y., Sang, G.W., Zhang, Y.D., Ma, Y.X., Zhang, C.L. , and Yang, R.M., 1991, *Acta Pharmacol. Sinica* 12:250-252.

3D STRUCTURE AT 2.7Å RESOLUTION OF NATIVE AND E202Q MUTANT HUMAN ACETYLCHOLINESTERASE COMPLEXED WITH FASCICULIN-II

Gitay Kryger,¹ Kurt Giles,^{1,2} Michal Harel,¹ Lilly Toker,² Baruch Velan,³
Ariel Lazar,³ Chanoch Kronman,³ Dov Barak,³ Naomi Ariel,³
Avigdor Shafferman,³ Israel Silman,² and Joel L. Sussman^{1,4}

¹Department of Structural Biology
Weizmann Institute of Science

²Department of Neurobiology
Weizmann Institute of Science
Rehovot 76100, Israel

³Israel Institute for Biological Research
Ness Ziona 70450, Israel

⁴Biology Department, Brookhaven National Laboratory
Upton, New York 11973

INTRODUCTION

Knowledge of the 3D structure of human acetylcholinesterase (AChE) is of importance for drug design, in particular of anti-Alzheimer drugs (1,2), for development of improved procedures for treatment of intoxication by nerve agents (3), and for the design of safer and more effective insecticides.

Vertebrate AChE occurs as an array of molecular forms which differ in the number of subunits which they contain and in their quaternary structure (4). Recombinant Human AChE (rHuAChE), expressed in HEK 293 cells, is secreted into the culture medium as a mixture of monomers, dimers and tetramers (5), and additional heterogeneity may arise due to variations in the extent of glycosylation (6) and to proteolytic 'nicking'. Such heterogeneity may severely impede crystallization. To partially alleviate this problem, a mutant of rHuAChE was constructed in which the C-terminus had been truncated to give rise to a homogeneous monomeric form (7).

EXPERIMENTAL

Mutagenesis and Generation of Truncated rHuAChE

Truncation of the C-terminus of the HuAChE T-subunit (8) was performed by DNA cassette replacement. Specifically, the 187 bp DNA fragment between *Bss*HII and *Sall* in pL5CA was replaced by the synthetic DNA duplex. The truncated DNA sequence was introduced into a tripartite expression vector expressing also the reporter gene *cat* and the selection marker *neo*. The expression vector coding for the expression of monomeric rHuAChE was introduced into HEK 293 cells. Stable clones, secreting high levels (> 4 U/ml/h) of truncated enzyme (Δ Ect-rHuAChE), were isolated and used in large scale production (9) so as to obtain amounts of purified enzyme adequate for crystallization. Purification of the recombinant enzyme was carried out by affinity chromatography (10). Catalytic activity was assayed by the Ellman method (11). Analytical sucrose density gradient centrifugation was performed on 5-20% sucrose gradients. A homologous truncated DNA sequence, in which site-directed mutagenesis afforded expression of the E202Q mutant (12), was generated, expressed and characterized similarly.

Crystallization and Data Collection

Both WT rHuAChE and the E202Q mutant were cocrystallized as a stoichiometric complex with the polypeptide toxin, fasciculin-II (FAS-II) (13), purified from the venom of the green mamba. Crystallization was from ammonium sulfate at neutral pH and room temperature. Crystal size and quality were improved by recrystallization from water. X-ray data were collected on the X12C beamline of the NSLS, at Brookhaven National Laboratory, in both cases from a single cryogenically cooled crystal.

Structure Solution and Refinement

Structure solution of the rHuAChE/FAS-II complex was carried out by molecular replacement, using the mouse AChE/FAS-II structure (PDB ID 1MAH, (14)) as a probe molecule and, subsequently, as a starting model for refinement. The model of the complex of *Torpedo californica* (Tc) AChE and FAS-II (PDB ID 1FSS, (15)) was used as a control to verify the molecular replacement solution. Diffraction data for the E202Q mutant were refined similarly, but using the rHuAChE/FAS-II structure as a starting model. The structure was refined using Xplor (simulated annealing (16)) and CNS (simulated annealing coupled with maximum likelihood technique (17)).

RESULTS AND DISCUSSION

Characterization of Δ Ect-rHuAChE

The T subunit expressed was devoid of the C-terminal hydrophobic sequence corresponding to residues 544-583, including C580, which forms the interchain disulfide in oligomeric forms (18). These residues were replaced by the pentapeptide, ASEAP, which is the natural C-terminal sequence in the H-subunit (4). The resulting truncated enzyme displays the following structural and catalytic characteristics: 1. Sucrose gradient centrifugation reveals a unique monomeric form, slightly slower than the monomer of the WT enzyme; 2. SDS-PAGE suggests that a similar degree of glycosylation-related microhet-

erogeneity is present in both the WT and the truncated enzyme; 3. The molecular weight of the truncated polypeptide, after removal of sugar side chains by glycanase, is 60kD, as compared to 64kD for the WT polypeptide. This difference in size is as predicted from the difference in chain length of the two forms. 4. The catalytic characteristics of the truncated enzyme, as well as the inhibition constants for its inhibition both by active and peripheral site ligands, are essentially identical to those for the WT enzyme.

X-Ray Data and Structure Refinement

Crystallization of both WT and E202Q rHuAChE produced crystals of irregular prism morphology, which grew within 1-3 weeks to 0.01-0.1 mm in size. Recrystallization resulted in larger, more suitable crystals, up to 0.8mm in size. The crystals exhibited rhombohedral symmetry of space-group R32, with unit cell dimensions of $a=b=150\text{\AA}$, $c=247\text{\AA}$, with a single copy of the complex in the asymmetric unit. The overall completeness of the 30Å-2.7Å data is 99.0% and 83.4%, with R_{merge} 8.1% and 9.1%, for WT and E202Q AChE, respectively. For the wild-type enzyme, the current R_{work} is 22% and the R_{free} is 29% , and for the E202Q structure, the corresponding figures are 21 and 24%, respectively. The electron density reveals residues 5- 490 and 497-543 of the HuAChE polypeptide chain, and all 61 residues of FAS-II. The 490-497 sequence is homologous to the external 485-490 sequence in *TcAChE*, which is not visible in the native 2ACE structure, but can be seen in the recently refined complex with E2020 (see Kryger *et al.*, this volume). In the published mouse structure (PDB ID 1MAH), residues 4-543 are all present but, judging from the temperature factors, residues 491-499 are poorly determined, especially at the 3.2Å higher resolution limit of this structure. The electron density of the WT rHuAChE structure shows the location of about 200 water molecules (none were reported for mAChE), one *N*-glycosylation site, at N350, seen also in the mAChE structure, and additional density near T504, which is a putative O-glycosylation site.

3D STRUCTURE COMPARISON OF AChE FROM THREE SPECIES

Close inspection of the rHuAChE/FAS-II model reveals a high degree of structural similarity between it and the two other, already published, complexes of AChE with FAS-II, viz. of *TcAChE* and mAChE (14,15), especially in the active-site region and within the aromatic gorge. Small variations can be found in some loops and in the insertion/deletion regions. Our results validate use of *TcAChE* as a model for gaining a general understanding of the structure of AChE, but also open the way to the study of subtle differences in structure which may account for species-dependent differences in specificity for substrates and inhibitors.

E202(199)Q MUTANT

Residue E202, which is adjacent to the active-site serine, S203(200), is one of three charged residues at the bottom of the active site gorge and plays an important role in HuAChE reactivity. Yet, the 3D structure of the E202(199)Q mutant is almost identical to that of the WT enzyme. The reduction in catalytic efficiency displayed by the E202Q mutant, either toward charged or uncharged substrates, and the marked concomitant decreases in rates of both phosphorylation and aging (12,19), was explained by the

participation of residue E202(199) in the chemical process involving the catalytic triad residue H447(440) (20). We proposed earlier that E202(199) plays a key role in maintaining a network of H-bonds that span the cross-section of the active site gorge (19). The role proposed for this network is to stabilize the functional architecture of the active center and to ensure proper positioning of E202(199), thereby stabilizing acylation and phosphorylation transition states. Central to this array are the two water molecules bridging residues E202(199)-E450(443) and E202(199)-Y133(131). Indeed, replacement of any of these three residues has similar effects in reducing catalytic activity (12). These water molecules appear to be conserved in the E202Q mutant. Replacement of E202 by D leads to an even greater decrease in enzymatic activity (K_{app} values for WT, E202Q and E202D are, respectively, 2640, 273 and $47 \times 10^{-6} \text{ M}^{-1} \text{ min}^{-1}$). Despite the fact that the charge in E202D is maintained, these data suggest that the H-bond network is disrupted due to the shorter side chain of D202. It will be of interest to investigate whether the H-bond network involving the water molecules is maintained in the E202D mutant.

ACKNOWLEDGMENTS

This work was supported by the U.S. Army Medical Research Acquisition Activity under Contracts DAMD17-96-C-6088 and DAMD17-97-2-7022, the Kimmelman Center for Biomolecular Structure and Assembly, Rehovot, Israel, the European Union, and the generous support of Tania Friedman. I.S. is Bernstein-Mason Professor of Neurochemistry.

REFERENCES

1. Weinstock, M. *Neurodegeneration* **1995**, *4*, 349-56.
2. Enz, A.; Amstutz, R.; Boddeke, H.; Gmelin, G.; Malanowski, J. *Prog. Brain Res.* **1993**, *98*, 431-8.
3. Millard, C. B.; Broomfield, C. A. *J. Neurochem.* **1995**, *64*, 1909-18.
4. Massoulié, Pezzementi, L.; Bon, S.; Krejci, E.; Vallette, F.-M. *Prog. Neurobiol.* **1993**, *14*, 31-91.
5. Velan, B.; Grosfeld, H.; Kronman, C.; Leitner, M.; Gozes, Y.; Lazar, A.; Flashner, Y.; Marcus, D.; Cohen, S.; Shafferman, A. *J. Biol. Chem.* **1991**, *266*, 23977-84.
6. Velan, B.; Kronman, C.; Ordentlich, A.; Flashner, Y.; Leitner, M.; Cohen, S.; Shafferman, A. *Biochem. J.* **1993**, *296*, 649-656.
7. Marchot, P.; Ravelli, R. B. G.; Raves, M. L.; Bourne, Y.; Vellom, D. C.; Kanter, J.; Camp, S.; Sussman, J. L.; Taylor, P. *Prot. Sci.* **1996**, *5*, 672-679.
8. Soreq, H.; Ben-Aziz, R.; Prody, C. A.; Seidman, S.; Gnatt, A.; Neville, L.; Lieman-Hurwitz, J.; Lev-Lehman, E.; Ginzberg, D.; Lipidot-Lifson, Y.; Zakut, H. *Proc. Natl. Acad. Sci. U S A* **1990**, *87*, 9688-92.
9. Kronman, C.; Velan, B.; Gozes, Y.; Leitner, M.; Flashner, Y.; Lazar, A.; Marcus, D.; Sery, T.; Papier, Y.; Grosfeld, H.; Cohen, S.; Shafferman, A. *Gene* **1992**, *121*, 295-304.
10. Sussman, J. L.; Harel, M.; Frolow, F.; Varon, L.; Toker, L.; Futerman, A. H.; Silman, I. *J. Mol. Biol.* **1988**, *203*, 821-823.
11. Ellman, G. L.; Courtney, K. D.; Andres, V., Jr.; Featherstone, R. M. *Biochem. Pharmacol.* **1961**, *7*, 88-95.
12. Shafferman, A.; Velan, B.; Ordentlich, A.; Kronman, C.; Grosfeld, H.; Leitner, M.; Flashner, Y.; Cohen, S.; Barak, D.; Ariel, N. *EMBO J.* **1992**, *11*, 3561-8.
13. Karlsson, E.; Mbugua, P. M.; Rodriguez Ithurralde, D. *J. Physiol. (Paris)* **1984**, *79*, 232-40.
14. Bourne, Y.; Taylor, P.; Marchot, P. *Cell* **1995**, *83*, 503-512.
15. Harel, M.; Kleywegt, G. J.; Ravelli, R. B.; Silman, I.; Sussman, J. L. *Structure* **1995**, *3*, 1355-66.
16. Brunger, A. T. *J. Mol. Biol.* **1988**, *203*, 803-16.
17. Adams, P. D.; Pannu, N. S.; Read, R. J.; Brunger, A. T. *Proc. Natl. Acad. Sci. U S A* **1997**, *94*, 5018-23.
18. Giles, K. *Protein Eng.* **1997**, *10*, 677-85.
19. Ordentlich, A.; Kronman, C.; Barak, D.; Stein, D.; Ariel, N.; Marcus, D.; Velan, B.; Shafferman, A. *FEBS Lett.* **1993**, *334*, 215-20.
20. Shafferman, A.; Ordentlich, A.; Barak, D.; Stein, D.; Ariel, N.; Velan, B. *Biochem. J.* **1996**, *318*, 833-40.